

# **The geology and structure of the Bushveld Complex metamorphic aureole in the Olifants River area**

by

Ronald Uken

Thesis submitted in partial fulfilment of the requirements  
for the degree of Doctor of Philosophy

*Department of Geology and Applied Geology  
University of Natal, Durban,  
South Africa*

December 1998

This is to certify that this thesis has not been submitted to any other university, and that unless specifically acknowledged, the work in this thesis is my own original work.

A handwritten signature in black ink, appearing to be 'R. Uken', written in a cursive style.

R. Uken

## ABSTRACT

The contact metamorphic aureole of the Rustenburg Layered Suite of the Bushveld Complex extends to a depth of over 5 km into the underlying mainly argillaceous Pretoria Group. When compared to other parts of the metamorphic aureole, the Olifants River area is unique in that it is characterised by a high degree of syn-Bushveld Complex deformation and very coarse grained pelitic assemblages. This is believed to have resulted from a combination of greater magma thickness, a deeper emplacement depth and a high degree of subsidence related deformation that was focused along the Thabazimbi-Murchison Lineament. This area also contains a laterally extensive and deformed quartz-feldspar porphyry sill, the Roodekrans Complex that is shown to represent a hypabyssal equivalent of the volcanic Rooiberg Group.

There are three main metamorphic zones. A wide andalusite zone dominated by staurolite, garnet and cordierite assemblages. This is followed by a narrow fibrolite zone without staurolite, and a wide inner aureole of migmatite. The migmatite zone is characterised by garnet-cordierite-aluminosilicate assemblages with corundum, spinel and orthopyroxene assemblages at the highest grades. Metamorphic pressure and temperature estimates indicate pressures of between 3 kb and 4 kb in the lower part of the andalusite zone at temperatures of approximately 550 °C.

Porphyroblast-matrix relationships reveal a close link between deformation and metamorphism resulting in a spectrum of textural relationships developed as a result of inhomogeneous strain. Porphyroblasts in low strain domains preserve textures of "static type" growth whereas syntectonic textures are found in foliated rocks. Pre-tectonic porphyroblasts in many foliated domains indicate that deformation outlasted porphyroblast growth and increased in intensity and extent with time. Retrograde porphyroblasts are post-tectonic. Evidence is presented for both rotation and non-rotation of porphyroblasts in relation to geographical coordinates during extensional top-to-south, down-dip shear in the floor.

The unique structural setting in this area triggered the growth of large diapiric structures in the floor of the Rustenburg Layered Suite that are preserved as periclinal folds on the margin and within the northeastern Bushveld Complex. Extreme gravitational loading and heating of the floor by a thickness of up to 8 km of mafic magma resulted in the generation of evenly spaced, up to 7 km diameter

wall-rock diapirs that penetrated the overlying magma chamber. Diapiric deformation is restricted to rocks above a decollement zone that is developed along competency contrasts and corresponds approximately with the 550 °C peak metamorphic isotherm.

Strongly lineated, boudinaged and foliated rocks are developed in the interpericlinal domains between adjacent periclinal. Migmatites in these domains are characterised by conjugate extensional ductile shears and associated asymmetrical boudinage suggesting bulk deformation by pure shear processes. The extension lineation was produced by lateral extension along flow lines directed toward dome culminations.

Each of the four diapiric periclinal is cut by a different erosional section enabling reconstruction of a typical diapir geometry. At the highest structural levels, periclinal have bulbous shapes with overturned limb geometries forming overhangs. The surrounding layered igneous rocks are locally deformed into a series of outward verging folds that define a broad rim syncline. Deformation within the periclinal cores is represented by constrictional deformation that produced radial curtain-type folds with steeply plunging lineations and concentrically orientated folds in the outer shell.

Diapirism is closely linked to magma emplacement mechanisms. Floor folds in the country rocks were initiated in the interfinger areas of a fingered intrusion. With further magma additions and the coalescence of intrusion fingers into a single sheet, interfinger folds matured into large diapiric periclinal which rose to the upper levels of the magma chamber. Strain rates estimated from strain analyses, periclinal geometry and model cooling calculations are in the order of  $10^{-14} \text{ s}^{-1}$ , corresponding to diapiric uplift rates of 0.6 cm/yr.

Diapirism is broadly compatible with a N-S extension in the Olifants River area during emplacement of the Rustenburg Layered Suite. On a regional scale, this is indicated by existence of a major EW dyke swarm that coincides with the long axis of the Bushveld Complex. The accommodation of the Bushveld Complex into the Kaapvaal Craton was facilitated by a combination of craton-wide extension that accompanied plume related magmatic underplating, and loading of the Bushveld Complex. Isostatic adjustment in response to Bushveld Complex subsidence resulted in further development of large basement domes around the perimeter of the Bushveld Complex.

## ACKNOWLEDGMENTS

This project was originally initiated to investigate the economic andalusite deposits on Hoogenoeg and the surrounding farms by Siegfried Lange and Tony Harwood. Out of this grew an interest in the structural geology of the area, driven by the enthusiasm and encouragement of my supervisor Mike Watkeys. Financial support was provided for by the FRD. Andy Killick and Chris Lee of JCI kindly also arranged for the use of a field vehicle for much of the mapping. Discussions on the geology of the area with the geological fraternity were diverse and numerous. Roger Gibson has been particularly helpful and interested in this research. I would also like to thank the staff and technical staff from the Department of Geology and Applied Geology, University of Natal for their assistance and support as well as the Department of Geochemistry, University of Cape Town for the use of their microprobe. Kindest thanks to my wife Deanna Meth without whom this would not have been possible, daughter Kaethe, family, extended family and friends who provided the moral support and encouragement to get this work on paper.

# TABLE OF CONTENTS

## ABSTRACT

## ACKNOWLEDGEMENTS

### CHAPTER 1 INTRODUCTION

1.1	GENERAL BACKGROUND	1
1.2	AIMS AND SCOPE OF WORK	2
1.3	LOCALITY, ACCESS AND PHYSIOGRAPHY	3

### CHAPTER 2 REGIONAL GEOLOGY AND STRUCTURAL SETTING

2.1	THE KAAPVAAL CRATON	5
2.2	THE TRANSVAAL SUPERGROUP	5
2.3	THE BUSHVELD MAGMATIC EVENT	11
2.3.1	The volcanic rocks	12
2.3.2	The Bushveld sills	12
2.3.3	The Bushveld Complex	13
2.4	THE WATERBERG GROUP	18
2.5	POST-TRANSVAAL SUPERGROUP DEFORMATION	18
2.5.1	The Kheis orogenic belt	19
2.5.2	Basement domes	20
2.5.3	The Vredefort Dome	21
2.5.4	Crustal lineaments	22
2.6	THE BUSHVELD CONTACT AUREOLE - HISTORICAL REVIEW	24
2.7	REGIONAL VARIATIONS IN THE AUREOLE	29
2.7.1	Introduction	29
2.7.2	Thickness of the aureole	29
2.7.3	Mineralogical variations	33

2.7.4	Metamorphic pressure variations	34
2.7.5	Textural variations	35
2.7.6	Conclusions	36

### **CHAPTER 3            LOCAL GEOLOGY AND LITHOSTRATIGRAPHY**

3.1	THE PRETORIA GROUP	37
3.1.1	Rooihooigte Formation	39
3.1.2	Timeball Hill Formation	39
3.1.3	Boshoek Formation	41
3.1.4	Hekpoort Andesite Formation	41
3.1.5	Dwaalheuwel Quartzite Formation	43
3.1.6	Strubenkop Shale Formation and Daspoort Quartzite Formation	44
3.1.7	Silverton Shale Formation	44
3.1.8	Magaliesberg Quartzite Formation	46
3.1.9	Vermont Hornfels Formation	46
3.1.10	Lakenvalei Quartzite Formation	47
3.2	INTRUSIVE ROCKS	48
3.2.1	Diabase sills	48
3.2.2	The Roodekrans Complex quartz-feldspar porphyry	48
3.2.2.1	Age relationships	50
3.2.2.2	Geochemistry	52
3.2.2.3	Comparison with the Rooiberg Group volcanics	54
3.2.2.4	Conclusions	59

### **CHAPTER 4            STRUCTURE**

4.1	INTRODUCTION	61
4.2	STRUCTURAL SETTING	62
4.2.1	Deformation events	65

4.2.2	ENE-trending structures	66
4.2.3	NS-trending structures	67
4.2.4	Terminology	68
4.3	SYN-BUSHVELD ( $D_2$ ) DEFORMATION OF THE PRETORIA GROUP	69
4.3.1	The Mathabatha domain	70
4.3.2	The Seropse domain	86
4.3.3	The Katkloof Fold domain	87
4.3.4	The Schwerin Fold domain	100
4.3.5	The Zaaikloof Fold domain	106
4.3.6	The Pramkoppies Fold domain	111
4.3.7	The Adriaanskop Fold domain	116
4.3.8	The Phepane Fold domain	123
4.3.9	Xenoliths	133
4.3.10	Conclusions	136
4.4	SYN-BUSHVELD ( $D_2$ ) DEFORMATION OF THE CHUNIESPOORT GROUP	
4.4.1	Introduction	138
4.4.2	$D_2$ structures	138
4.4.2	$D_3$ structures	142
4.4.3	Conclusions	144
4.5	SYN-BUSHVELD ORIENTATION OF THE $D_2$ STRAIN ELLIPSE	144

## CHAPTER 5      PORPHYROBLAST-MATRIX RELATIONSHIPS

5.1	INTRODUCTION	147
5.2	PREVIOUS WORK	148
5.3	SAMPLE PREPARATION	150
5.4	INTERPERICLINAL DOMAINS	150
5.4.1	Pretectonic porphyroblast growth ( $P < D_{2a}$ )	150
5.4.2	Syntectonic porphyroblast growth ( $D_{2a} > P$ )	158
5.4.3	Post-tectonic porphyroblast growth ( $D_{2a} < P$ )	164
5.5	PERICLINAL DOMAINS	165



5.5.1	Pretectonic porphyroblast growth ( $P < D_{2a}$ and $D_{2b}$ )	165
5.5.2	Syntectonic porphyroblast growth	165
5.6	SEQUENTIAL PORPHYROBLAST AND MATRIX GROWTH	171
5.7	RELATIVE ROTATION OF PORPHYROBLASTS	173
5.8	CONCLUSIONS	175

## CHAPTER 6 METAMORPHISM

6.1	METAMORPHIC ZONES	179
6.2	THE ANDALUSITE ZONE	183
	<i>Andalusite</i>	183
	<i>Staurolite</i>	186
	<i>Biotite</i>	189
	<i>Plagioclase</i>	190
	<i>Garnet</i>	191
	<i>Cordierite</i>	191
	<i>Orthoamphibole</i>	194
	<i>Chloritoid</i>	195
6.3	THE FIBROLITE ZONE	197
	<i>Andalusite</i>	199
	<i>Fibrolite</i>	199
	<i>K-feldspar</i>	201
	<i>Biotite</i>	201
6.4	MIGMATITE ZONE	201
	<i>Andalusite</i>	203
	<i>K-feldspar</i>	203
	<i>Cordierite</i>	204
	<i>Garnet</i>	205
	<i>Spinel</i>	205
	<i>Orthopyroxene</i>	207
	<i>Corundum</i>	207

6.5	PELITE COMPOSITION	210
6.6	THERMOBAROMETRY	212
6.6.1	The garnet - biotite geothermometer	212
6.6.2	The garnet-cordierite geothermometer	215
6.6.3	The garnet-staurolite geobarometer	216
6.7	PT CONDITIONS AND THE KFMASH GRID	217
6.7.1	Andalusite zone	217
6.7.2	Migmatite zone	220
6.8	DISCUSSION AND CONCLUSION	221

## **CHAPTER 7           TECTONOMETAMORPHIC MODEL**

7.1	INTRODUCTION	224
7.2	DIAPIRISM	224
7.2.1	Pericline geometry and effective viscosity	227
7.2.2	Pericline arrangement	230
7.2.3	Pericline spacing	232
7.2.4	Pericline-Rustenburg Layered Suite relationship	233
7.2.5	Internal pericline structures	235
7.2.6	Interpericlinial structures	239
7.3	RATES OF PROCESSES	241
7.3.1	Magma accumulation rates	241
7.3.2	Aureole deformation rates	241
7.3.3	Rates of foliation development and porphyroblast growth	247
7.4	RATE DEPENDENT EMPLACEMENT MECHANISMS	248
7.4.1	Pre-Bushveld Complex uplift	248
7.4.2	Bushveld Complex subsidence	249
7.5	A DIAPIRIC ORIGIN FOR THE BUSHVELD COMPLEX DOMES	251
7.5.1	Basement domes	251
7.5.2	Transvaal Supergroup domes	252
7.5.3	Pretoria Group domes	252

7.5.4	Diapiric origin for the domes	252
7.6	THE BUSHVELD COMPLEX FEEDERS	257
7.6.1	EW-trending dykes: a Rustenburg Layered Suite trend	258
7.7	CONCLUSION	261
<b>REFERENCES</b>		263

## **APPENDIX 1                    1: 50 000 SCALE GEOLOGICAL MAPS**

- F     Key to farm names
- G     Aeromagnetic Map

### ***(IN BACK FOLDER)***

- A Geological map of the Katkloof area
- B Geological map of the Schwerin area
- C Geological map of the Zaaikloof area
- D Geological map of the Phepane area
- E Legend

## **APPENDIX 2            MINERAL ASSEMBLAGES**

- A     Mineral assemblages from the andalusite zone
- B     Mineral assemblages from the fibrolite zone
- C     Mineral assemblages from the migmatite zone

## **APPENDIX 3            GEOCHEMISTRY**

- A     Analytical methods and operating conditions for XRF analysis
- B     Whole rock major element chemistry
- C     Analytical methods used in microprobe analysis
- D     Mineral analysis used for geothermometry and geobarometry

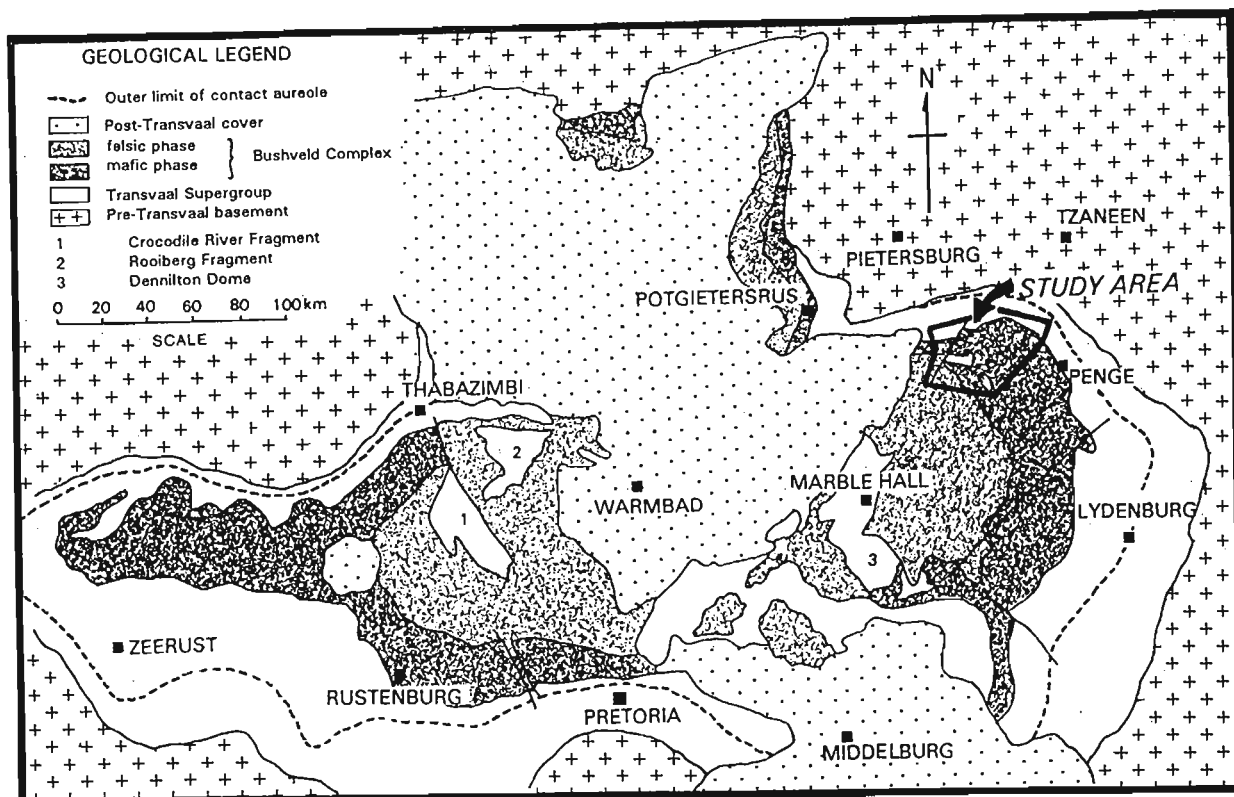
# CHAPTER 1

## INTRODUCTION

### 1.1 GENERAL BACKGROUND

The world's largest layered mafic intrusion, the ca 2060 Ma Rustenburg Layered Suite of the Bushveld Complex, has an equally impressive contact metamorphic aureole that extends up to a depth of over 5 km into the underlying ~2.6 to ~2.0 Ga Transvaal Supergroup (Figure 1.1). Bushveld magmatism commenced with mafic and felsic volcanism (Dullstroom Basalt Formation and Rooiberg Group) and the associated emplacement of numerous diabase and granophyric sills. This was closely followed by, and may have been largely synchronous with, the emplacement of the Rustenburg Layered Suite as a succession of sub-volcanic mafic and ultramafic intrusions that attain a maximum thickness of almost 10 km. The final phase of magmatism is represented by the emplacement of an approximately 5 km thick sheet of Bushveld Granite, which intrudes and overlies the Rustenburg Layered Suite, and underlies the 6 km thick roof succession of mafic and felsic lavas.

Regionally the contact aureole shows marked variations in rock texture, mineral assemblage, deformation style and deformation intensity. Since igneous intrusions and their aureoles can be regarded as linked systems, each of these characteristics forms an integral part of the magmatic evolution and genesis of the Bushveld Complex itself. Once syn-emplacement features are identified, the details of successive metamorphic and deformation events within the aureole can provide an insight into magma emplacement mechanisms, deformation rates and the physical conditions prevailing during the time of emplacement. Not only does the aureole provide a record of the syn-Bushveld mechanical and kinematic processes, it also serves as a significant time marker within the framework of regional deformation. This is useful in unravelling the timing of the numerous and complex post-Transvaal age deformations recognised from various parts of the Kaapvaal Craton.



**Figure 1.1** Simplified regional geological map showing the location of the study area, the distribution of the Transvaal Supergroup, the Bushveld Complex and the outer limit of the contact metamorphic aureole.

In addition to the vast chromite, platinoid and vanadium deposits of the Bushveld Complex, the thermal aureole also hosts the world's largest reserves of refractory grade andalusite which are mined from a number of deposits in the eastern, northwestern and southwestern parts of the contact aureole. Other economic deposits found within the confines of the Bushveld Complex aureole include vast asbestos deposits, exploited in the past along the northern margin of the eastern Bushveld Complex, the iron ores of the Thabazimbi area, shear-zone hosted gold deposits of the Pilgrims Rest area, tin and fluorspar deposits within the roof zone of the complex, and scattered occurrences of base metals.

## 1.2 AIMS AND SCOPE OF WORK

This project was initiated to investigate the geology, metamorphism and structural history of the contact aureole in the northern margin of the eastern Bushveld Complex (Figure 1.1). When compared to other parts of the aureole, this area is the most striking in that it is characterised

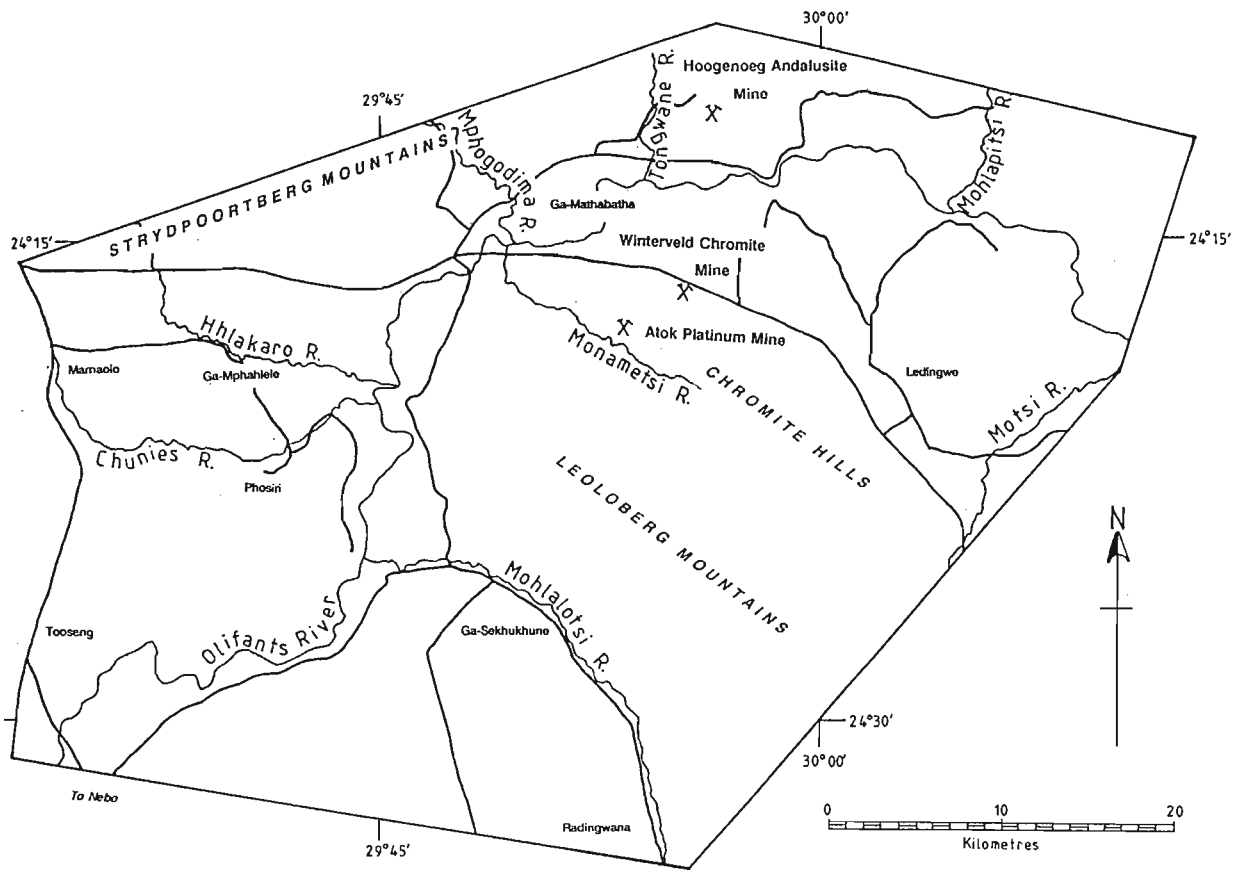
by the pervasive development of schistose rocks and an exceptional aureole thickness of almost 5 km. Of particular interest is the tectonometamorphic evolution of wall rock response to the emplacement of the Bushveld Complex magmas, providing clues to magma emplacement mechanisms and the structural history of the Bushveld Complex.

The project involved extensive field mapping, mostly in the winter months between 1988 and 1991, and laboratory based petrographic and geochemical studies. Mapping was done on 1:12 500 scale topographical base maps, with the aid of 1:30 000 scale air photographs. The data from these maps were used to compile a series geological maps to a scale of 1:50 000. These are included as four separate sheets and a geological legend in Appendix 1. During the course of the fieldwork, attention was given to identifying and mapping out the distribution of metamorphic zones and isograds in the pelitic sequences and the associated metamorphic fabrics and structures.

Thin sections were made of rocks collected and used to identify mineral assemblages, mineral reactions, and most importantly microstructural relationships between porphyroblasts and the matrix foliation. From these samples, further samples were selected for more detailed petrochemical studies involving electron microprobe, scanning electron microscopy and x-ray fluorescence spectroscopy. This was done to determine peak metamorphic conditions of temperature and pressure within the aureole using selected geothermometers and geobarometers and to constrain the metamorphic pressure-temperature path.

### **1.3 LOCALITY, ACCESS AND PHYSIOGRAPHY**

The study area is situated within the magisterial districts of Thabamopo, Pietersburg and Sekhukhuneland of the Northern Transvaal Province and lies between 29°30' and 30°08' west and 24°08' and 24°30' south (Figure 1.2). It has an east-west length of approximately 60 km and a width of 45 km. Access to the southwestern part of the area is gained by the Chuniespoort-Nebo road which also forms the western boundary of the study area. The main tarred road between Pietersburg and Burgersfort provides access to the northern and eastern portions of the study area. Numerous secondary roads and isolated tracks, leading off these main roads towards smaller isolated rural settlements, old mineral prospects and mines, provide access to more remote parts of the area.



**Figure 1.2** Map of the study area showing the location of major access roads, rivers, settlements and mines.

The study area is located in mountainous terrain with a local relief variation of approximately 720 metres, ranging from 780 metres above sea level on the Olifants River to approximately 1500 metres above sea level. The topography of the region closely follows the geology. Erosion-resistant quartzite units within the Pretoria Group of the Transvaal Supergroup, produce a positive relief, often forming cuestas with steep scarp and extensive dip-slope surfaces. Argillaceous units are generally more poorly exposed, forming low lying, usually alluvium-covered plains.

The area is bounded in the north by rugged mountainous terrain of the Strydpoortberg Range, which is underlain by intensely deformed volcanosedimentary sequences of the Wolkberg Group and dolomites and banded ironstones of the Chuniespoort Group. This mountain range is the source of many tributaries to the perennial east flowing Olifants River.

# CHAPTER 2

## REGIONAL GEOLOGY AND STRUCTURAL SETTING

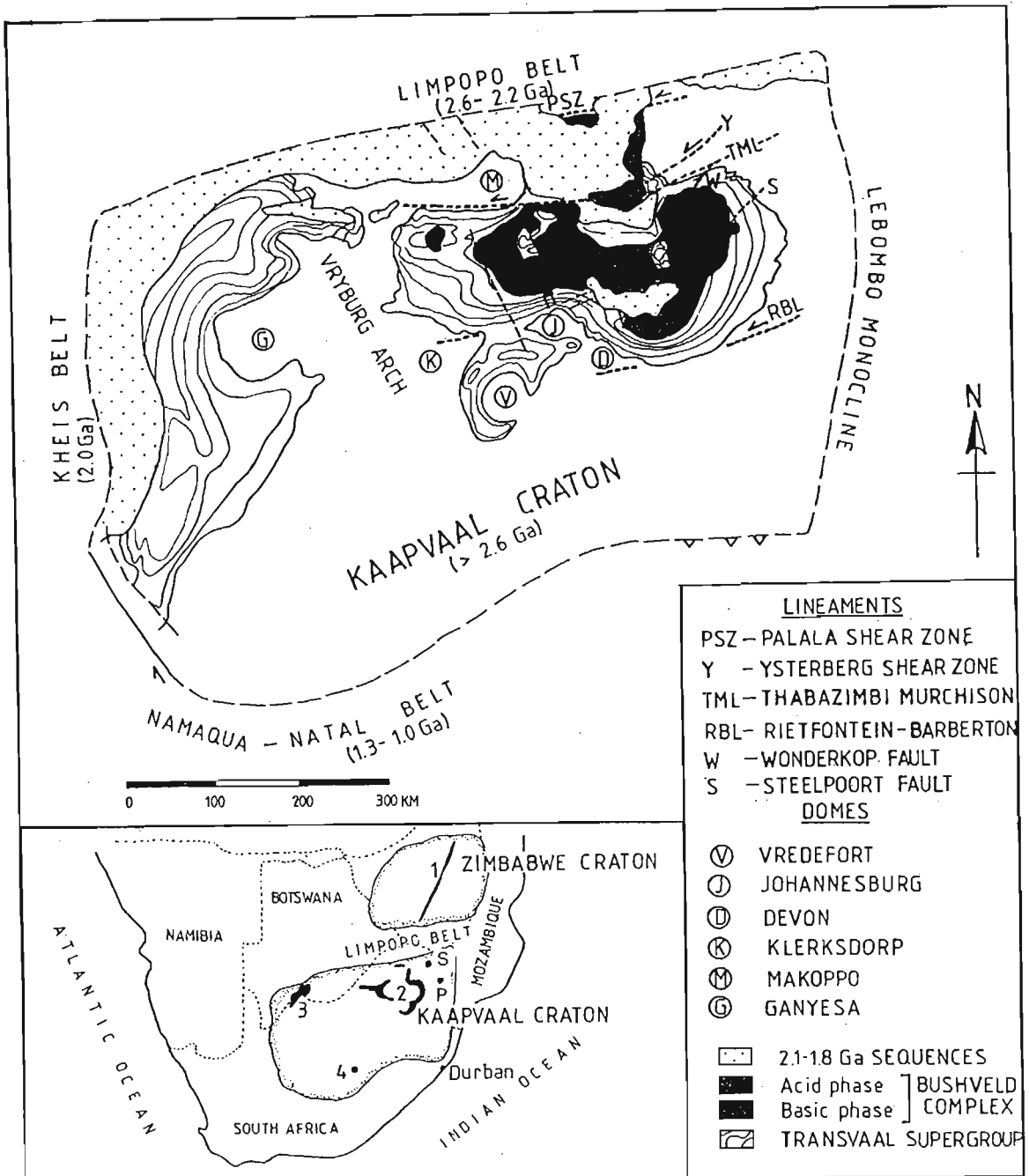
### 2.1 THE KAAPVAAL CRATON

The Kaapvaal Craton (Figure 2.1) constitutes the remnants of an Archaean continental fragment, which stabilised and reached its maximum thickness of about 35 km approximately 2.6 Ga ago (Hunter and Hamilton, 1975). It is separated from the Zimbabwe Craton in the north by the polymetamorphic (2.6-2.7 Ga) Limpopo Belt (De Wit *et al.*, 1992b). Proterozoic mobile belts define the western and southern margins, and the Lebombo monocline comprising Jurassic volcanics defines the eastern margin (Figure 2.1). Two major stages of cratonic development have been recognised (De Wit *et al.*, 1992b). The earliest (3.7 - 3.1 Ga) is represented by tonalitic, calc-alkaline type plutonic rocks and remnants of volcano-sedimentary supracrustal sequences that together form the typical granite and greenstone terrain of the Craton. The final stages (3.1 - 2.6 Ga) culminated in the formation of ensialic sedimentary basins such as the Witwatersrand, Pongola and the Ventersdorp basins. These events produced a relatively rigid, yet structurally heterogeneous basement, composed of a mosaic of subdomains separated mainly by thrust and strike-slip boundaries of various ages (De Wit *et al.*, 1992b). These structures are considered to have further influenced the deposition and the deformation of subsequent Proterozoic intracratonic platform cover sequences, such as the Transvaal Supergroup (Button, 1973), and played an important part in the siting of the Bushveld Complex (Hunter, 1975; Du Plessis and Walraven, 1990).

### 2.2 THE TRANSVAAL SUPERGROUP

The Palaeoproterozoic Transvaal Supergroup (Table 2.1) unconformably overlies rocks of the Witwatersrand and Ventersdorp Supergroups and the granite-greenstone basement of the Kaapvaal Craton. Within the Transvaal Supergroup depository, east of the Vryburg arch (Figure 2.1), Eriksson and Reczko (1995) subdivided the 10 000 m to 12 000 m thick succession into the following five units: (1) protobasinal volcanoclastics of the Wolkberg Group; (2) quartzites of the Black Reef Quartzite Formation; (3) carbonates and banded





**Figure 2.1** Diagrammatic map of the Kaapvaal Craton after Hunter (1975) showing the regional distribution of the Transvaal Supergroup and the Bushveld Complex. Trend lines highlight post-Transvaal deformation features. Inset shows the distribution of large layered complexes in southern Africa. (S) Schiel Complex, (P) Phalaborwa Complex, (1) Great Dyke, (2) Bushveld Complex, (3) Molopo Farms Complex, (4) Trompsburg.

ironstones of the Chuniespoort Group; (4) argillaceous and arenaceous rocks of the Pretoria Group; and (5) mafic and felsic volcanics of the Dullstroom Basalt Formation and Rooiberg Group. The erosional remnants of this succession cover a large portion of the Kaapvaal Craton (Figure 2.1) constituting the Transvaal Supergroup in the east, which is broadly correlated with successions preserved along the western margin of the Kaapvaal Craton in the Griqualand West basin, and the Kanye basin in Botswana. It has also been suggested that the Transvaal Supergroup may correlate with units within the Pilbara Craton in western Australia, greatly extending the size of the Transvaal-age depository (Cheney *et al.*, 1988).

The 2600 m thick Wolkberg Group (Figure 2.2) in the Northern Transvaal Province is the most widespread of the protobasinal successions. It consists of a lower unit of texturally immature conglomerates and sandstones, a mafic volcanic unit, and an upper unit of fine-grained sandstones, argillaceous rocks and carbonates (Button, 1973; Myers, 1990). The idea of a protobasinal succession as a forerunner to the more extensive Transvaal basin (Button, 1973), is open to reinterpretation as the Wolkberg Group predates the  $2642.2 \pm 2.3$  Ma age determined for the Vryburg Formation (Walraven and Martini, 1995), a Griqualand West basin correlate of the Black Reef Quartzite Formation. This supports the chronological correlation of the "protobasinal sequences" with the Ventersdorp Supergroup (Table 2.1), whose basal lavas provide an age of 2714 Ma (Armstrong *et al.*, 1991). Pre-Black Reef deformation (Myers, 1990; Hilliard, 1994) suggests that the protobasinal sequences represent an erosional remnant of previously more extensive stratigraphic units (Tankard *et al.*, 1982; Cheney *et al.*, 1990) or that they represent isolated remnants of smaller strike-slip pull-apart and extensional grabens (Eriksson and Reczko, 1995).

The Black Reef Quartzite Formation is overlain by the up to 3300 m thick Chuniespoort Group. It consists of a lowermost dolomite and chert unit, the Malmani Subgroup, and two upper units, the Penge and Deutschland Formations, comprising banded ironstone and limestone with a subordinate amount of clastic material. An epeiric marine environment in which the dolomites were deposited as a carbonate ramp succession in a tidal environment is the generally accepted model for the deposition of the Malmani Subgroup (Eriksson, *et al.*, 1975; Beukes, 1986; Clendenin, 1989). The lack of clastic material suggests a period of tectonic stability with

deposition controlled by thermally-induced flexural subsidence of the protobasinal fault systems (Clendenin, 1989; Eriksson and Reczko, 1995). Walraven and Martini (1995) established a single zircon Pb-evaporation age of  $2550 \pm 3$  Ma from a tuff layer in the Malmani Subgroup in the southern part of the basin.

**Table 2.1** Lithostratigraphy for the Transvaal Supergroup and associated pre- and post-Transvaal successions.

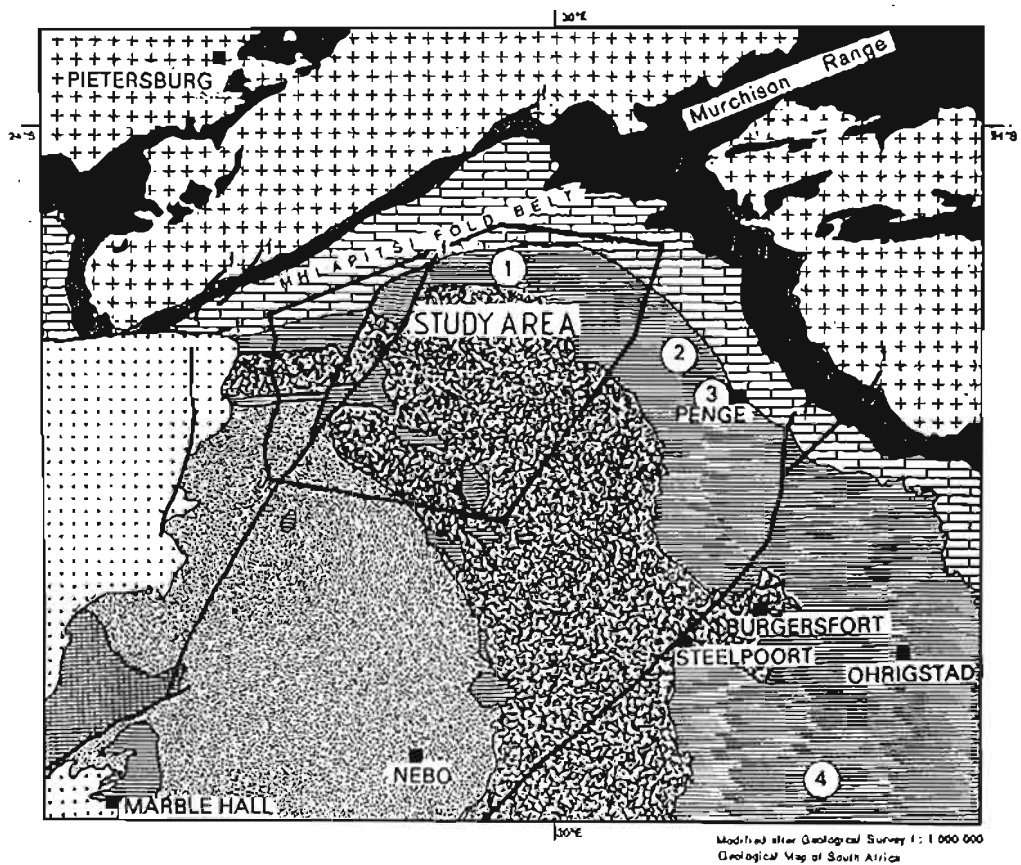
WATERBERG GROUP		
BUSHVELD MAGMATISM (Volcanics)	ROOIBERG GROUP ~5000m	Schrikkloof Formation Kwaggasnek Formation Damwal Formation Dullstroom Basalt Formation
TRANSCVAAL SUPERGROUP	PRETORIA GROUP ~7000m	Houtenbek Formation Steenkampsberg Quartzite Formation Nederhorst Formation Lakenvalei Quartzite Formation Vermont Hornfels Formation Magaliesberg Quartzite Formation Silverton Shale Formation Daspoort Quartzite Formation Strubenkop Shale Formation Dwaalheuvel Quartzite Formation Hekpoort Andesite Formation Boshoek Formation Timeball Hill Formation Rooihoogte Formation
	CHUNIESPOORT GROUP ~3300m	Duitschland Formation Penge Formation  Malmani Subgroup (5 formations)
		Black Reef Quartzite Formation
VENTERSDORP SUPERGROUP	WOLKBERG GROUP ~2600m	Sadowa Shale Formation Mabin Quartzite Formation Selati Shale Formation Schelem Formation Abel Erasmus Basalt Formation Sekororo Formation

The origin of the banded ironstones of the Penge Formation is more contentious. They have been interpreted as representing chemical precipitation of iron from an  $Fe^{2+}$ -enriched hydrothermal source (Clendenin, 1989; Klein and Beukes, 1989; Beukes *et al.*, 1990);

precipitation from a fluvial source derived from weathered Ventersdorp Supergroup lavas (Hälbich *et al.*, 1992, 1993); and precipitation as an evaporite in an anaerobic, shallow marine setting (Klemm, 1991). The Duitschland Formation which comprises dolomitic argillite, dolomite, minor quartzites and chert breccias is found only in the northeastern part of the Transvaal basin. Clendenin (1989) suggested that these rocks represent the final regressive cycle of the sea from the Kaapvaal Craton. Eriksson and Reczko (1995) however, suggested that deposition may have occurred in localised lacustrine flexural subsidence basins, with material derived from uplift and erosional loss of the underlying Chuniespoort Group stratigraphy in the southern and southeastern part of the Transvaal basin.

The Pretoria Group is characterised by a predominance of alternating mudrock and sandstone formations, three basaltic-andesite formations, subordinate conglomerate, diamictite and carbonate. The onset of Pretoria Group deposition is considered to represent a renewed period of clastic influx into the shallow marine environment alternating with tidal-shelf deposits and offshore-shelf deposits (Tankard *et al.*, 1982). More recent models have suggested a continental rift basin setting (Eriksson and Clendenin, 1990), and in a revised version, a predominance of thermal subsidence with subordinate mechanical subsidence on the periphery of the basin is suggested (Eriksson and Reczko, 1995). In the lowermost units of the Pretoria Group, the Rooihogte, Timeball Hill and Boshhoek Formations, evidence for a periglacial influence has been reported (Visser, 1971; Eriksson *et al.*, 1993). Immature clastic units of the Rooihogte, Boshhoek and Dwaalheuwel Formations are considered to represent distal delta-fan deposits (Eriksson and Reczko, 1995). The thick and extensive argillaceous units of the Timeball Hill Formation are considered to represent basinal and turbiditic mudrocks. A fluviodeltaic unit is represented by the Klapperkop Member (Eriksson and Reczko, 1995). The lavas of the Hekpoort Andesite Formation have been interpreted as mainly subaerial (Harmer and von Gruenewaldt, 1991) with a Rb-Sr isochron age of  $2224 \pm 21$  Ma (Burger and Coertze, 1975). The argillaceous rocks of the Silverton Shale Formation are generally accepted to represent epeiric marine deposits (Button, 1973) with transgression after the deposition of the fluvial deposits of the Daspoort Formation (Eriksson *et al.*, 1993). The carbonates and mafic volcanics of the Machadodorp Member within the Silverton Shale Formation are interpreted as having formed in shallow marine conditions (Button, 1973). The Magaliesberg Quartzite

Formation is interpreted as a shallow marine deposit (Burton, 1973), deposited as a regressive sandy coastline to the Silverton marine basin (Eriksson and Reczko, 1995). The Post-Magaliesberg Formations are considered to reflect renewed tectonic instability and deposition by fans, fan-deltas and lacustrine processes within restricted basins (Eriksson *et al.*, 1993).



#### LEGEND




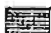
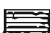
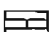



- |   |  |                    |                                  |
|---|--|--------------------|----------------------------------|
|  | Karoo Supergroup                         |                    |                                  |
|  | Lebowa Granite Suite                     | } Bushveld Complex | 1 - Hoogenoeg Andalusite Mine    |
|  | Rustenburg Layered Suite                 |                    | 2 - Havercroft Andalusite Mine   |
|  | Rooiberg Group                           |                    | 3 - Annesley Andalusite Mine     |
|  | Pretoria Group                           |                    | 4 - Krugers Post Andalusite Mine |
|  | Chuniespoort Group                       |                    |                                  |
|  | Black Reef Quartzite Formation           |                    |                                  |
|  | Wolkberg Group                           |                    |                                  |
|  | Archaean granite and greenstone basement |                    |                                  |

Figure 2.2 Geological map of the northeastern Bushveld Complex showing the study area in relation to the regional geology, the Mhlapitsi Fold Belt and the major andalusite producing mines within the Bushveld contact aureole.

### 2.3 THE BUSHVELD MAGMATIC EVENT

Magmatism towards the end of Transvaal Supergroup deposition has traditionally been subdivided into five major components that were considered to have formed before and during the emplacement of the Bushveld Complex (Hall, 1932; Willemse, 1964, 1969).

- 1) The initial volcanic phase: volcanic rocks interstratified with the Pretoria Group, the Machadodorp Member and Hekpoort Andesite Formation.
- 2) The sill phase: emplacement of the pre-Bushveld Complex mafic sills mainly into the Pretoria Group.
- 3) The epicrustal phase: extrusion of the felsic lavas of the Rooiberg Group, forming the upper Transvaal Supergroup and the roof to the Bushveld Complex.
- 4) The main plutonic phase: emplacement of the main layered ultramafic and mafic rocks of the Rustenburg Layered Suite.
- 5) The late plutonic phase: emplacement of the granitic rocks of the Bushveld Complex.

Geochronological data (Table 2.2) now provide strong evidence for a host of ~2050 to 2060 Ga magmatic events, including two large alkaline complexes, the Phalaborwa and Schiel Complexes (Figure 2.1) that intrude the northeastern part of the Kaapvaal Craton.

**Table 2.2** Geochronological data for the Bushveld Complex and temporally related magmatic events on the Kaapvaal Craton.

Magmatic unit	Age	Method	Reference
Lebowa Granite Suite	2054 ± 2 Ma	Single zircon Pb-evaporation	Walraven & Hattingh (1993)
Phalaborwa Complex	2060.6 ± 0.5 Ma	U/Pb Single baddeleyite	Reischmann (1995)
Schiel Complex	2059 ± 35 Ma	Pb-whole-rock	Walraven <i>et al.</i> (1992)
Rustenburg Layered Suite	2061 ± 27 Ma	Rb-Sr whole-rock	Walraven <i>et al.</i> (1990)
Rashoop Granophyre Suite	2060 ± 2 Ma	Single zircon Pb-evaporation	Walraven (1997)
Rooiberg Group - Dullstroom Basalt Formation	2061 ± 2 Ma	Single-zircon Pb-evaporation	Walraven (1997)

### 2.3.1 The volcanic rocks

Volcanism at the end of Pretoria Group times is represented by the Dullstroom Basalt Formation consisting of up to 1400 m of basaltic andesite and andesite with subordinate felsite and sedimentary intercalations (Cheney and Twist, 1988). The recognition of a basal unconformity and marked geochemical affinity with the overlying Rooiberg Group felsites (Cheney and Twist, 1988) implies that the Dullstroom Basalt Formation does not form part of the Pretoria Group as represented by SACS (1980), but should be included within the Rooiberg Group (Table 2.1). This is supported further by more detailed geochemical work by Eriksson *et al.*, (1993) and Schweitzer *et al.* (1995). The Rooiberg Group is represented by voluminous rhyolitic and rhyodacitic lavas up to 5000 m in thickness with minor mafic lavas at the base and subordinate pyroclastics and sedimentary intercalations (Twist, 1985; Twist and Harmer, 1987). As already mentioned, zircon dating of the Rooiberg Group felsites has also indicated the synchronous genesis of the Rooiberg lavas with the Bushveld Complex, suggesting that the complete upper succession of lavas should be considered a part of the Bushveld Complex magmatic event (Hatton and Schweitzer, 1995) (Table 2.2). The Bushveld magmatic event thus includes all the magmatic components except the two volcanic units of the Pretoria Group, the Hekpoort Andesite Formation ( $2224 \pm 21$  Ma; Burger and Coertze, 1975) and the Machadodorp Member lavas (Table 2.1).

### 2.3.2 The Bushveld sills

A significant part of the Bushveld Complex floor comprises numerous diabase sills, that have generally been accepted to represent precursors to the intrusion of the main mafic layered sequence of the Bushveld Complex (Hall, 1932; Willemse, 1959; Engelbrecht, 1990a). These are represented by diabase sills, unaltered pyroxenites and gabbros and the more felsic Roodekrans quartz-feldspar porphyry. In line with the proposals by Hatton and Schweitzer (1995), the hypabyssal intrusions should also form part of the Bushveld magmatic event, together with the Rooiberg Group lavas.

In parts of the eastern Transvaal basin, the mafic sills have a combined thickness of almost 2500 m (Sharpe and Snyman, 1980). In this area, Sharpe (1984) recognised two distinct mafic

sill types: highly altered amphibolitic sills and unaltered pyroxene-bearing sills. He suggested that the highly altered amphibolitic sills were of pre-Bushveld Complex age, whereas the unaltered sills were of syn-Bushveld Complex age and were related to the marginal border groups of the Bushveld Complex. Engelbrecht (1990a) working in the western Bushveld Complex, however, found that the two sill types were chemically similar and were spatially related to their position within the contact aureole. He suggested that hydration of norite sills in the outer parts of the aureole gave rise to the amphibolitic sills and the unaltered norite sills remained unaffected in the inner, higher grade parts of the contact aureole.

The only felsic sill in the Bushveld Complex floor is found in northeastern Bushveld Complex and is informally named the Roodekrans Complex (Sharpe and Chadwick, 1981). The age relative to the mafic sills and the Bushveld Complex and the origin of the intrusion is not well established. The most recent Geological Survey maps have included it with the Rushoop Granophyre Suite, a diverse group of granophyric rocks, for which numerous and often contradictory origins have been proposed (Tankard *et al.*, 1982; Walraven, 1985). These rocks are discussed in more detail in Chapter 3.

### **2.3.3 The Bushveld Complex**

The Bushveld Complex can be subdivided into a number of compartments forming four major lobes that are arranged about an east-west and a northwest-southeast trending axis (Figure 2.1). A broad compositional range of rock types, from ultrabasic to acid is represented by the three lithological subdivisions: the Rustenburg Layered Suite, the Lebowa Granite Suite, and the Rushoop Granophyre Suite (SACS, 1980). The four lobes are considered to represent separate conical-shaped compartments, each with a central gravity-high, interpreted as a feeder site (Cousins, 1959, Sharpe and Snyman, 1980). The maximum thickness of the Bushveld Complex is estimated at approximately 13 000 m. In the eastern compartment, the thickness of the Rustenburg Layered Suite alone is estimated to be about 5000 m (Hattingh, 1980; Molyneux and Klinkert, 1978), with a maximum composite thickness of 9000 m (Von Gruenewaldt, 1973).

Over most of the Bushveld Complex, the Pretoria Group forms the immediate floor to the



Rustenburg Layered Suite and the felsic volcanics of the Rooiberg Group the roof. The footwall contact transgresses the floor rocks, progressively cutting down through the Transvaal Supergroup from south to north, coming to rest on the Archaean basement to the north of Potgietersrus. Until recently, most models for this relationship have assumed that the footwall rocks were displaced upwards to a position above the Rustenburg Layered Suite (Willemse, 1959; Von Gruenewaldt, 1973; Button, 1973, 1976). Cheney and Twist (1988, 1991) challenged this proposal arguing that the xenoliths are too small to account for the missing strata and no evidence of major assimilation exists. This led them to propose that a previously unrecognised unconformity exists in the upper Pretoria Group at the base of the Dullstroom Basalt Formation, and that the Rustenburg Layered Suite was regionally emplaced along this contact.

Until recently, the lack of volcanic equivalents of the layered mafic rocks was considered to indicate that magma additions remained in the magma chamber (Sharpe, 1985) and were accommodated by lateral expansion of the magma body, producing pronounced transgressions between successive zones (Hatton and Von Gruenewaldt, 1989). This has now been resolved by the suggestion that the lavas of the Dullstroom Basalt Formation and the Rooiberg Group comprise the "missing volcanics" that were extruded synchronously with the emplacement of the Rustenburg Layered Suite (Hatton and Schweitzer, 1995).

The Rustenburg Layered Suite (Table 2.3) is subdivided informally into the marginal, lower, critical, main and upper zones. Detailed descriptions of the lithologies are presented by Vermaak (1970), Von Gruenewaldt (1973), Cameron (1978, 1980, 1982) and Von Gruenewaldt *et al.* (1985). In the eastern compartment, the marginal zone comprises a diverse assemblage of fine-grained variably textured norites, pyroxenites and ultramafic rocks. The lower zone consists mainly of alternating bronzitite, harzburgite, and dunite, and is considered to have been mainly responsible for the development of the contact aureole.

**Table 2.3** Lithostratigraphy of the Bushveld Complex in the eastern Transvaal basin showing the major lithological units and the informal zonal classification after SACS (1980).

	INFORMAL SUBDIVISION		THICKNESS	FORMAL SUBDIVISION
LEBOWA GRANITE SUITE			~3000m	Makutso Granite Nebo Granite Verena Porphyritic Granite Klipkloof Granite Bobbejaankop Granite Lease Granite Balmoral Granite
RASHOOP GRANOPHYRE SUITE				Stavoren Granophyre Rooikop Granophyre Porphyry Zwartbank Pseudogranophyre
RUSTENBURG LAYERED SUITE	UPPER ZONE		~2300m	Luipershoek Olivine Diorite Ironstone Magnetite Gabbro Magnet Heights Gabbro-Norite
	MAIN ZONE		~3600m	Leolo mountain Gabbro-Norite Winnarshoek Norite-Anorthosite
	CRITICAL ZONE	upper subzone	~1400m	Winterveld Norite-Anorthosite
		lower subzone		Mooihoek Pyroxenite
	LOWER ZONE		~1700m	Serokolo Bronzitite Jaglust Harzburgite Rostock Bronzitite Clapham Bronzitite
MARGINAL ZONE		0-100m	Shelter Norite	

Floor folds in the metamorphosed Pretoria Group separate the lower zone into a number of individual troughs, each with a separate ultramafic succession (Sharpe, 1986). The critical zone oversteps the lower zone. It is subdivided into a lower subzone comprising mainly feldspathic pyroxenite, and an upper subzone comprising norites, leuconorites and anorthosites, characterised by the economically important chromitite seams and platinumiferous Merensky Reef. The main zone consists of a thick, relatively homogeneous sequence of norites and gabbros. The upper zone is characterised by cumulus magnetite forming thick magnetite layers and ferrogabbros.

The same cumulate succession is recognised in each compartment, suggesting a connection to a common magma chamber (Sharpe, 1986; Hatton and Von Gruenewaldt, 1989). The

development of igneous layering in large mafic igneous complexes is generally ascribed to a combination of crystallisation processes coupled with the intermittent addition of magmas during crystallisation. Most publications on the magmatic evolution of the Rustenburg Layered Suite propose multiple magma pulses (Hamilton, 1977; Sharpe *et al.*, 1986; Kruger *et al.*, 1986). The number of magma additions, the timing and compositions of successive magmas and the degree of interaction between these additions are poorly understood. Coertze (1974) suggested up to nine separate magmas explaining the various lithologies in the layered mafic sequence in the western Bushveld Complex. Isotopic investigations suggest at least three major magma additions (Walraven and Coertze, 1988; Hatton and Von Gruenewaldt, 1989).  $^{87}\text{Sr}/^{86}\text{Sr}$  ( $\text{Sr}_i$ ) profiles indicate discontinuities between the lower critical and upper critical zones and between the upper critical and main zones (Kruger and Marsh, 1982; Sharpe, 1985). Two different parental magmas have been recognised. A tholeiitic (type "A") magma and a bonninitic (type "U") magma (Kruger and Marsh, 1982; Sharpe, 1985; Hatton and Von Gruenewaldt, 1987).

A diversity of hypotheses have been proposed for the origin of the Bushveld Complex. The outlandish model of the transformation of sedimentary to igneous rocks by fugitive fluids (S. van Biljon, 1949) has generally been rejected and a magmatic origin is accepted by all workers. Most hypotheses take into account a structural control on the position and origin of the complex (Hall, 1932; Brock, 1956, 1957; Cousins, 1959) in response to major lineaments or megafaults in the crust. Hunter (1974) proposed that the Bushveld Complex formed at the confluence of linear and domal structures in the Kaapvaal basement.

Extensional conditions for emplacement have been suggested by W.J. van Biljon (1976) and also by Stowe (1993, 1994), the former suggesting a failed rift setting and the latter extensional conditions associated with mantle diapirism. These models contrast to those of Sharpe and Chadwick (1981, 1982) who considered emplacement under compressive conditions.

Geochemical interpretations suggest that the bonninitic (type "U") magmas were derived from a depleted mantle source metasomatized by fluids from subducted sediments and that the tholeiitic (type "A") magmas were derived from subducted ocean lithosphere in a region of

back-arc spreading (Hatton, 1989). The extensional conditions are considered to have developed during the collision of the Kaapvaal and Zimbabwe cratons (Hatton, 1989).

Evidence for a meteorite impact origin for the Vredefort structure and its close proximity in time and space with the Bushveld Complex, prompted the theory of an origin for both structures by a meteorite impact (Dietz, 1963; Hamilton, 1970; Rhodes, 1975). Alternatively, the suggestion of an internal origin for the Vredefort structure (Nicolaysen and Ferguson, 1990) compels a similar related origin for the Bushveld Complex (Sharpe *et al.*, 1981). Other hypotheses imply that both the Vredefort and the Bushveld Complex were developed coincidentally at about the same time but by unrelated processes. For example, Master (1990) suggested that the magmas had been generated in a subduction zone to the northwest of the Kaapvaal Craton, but were released into the upper crust by meteorite impact. Martini (1992) however, suggested that the emplacement of the Bushveld Complex represented a slightly earlier regional extension event on the Kaapvaal Craton about 2050 Ma that was followed by a meteorite impact at Vredefort about 50 Ma later. More recent data now constrain the time difference between the earlier Bushveld magmatic event and the subsequent Vredefort event to 30 Ma (Kamo *et al.*, 1995).

An origin related to a mantle diapir is presented by Hatton and Schweitzer (1995). They provide evidence for a single comagmatic Bushveld event that includes the Dullstroom Basalt Formation and Rooiberg Group lavas. The model proposes the relatively shallow intrusion of a mantle plume into the middle crust with a high degree of crustal melting. Early crustal melts produced highly contaminated lavas at the base of the Rooiberg Group (Dullstroom Basalt and Damwal Formations) that formed the roof to the lower zone magmas. With expansion of the plume head, further crustal melting produced the more felsic and widespread eruptions of the Kwaggasnek and Schrikkloof lavas during which time more contaminated magmas of the critical and main zones are emplaced.

The various hypotheses for the origin of the Bushveld Complex have generally not been supported by or integrated with any structural analysis of syn-Bushveld tectonism. Little account has been taken of the pre-Bushveld development of the Archaean basement, Transvaal

Supergroup, or syn- and post-Bushveld deformation (Sharpe, 1986). In this regard the much neglected Bushveld Complex contact metamorphic aureole can provide valuable information of the events leading up to, during and post-dating this major magmatic event. It also provides an important framework for investigating the timing relationships with other 2.0 Ga events on the Kaapvaal Craton, such as the development of the Vredefort Dome and other large basement domes.

#### **2.4 THE WATERBERG GROUP**

Post-Transvaal Supergroup Mesoproterozoic continental sequences, the Waterberg, Soutpansberg and Matsap Groups were deposited after the emplacement of the Bushveld Complex. Together with the correlates in Griqualand West basin, the Olifantshoek Supergroup, they presently cover most of the western and northern margin of the Kaapvaal Craton (Figure 2.1). Jansen (1970) considered sedimentation of the lowermost Waterberg Group to have been contemporaneous with the emplacement of the Bushveld granite and Coertze *et al.* (1977) found no major hiatus between the Transvaal Supergroup and the Waterberg Group. This has come into question as the Hartley Basalt Formation - a Waterberg Group correlate in the Griqualand West basin - has an age of  $1928 \pm 3$  Ma (Cornell *et al.*, 1997). The Waterberg Group comprises approximately 5000 m of intracratonic minor volcanics and predominantly coarse clastic rocks which represent the earliest red beds deposited on the Kaapvaal Craton. Du Plessis (1987) suggested that early Waterberg Group sedimentation was initiated in isolated pull-apart basins related to left-lateral strike-slip movement along the Thabazimbi-Murchison Lineament. Deformation of the Waterberg Group is characterised by open folds mainly to the south of the Thabazimbi-Murchison Lineament with more intense deformation localised along the lineament. Du Preez (1944) and Meinster (1974) attributed the deformation to northward-directed thrusting and associated folding, whereas du Plessis (1987) suggested the existence of a positive flower structure related to left-lateral strike-slip movement along the lineament in post-Pilanesberg time at approximately 1.3 Ga (Martin *et al.*, 1988).

#### **2.5 POST-TRANSVAAL SUPERGROUP DEFORMATION**

The most prominent structural features responsible for the present outcrop pattern on the Kaapvaal Craton are large basement domes and major ENE-trending cratonic-scale lineaments

(Figure 2.1). Numerous deformations involving compressional, extensional and translational events within the Transvaal Supergroup have been recognised (Andreoli, 1988). The origin, age and relative timing of these structures is still poorly understood (Roering *et al.*, 1990). Courtnege *et al.* (1995) revealed widespread polyphase deformation and dynamothermal metamorphism with up to four ductile events recognised within the Transvaal Supergroup in the area between the Johannesburg Dome and the Bushveld Complex.

Some of the earliest post-Transvaal structures may be those recognised by Crockett (1971) who mapped highly deformed Transvaal Supergroup strata in southeastern Botswana. He suggested that the deformation there was of post-Transvaal, pre-Bushveld age and closely related to the development of the Vryburg arch (Figure 2.1). Relative vertical movement on the arch resulted in gravitational slides towards deeper parts of the basin and off the axis of the arch that now separates the Transvaal and Griqualand basins.

Many of the structures appear to have been repeatedly reactivated from Archaean to Jurassic times and this may explain the structural complexity observed in the Transvaal Supergroup. The NNW-trending Vryburg arch, for example is considered to have been active during Transvaal Supergroup times controlling the sedimentation, erosion, and subsequent deformation of the Transvaal Supergroup (Crockett, 1972; Hunter, 1975). The ENE-trending lineaments, initiated during the development of the Limpopo Belt (McCourt and Vearncombe, 1992), are considered to have been repeatedly reactivated during the deposition and deformation of the successive intracratonic basins: the Witwatersrand basin (McCarthy *et al.*, 1986; De Wit *et al.*, 1992b); the Ventersdorp basin (Clendenin *et al.*, 1988; Clendenin *et al.*, 1991); the Transvaal basin (Button, 1973; Eriksson *et al.*, 1991; Potgieter, 1991); the Waterberg basin (Du Plessis, 1987); and the Karoo Basin (Watkeys and Sweeney, 1988).

### 2.5.1 The Kheis orogenic belt

Along the western margin of the Kaapvaal Craton, post-Transvaal tectonism known as the Kheis belt is well documented (Cousins, 1959; Stowe, 1986; Beukes and Smit, 1987; Hilliard, 1997). The Kheis orogeny pre-dates the younger 1300-1000 Ma Namaqua-Natal tectogenesis and is generally considered to be related to the Palaeoproterozoic Ubendian Event (Master,

1991). Structures are typically eastward verging, with thin-skinned style thrusting and folding (Stowe, 1986). Post-Pretoria Group, pre-Bushveld folding in the western Bushveld Complex was considered by Engelbrecht (1988) to be related to this event. Recent investigations by Courtage *et al.* (1995) have also suggested that eastward verging Kheis-related fabrics may have extended as far east as Johannesburg. Duane and Kruger (1991) and Duane *et al.* (1991) consider the Kheis orogeny to be a "Cordilleran" type orogeny with an age between 2.1 Ga and 1.9 Ga, which suggests that the Bushveld Complex was emplaced into an east-directed stress field within the Kaapvaal Craton. This possibility is investigated in more detail in later chapters. The age of the Kheis orogeny however, may be much younger, post-dating the Bushveld Complex. Hilliard (1997) recently concluded that the Kheis orogeny is poorly constrained between ~1.9 - 1.2 Ga. Nevertheless the Kheis orogeny remains an important component of the post-Transvaal Supergroup deformation.

### 2.5.2 Basement domes

The close association of basement domes (Figure 2.1) with the Bushveld Complex has been recognised for some time. Most interpretations have suggested that these structures are the result of craton-scale interference folding resulting from two near orthogonal ENE and NNW orientated axes. Pretorius (1964) and Hunter (1975) interpreted the structures as a product of several orders of folds, progressively increasing in wavelength, that compliment each other and assist in building antiforms and synforms. The age and sequence of the regional folding along these two trends is controversial. Du Plessis and Walraven (1990), and Dietvorst (1991) were of the opinion that the ENE-trending folds were of pre-Bushveld age, and the NNW-trending folds were of syn-to post-Bushveld age. Vermaak (1970) and Hunter (1975) on the other hand argued for an early NNW folding followed by ENE-trending folds.

Hunter (1975) ascribed the domes to compression in the upper crust, following progressive subsidence of the Kaapvaal Craton from a period of maximum continental inflation at about 3000 Ma. He stated that it was into this upper crustal compressional setting that the Bushveld Complex was emplaced. Stress conditions favoured sill formation along the chord position, as a sequence of upward stacking sills with continued depression. Hartzler (1995) supported this model, but suggested that the initial interference folds were subsequently accentuated by

the intrusion of the Bushveld Complex and by post-Bushveld Complex regional deformation.

### 2.5.3 The Vredefort Dome

In comparison to the other basement domes on the Kaapvaal Craton, the Vredefort Dome is considered unique as numerous features suggest an impact origin for the structure (see review in Reimold, 1993). Intensely deformed rocks of the Transvaal Supergroup, and underlying Archaean Witwatersrand and Ventersdorp Supergroups, form a rim syncline and overturned collar to the dome. Metamorphic studies by Bisschoff (1969, 1982), Schreyer (1983) and Stepto (1990) show a zonation with metamorphic grades increasing towards the core of the dome, from regional greenschist facies in the Witwatersrand basin to mid-amphibolite facies in the lowest parts of the Witwatersrand Supergroup exposed in the collar, to granulite grades in the core of the dome. They considered the origin of the metamorphism to be a localised effect related to contact metamorphism associated with hidden igneous plutons in the dome.

As already discussed, the close spatial and temporal relationships between the Vredefort Dome and the Bushveld Complex at approximately 2 Ga ago prompted numerous proposals for a common origin by an external impact origin (Dietz, 1961, 1963; Hamilton, 1970; Rhodes, 1975; Master, 1990, Elston 1995) or by endogenous processes (Nicolaysen and Ferguson, 1990). This relationship led to further detailed investigations of the metamorphism associated with the dome (Gibson, 1993). These studies (Gibson and Wallmach, 1995) and more recently Stevens *et al.* (1996) concluded that the metamorphism in the Vredefort rocks involved a two stage P-T path and was not simply related to localised contact metamorphism. They identified an initial regional low-pressure, high-temperature metamorphic event that was followed by a stage of near isobaric cooling then by rapid decompression during the uplift of the Vredefort Dome. The initial metamorphic event was considered to have been associated with magmatic intraplate by Bushveld-age magmas at 2.06 Ga. This was followed, approximately 30 Ma later, by impact cratering and uplift of the thermally elevated rocks in the Vredefort Dome, resulting in a combination of high-grade crustal metamorphism and ultra-high pressure shock metamorphism due to both endogenous and exogenous events.

Most researchers now favour the impact origin for the Vredefort Dome as suggested by the



abundant evidence of shock deformation features in the form of shatter cones, planar microdeformation features, the minerals coesite and stishovite, and voluminous pseudotachylite. These aspects have been comprehensively reviewed by Reimold (1993). New geochronological evidence indicates that the development of pseudotachylite was a single event, dated at approximately 2025 Ma (Kamo *et al.*, 1995).

Since no evidence has been found for an impact origin in any of the other domes surrounding the Bushveld Complex, they must therefore be explained by other processes that are closely associated with the Bushveld event. The origin of these domes is considered to be of vital importance in understanding Transvaal Supergroup deformation and will be explored in more detail in the latter part of this thesis.

#### 2.5.4 Crustal lineaments

In the same way that large basement domes have strongly influenced the geometry and deformation of the Transvaal Supergroup and the Bushveld Complex, crustal-scale lineaments played an important part in siting and the deformation of the Bushveld Complex (Hunter 1975, Du Plessis and Walraven, 1990). Repeated lineament reactivation in pre-, syn- and post-Bushveld Complex times has resulted in a complex structural history associated with each lineament. The most important lineaments include the ENE-trending Palala Shear Zone, the Thabazimbi-Murchison Lineament and the Rietfontein-Barberton Lineament.

The Palala Shear Zone truncates the northern lobe of the Bushveld Complex (Figure 2.1) and pre-dates the deposition of the Waterberg Group sediments, indicating that the ENE-trending lineaments were active as major sinistral shears during post-Bushveld times. Smit *et al.* (1992) and McCourt and Vearncombe (1987, 1992) considered this to represent a reactivation of an older crustal structure developed during Limpopo times. Watkeys (1984) argued that the Zimbabwe Craton and the Central Zone were juxtaposed with the Kaapvaal Craton along the Pala Shear Zone at ~2.0 Ga.

South of the Palala Shear Zone, the Thabazimbi-Murchison Lineament (TML) marks the northern margin of the eastern and western Bushveld Complex (Figure 2.1) and for this reason

has also been termed the Northern Bushveld Margin or NBM (Sharpe, 1986). The TML is a complex deformation zone that is represented by a 25 km, ENE-WSW trending fold and fault belt that extends over a distance of 400 km, transecting most of the Kaapvaal Craton.

The zone has been subjected to a long history of reactivation (Good and De Wit, 1997). The earliest record of deformation is represented by Archaean-age pre-Transvaal deformation as SW-directed reverse-sinistral shears within the Murchison Greenstone Belt which are considered to be an integral part of the Limpopo event (McCourt and Vearncombe, 1992). This was followed by extensional tectonics along the TML which sited the depositional axis of the Wolkberg-Buffelfontein Groups. These volcanosedimentary successions either represent a protobasin to the Transvaal Supergroup (Button, 1973; SACS, 1980) or form erosional remnants of the Ventersdorp Supergroup (Tankard *et al.*, 1982; Cheney *et al.*, 1990; Eriksson and Reczko, 1995). Deposition probably occurred in a narrow rift that preceded the deposition of the Transvaal Supergroup (Clendenin *et al.*, 1988; Clendenin *et al.*, 1991).

In post-Chuniespoort Group times, compressional reactivation of the TML produced a pre-Pretoria Group deformation that is recognised in the Mhlapitsi Fold Belt (Potgieter, 1991) (Figure 2.2). Du Plessis and Walraven (1990) attributed this deformation to right-lateral wrenching on the TML due to NW-SE directed compression and pre-Pretoria Group erosion. Extensional reactivation along the TML may then have initiated Pretoria Group deposition in a series of continental half-grabens as suggested by Eriksson *et al.* (1991).

Post-Bushveld, left-lateral strike-slip reactivation of the TML was not evident in the Mhlapitsi Fold Belt but rather extended from Thabazimbi towards Pietersburg. Sinistral faults of this age cut across the TML and the Mhlapitsi Fold Belt (The Wonderkop and Steelpoort Faults). This event is believed to have initiated Waterberg Group sedimentation at ca. 2.0 Ga in a pull-apart basin setting (Du Plessis, 1987; Du Plessis and Walraven, 1990) and left-lateral movement on this structure continued after the ca 1.3 Ga Pilanesberg syenite dyke swarm (Martin *et al.*, 1988). Previous workers however, suggested that the structural style was typified by post-Waterberg age thrust-faulting and folding (Mellor, 1908; Du Preez, 1944; Meinster, 1974).

As indicated above, the complete length of the TML may not have been active at any one particular time as contrasting tectonic styles and histories are found along the belt. In the northern margin of the western Bushveld Complex, folding and transpressional strike-slip faulting with the development of positive flower structures occur in a narrow belt in the Thabazimbi area (Martin *et al.*, 1988; Du Plessis and Clendenin, 1988). The lack of these features in the northern margin of the eastern Bushveld Complex suggests that this movement was rather focussed on the Pietersburg Greenstone Belt forming the Ysterberg Shear Zone (Figure 2.1). This shear zone is, as in the Thabazimbi area, characterised by extensive sinistral post-Transvaal strike-slip faulting with a compressional flower structure (De Wit *et al.*, 1992a; Good and De Wit, 1997).

In the study area, post-Bushveld Complex sinistral faulting on the Wonderkop Fault (Figure 2.1) is considered to be related to this deformation event. This will be discussed in more detail later in the thesis.

A similarly complex reactivation history is believed to have affected the ENE-trending Rietfontein-Barberton Lineament (Figure 2.1) coinciding approximately with the southern margin of the Bushveld Complex (McCarthy *et al.*, 1986; Spencer, 1986; Stanistreet *et al.*, 1986; Eriksson *et al.*, 1991).

The linear array of basic igneous intrusions (Figure 2.1) and their presumed decrease in age northwards from the Trompsburg Complex to the Great Dyke, was considered an important factor in the siting of the igneous complexes (Cousins, 1959; Vail, 1977) and the associated deformation (Sharpe 1986). In view of the post-emplacement displacements recognised along the ENE-trending lineaments however, this alignment is now regarded as entirely fortuitous (Roering *et al.*, 1990).

## **2.6 THE BUSHVELD CONTACT AUREOLE - HISTORICAL REVIEW**

The first mention of the Bushveld Complex metamorphic aureole was made by Molengraaff (1894) where the petrographic characteristics of chistolite slate from Zeerust in the western Transvaal basin are given and interpreted as belonging to the contact belt of an extensive

granite mass. He also dealt with the tectonic effects of Bushveld emplacement, explaining the centrally directed dip of the encircling Transvaal Supergroup as being due to subsidence, which caused folding and oblique faulting. This was followed by descriptions of contact metamorphic rocks in the western Transvaal basin by Hatch (1905) and Holmes (1906).

In 1906, Kynaston gave the first report of associated contact and dynamic metamorphism in the northeastern Transvaal basin, describing a cordierite-sillimanite-biotite schist. Molengraaff (1906) described various rock specimens from the contact aureole of the Pretoria Group. He ascribed the schistose character of some of the rocks to pressure at the bottom of the intrusive mass. Gau (1907) described chiastolite and andalusite schists in the Pretoria Group together with various serpentine and pyroxene marbles in the Elands River area near Marble Hall.

Hall (1907) was the first to study the aureole in more detail in the Lydenburg district, recognising an inner and an outer belt consisting of dark holocrystalline hornfels and chiastolite slate respectively. In numerous publications that followed, he was able to subdivide the aureole into four distinct types (Hall, 1932):

*The Groothoek type:* an inner, strongly metamorphosed zone consisting of dark-coloured, even-grained, holocrystalline cordierite hornfels, the original nature of the rock being no longer apparent in hand specimen.

*The Longsight type:* an outer, less strongly metamorphosed zone, where the original nature of the rocks is still recognisable, with characteristic development of porphyroblastic minerals such as chiastolite, andalusite, biotite, staurolite, garnet and chloritoid.

*The Malips River type:* characterised by completely recrystallised paragneisses with a pronounced schistose fabric due to pressure effects.

*The Doornpoort type:* a localised occurrence of highly metamorphosed, very coarsely crystalline glassy quartzite found near the contact or as xenoliths within the Bushveld norites.

Hall's extensive fieldwork served as a basis to explain the major regional characteristics of the aureole, such as its variation in width, the combination of thermal and pressure effects in the northeastern Transvaal basin, and the metamorphic effects of basic sills in the floor rocks. Daly

(1928) considered the influence of connate waters to explain the immense width of the metamorphic aureole in some areas.

Interest in the aureole was further stimulated by the growing economic value of andalusite for refractory purposes. Several surveys were conducted initially in the western Transvaal basin and then in the eastern Transvaal basin along the andalusite horizons (Partridge, 1934; Bosazza and Levin, 1939; Van Rooyen, 1951; Blain, 1974, 1975; Human and Collins, 1986; Hammerbeck, 1986). Schwelnuus (1956) mapped the Bushveld floor relationships in the northeastern Transvaal basin along the Olifants River. He also investigated the petrographic and chemical controls on the formation of staurolite and garnet in rocks collected from the area. This study was the start of more detailed petrochemical investigations.

Willemse (1959) produced the next comprehensive study of the Bushveld Complex and its relationship to the floor. He used geochemical techniques to establish the chemical relationships of the metamorphic rocks and the effects of whole-rock chemistry on the mineralogy, particularly in the development of andalusite, cordierite, staurolite, garnet and chloritoid. He utilised the metamorphic facies principle to characterise the rocks, revising the original classification of Hall (1932). Chloritoid and chistolite-bearing rocks were retained in Hall's Longsight type (outer zone) and staurolite-bearing rocks were placed in the Groothoek type. Cordierite-sillimanite gneiss, being a product of high-grade thermal metamorphism with a subordinate dynamic component, was removed from the Malips River type and assigned to the pyroxene-hornfels facies. The schistose rocks of the Malips River type were considered to have formed later than the hornfels and this type of metamorphism was suggested to refer only to those rocks that show a schistose character or dynamic effects without high temperature.

Schwelnuus *et al.* (1962) compiled the first detailed Geological Survey map and explanation of the northeastern Transvaal basin (1:125 000 Chuniespoort-Wolkberg sheet). The major structural features, some of the controls on the formation of certain metamorphic minerals, as well as the age relationships of the metamorphism and deformation were discussed. Bastin (1968) continued working in the same area investigating the major structural relationships, and

was able to identify three stages of deformation in the Transvaal Supergroup rocks: initial pre-Pretoria Group folding of the underlying Wolkberg and Chuniespoort Groups, followed by post-Pretoria Group folding related to the emplacement of the Bushveld Complex, and finally post-Bushveld Complex tear faulting and reverse faulting.

Studying the regional stratigraphy and development of the Transvaal basin in the eastern and northeastern parts, Button (1973) recognised two periods of metamorphism. The first metamorphic event was related to the intrusion of sills prior to the emplacement of the Bushveld Complex and the second, superimposed on the first, due to the intrusion of the complex itself. He reported the occurrence of cleavages within certain horizons in the Pretoria Group and ascribed these to zones of intrastratal slippage. Human (1975) also recognised two metamorphic events in a study of the metamorphic petrology of pelitic rocks from the Havercroft area near Penge in the northeastern Transvaal basin.

In 1976, Button gave an account of the stratigraphy and stratigraphic relations of the Transvaal Supergroup and established two isotherms in the contact aureole in the eastern Transvaal. From these he was able to show that the deeper penetration of metamorphic effects from south to north are related to a greater proportion of ultramafics and a thicker pile of mafic igneous rocks in that direction. In the same year, Engelbrecht (1976) studied the metasediments in the Marico area using petrochemical techniques and gave an estimate of the physical conditions that prevailed during metamorphism.

Sharpe and Chadwick (1981, 1982) investigated the geometry and origin of structures in the Transvaal Supergroup rocks related to the eastern compartment of the Bushveld Complex. They described the tectonometamorphic fabrics associated with these structures and investigated the age relations of deformation and metamorphism. Metamorphic pressure and temperature calculations for pelitic rocks in the eastern Bushveld Complex were made by Hulbert and Sharpe (1981) who gave pressure estimates of metamorphism between 5 kb and 6 kb.

Lapinsky (1981), using whole-rock and microprobe analysis, investigated the petrography and

mineralogy of various pelitic assemblages found in the northeastern Bushveld Complex metamorphic aureole. Nell (1984, 1985) investigated the metamorphic aureole in the Potgietersrus area. This study concentrated on the thermodynamic and geochemical controls in the formation of mineral assemblages in the pelitic and calcareous rocks. Using various geothermometers and geobarometers, constraints were placed on the equilibrium temperatures and pressures. Based on these calculations he postulated two stages of metamorphism which were equated with two major pulses of Bushveld magma emplacement. An early low pressure event, at about 2 kb, followed by a later higher pressure metamorphic event, between 4 kb and 5 kb.

Engelbrecht (1988, 1990a, 1990b) gave an account of the metamorphic aureole in the Marico district in the western Transvaal basin. Three metamorphic zones were recognised in the field: an outer low grade chiastolite zone, an intermediate cordierite zone, and an inner high grade orthopyroxene zone. These zones are all superimposed on earlier burial metamorphism. Geothermobarometry was used to establish a metamorphic loop for the area whereby contact metamorphism reached a peak with the intrusion of marginal, lower, critical and lower main zone magmas at relatively low pressures but were reset to higher pressures with subsequent intrusion of the major part of the main and upper zones.

Wallmach (1986) and Wallmach *et al.* (1989) using metamorphic mineral assemblages from calc-silicate xenoliths in the eastern Bushveld Complex constrained the pressure and temperature conditions of magma emplacement. Load pressures of 0.6 - 1.6 kb for the critical zone and 1.1 - 2.4 kb for the marginal zone magmas were inferred, with magma temperatures between 1200 °C and 1400 °C, and lower peak temperatures occurring in the marginal zone.

Hartzer (1988, 1989, 1995) investigated the deformed and metamorphosed rocks of the Transvaal Supergroup in the Crocodile River Fragment. Three periods of deformation, and three phases of Bushveld thermal metamorphism, two progressive (hornblende-hornfels facies) and one retrogressive were identified. He concluded that interference folding in the Transvaal basin occurred before the intrusion of the Bushveld Complex and that thermal metamorphism was mostly post-tectonic. He suggested that any subsequent deformation was related to

isostatic readjustment due to the emplacement of the Bushveld Complex, which in places accentuated the deformation. Interference folding was controlled by the ENE-trending Thabazimbi-Murchison trend and a NW-trending set of faults.

Kaneko and Miyano (1990) sampled a cross section of the contact aureole in the northeastern Bushveld Complex and established metamorphic pressures between  $2.1 \pm 0.4$  kb at 5.4 km and  $2.4 \pm 0.9$  kb at 8.9 km distance from the contact with the Bushveld Complex. They used this to determine a geothermal gradient for the aureole of  $80 \pm 20^\circ\text{C}/\text{km}$ .

The most recent work on the Bushveld Complex contact aureole by Courtnage *et al.* (1995) in an area northwest of Johannesburg, described complex porphyroblast-matrix relationships. These were identified as pre-, syn-, and post-tectonic in origin and interpreted as being related to a number of pre-, syn- and post-Transvaal Supergroup deformations.

## **2.7 REGIONAL VARIATIONS IN THE AUREOLE**

### **2.7.1 Introduction**

Variations in aureole characteristics can be related to numerous factors. The most important being depth, size of intrusion, magma and country-rock composition, and volatile content and composition (Barton *et al.*, 1991). Other factors that need to be considered include the absolute and relative timing of intrusive events, emplacement mechanisms, tectonic setting, the local and regional stress state, structural grain, and prior thermal history (Barton *et al.*, 1991).

Although the Bushveld Complex is remarkable for its extensive lateral uniformity and the floor rocks throughout most of the complex comprise the same lithostratigraphic formations, considerable variations in the nature and extent of the aureole have been recognised (Hall, 1932; Willemse, 1964; Saggerson and Turner, 1995). The most important are the extent and true width of the aureole, mineralogical and textural variations, and the structural setting.

### **2.7.2 Thickness of the aureole**

The extent of the contact aureole was first documented by Hall (1932) and an updated version is provided by Saggerson and Turner (1992). From these maps it is clear that the surface extent



of the aureole (Figure 2.3) is strongly influenced by the regional dip of the strata and the degree of erosion. In the western Transvaal basin the exceptionally wide aureole has been ascribed to previously overlying Bushveld Complex (Hall, 1932; Engelbrecht, 1976).

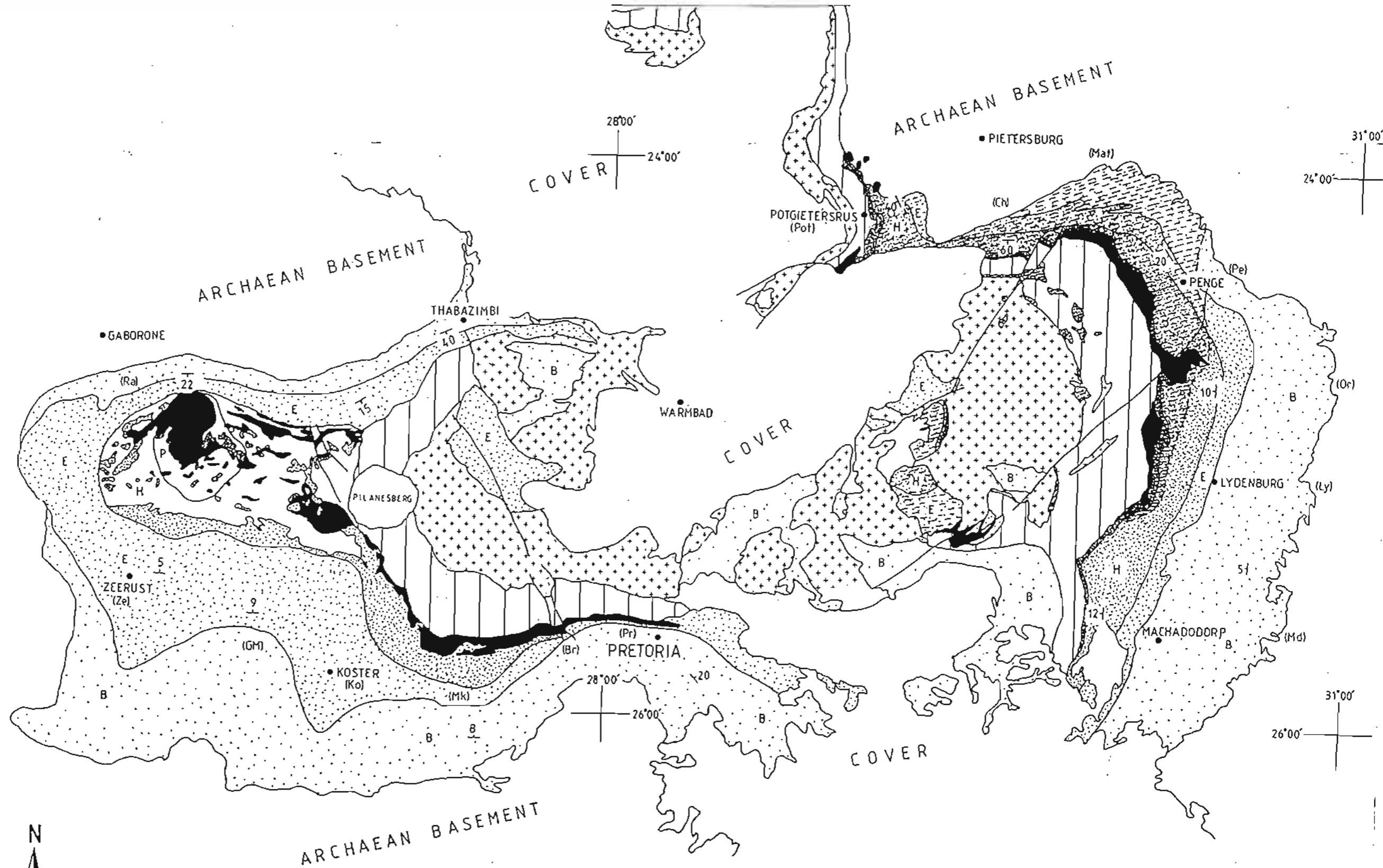
The outer limit of the aureole is represented by the appearance of chloritoid spotting in argillaceous rocks of the Pretoria Group, but is poorly defined where it occurs within the dolomites of the Chuniespoort Group. This is primarily due to a lack of information concerning the degree of recrystallisation attributed solely to contact rather than diagenetic effects in the dolomites (Saggerson and Turner, 1995).

In the eastern Bushveld Complex, the total thickness of pre-Bushveld sills does not seem to have influenced the total thickness of the aureole. Aureole isotherms transgress the sill contacts (Hulbert and Sharpe, 1981). The thickness of the aureole changes even though the number, and total accumulated thickness of the sills remains almost constant.

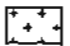


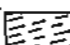
Aureole thickness variations are best represented by true thickness sections constructed at twelve selected localities around the Bushveld Complex together with the associated ultramafic and total Rustenburg Layered Suite thickness at each locality (Figure 2.4). Thicknesses were determined from 1:250 000 scale Geological Survey maps and the 1:1 000 000 scale metamorphic map of South Africa. Regionally, the aureole thickens towards the southwestern portion of the western Bushveld Complex and the northern margin of the eastern Bushveld Complex, thinning markedly over the southern central portion in the Pretoria area. This correlates broadly with the exposed magma thicknesses which thicken northwards, westwards and eastwards of Pretoria (Figure 2.4).

The aureole has a minimum width in the Pretoria area of less than 100 m, with some cordierite developed in the Pretoria Group pelites above the Magaliesberg Quartzite Formation (Hall, 1932). The aureole widens westwards with the outer limit transgressing downwards across the stratigraphy until almost the entire thickness of the Transvaal Supergroup is affected (Figure 2.3). In this area, andalusite is found over 28 km from the floor contact of the Rustenburg Layered Suite and the outer limit of contact metamorphism is represented by talc-bearing

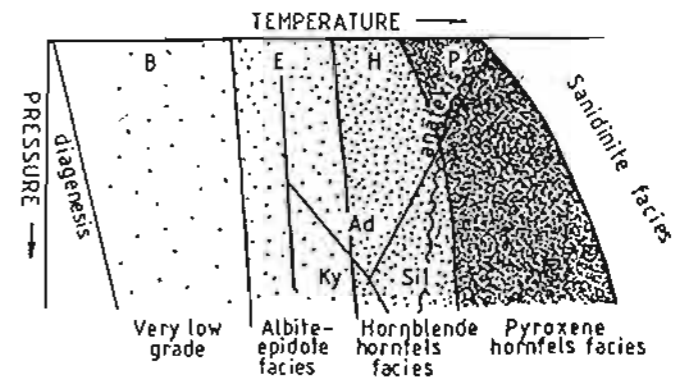
Figure 2.3 The distribution of the Bushveld Complex contact aureole after Saggerson and Turner (1992) showing regional metamorphic facies variations and the locations of aureole true thickness estimates shown in Figure 2.4.



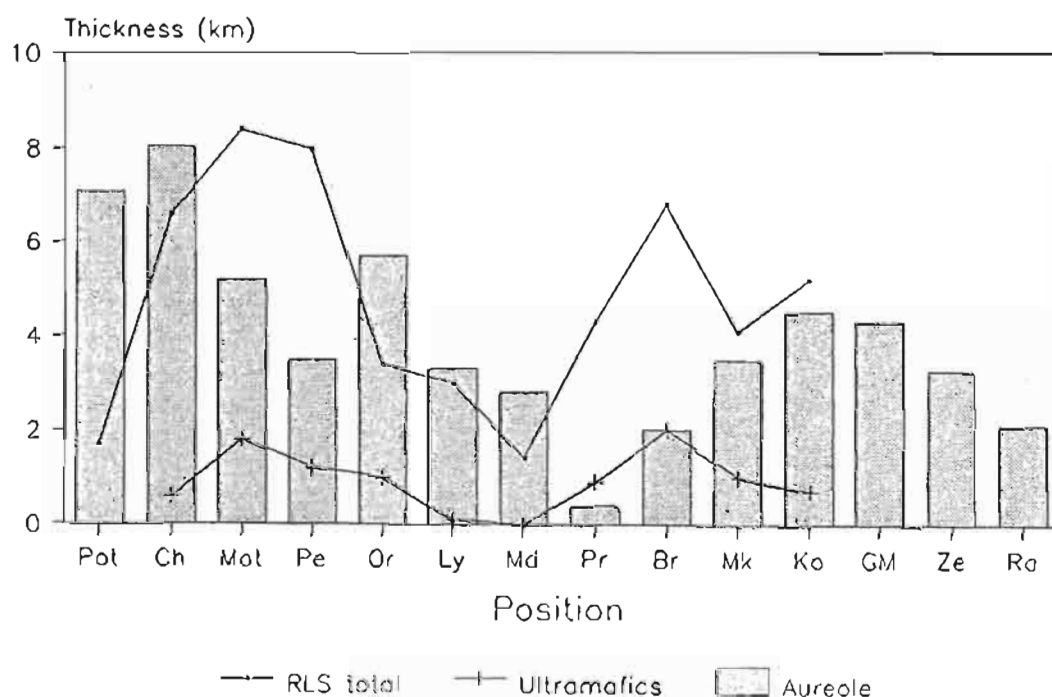
### BUSHVELD COMPLEX

-  LEBOWA GRANITE SUITE
  -  Mafic rocks
  -  Ultramafic rocks
  -  PENETRATIVE FABRIC
- } RUSTENBURG LAYERED SUITE

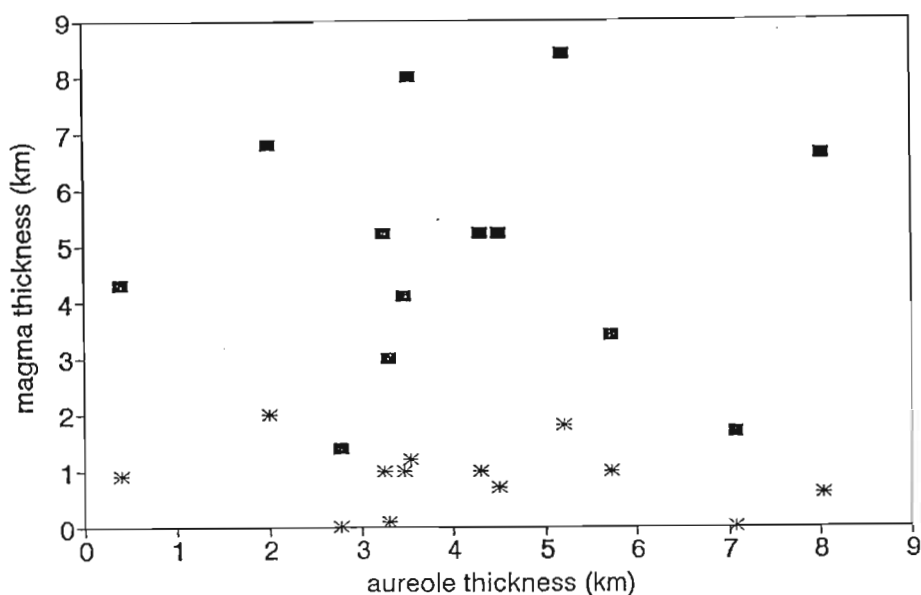
### CONTACT METAMORPHIC FACIES



assemblages in the underlying Chuniespoort Group (Saggerson and Turner, 1995). Similarly, the aureole progressively widens northwards in the eastern Bushveld Complex until the entire thickness of the Transvaal Supergroup is affected in the Potgietersrus area. Two marked discrepancies however, are also evident from Figure 2.3 and Figure 2.4: the exceptional thickness of the aureole in the Potgietersrus area in comparison to the relatively thin overlying Rustenburg Layered Suite, and the poorly developed contact aureole in the Pretoria area which cannot simply be explained by a thin Rustenburg Layered Suite. Attempts to correlate magma thickness with aureole thickness (Figure 2.5) further indicate that no simple correlation exists and that other factors must have had an important influence on the development and extent of the contact aureole.



**Figure 2.4** True thickness estimates for the Bushveld contact aureole (histogram) in relation to the overlying thickness of the ultramafic portion of the Rustenburg Layered Suite (RLS) (+) and the complete RLS (•). Note thick aureole in Potgietersrus area with thin RLS, and thin aureole in Pretoria area with thicker RLS and ultramafics. (Pot)-Potgietersrus, (Ch)-Chuniespoort, (Mat)-Mathabatha, (Pe)-Penge, (Or)-Ohrigstad, (Ly)-Lydenburg, (Md)-Machadodorp, (Pr)-Pretoria, (Mk)-Marikana, (Ko)-Koster, (GM)-Groot Marico, (Ze)-Zeerust, (Ra)-Ramoutsa.



**Figure 2.5** Plot of aureole thickness versus the ultramafic portion of the Rustenburg Layered Suite (\*) and the total thickness of the Rustenburg Layered Suite (■) for the same localities shown in Figure 2.4.

### 2.7.3 Mineralogical variations

The metamorphic zonation of the aureole can be subdivided into four facies of contact metamorphism (Table 2.4) (Saggerson and Turner, 1995). Sanidinite facies rocks are found as small isolated pelitic and calc-silicate xenoliths within the Rustenburg Layered Suite (Willemsse and Bensch, 1964; Willemsse and Viljoen, 1970; Wallmach *et al.*, 1989). Pyroxene-hornfels facies rocks are locally developed along the Bushveld Complex contact, grading outwards into hornblende-hornfels facies, albite-epidote facies and the unaffected regionally burial-metamorphosed Transvaal Supergroup rocks.

The development and extent of the metamorphic facies is related to the thickness of the aureole (Figure 2.3). Where the aureole is poorly developed, such as in the Pretoria area, not all the facies of contact metamorphism are recognised. As the width of the aureole increases, it is accompanied by a corresponding increase in metamorphic grade and the development of all facies of contact metamorphism.

The hornblende-hornfels facies is the most extensive, characterised by the widespread development of andalusite (mainly chiastolite) in pelites. Within this zone, the most pronounced mineralogical differences are noted between the western and the eastern Bushveld Complex aureole. In the northeastern aureole, the pelites are characterised by an extensive zone of

**Table 2.4** Dominant pelitic and calc-silicate assemblages from the Bushveld Complex aureole in the four facies of contact metamorphism, after Saggerson and Turner (1995). Mineral abbreviations after Kretz (1983).

	Albite-epidote facies	Hornblende-hornfels facies	Pyroxene-hornfels facies	Sandinite facies
pelitic	Qtz-Bt-Chl	Bt-Crd-Mus Bt-Mus-And Bt-And-Chl-Crd Bt-And-Cld-Crd-St Bt-Grt-St-And	Bt-Grt-Crd-Sill Bt-Crd-Ksp Bt-Opx-Crd Bt-Opx-Crd-And	Crd-Spl Crn-Crd-Pl-Rt Crd-Mul-Spl-Crn Pl-Crn-Spl-Spa
calc - silicate	Qtz-Cal-Tlc Qtz-Chl-Ep	Cal-Dol-Plh Cal-Dol-Hbl-Ttn Cal-Dol-Di-Grs Cal-Dol-Ep Qtz-Ep-Am-Ttn-Kfs Hbl-Bt-Pl	Pl-Kfs-Cpx-Idc Idc-Wo-Di-Adr Di-Mtc-Ak Mtc-Ak-Spl Spl-Di	Per(Brc)-Mtc-Mer Mtc + Fo (exsol) Mer-Spl Mer Mer-Mtc

staurolite-bearing felses which are absent in the western (Engelbrecht 1990b) and northern aureole in the Potgietersrus area (Nell, 1984; 1985).

These features can be explained by regional compositional variations in the Pretoria Group protolith, related to regional facies variations within the Transvaal basin (Eriksson *et al.*, 1991), but are also suggestive of regional pressure variations. Pattison and Tracy (1991) showed that pressure is of primary importance in the development of different facies series. Staurolite is generally absent from most contact aureoles except the highest pressure facies series for a given composition corresponding to the Pattison and Tracy (1991) facies series type 2b to 4.

#### 2.7.4 Metamorphic pressure variations

Estimates of metamorphic pressure from various parts of the aureole are poorly constrained. The most recent geobarometric calculations from mineral equilibria by Engelbrecht (1990b) give pressures of between 2.1 and 3.2 kb for the western Bushveld Complex and between 4 and 5 kb for the Potgietersrus area in the northern Bushveld Complex (Nell, 1984). Hulbert and

Sharpe (1981) established pressures of up to 5 kb for the northeastern Bushveld Complex aureole. This is in marked contrast to the significantly lower pressures established for the same area by Kaneko and Miyano (1990) of between 2.1 and 2.4 kb.

### 2.7.5 Textural variations

Quantitative grain size profiles of the contact aureole are not available, although andalusite crystal sizes from andalusite mines in the eastern and western aureole provide some indication of grain size variations in the different regions of the contact aureole (Figure 2.6). Andalusite from the western Bushveld Complex has an average length of 40  $\mu$ m with a width of 2 - 4  $\mu$ m. This is a few orders of magnitude smaller than the andalusite mined in the northeastern Transvaal basin which attain lengths in excess of 200  $\mu$ m and has a width of about 10  $\mu$ m. Similarly, other associated porphyroblastic minerals such as biotite, garnet, staurolite and muscovite are considerably coarser-grained in the northeastern Bushveld aureole than in the western aureole.

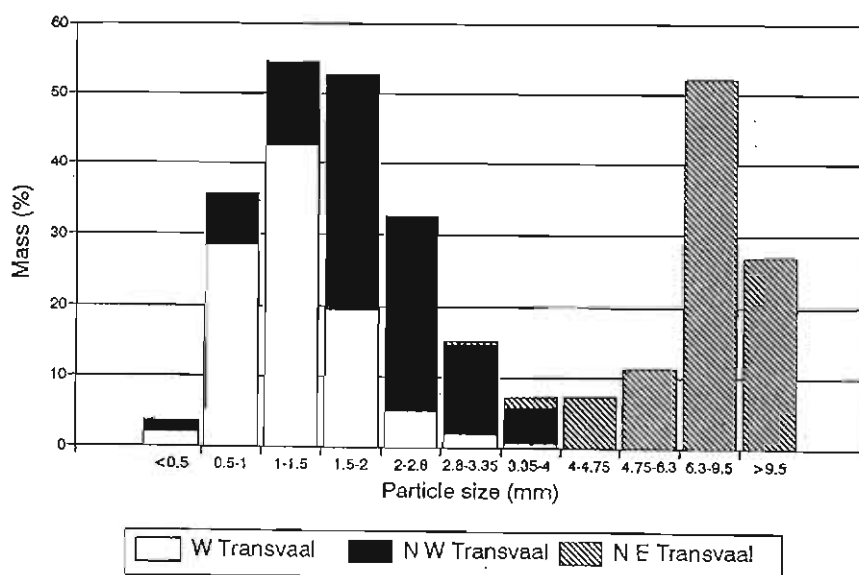


Figure 2.6 Histogram plot of andalusite product grain size distributions from the main andalusite producers in the contact aureole.

The most coarse-grained contact metamorphosed rocks are also found associated with the area which has the most pronounced development of penetrative metamorphic fabric. Schistose rocks, the type area being at Malipsdrif (Hall, 1932), are found throughout the northeastern part of the eastern Bushveld Complex, both in the Bushveld Complex floor, and associated with

highly deformed Transvaal Supergroup fragments within the complex (Figure 2.3). Further south, in the Machadodorp area, the penetrative nature of the fabric decreases, and the only evidence of possible Bushveld Complex related deformation is found as thin bedding-parallel eastward-directed thrusts (Harley and Charlesworth, 1991, 1993, 1995). Limited fabric and structural data exist from other parts of the contact aureole, but visits by the author to the Potgietersus area and the northern margin of the far western Bushveld Complex indicated a poorly developed fabric in comparison to that in the northeastern Transvaal basin.

### 2.7.6 Conclusions

The regional thickness variations in the aureole cannot solely be attributed to variations in the thickness of the Rustenburg Layered Suite and of the lower zone magmas, as was originally suggested by Hall (1932). The above textural observations and thickness variations may also be interpreted as being due to variations in emplacement depth or the degree of syn-Bushveld Complex subsidence. This is to some extent also supported by mineralogical and sparse geobarometric data.

As a rule, grain, size distributions in isochemical aureoles are strongly depth dependant, increasing with increasing depth of crystallisation, proximity to the intrusion and the size of the intrusion (Spry, 1969). It has also been found that upper crustal aureoles are mainly hornfelsic and penetrative fabrics are mostly associated with deeper aureoles (Barton *et al.*, 1991).

Based on this interpretation, the deepest and most highly tilted and deformed part of the aureole is represented by the northern margin of the eastern Bushveld Complex. The eastern Bushveld Complex resembles a strongly asymmetrical, half-graben-type structure with a maximum zone of subsidence and accompanying deformation along the northern margin. In this area, metamorphic conditions were such that regional strain was focused along the Thabazimbi-Murchison Lineament. At higher structural levels, such as exposed in the southern and western Bushveld Complex not all of the facies of contact metamorphism are represented (Saggerson and Turner, 1995). In these areas, the aureole is narrower and deformation conditions were more brittle, with the localised development of bedding-parallel thrusts (Harley and Charlesworth, 1991) rather than a penetrative fabric.



# CHAPTER 3

## LOCAL GEOLOGY AND LITHOSTRATIGRAPHY

### 3.1 THE PRETORIA GROUP

Within the study area the entire Pretoria Group rocks are metamorphosed from medium to high grades with the zonal development of various porphyroblastic mineral assemblages. Despite this, regional stratigraphic correlations across the area are generally possible, as primary sedimentary features are usually well preserved and are often accentuated by metamorphic minerals. Identification of the stratigraphic units exposed within the Bushveld Complex as xenoliths and fragments is particularly important and vital for a structural interpretation of the contact aureole. In a few areas however, structural complexity, intense metamorphism and feldspathisation makes the field identification of units, and correlation between xenoliths and fragments difficult.

The Pretoria Group attains a total thickness of approximately 7000 m in the southeastern Transvaal basin (Button, 1973). Only the lower portion of the Pretoria Group is represented in the study area, comprising the stratigraphy from the Rooihogte Formation to the Lakenvalei Quartzite Formation, a thickness of approximately 4000 m (Figure 3.1, Appendix 1). Locally, xenoliths within the Rustenburg Layered Suite may represent poorly preserved remnants of the Lakenvalei Quartzite Formation. Nowhere in the area is the overlying stratigraphy preserved in any of the xenoliths forming the roof to the Bushveld Complex. This indicates that these formations were either not deposited in this area, or as suggested by Cheney and Twist (1991), were removed prior to the development of the sub-Dullstroom Formation unconformity, which later provided a suitable pathway for the Bushveld magmas. This would explain the regional transgressive nature of the Bushveld Complex floor contact which is evident in the study area. In the southern part of the area, the highest level of intrusion corresponds to the Lakenvalei Quartzite Formation, passing downwards locally to below the Magaliesberg Quartzite Formation in the northwestern portion.

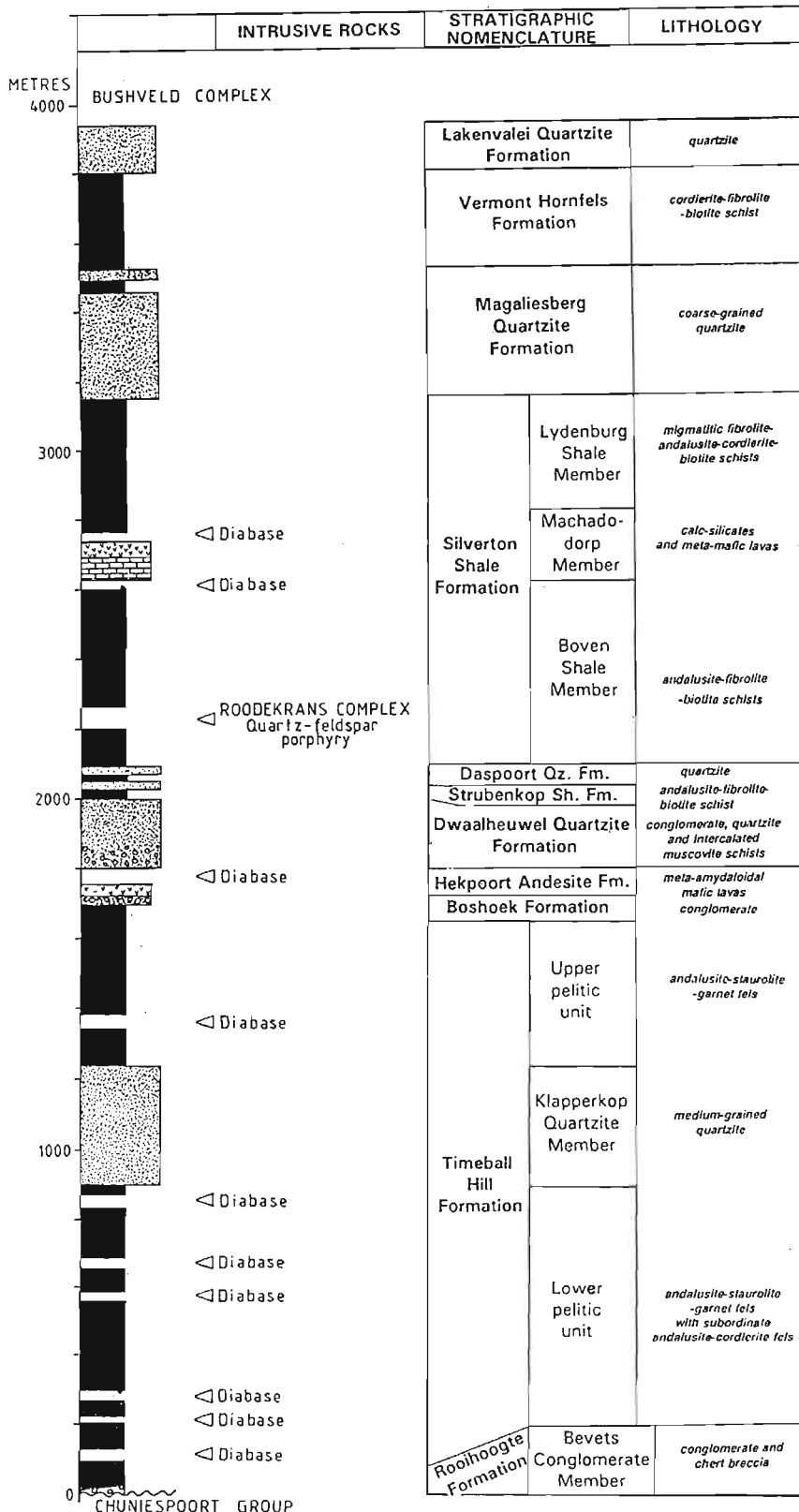


Figure 3.1 Lithostratigraphy of the Pretoria Group and the positions of the intrusive sills in the study area. Stratigraphic nomenclature after SACS (1980) except for the Klapperkop Quartzite Member (after Eriksson and Clendenin, 1990). Lithology of the argillaceous units is indicated by the dominant and characteristic metamorphic assemblages.

### 3.1.1 Rooihoogte Formation

The Rooihoogte Formation is present in the study area only as sporadic occurrences of the Bevet Conglomerate Member consisting of chert breccia and ferruginous chert breccia up to a thickness of approximately 3 m. Individual fragments or clasts are rectangular in shape, up to 10 cm in length and set in a chert matrix.

### 3.1.2 Timeball Hill Formation

The Timeball Hill Formation comprises three major units: the lower pelitic unit, the Klapperkop Quartzite Member and the upper pelitic unit. The lower pelitic unit is approximately 900 m in thickness and overlies the Rooihoogte Formation with a 40 m - thick unit of black fine-grained carbonaceous pelite. Metamorphic porphyroblasts in this unit are small in comparison to the overlying, less carbonaceous units. Porphyroblasts of staurolite are typically up to 5 mm in length, and smaller biotite flakes are visible in hand specimen. Chiasmatic andalusite porphyroblasts up to 10 mm in length are usually completely pseudomorphed by muscovite (Figure 3.2), which may be associated with microscopic chloritoid. The remainder of the sequence consists predominantly of banded, coarse grained, andalusite-staurolite-biotite fels, in which some horizons are particularly rich in chiasmatic andalusite and have economic potential (Figure 3.3).

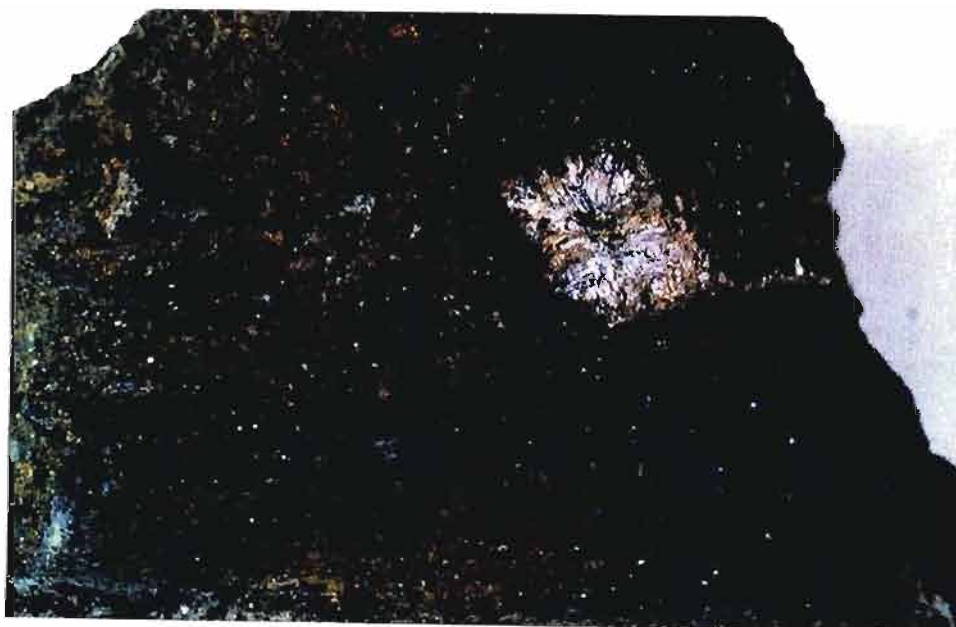


Figure 3.2 Large porphyroblasts of andalusite pseudomorphed by muscovite from the lower pelitic unit of the Timeball Hill Formation on the farm Uitkyk. Andalusite crystal has a width of 10 mm.



**Figure 3.3** Typical andalusite ore from the Hoogenoeg Andalusite Mine in the upper part of the lower pelitic unit, Timeball Hill Formation. Large white chiasolite porphyroblasts in a groundmass assemblage of staurolite, garnet and biotite. Scale length = 14 cm.

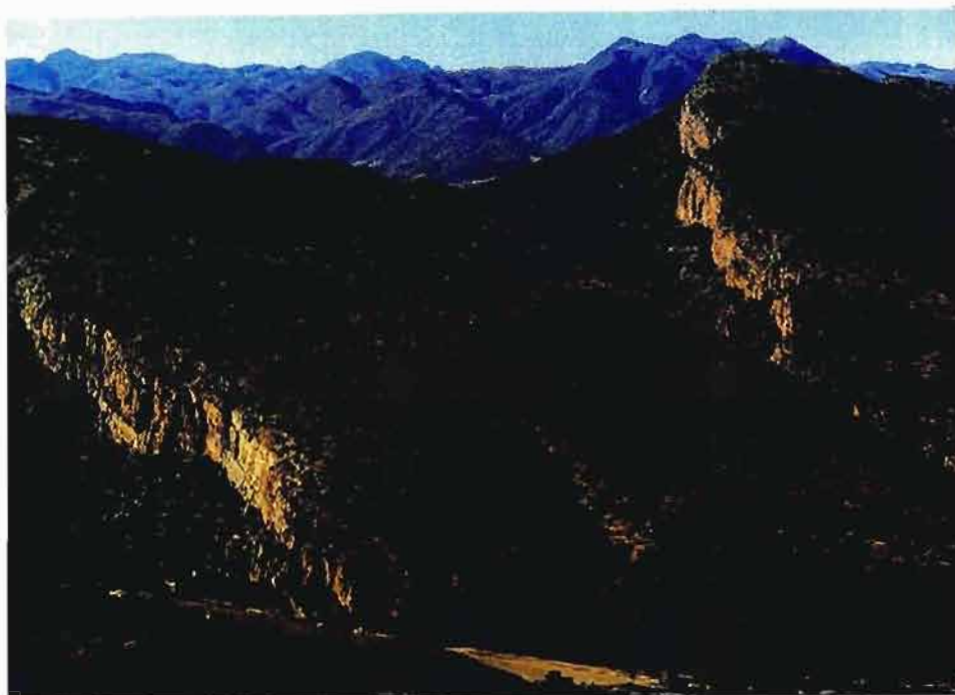
In some horizons, chiasolite andalusite porphyroblasts may reach impressive lengths of over 300 mm and twinned staurolite crystals up to 30 mm in length are common. In the lower part of the sequence chloritoid is usually associated with the andalusite-staurolite-biotite assemblages and is commonly found within the cores of large andalusite crystals.

In the upper part of the sequence, cordierite and almandine-bearing assemblages become more predominant. Garnet-amphibole rocks become common, forming resistant fine-grained quartzitic horizons up to 1 m in thickness interbedded with the pelitic and semi-pelitic rocks.

The lower pelitic unit grades into the Klapperkop Quartzite Member (Figure 3.4) which attains a thickness of approximately 250 m with a central more argillaceous unit of a few metres in thickness. Recrystallisation due to Bushveld metamorphism is not apparent in the arenite hand specimen.

The 500 m thick upper pelitic unit consists mainly of banded argillaceous rocks, similar to those of the lower pelitic unit, comprising various associations of garnet, biotite, staurolite, andalusite

and cordierite. Minor interbedded siliceous marl associations, thin quartzites and ironstones have also been documented (Button, 1973).



**Figure 3.4** Large dip slope exposures of the Klapperkop Quartzite Member of the Timeball Hill Formation on the farms Lot 288, 289 and 290 on the Olifants River. View towards the northeast from Roodekrans. The distant hills lie in the Mhlapitsi River catchment area and consist of deformed Chuniespoort and Wolkberg Group strata.

### **3.1.3 Boshhoek Formation**

Button (1973) reported a conglomerate and diamictite unit within the upper pelitic unit of the Timeball Hill Formation and immediately underlying the Hekpoort Andesite Formation. Only the diamictite unit was found in the study area and it has been equated with the Boshhoek Formation. It consists of an approximately 8 m thick unit of matrix supported, sub-rounded quartz pebble conglomerate with a sandy matrix (Figure 3.5). Button (1973) found that the Boshhoek Formation locally unconformably overlies folded Timeball Hill Formation shales. This has been interpreted by Eriksson (1988) as the result of tectonic instability which preceded Hekpoort volcanism with deposition taking place by gravity flow mechanisms in a fan and fan-delta environment.

### **3.1.4 Hekpoort Andesite Formation**

The Hekpoort Andesite Formation is poorly developed in the area and nowhere does the

thickness exceed 10 m. These meta-lavas are typically amygdaloidal, dark green in colour, consisting of plagioclase and hornblende with amygdales filled by the same minerals (Figure 3.6). Sharpe *et al.* (1983) suggested that the Hekpoort lavas are the product of partial melting at the base of the crust due to the depression of the Transvaal basin.



Figure 3.5 Matrix supported diamictite of the Boshhoek Formation on the farm Copper. Hammer head length = 9 cm.

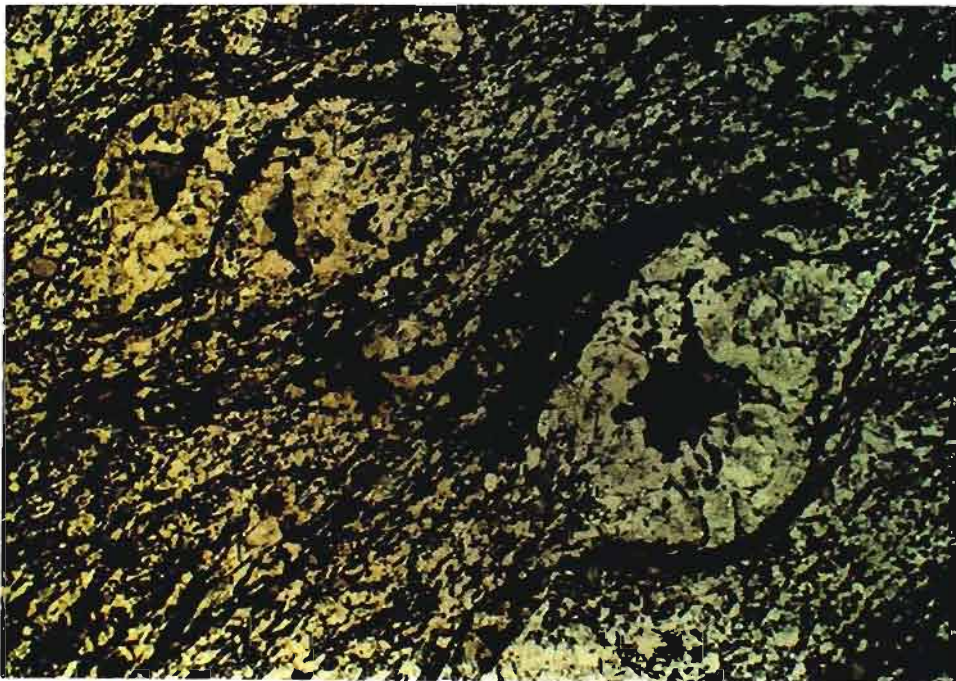


Figure 3.6 Photomicrograph of deformed "augen" in Hekpoort amygdaloidal lava. Katkloof farm. Plane polarised light. Width of view = 6mm.

### 3.1.5 Dwaalheuwel Quartzite Formation

Overlying the Hekpoort lavas is an up to 200 m thick sequence of medium- to coarse-grained, cross-bedded quartzites with chert and quartz pebble conglomerates at the base. This formation forms a prominent dip and scarp slope in the area (Figure 3.7). As opposed to the relatively undeformed and unrecrystallised Klapperkop Quartzite Member, fine-grained units are typically altered to quartz-muscovite schists, and pebbles in conglomeratic horizons are usually deformed.

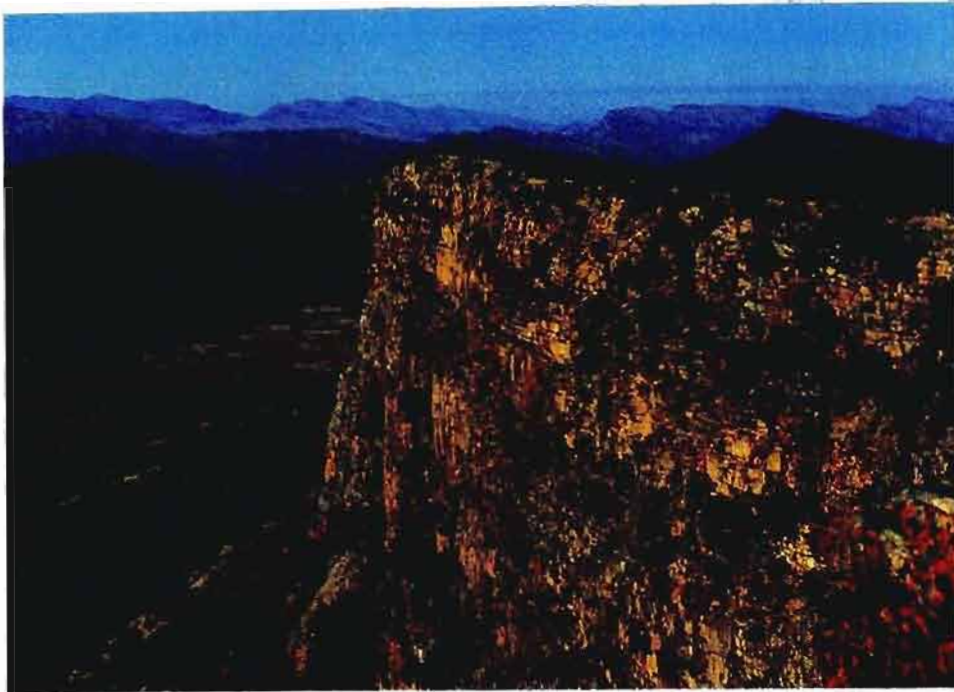


Figure 3.7 Cliff exposure of the Dwaalheuwel Quartzite Formation on the farm Roodekrans. View towards the east along the Olifants River Valley.

Button (1973) referred to these rocks as the lateral continuation and northern exposure of the Dwaalheuwel Formation, which Schweltnus *et al.* (1962) had previously mapped as the Daspoort Quartzite Formation. Button (1973) was of the opinion that the highly attenuated lenses and layers in the basal zone of the Silvertown Shale Formation, mapped by Schweltnus *et al.* (1962), were the northern facies of the Daspoort Quartzite Formation. The discrepancies have still not been resolved, and the latest 1:250 000 Nylstroom 2428 Geological Survey sheet has left the unit as undifferentiated. SACS (1980) has used the nomenclature of Button (1973), naming the conglomerate and quartzite unit immediately overlying the Hekpoort Andesite Formation, the Dwaalheuwel Quartzite Formation. To prevent confusion, the nomenclature used here is that of SACS (1980).

The upper portion of the Dwaalheuwel Quartzite Formation is generally feldspathic, but in places it is capped by a 5 m thick medium to coarse-grained planar bedded quartzite.

### **3.1.6 Strubenkop Shale Formation and Daspoort Quartzite Formation**

A 10 m thick unit of andalusite-fibrolite-biotite schist, interpreted as the Strubenkop Shale Formation, overlies the Dwaalheuwel quartzites. This is overlain by two thin, 3 to 4 m thick, laterally discontinuous, quartzite units separated by a 5 m thick pelitic schist. These are considered to be the northern equivalent of the Daspoort Quartzite Formation (Button, 1973).

### **3.1.7 Silverton Shale Formation**

The Silverton Shale Formation is subdivided into three members: a lower unit, the Boven Shale Member which is separated from the upper Lydenburg Shale Member by the Machadodorp Member. The 500 m thick Boven Shale Member consists of various pelitic rocks of which the most dominant rock type is a chistolite-fibrolite-biotite schist in which andalusite, together with fibrolite is usually present. Andalusite is abundant in a horizon at the base of the unit, and eluvial concentrations derived from this have been exploited in the past. No staurolite-bearing assemblages were found in these rocks, a function either of the original composition of the shales, or of metamorphic grade.

The Machadodorp Member (Figure 3.8) consists of a lower 10 to 30 m thick calc-silicate unit with occasional graphite-rich metapelite at the base, and an upper 30 to 50 m thick upward-fining pyroclastic unit. The calc-silicate unit consists mainly of dolomite with occasional chert layers. Impure carbonate units are characterised by a range of metamorphic calc-silicate assemblages. Samples from a number of localities in the study show elevated  $\delta^{13}\text{C}$  compositions (Buick *et al.*, 1997) when compared to the Malmani Dolomites that underlie the Pretoria Group and carbonates in the overlying Vermont Hornfels Formation. The pyroclastic unit is typified by a poorly sorted meta-volcanic clast-supported breccia (Figure 3.9) fining upwards into well sorted fine-grained volcanoclastics. Metamorphic assemblages are typified by hornblende and plagioclase. Over most of the area, the entire Machadodorp Member is confined between two diabase sills.

The 400 m thick Lydenburg Shale Member is characterised by andalusite, fibrolite and K-



feldspar-bearing pelitic assemblages. Andalusite in these rocks is typically small, up to 10 mm in length, compared to the large crystals found in the Timeball Hill Formation. Near the top of the sequence, migmatites are developed from partial melting of pelites, resulting in the segregation of mafic paleosome and felsic leucosome.

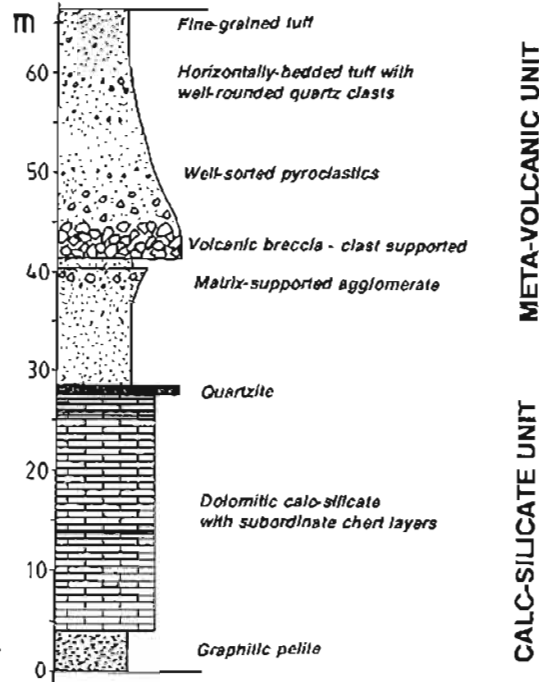


Figure 3.8 Lithological section of the Machadodorp Member as exposed on the farm Schwerin.



Figure 3.9 Deformed and metamorphosed Machadodorp Member meta-volcanic breccia from the farm Zaaikloof. Scale length = 13 cm.

### 3.1.8 Magaliesberg Quartzite Formation

The Magaliesberg Quartzite Formation is between 200 and 300 m thick and over most of the study area forms the immediate floor to the Rustenburg Layered Suite. In some areas however, such as in the Katkloof Fold, the formation is absent from the floor succession. Here, a large section of the Magaliesberg Quartzite Formation has been detached from the floor rocks by the intrusion of the mafic Bushveld magmas. In places remnants of these rocks remain as quartzite xenoliths within the Rustenburg Layered Suite. The quartzites are generally medium-grained with abundant trough cross-stratification structures which range in thickness between 15 and 30 cm. Due to intense metamorphism accompanied by ductile deformation, primary structures are often obliterated with the production of schlieren-type structure (Figure 3.10).

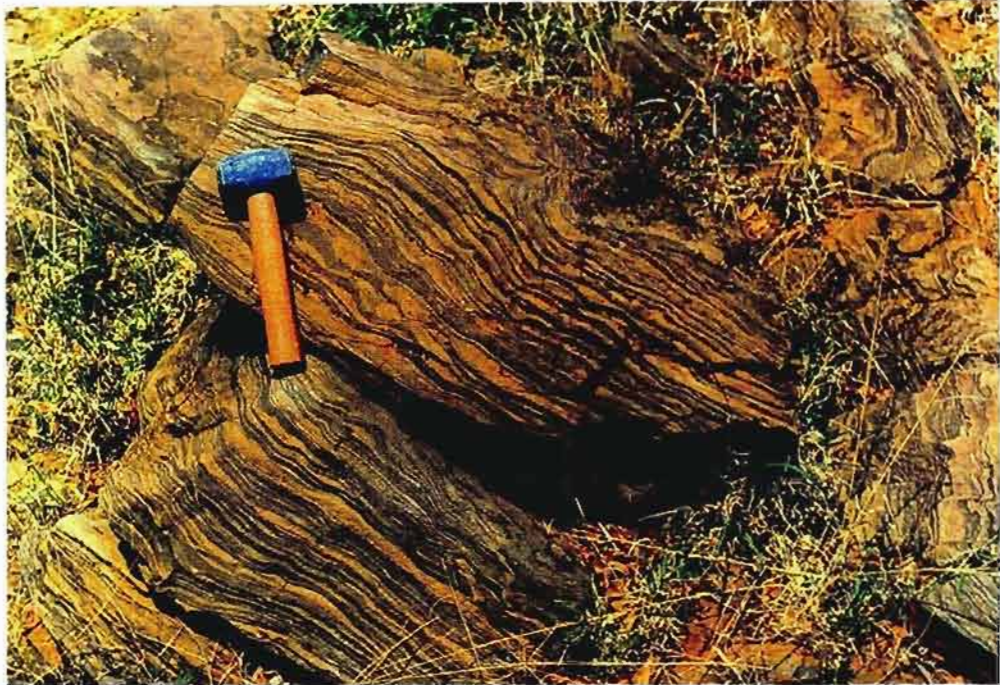


Figure 3.10 Intensely metamorphosed and deformed Magaliesberg Quartzite Formation with schlieren structure from Adriaanskop. Scale size = 14 cm.

### 3.1.9 Vermont Hornfels Formation

The Magaliesberg Quartzite Formation passes gradationally upwards into a succession of predominantly semi-pelitic rocks of the approximately 300 m thick Vermont Hornfels Formation (SACS, 1980). The unit is best exposed in the southern portion of the area, the Zaaikloof and Phepane areas, where it contains minor quartzite and calc-silicate horizons.

Pelitic and semipelitic units are typically migmatitic (Figure 3.11) with cordierite and fibrolite-bearing assemblages most common. Occasional high-grade orthopyroxene-bearing pelitic xenoliths within the Rustenburg Layered Suite are considered to represent fragments of the Vermont Hornfels Formation such as found on the farm Driekop.



**Figure 3.11** Migmatitic semi-pelite of the Vermont Hornfels Formation on the farm Jobskop. Scale length = 25 cm.

#### **3.1.10 Lakenvalei Quartzite Formation**

The Lakenvalei Quartzite Formation is the uppermost recognisable unit of the Pretoria Group represented in the area. It is only found in the southwestern and eastern part of the area. The unit comprises coarse-grained quartzite and feldspathic quartzites. Intense feldspathisation and the development of leptonite is often associated with these rocks where they are in contact with the Nebo Granite.

## **3.2 INTRUSIVE ROCKS**

### **3.2.1 Diabase sills**

It is generally accepted that the diabase sills are the precursors to the intrusion of the Rustenburg Layered Suite (Hall, 1932; Willemsse, 1959; Engelbrecht, 1990a). As mentioned in the discussion on the regional geology, Sharpe (1984) classified the sills into hydrated amphibolitic pre-Bushveld sills and anhydrous pyroxene-bearing syn-Bushveld sills. Engelbrecht (1990a) however, suggested that the sills were of similar age with differences in mineralogy reflecting their relative position within the contact aureole.

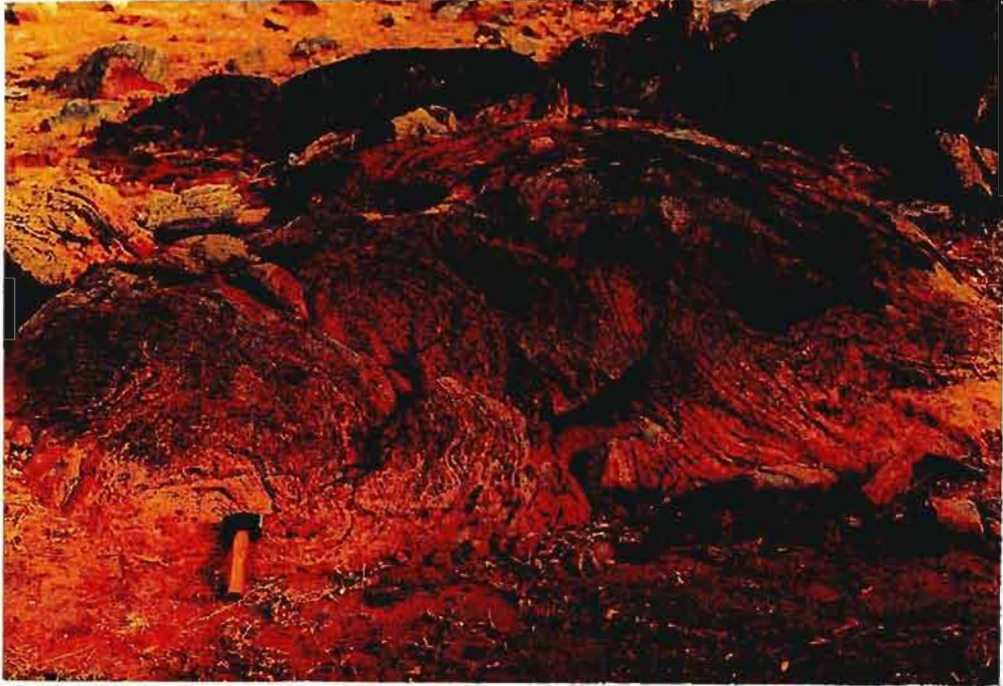
In the study area, sills are up to 50 m thick, and are predominantly found in the lower parts of the Pretoria Group (Appendix 1). They consist mainly of hornblende, chlorite and saussuritized plagioclase assemblages. Occasional granophyric quartz-feldspar intergrowths may be observed in some sills. Primary textures are generally obliterated, but a sill below the Dwaalheuwel Quartzite Formation has a characteristic spotted appearance in which palimpsest pyroxene is mantled by hornblende. The position of this sill just below the fibrolite-in isograd is thought to represent the position below which hydration reactions have gone to completion and above which sills tend to be relatively unaltered and hydration is limited. Sills found in the Silverton Shale Formation are less altered and contain assemblages of plagioclase, pyroxene and commonly biotite.

No local contact metamorphic effect is evident adjacent to the sills. This suggests that any contact effects were overprinted and obliterated by the development of the main contact metamorphic aureole related to the emplacement of the Rustenburg Layered Suite. These observations support the arguments of Engelbrecht (1990a) for a pre-contact aureole emplacement of the sills and that the distribution of altered and unaltered sills is related to their position within the contact aureole.

### **3.2.2 The Roodekrans Complex quartz-feldspar porphyry**

These rocks are usually dark grey in colour and occur as a laterally extensive 30 to 50 m thick sill in the Boven Shale Member of the Silverton Formation (Appendix 1A,B,C). The rock can be texturally very inhomogeneous. In some areas the rock is massive and unlayered, but more commonly it is characterised by zones of flow banding exhibiting flow folding (Figure 3.12).

Layering is defined by a variation in phenocryst content ranging between about 5 and 20 percent. In the field they resemble volcanic rocks, but the occasional quartzite xenolith near the contact with the surrounding rocks suggests an intrusive relationship. Some areas are brecciated (Figure 3.13) with early quartz-feldspar porphyry xenoliths set in a slightly darker groundmass, suggesting at least two intrusive pulses.



3.12 Flow folding and layering in the Roodekrans quartz-feldspar porphyry on the farm Jobskop. Scale length = 25 cm.



Figure 3.13 Igneous breccia within the Roodekrans Complex quartz-feldspar sill from the farm Jobskop. Scale length = 25 cm.

The phenocrysts consist mainly of subhedral to euhedral plagioclase ( $Ab_{65}$ ), up to 10 mm in length and minor, round "opalescent" blue-quartz up to 10 mm in diameter set in a quartz, plagioclase, K-feldspar and hornblende groundmass (Figure 3.14). Biotite and chlorite become common in sheared rocks. Accessory minerals include apatite, zircon, pyrite and other opaque phases. Schwelnus (1956) also reported the presence of secondary carbonate and garnet. Schwelnus (1956) identified the rock as a dacite porphyry and quartz porphyry, and later (Schwelnus *et al.*, 1962) as a microgranodiorite porphyry. More recent 1:250 000 scale Geological Survey maps refer to it simply as a granodiorite. Sharpe and Chadwick (1981) gave the name Roodekrans Complex to these rocks, after the farm Roodekrans within the Schwerin Fold, on which some of the best exposures in the area are found.

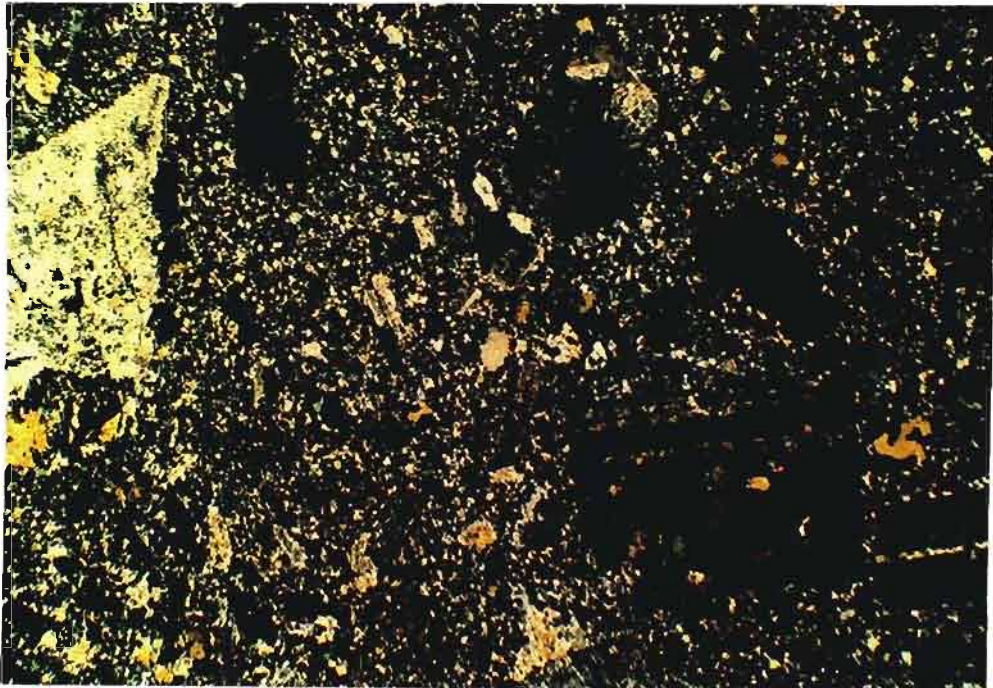


Figure 3.14 Photomicrograph of the Roodekrans quartz-feldspar porphyry. Phenocrysts of quartz and plagioclase in a groundmass of quartz, hornblende, biotite and chlorite. Crossed polarised light. Width of view = 6 mm.

### 3.2.1.1 Age relationships

Various age interpretations have been given to the quartz-feldspar porphyry sill. Schwelnus (1956) considered the unit to be of pre-Rustenburg Layered Suite age, as it was deformed with the Pretoria Group and occurs in Pretoria Group rafts within the Rustenburg Layered Suite. Blain (1975) considered these rocks to grade laterally into the Machadodorp volcanics of the

Pretoria Group. Button (1978) suggested that the emplacement of the quartz-feldspar porphyry was related to the development of large diapiric floor folds in the Bushveld Complex. He believed that this process promoted the emplacement of the Roodekrans Complex, as a phacolith along a decollement zone in the core of the rising diapir, such as the Schwerin Fold.

The Geological Survey 1:250 000 scale Nylstroom 2428 sheet (1978), has included the Roodekrans quartz-feldspar porphyry with the Rashoop Granophyre Suite, a diverse group of granophyric rocks, for which numerous and often contradictory origins have been proposed (Tankard *et al.*, 1982). The most recent geochemical work by Schweitzer *et al.* (1995) found that the vast majority of the granophyres were co-magmatic with Rooiberg volcanism and emplaced as compositionally similar sills into older felsites below their corresponding volcanics, supporting the original ideas of Walraven (1985) who suggested that the Rooiberg Group volcanics and the granophyres had the same parent magma.

Field relations from this study indicate that the Roodekrans quartz-feldspar porphyry pre-dates peak contact metamorphic conditions and deformation in the aureole. The intrusion is far more extensive than originally mapped, occurring in all the fold structures and interfold areas. It does not occur as a phacolithic intrusion confined to the cores and basal decollement zones of the fold structures as proposed by Button (1978). Button however, did suggest that the intrusion was synchronous with deformation. This may explain the common occurrence of flow folding (Figure 3.12). Flow folding predates the foliation, suggesting that intrusion may have been synchronous with the early stages of deformation. Only once the magma was solidified was a foliation developed.

This close association with the tectonothermal events in the contact aureole further suggests that the intrusion is, as with the diabase sills, part of the Bushveld magmatic event. No field relationships were found between the quartz-feldspar porphyry and the diabase sills. The relative timing of the two magma types thus remains unknown. The quartz-feldspar porphyry however, may represent a hypabyssal phase to either the Dullstroom Formation or the Rooiberg Group volcanics which are considered immediate precursors to (Twist, 1985; Walraven, 1985), or synchronous to (Hatton and Schweitzer, 1995) the plutonic episodes of the Bushveld Complex. This is further explored below.

### 3.2.1.2 Geochemistry

Five 20 kg size bulk samples of the Roodekrans quartz-feldspar porphyry were collected from the farm Jobs Kop. The samples represent the range of textural and colour variations found in the area. Whole-rock powders were analysed for major and selected trace elements by X-ray fluorescence techniques at the Department of Geochemistry, University of Cape Town. For analytical methods, procedures and accuracy and precision data, see Duncan *et al.* (1984).

Geochemical analyses are presented in Table 3.1. Included is an analysis of the same rock type (SCH-1) collected on the neighbouring farm Stellenbosch by Schweltnus (1956). Major elements are presented as Harker binary plots (Figure 3.15) indicating a general positive correlation between Na<sub>2</sub>O, TiO<sub>2</sub>, and CaO with SiO<sub>2</sub>, and a negative correlation between MgO, K<sub>2</sub>O, MnO, Fe<sub>2</sub>O<sub>3</sub>, and SiO<sub>2</sub>. Sample (RK-3) has anomalously lower Na<sub>2</sub>O, and higher K<sub>2</sub>O and CaO than the other samples. As the other elements are not affected, it may be related to

**Table 3.1** Geochemical analyses of major and trace elements for the Roodekrans quartz feldspar porphyry (RK-1 to RK-5, this study) and major elements only (SCH-1) from Schweltnus (1956).

SAMPLE NO.	RK-1	RK-2	RK-3	RK-4	RK-5	SCH-1
SiO <sub>2</sub>	69.68	69.04	69.80	69.62	74.77	64.41
TiO <sub>2</sub>	0.96	0.92	0.84	0.97	1.01	0.85
Al <sub>2</sub> O <sub>3</sub>	12.53	12.19	12.05	13.22	13.28	13.59
Fe <sub>2</sub> O <sub>3</sub>	5.91	5.68	5.45	4.66	1.87	8.38
MnO	0.09	0.12	0.12	0.10	0.05	0.13
MgO	0.96	0.70	0.78	0.70	0.17	2.18
CaO	2.24	3.28	2.87	2.44	2.33	2.06
Na <sub>2</sub> O	4.63	3.88	2.34	4.56	6.12	3.86
K <sub>2</sub> O	2.41	2.34	4.32	2.54	0.46	2.51
P <sub>2</sub> O <sub>5</sub>	0.32	0.32	0.27	0.34	0.37	0.13
H <sub>2</sub> O-LOI	0.08	0.16	0.13	0.13	0.12	0.06
	0.67	1.76	1.32	1.01	0.58	
TOTAL	100.48	100.38	100.27	100.31	101.14	99.86
Mo	2	1	1	1	0	
Nb	10	9	9	9	9	
Zr	187	183	199	193	189	
Y	30	30	31	29	27	
Sr	348	139	98	223	169	
U	2	3	2	2	1	
Rb	65	73	90	56	12	
Th	6	6	6	5	6	
Pb	15	9	19	16	10	
Ba	1006	663	1334	3048	209	
Sc	12	12	12	13	2	
S	59	606	5	35	5	
La	29	29	29	19	22	
Ce	58	62	68	41	54	
Nd	28	31	34	23	27	
Cs	5	5	5	5	4	
Co	3	7	6	4	2	
Kn	716	946	929	810	356	
Cr	3	4	2	2	2	
V	35	33	21	32	11	
Ga	13	17	15	17	12	
Zn	88	63	92	51	21	
Cu	5	4	3	2	2	
Ni	2	2	2	2	1	



element mobility and alteration which led to a loss in Na and gain in K and Ca. Other elements, such as Ti, Zr, Nb, Y show small and systematic variations, and are considered to have been less mobile during metamorphism and alteration.

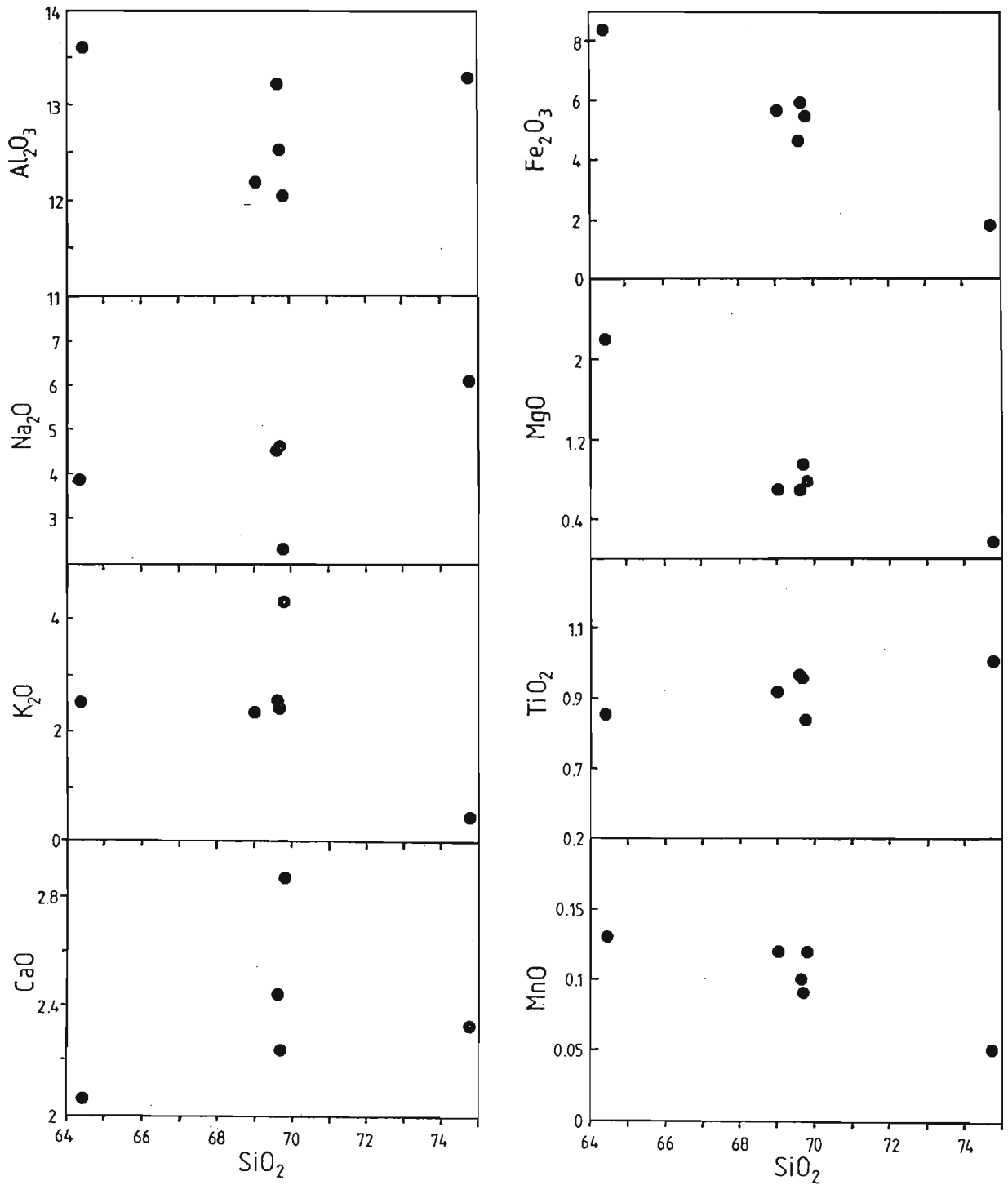


Figure 3.15 Harker-type plots for the major elements from the Roodekrans quartz-feldspar porphyry.



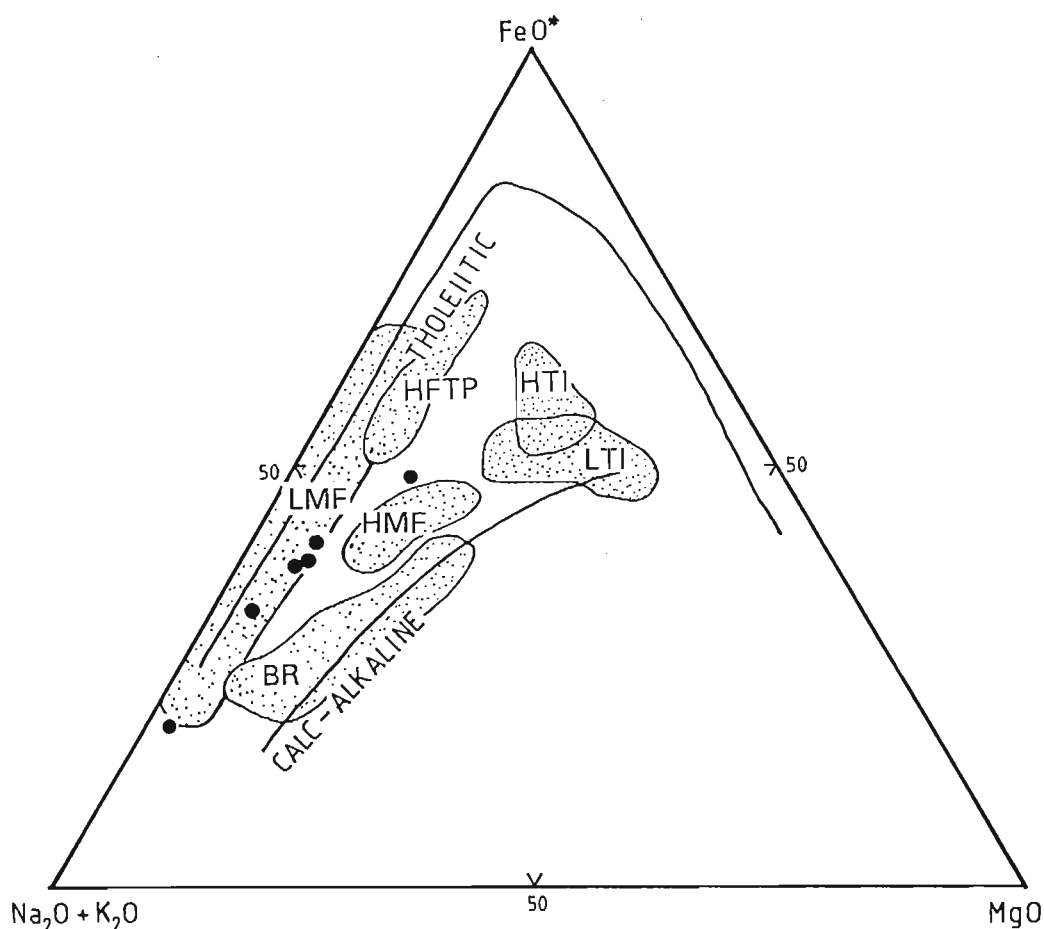
with limited data, he found no significant major element correlation. Since then, a much larger chemical data set for the Dullstroom and Rooiberg volcanics, the Rashoop Granophyre Suite and Lebowa Granite Suite has become available.

Schweitzer *et al.* (1995) and Hatton and Schweitzer (1995) subdivided the Rooiberg Group into four formations, including the Dullstroom Formation, and recognised nine magma types (Table 3.2). They found that the most common magma type, constituting the majority of the Damwal Formation, the entire Kwaggasnek and Schrikkloof Formations is a low-Mg felsite (LMF). The lowermost Dullstroom Formation however, is compositionally diverse with all nine magma types identified. In the order of appearance, the earliest magmas are low-Ti (LTI) basaltic andesites followed by basal rhyolites (BR), high-Mg felsite (HMF), high-Ti (HTI) basalt, high Fe-Ti-P lavas (HFTP) and the Bothasberg low-Mg felsites (LMF) which form the bulk of the overlying Damwal Formation.

**Table 3.2** Regional stratigraphy of the Rooiberg Group and the stratigraphic distribution of magma types as identified by Schweitzer *et al.* (1995). (HTI) High-Ti basalt, (LTI) Low-Ti basaltic andesite, (HFTP) High-Fe-Ti-P basaltic andesite, (LMF) Low-Mg felsite, (HMF) High-Mg felsite, (BR) Basal rhyolite.

FORMATION	LITHOLOGY	MAGMA TYPE
Schrikkloof	Flow-banded rhyolites with minor quartzite xenoliths	LMF
Kwaggasnek	Rhyolite with pyroclastics and sedimentary rocks	LMF
Damwal	Massive amygdaloidal dacites and rhyolites with intercalated quartzite and pyroclastics	LMF HFTP
Dullstroom	Mafic and felsic magma types becoming increasingly siliceous towards top	BR LTI HTI HMF LMF

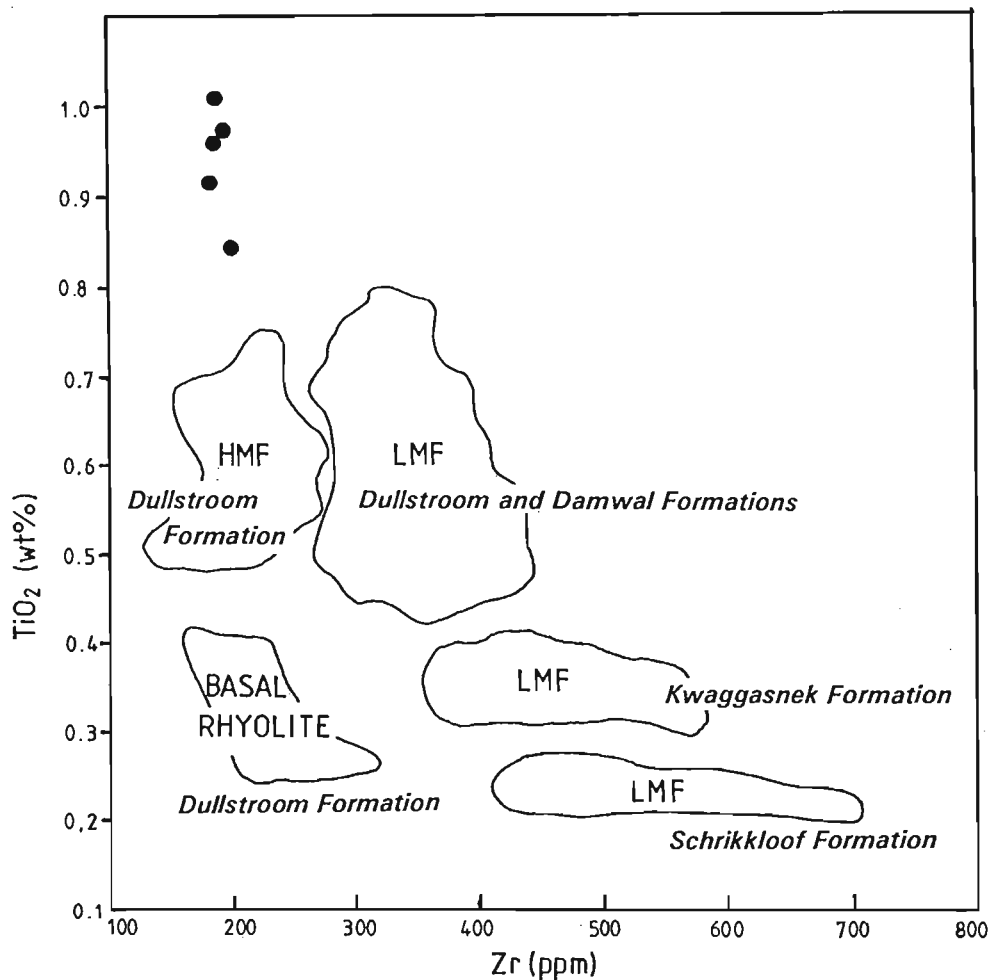
Plotted on a ternary AFM diagram (Figure 3.17), the Roodekrans rocks show a tholeiitic line of descent and plot mainly amongst the LMF magma type of Hatton and Schweitzer (1995). They are also characterised by low Cr, V and Ni concentrations (Table 3.1), a feature common to the LMF magma type (Hatton and Schweitzer, 1995).



**Figure 3.17** Ternary AFM plot for the Roodekrans rocks showing an iron-enrichment trend with tholeiitic affinity and magma type fields for the Rooiberg Group after Hatton and Schweitzer (1995). (HTI) High-Ti basalt, (LTI) Low-Ti basaltic andesite, (HFTP) High-Fe-Ti-P basaltic andesite, (LMF) Low-Mg felsite, (HMF) High-Mg felsite, (BR) Basal rhyolite.

When the Roodekrans rocks are compared to the  $\text{TiO}_2$  versus Zr compositional fields for the Rooiberg Group of Schweitzer *et al.* (1995), they plot outside but closest to the Bothasberg HMF and LMF compositional fields (Figure 3.18). The high  $\text{TiO}_2$  and low Zr content is most characteristic of the lowermost formations of the Rooiberg Group, the Dullstroom and Damwal

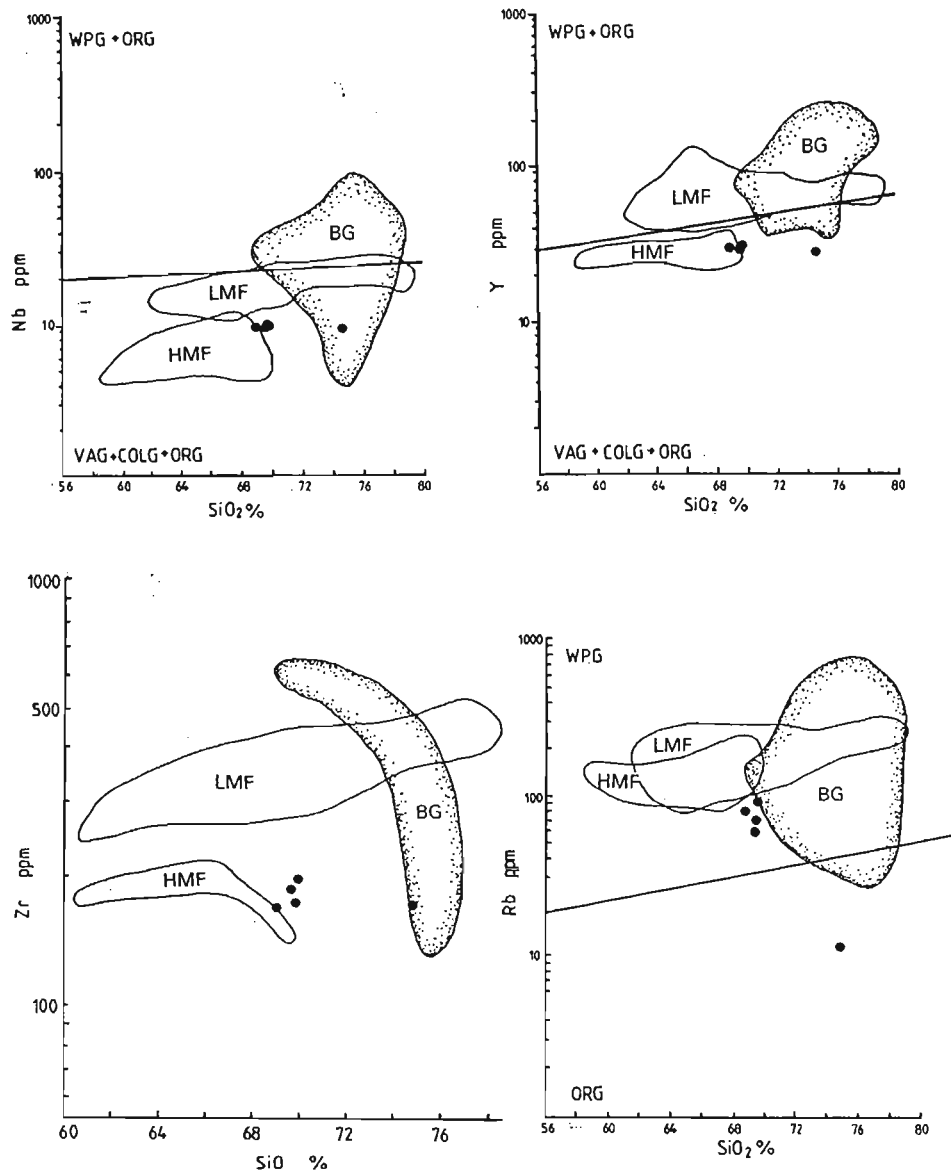
Formations. These compositions are easily distinguished from the basal rhyolites of the Dullstroom Formation and the LMF compositions of both the Kwaggasnek and Schrikkloof Formations. Schweitzer *et al.* (1995) also noted that the LMF type lavas are characterised by decreasing TiO<sub>2</sub> and increasing Zr concentrations towards the top of the Rooiberg Group. This may suggest that the Roodekrans rocks represent a very early, high TiO<sub>2</sub> low Zr, part of this trend.



**Figure 3.18** The Roodekrans quartz-feldspar porphyry plotted against the main chemostratigraphical compositional fields of Schweitzer *et al.* (1995) for the Bothasberg package of the Rooiberg Group in the eastern Bushveld Complex.

The low Nb, Y, Zr and Rb values of the Roodekrans rocks however, compare best to the HMF magma type of the Dullstroom Formation which have lower concentrations of these elements when compared to the LMF magma type of Schweitzer *et al.* (1995). This is best illustrated on the bivariate silica versus trace element tectonic discrimination diagrams after Pearce *et al.*

(1984). These were used by Twist and Harmer (1987) to distinguish the HMF, LMF and Bushveld Granite compositions (Figure 3.19).

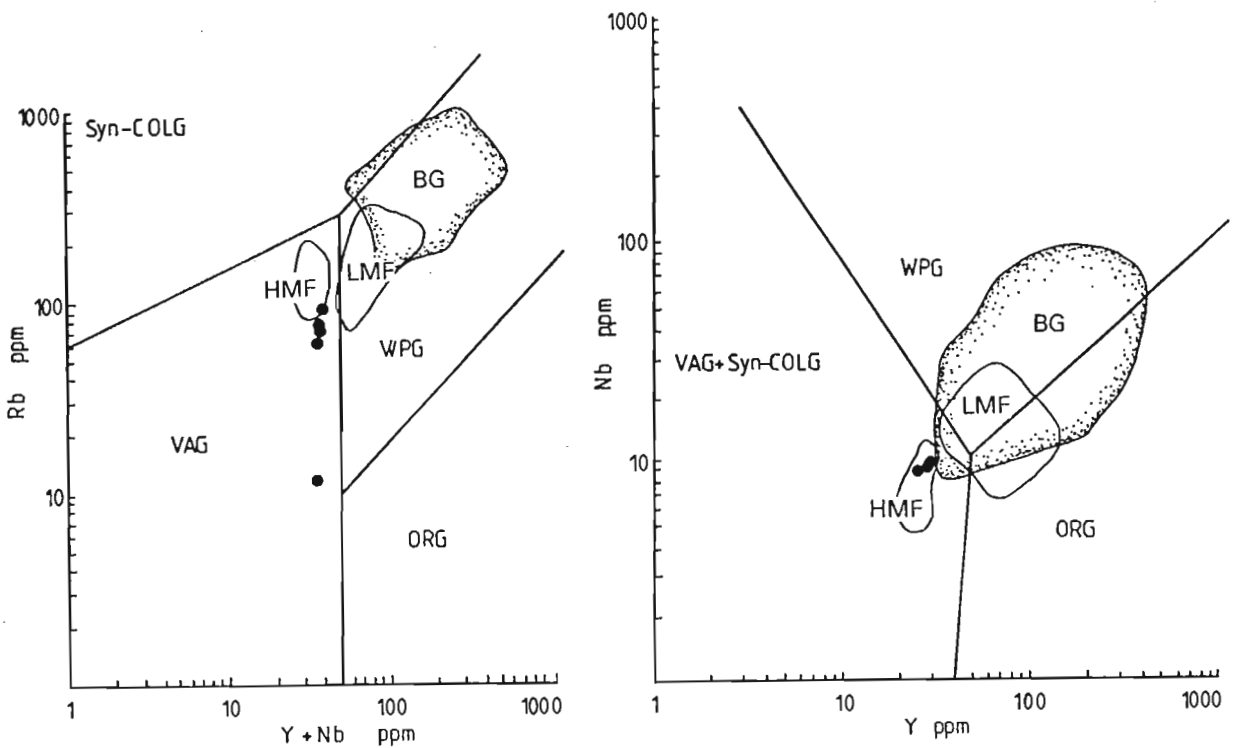


**Figure 3.19** Bivariate silica versus trace element tectonic discrimination diagrams after Pearce *et al.* (1984): (WPG) within plate granite, (ORG) ocean ridge granite, (VAG) volcanic arc granite, (COLG) collision granite. Fields of Bushveld granite (BG), High-Mg felsite (HMF), and Low-Mg felsites (LMF) after Twist and Harmer (1987).

Plots show a linear trend with respect to silica, falling on the same trend as the HMF felsites within the field represented by volcanic arc granites (VAG), collision granites (COLG), and ocean ridge granite (ORG). Rb versus SiO<sub>2</sub> plots are less convincing, with sample RK-5 having anomalously low Rb. Twist and Harmer (1987) however, showed that Rb in Bushveld rocks

was subject to alteration. Anomalously low Rb values in Bushveld granites were ascribed to late stage hydrothermal alteration and fell outside the within-plate field. The other values all fall in the within-plate field showing affinity to the HMF felsite trend.

In Figure 3.20, on the Rb versus Y+Nb binary diagram, all the analyses, including RK-5, fall in the volcanic arc granite field together with the HMF felsites. The same is true for the Nb versus Y diagram.



**Figure 3.20** Rb versus Y+Nb and Nb versus Y tectonic discrimination diagrams after Pearce *et al.* (1984). (WPG) within plate granite, (ORG) ocean ridge granite, (VAG) volcanic arc granite, (COLG) collision granite. Fields of Bushveld granite (BG), High-Mg felsite (HMF), and Low-Mg felsites (LMF) after Twist and Harmer (1987).

#### 3.2.1.4 Conclusions

The timing of the intrusion relative to contact metamorphism, field relationships and geochemistry suggest that the Roodekrans quartz-feldspar porphyry is part of the Bushveld magmatic event, having the closest affinities to the HMF and LMF-type volcanics of the

Dullstroom and the Damwal Formations. Exactly which magma type is not clear, but immobile trace element relationships show the closest affinity to the HMF magma type and the Roodekrans quartz-feldspar porphyry may therefore represent a hypabyssal equivalent of these felsites.

Twist (1985) suggested that the HMF and LMF magma types identified about 100 km to the south of the Roodekrans rocks, were derived from two isolated magma chambers that were normally and reversely zoned. The magma developed by deep crustal anatexis as the mafic Bushveld magmas began their ascent. Melting above a rising mantle plume at progressively higher crustal levels was suggested by Hatton and Schweitzer (1995) with melts undergoing a complex history of partial melting, magma mixing and crustal contamination. Variations within the LMF and HMF were considered by Twist and Harmer (1987) to have resulted from fractionation of similar mineral assemblages during partial melting from chemically distinct sources. They considered the felsites to have developed by partial melting processes, whereas the Bushveld granites represent the product of fractional crystallisation.



# CHAPTER 4

## STRUCTURE

### 4.1 INTRODUCTION

Deformation features in thermal aureoles are a common occurrence, and are particularly well documented from country rocks surrounding steep-sided silicic plutons and batholiths (Buddington, 1959; Pitcher and Berger, 1972; Castro, 1987). In most cases the deformation features are localised within the immediate contact aureole, triggered by a rise in country rock temperature. When areas are intruded by a large number of closely spaced plutons, contact aureole deformation may form a significant part of the total deformation observed in orogenic belts (Hollister and Crawford, 1986; Gastil *et al.*, 1975). According to Buddington (1959) brittle processes such as stoping, block-faulting and cauldron subsidence are commonly associated with shallow plutons whereas ductile deformation processes are evident from deeper intrusions. The Buddington model has more recently been reviewed by Bateman (1984) and Castro (1987). They show that considerable controversy still exists regarding magma ascent processes and the relative importance of various emplacement mechanisms.

Tectonism accompanying the emplacement of flat-lying concordant tholeiitic mafic intrusions (sills and lopoliths) is generally far less spectacular than that found in aureoles associated with discordant silicic plutons. Hornfelsic "static type" contact metamorphism is commonly reported suggesting passive emplacement mechanisms with the magma accommodated by vertical rather than horizontal dilation (Barton *et al.*, 1991). In exceptionally large mafic sill-like intrusions such as the Bushveld Complex however, more complex country rock deformation processes are reported (Hall, 1932). As discussed previously, the most intensely deformed contact metamorphic rocks characterised by schistose rocks are found along the northern margin of the eastern Bushveld Complex. In this area the contact metamorphosed floor dips steeply beneath the Bushveld Complex at between 20° and 80°. The aureole is also at its thickest, possibly representing the deepest exposed part of the contact aureole (Section 2.8.1 and Uken and Watkeys, 1995). Country rocks and xenoliths in the area have a complex deformation history with a range of deformation styles and intricate tectonometamorphic timing relationships (Uken

and Watkeys, 1990, 1994, 1995).

This structural analysis follows the investigations undertaken by Sharpe and Chadwick (1981) who provided a classification of the main structures in the area and examined the associated fabrics, proposing timing constraints on their development. Earlier regional geological mapping (Schwellnus, 1956; Schwellnus *et al.*, 1962; Bastin, 1968) provided evidence for large fold structures in the Bushveld Complex floor and in large xenoliths within the Bushveld Complex. Observations of tectonic fabrics, and dynamothermal metamorphism were also made by Button (1973) and Blain (1975), who noted the occurrence of bedding parallel fabrics in some pelitic units of the Pretoria Group.

#### 4.2 STRUCTURAL SETTING

The northern margin of the eastern Bushveld Complex is characterised by two dominant structural trends; the ENE-trending Mhlapitsi Fold Belt, affecting rocks of the Chuniespoort and Wolkberg Groups (Button, 1973) and large approximately NS-elongated periclinal folds in the immediate floor of the Bushveld Complex, confined only to the contact metamorphosed Pretoria Group (Figure 4.1). Numerous interpretations regarding the relative timing and relationships between these two structural trends for this area have been suggested. Bastin (1968) reported no evidence for interference folding between the two deformation trends and found that they were separated by major decollement surfaces that coincided approximately with the base of the Pretoria Group. This is also indicated on the 1:250 000 scale Geological Survey map sheets, Nylstroom 2428 (1978) and Pilgrims Rest 2430 (1986). These show the sub-Pretoria Group, ENE-trending Mhlapitsi Fold Belt structures, unaffected by the large NNW-trending folds in the overlying Pretoria Group.

Other workers have recognised these two trends throughout the Kaapvaal Craton (Brock and Pretorius, 1964; Hunter, 1974, 1976; Jansen 1975; Clubley-Armstrong and Sharpe 1979). In certain areas the intersection of these trends is considered to have led to interference folding and the development of dome and basin type geometries in the Transvaal Supergroup rocks associated with the Bushveld Complex (Leube, 1960; Verwoerd, 1963; De Waal, 1970; Hunter 1973, 1975; Stear, 1976; Hartzler, 1988, 1989, 1995). Interpretations vary regarding the origin and relative timing of the two structural trends and their deformation in relation to the

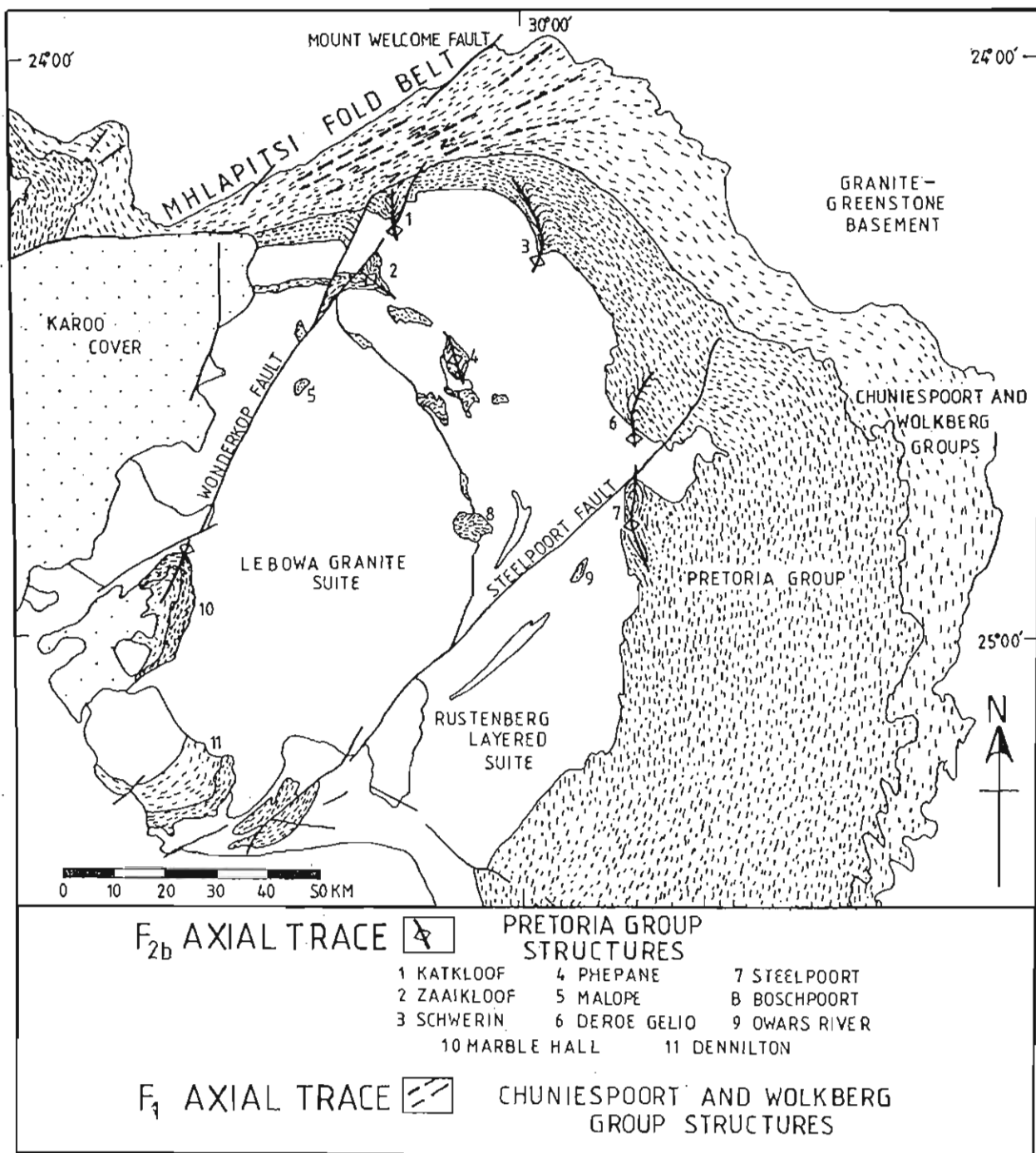


Figure 4.1 Regional structural map of the eastern Bushveld Complex, modified from Sharpe and Chadwick (1981). Form lines show the relationship between the ENE-trending fold axial traces in the Mhlapitsi Fold Belt, the approximately NS-elongated structures in the Pretoria Group, and major faults.

emplacement of the Bushveld Complex. Du Plessis and Walraven (1990) proposed a regional strike-slip tectonic model for the Bushveld Complex. They suggested a period of pre-Bushveld Complex dextral movement in the Thabazimbi-Murchison Lineament (TML) to produce the Mhlapitsi folding. This was followed by a re-orientation of the stress field, resulting in sinistral reactivation of the TML with associated N to NW-trending en-echelon folding by gravity inversion tectonics in the Bushveld Complex floor. Sinistral movement on the TML continued in post-Bushveld times, initiating Waterberg sedimentation and folding of the Bushveld Complex.

Other interpretations have also been made for the origin of the deformed Transvaal Supergroup within the Bushveld Complex. For example, models for the origin of the Crocodile River Fragment (Hartzer, 1989 and references therein) range between: pre-Bushveld folding and doming models; syn-Bushveld Complex xenolith development accompanied by a range of emplacement processes; syn-Bushveld Complex doming and diapirism; and post-Bushveld Complex thrusting models.

#### **4.2.1 Deformation events**

The timing of structural events in the contact aureole can be subdivided into three deformation phases in relation to the emplacement of the Rustenburg Layered Suite of the Bushveld Complex:

- D<sub>1</sub>** - Structures of pre-Bushveld Complex age.
- D<sub>2</sub>** - All syn-Bushveld Complex (Rustenburg Layered Suite) age deformation.
- D<sub>3</sub>** - Post-Bushveld Complex deformation.

Using the above scheme, the interpretations for the ages and origins of the deformations in the study area by previous workers are summarised in Table 4.1.

**Table 4.1** Summary of the major structural events and terminology for the Transvaal Supergroup along the northern margin of the eastern Bushveld Complex as interpreted by previous researchers and for this investigation.

	<b>D1 PRE - BUSHVELD DEFORMATION</b>	<b>D2 SYN - BUSHVELD DEFORMATION</b>	<b>D3 POST - BUSHVELD DEFORMATION</b>
<b>SCHWELLNUS ET AL. (1962)</b>	Gentle Pre-Pretoria Group folding of the Wolkberg and Chuniespoort Groups	Thermal metamorphism followed by folding during the emplacement of the Hendriksplaas Norite	Post-Waterberg faulting and associated intense folding of the Wolkberg and Chuniespoort Groups
<b>BASTIN (1968)</b>	Pre-Pretoria Group folding of the Wolkberg and Chuniespoort Groups	Syn-Bushveld folding affecting only the Pretoria Group with no interference folding of pre-Pretoria structures	Post-Waterberg faulting and folding with some tightening of Pre-Pretoria folds
<b>BUTTON (1973)</b>	Pre-Pretoria Group folding of the Wolkberg and Chuniespoort Groups	Syn-Bushveld folding of the Pretoria Group as diapiric structures (Button, 1978)	Post- Waterberg Deformation
<b>SHARPE AND CHADWICK (1981)</b>	-	Pretoria Group folding due to E-W compression related to subsidence of the Rustenburg Layered Suite	-
<b>DREYER (1982)</b>	All deformation post-dates the Pre-Pretoria Group unconformity		
<b>DU PLESSIS AND WALRAVEN (1990)</b>	Pre-Pretoria Group, Mhlapitsi Belt folding and thrusting due to dextral movement on the TML	Folding of the Bushveld Complex floor as en-echelon folds related to sinistral movement on the TML and gravity inversion tectonics	Continued sinistral TML movement offsetting earlier Mhlapitsi belt structures
<b>MIYANO ET AL. (1987)</b>	-	-	Mhlapitsi Fold Belt is post-Waterberg in age

POTGIETER (1991)	D1 Pre-Pretoria F1 kink folding in Wolkberg and Chuniespoort Groups	D2 Syn-Bushveld tightening of F1 folds in Mhlapitsi Fold Belt		
THIS STUDY	D1 Pre-Pretoria Group deformation (S1 is not developed in the Pretoria Group)  <i>F1 folds and uplift to produce sub-Pretoria Group unconformity</i>	D2 Syn-Bushveld Deformation		D3 Post-Waterberg deformation
		D2a  <i>F2a folds in Chuniespoort Group</i>  <i>S2a fabric and L2a lineations in the Pretoria Group</i>	D2b  <i>F2b folds in Pretoria Group only</i>  <i>S2b axial planar cleavage fabric</i>	<i>Strike-slip faulting and local modification of F2 folds</i>

#### 4.2.2 ENE-trending structures

Most of the interpretations regarding the age of the ENE-trending Mhlapitsi Fold Belt structures considered the deformation to be unrelated to Syn-Bushveld Complex tectonism (Schwellnus *et al.*, 1962; Bastin, 1968; Button, 1973; Miyano *et al.*, 1987; du Plessis and Walraven, 1990). Schwellnus *et al.* (1962) were of the opinion that most of the deformation was synchronous with strike-slip faulting along the Wonderkop Fault in post-Bushveld Complex, post-Waterberg time. They did however indicate that "milder" folding in the Wolkberg and Chuniespoort Groups was of pre-Pretoria Group age. Bastin (1968) however, considered that most of the deformation was earlier, of pre-Pretoria Group age, but was modified by later post-Waterberg deformation associated with the development of the Wonderkop Fault. This view was supported by Button (1973) and more recently by du Plessis and Walraven (1990), who similarly suggested that the Mhlapitsi folding pre-dated the Bushveld Complex and also the pre-Pretoria Group unconformity. Other researchers such as Miyano *et al.* (1987) suggested that all the deformation in the Mhlapitsi Fold Belt was much younger in age, and developed during post-Waterberg times.

Dreyer (1982), working on the asbestos deposits in the Chuniespoort Group, similarly

concluded that the deformation was post-Pretoria Group in age as pre-Bushveld Complex sills that transect the pre-Pretoria Group unconformity were deformed within the Chuniespoort Group. K. Weber (pers. comm., 1991) also suggested that the development of asbestos fibres in the Chuniespoort Group banded ironstones of the Penge area, most likely developed syntectonically during Bushveld metamorphism. This would imply that at least some of the deformation in the Mhlapitsi Fold Belt was synchronous with the emplacement of the Bushveld Complex. This view was also expressed by Potgieter (1991), who indicated the presence of two fold phases in the sub-Pretoria Group strata which he termed  $F_1$  and  $F_2$  folds. He found that both  $F_1$  and  $F_2$  folds were nearly coaxial.  $F_1$  folds, characterized by north-vergent  $F_1$  kink-folds, were interpreted as pre-Pretoria Group in age ( $D_1$ ) whereas tight  $F_2$  isometric-folds, occurring only in the vicinity of the Bushveld Complex, were interpreted as post-Pretoria Group, Syn-Bushveld age.

#### 4.2.3 NS-trending structures

Most researchers concluded that the large floor folds found only in the Pretoria Group are in some way related to the emplacement of the Bushveld Complex and distinct from the ENE-trending Mhlapitsi Fold Belt. These form the main  $D_2$  structures of Syn-Bushveld Complex age. Schweltnus (1956), Schweltnus *et al.* (1962) and Bastin (1968) considered the folds to have developed as a direct result of forceful emplacement of the Hendriksplaas Norite into the Pretoria Group. Other interpretations considered regional compression as a possible mechanism for the development of the fold structures (Snyman, 1958; De Waal, 1970; du Plessis and Walraven, 1990).

Button (1978) proposed that the structures may be of diapiric origin. He envisaged ductile deformation and buoyant rise of the Transvaal rocks into the magmas of the Bushveld Complex. Sharpe and Chadwick (1981) however, concluded that although diapiric rise may have assisted in the development of the fold structures, the most important mechanism was due to compressional forces. They suggested that basin-wide compression in the Transvaal Supergroup resulted from subsidence of the Transvaal basin and subsequent emplacement of the Bushveld Complex. Heating of the floor by the Bushveld Complex increased ductility and buckling of the floor strata and deformation proceeded readily in response to the subsidence induced compressions as modelled by Sharpe and Snyman (1980). Du Plessis and Walraven (1990) on the other hand, although acknowledging the importance of gravity inversion

tectonics, suggested that the folds developed in a sinistral strike-slip setting as linked en-echelon folds.

#### 4.2.4 Terminology

For the purposes of this investigation, Potgieter's (1991) terminology for the ENE-trending fold structures is maintained (Table 4.1). Early pre-Bushveld Complex ( $D_1$ ) structures within the contact aureole are represented by the  $F_1$  folds described by Potgieter (1991) and are truncated by the pre-Pretoria Group unconformity.  $S_1$  is not developed in the Pretoria Group. Syn-Bushveld Complex ( $D_2$ ) structures, represented by the  $F_2$  folds recognised by Potgieter (1991) in the Mhlapitsi Fold Belt are here termed  $F_{2a}$  fold structures, and the large floor folds within the Pretoria Group,  $F_{2b}$  folds. Planar and linear fabrics associated with the Pretoria Group strata in the interpericlinal domains are termed  $S_{2a}$  and  $L_{2a}$  whereas planar and linear fabrics found within the large Pretoria Group folds (periclinal domains) are termed  $S_{2b}$  and  $L_{2b}$  respectively (Table 4.2).

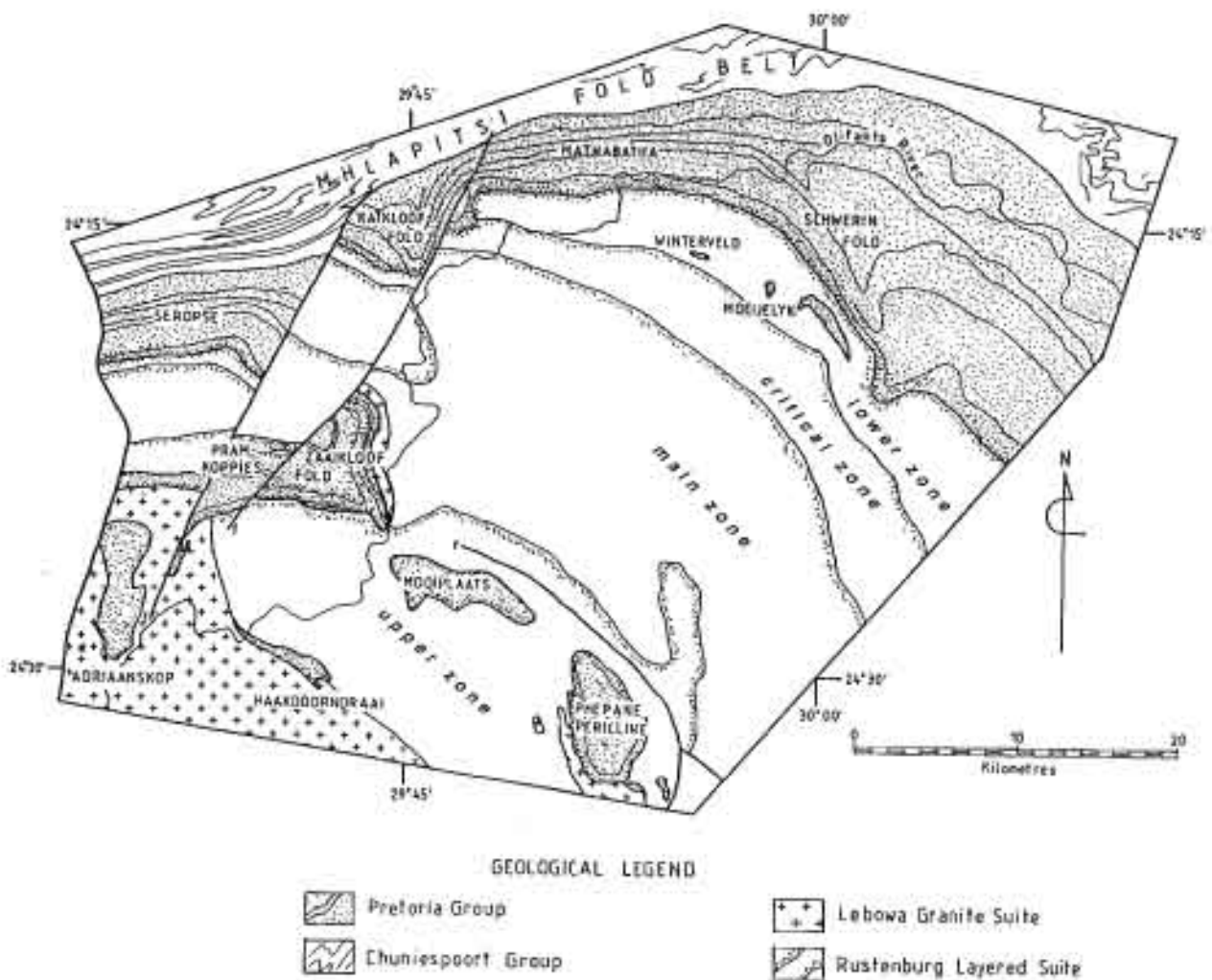
**Table 4.2** Classification and subdivision of the major  $D_2$  domains within the Bushveld Complex. The relationship of the country-rock fragments within the Bushveld Complex can be subdivided into xenoliths or up domed and folded Pretoria Group floor.

FLOOR ATTACHED PRETORIA GROUP		PRETORIA GROUP EXPOSURES WITHIN THE BUSHVELD COMPLEX	
INTERPERICLINAL DOMAINS (Unfolded floor) $S_{2a}$ , $L_{2a}$ foliation	PERICLINAL DOMAINS (Folded floor rocks) $S_{2b}$ , $L_{2b}$ foliation		XENOLITHS
Mathabatha domain  Seropse domain	Katkloof Fold domain  Schwerin Fold domain	Zaakloof-Prankoppies Fold domain  Adriaanskop domain  Phepane Fold domain	Mooiplaats/ Haakdoorn-draai domain  Winterveld/Moeijelyk domain



### 4.3 SYN-BUSHVELD (D<sub>2</sub>) DEFORMATION OF THE PRETORIA GROUP

The Pretoria Group rocks can be subdivided into two categories: Strata that are either visibly attached to the underlying Chuniespoort Group and strata that occur within the Bushveld Complex as isolated fragments (Table 4.2). The relationship of the "fragments" with the Bushveld Complex is debatable, representing either xenoliths detached or partly detached from the Transvaal Supergroup floor or large inliers of up domed or faulted floor within the complex. This simple classification forms the basis of the subdivision of the contact metamorphosed Pretoria Group in the study area into the various structural domains shown in Figure 4.2.



**Figure 4.2** Map of the study area showing the distribution of the Pretoria Group rocks in relation to the Bushveld Complex and the domainal subdivisions. Along the northern margin of the study area, the Pretoria Group is still visibly attached to the underlying Chuniespoort Group rocks, but its relationship to the floor within the Bushveld Complex is debatable.

The floor-attached domains comprise the two large  $D_2$ ,  $F_{2b}$  floor folds, the Katkloof and Schwerin Fold domains and the unfolded Mathabatha and Seropse domains. Two major  $F_{2b}$  folds occur as "fragments" within the Bushveld Complex, forming the Zaaikloof Fold domain and the Phepane Fold domain. The term "fragment" historically refers specifically to the large country-rock inliers within the Bushveld Complex and does not imply that they are true xenoliths. The other domains form smaller fragments and xenoliths between these larger structures.

Fabric data collected in the field from various stations in each structural domain are presented as lower hemisphere, equal-angle stereographic projections. These are supplemented by microtextural studies on orientated samples collected at these localities. The microtextural relationships between porphyroblasts and cleavage are useful for determining the relative timing of porphyroblastic growth and fabric-forming events. This topic is therefore of considerable importance and is discussed separately in Chapter 6.

#### **4.3.1 The Mathabatha domain**

The Mathabatha domain comprises the area between the Katkloof Fold in the west and the Schwerin Fold in the east, extending along strike for a distance of approximately 20 km (Appendix 1:map sheet B). Structural data for the area are presented in Figure 4.3. The structure is characterised by southward dipping, east-west striking, floor-attached Pretoria Group strata (Figure 4.4). Superimposed on this is a more steeply southward dipping to bedding parallel  $S_2$  fabric with a commonly associated  $L_2$  linear fabric. L-S tectonites are found throughout the Pretoria Group, but are not penetrative in the complete succession and are mainly confined to low competency, pelitic and micaceous units. Igneous layering in the overlying Rustenburg Layered Suite is slightly discordant to the floor rocks, having a similar strike but dipping at a slightly shallower angle towards the south.

Sedimentary stratification is well preserved throughout the area. On an outcrop scale, primary sedimentary features are usually visible and are often accentuated by a change in the degree of crystallinity, metamorphic mineral assemblage, and grain size. In pelitic and semi-pelitic rocks for example, fine ripple laminations, graded bedding, and ripple marks on bedding surfaces are usually present (Figure 4.5). Graded beds are usually in the order of 10 cm in thickness. The upper finer-grained argillaceous portions of the rhythmic units consist of the

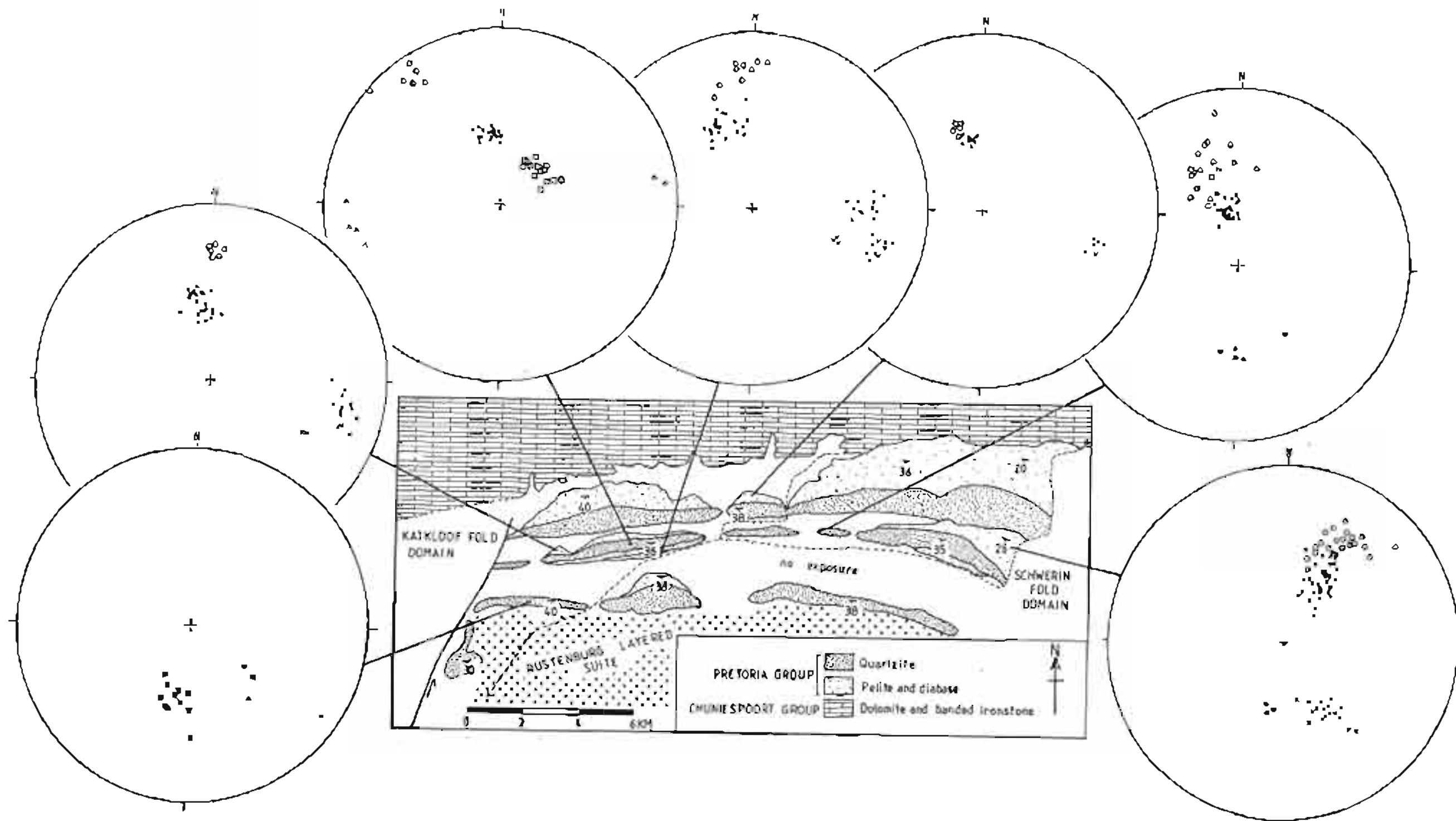


Figure 4.3 Equal angle, lower hemisphere projections of structural data from various stations in the Mathabatha domain. Poles to moderately southward dipping strata (●) and poles to more steeply southward dipping  $S_{2s}$  planar foliation (○) with an eastward plunging  $L_{2s}$  linear fabric (x).  $D_1$  boudins (◆), mesoscale  $F_1$  folds (■), a flat-lying  $S_3$  crenulation cleavage (□), and late stage, near vertical kinkbands (△) are locally represented.



**Figure 4.4** View towards the east across the Malips River of the Mathabatha domain showing the southward dipping strata. The three ridges, from left to right are formed by the Klapperkop Quartzite Member of the Timeball Hill Formation, the Dwaalheuwel Quartzite Formation and the Magaliesberg Quartzite Formation.



**Figure 4.5** Typical outcrop of alternating darker pelitic layers (garnet-biotite-staurolite-andalusite assemblages) with semi-pelitic layers (biotite-quartz assemblages) in the upper part of the lower pelitic unit of the Timeball Hill Formation on the farm Uitkyk. Note the excellent preservation of sedimentary structures. Scale length = 14 cm.

coarsest porphyroblasts, producing a reversal in grain-size, in comparison to the original grading. On a micro-scale helicitic textures are common, with the original layering still discernable within large porphyroblasts (Figure 4.6).  $S_0$  becomes increasingly difficult to recognise as the contact with the Bushveld Complex is approached, where schistose fabrics are more intensely developed and partial melting has occurred. Within the Mathabatha domain, dips increase from east to west, ranging from about  $25^\circ$  to  $55^\circ$  towards the south.



Figure 4.6 Photomicrograph of helicitic staurolite (pale euhedral crystals) and biotite porphyroblasts (dark elliptical flakes) from a staurolite-chiastolite-biotite contact fels on the farm Hoogenoeg. Plane polarised light. Width of view = 20 mm.

### *$S_2$ cleavage fabric*

The  $D_2$ ,  $S_2$  foliation is most pronounced in relatively incompetent pelitic units (Figure 4.3) and is often absent in more competent quartzitic rocks and diabase sills. The inhomogeneous nature of the lithologies within the thermal aureole has resulted in strain partitioning during the development of  $S_2$ , with the development of higher and lower strain zones. Cleavage refraction between various layers results in near-bedding-parallel  $S_2$  cleavage in highly incompetent micaceous layers and a steeper dipping fabric in relatively more competent units.

In general the foliation intensity also increases with metamorphic grade and mica coarsening. In the migmatite zone (Figure 6.2), leucosomes are generally bedding parallel (compositional banding) with biotite-rich melanosomes defining a pronounced schistose fabric. In the Dwaalheuwel Quartzite Formation, sericite in the groundmass and elongate recrystallized quartz grains define the cleavage fabric. The intrusive quartz-feldspar porphyry in the eastern part of the area on the farm Groenfontein is structureless, but becomes foliated with  $S_2$  to the west of the farm Mathabatha. Phenocrysts have recrystallized quartz and plagioclase strain shadows developed in the  $S_2$  plane of orientated biotite and hornblende grains.

Throughout the area, cleavage bedding relationships indicate northward-vergence with  $S_2$  striking subparallel to  $S_0$  but dipping more steeply towards the south (Figure 4.3). Close examination of  $S_2$  -  $S_0$  relationships and porphyroblast-matrix microstructural relationships however, indicate that the fabric is an extensional shear fabric, with a top toward south shear component. This is described in greater detail in Chapter 6.

A general increase in the extent of the development of the  $S_{2a}$  cleavage fabric was noted from the east towards the west within the Mathabatha domain. In the eastern part of the area, the lower pelitic unit of the Timeball Hill Formation has a poorly developed fabric which gradually increases in intensity towards the western part of the area. This feature is important within the context of the overall model for the deformation within the aureole and will be addressed below.

### *D<sub>2</sub> boudin structures*

Large metre-scale boudins are developed in the more competent coarse-grained arenaceous and conglomeratic units within the Dwaalheuwel Quartzite Formation. Dilational quartz veins fill the areas between respective boudins, with some degree of matrix flow into the neck region as a scar fold (Figure 4.7). This combination suggests that boudins were developed during tensile failure under brittle-ductile conditions (Price and Cosgrove, 1990). Under these conditions (upper andalusite zone) pelitic units within quartzitic multilayers behave as the incompetent layers. Boudin axes trend approximately north-south, plunging towards the south at between  $38^\circ$  and  $42^\circ$ , sub-parallel to the local  $S_0$  dip direction. Occasional north-south orientated lensoid-shaped quartz veins up to 5 m in length are also found within the lower pelitic unit of

the Timeball Hill Formation on the farm Voerspoed. This orientation is almost  $90^\circ$  to the mineral stretching  $L_2$  lineation, and therefore consistent with a maximum extension in the east-west direction during  $D_2$  deformation in this domain.



**Figure 4.7** Large boudin structures in a pebbly quartzite layer of the Dwaalheuwel Quartzite Formation from the farm Mathabatha. Note the quartz dilational veins in the boudin neck and the limited flow into the neck region of less competent micaceous material. Scale size = 25 cm.

In the Magaliesberg Quartzite Formation, within the partial melt or migmatite zone of the aureole, boudins are typically asymmetrical in shape (Figure 4.8a and b), associated with sigmoidal pinch and swell structures (Figure 4.8c), conjugate extensional ductile shears (Figure 4.8d) and oversteepened sigmoidal-shaped crossbeds. The spectrum of boudin geometries is a reflection of the wide range in rheological behaviour and competency contrasts within the Magaliesberg Quartzite Formation. Contrary to the boudins at lower metamorphic grades (andalusite zone), at these grades, the pelitic units within the quartzitic multilayers behaved as the relatively more competent layers (Figure 4.8a). Similar temperature-composition-viscosity relationships were experimentally produced in a quartzite-marble multilayer (Parrisch *et al.*, 1976). Wet quartzite viscosity was found to be more strongly temperature dependant in

comparison to marble viscosity, resulting in a viscosity ratio switch at about 550°C when quartzite becomes less competent than the marble. In this case the pelite-quartzite viscosity switch in the aureole corresponds approximately to upper part of migmatite zone of the aureole. At lower grades quartzitic units enclosed in a pelitic unit are boudinaged. At metamorphic grades within the migmatite zone, quartzofeldspathic leucosomes approach Newtonian ductility whereas the melanosome or restite remains less ductile and deforms incompetently as boudins within the ductile matrix. This is particularly pronounced in the Magaliesberg Quartzite Formation where thin pelitic beds occur within a predominantly quartzofeldspathic succession.

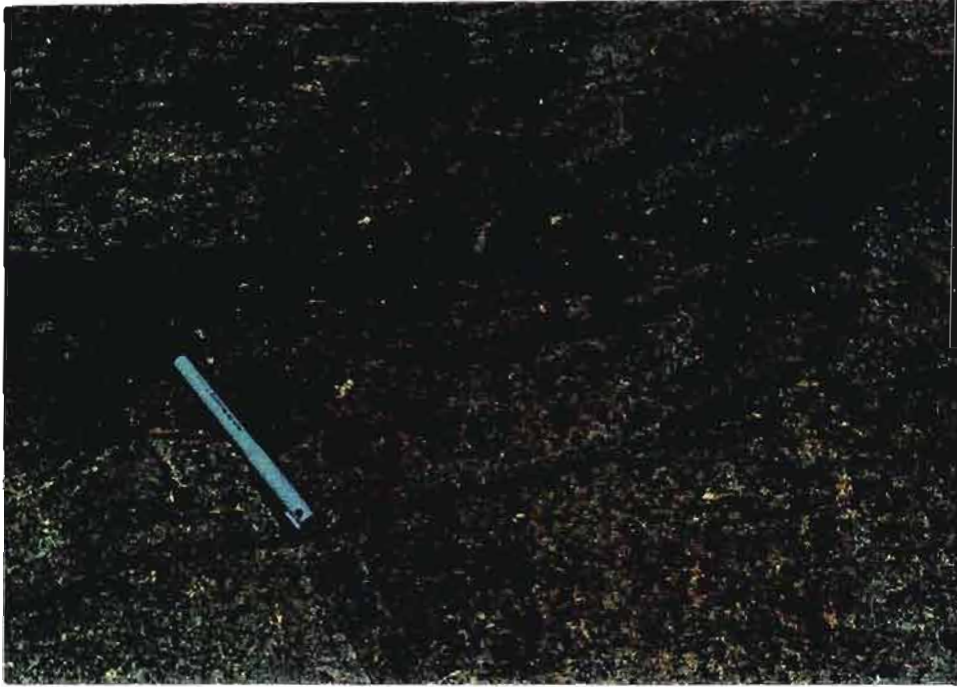
Down-plunge sections on a single exposure of boundinage in the Magaliesberg Quartzite Formation, indicate both relative clockwise (Figure 4.8a) and anticlockwise rotation (Figure 4.8b) of individual boudin units in various parts of the exposure. The largest apparent rotation is developed in boudins with the lowest cross-sectional aspect-ratio.

Experimental models have shown that asymmetrical boudinage is commonly produced when the layering is orientated obliquely to the principle strains within the zone of extension (Ramsay, 1967). This however, would tend to produce a consistent rotation sense rather than an opposing sense of rotation within a single exposure. Closer examination indicates that some boudins are separated by discrete conjugate extensional ductile shears (Figure 4.9d) producing an asymmetrical internal boudinage (Cobbold *et al.*, 1971; Platt and Vissers, 1980) explaining the apparent opposite sense of rotation within a single outcrop.

Acute and obtuse bisectors of the conjugate ductile shear surfaces provide the principle stress orientations and the orientation of the  $D_2$  strain ellipsoid (Figure 4.9). The maximum shortening direction, in contrast to brittle shear failure, is determined by the obtuse angle between the shears, which in this case is approximately 122°. Typically this angle ranges between 90° and 130° (Ramsay, 1980). The boudin structures are consistent with a strain ellipsoid orientated with the maximum extension direction normal to the boudin axes and parallel to the  $L_2$  mineral lineation direction. The intermediate stress orientation approximates the boudin axis orientation and the maximum compressive direction is approximately normal to the  $S_{2a}$  foliation orientation.



**a**

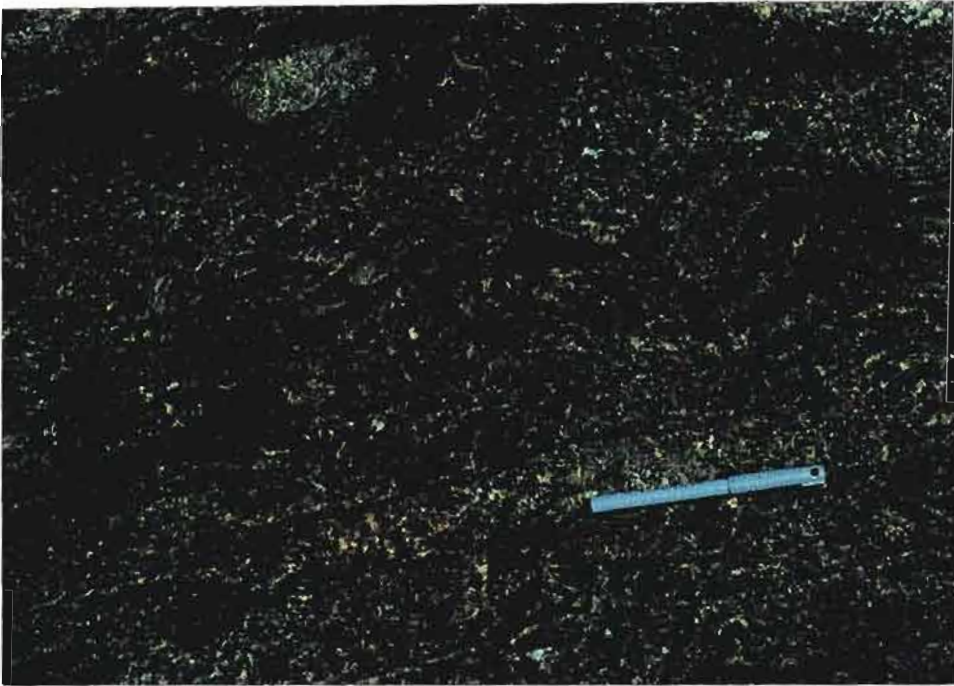


**b**



**Figure 4.8** Downdip view of structures in the Magaliesberg Quartzite Formation near Malips Drif. **a)** Asymmetrical, rhomboidal-shaped boudinage in an andalusite-fibrolite-biotite layer in matrix quartzite with a clockwise rotation sense. **b)** Asymmetric boudinage with anticlockwise rotation. Scale size = 14 cm.

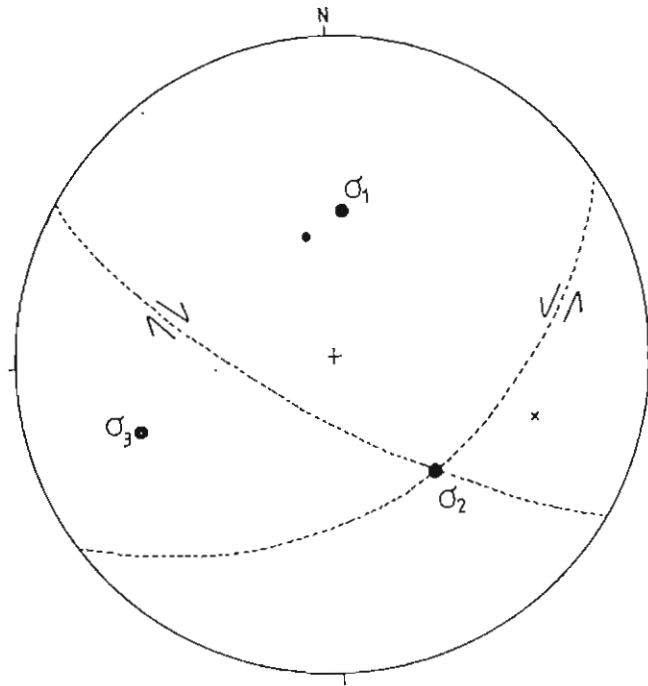
**c**



**d**



**Figure 4.8 cont.** c) Sigmoidal pinch and swell structures indicating left-lateral sense of shear. d) Asymmetric boudinage associated with discrete extensional ductile shear immediately right of pen. Scale size = 14 cm.



**Figure 4.9** Lower hemisphere, equal angle stereographic projection showing the relationship between conjugate extensional ductile shears (---), associated with the asymmetrical boudinage, and the orientations of the  $D_{2a}$  principle stress axis ( $\sigma_1$ ,  $\sigma_2$ ,  $\sigma_3$ ). Average poles to bedding (●)  $L_{2n}$  linear fabric (x).

In addition, the common occurrence of deformed cross-bedding, usually seen as sigmoidal-shaped sets within the bedding, suggests that deformation proceeded by a process of pure homogeneous shear within certain domains, and not only as spaced ductile shears. In the Mathabatha area crossbed geometries, viewed down-dip are consistent with a dominantly sinistral, close to bedding-parallel shear sense.

This would suggest that the bulk deformation within the Magaliesberg Quartzite Formation in the interpericlinal domains was dominated by pure shear and that deformation proceeded via a combination of bedding parallel shearing and conjugate extensional shear bands. This has produced a series of deformed cross beds and individual beds undergoing back rotation between conjugate sets of extensional shears.

### *$L_2$ mineral stretching lineations*

The chistolite schists within the fibrolite zone are usually strongly lineated (Figure 4.10). Lineations are defined by quartz pressure shadow zones in boudinaged chistolite crystals

**a**



**b**



Figure 4.10 a) Chiastolite-biotite-muscovite schist exposed in old andalusite workings on the farm Mathabatha, showing prominent southward dipping  $S_{2s}$  fabric and easterly plunging  $L_{2s}$  lineation. b) Boudinaged chiastolite crystals with quartz infill (arrowed) defining the  $L_{2s}$  lineation. Bedding is visible as colour banding. Outcrop on the farm Copper. Scale length = 14 cm.

elongated in the direction of maximum finite extension. Sanderson and Meneilly (1981) showed that these can be useful strain indicators. Measurement of some boudinaged chistolite crystals showed a maximum elongation of approximately 30 percent, parallel to the lineation direction in the plane of the  $S_{2a}$  schistosity. These microtextures and their interpretations are discussed in more detail in Chapter 6.

Stretching lineations over most of the Mathabatha domain plunge at shallow angles (between  $15^\circ$  and  $30^\circ$ ) towards the east, and locally steepen in the eastern portion of the domain (Figure 4.3). The steeper plunging lineations were possibly deformed by the  $F_3$  Schwerin Fold and this aspect is investigated in more detail below.

### *Deformed pebbles*

Quartz pebbles in the Dwaalheuwel Formation are deformed with an east-west elongation direction, sub-parallel to the strike of the strata. Direct measurements of deformed pebbles on the farm Mathabatha, give axial ratios of 1 : 1.1 : 1.8. (n=40). This provides an estimate of the  $D_2$  strain ellipsoid which is prolate in shape, plotting in the apparent constrictional field of the Flinn diagram with a k-value of 6.6 (Figure 4.11a).

Strain analysis using the methods described by Ramsay and Huber (1983) are presented in Figure 4.11b. These data provide an estimated minimum tectonic strain ratio ( $R_T$ ) of 2.61 as the pebbles had a variable initial shape ratio and a primary depositional preferred orientation. An added problem is produced by strain partitioning between pebble and matrix, and varying pebble composition (Ramsay, 1967).

### *$F_2$ folds*

Metre-scale open folds were observed in the Magaliesberg Quartzite Formation on Holla mountain on the farm Koedoeskop and Mathabatha and further to the west on the farm Inkomst (Appendix 1A and 1f). Where partial melting has occurred in the pelitic rocks nearest the contact with the Bushveld Complex, quartzofeldspathic veinlets are generally concordant with the  $S_0$  bedding surfaces, but in places, they are deformed into small, often intrafolial folds within the  $S_{2a}$  schistosity, with fold axes generally subparallel to the  $L_{2a}$  lineation direction (Figure 4.12).

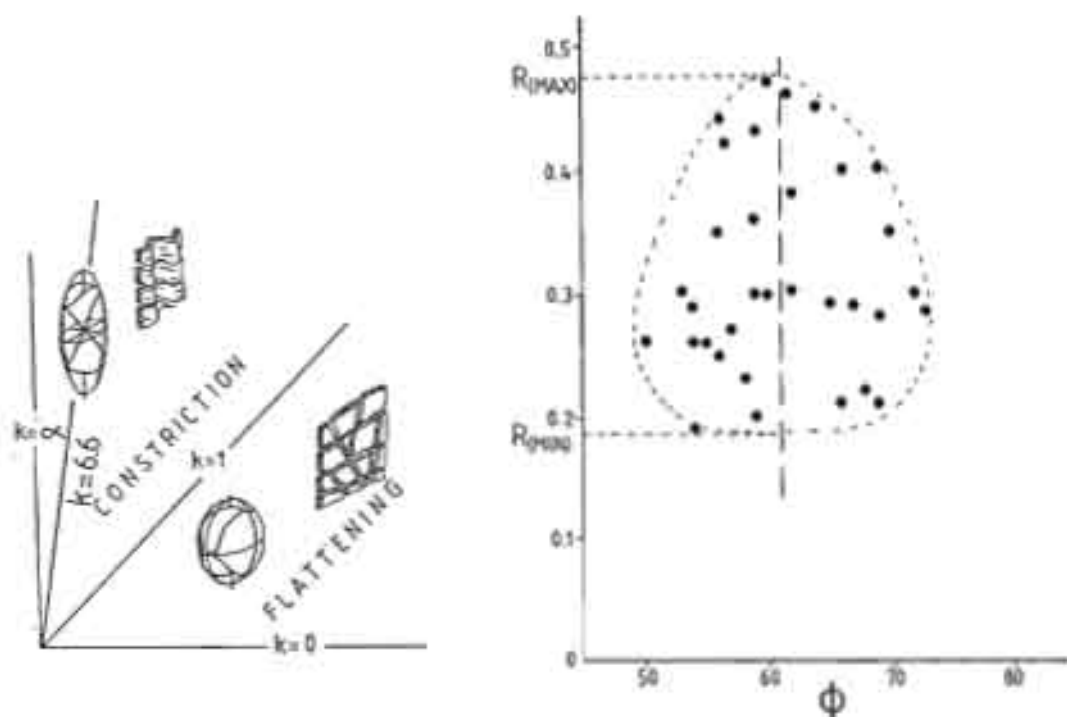


Figure 4.11 a) Plot of the strain ellipsoid on the Flinn graph (after Ramsay and Huber, 1983). ( $R_{YZ} = 1.05$ ,  $R_{XY} = 1.33$ ,  $K = 6.6$ ). b)  $R_T / \phi$  plot of deformed pebbles from the Dwaalheuvel Quartzite Formation from the farm Mathabatha ( $R_T = 2.61$ , where  $R_T = R_{MAX} / R_{MIN}$ ).

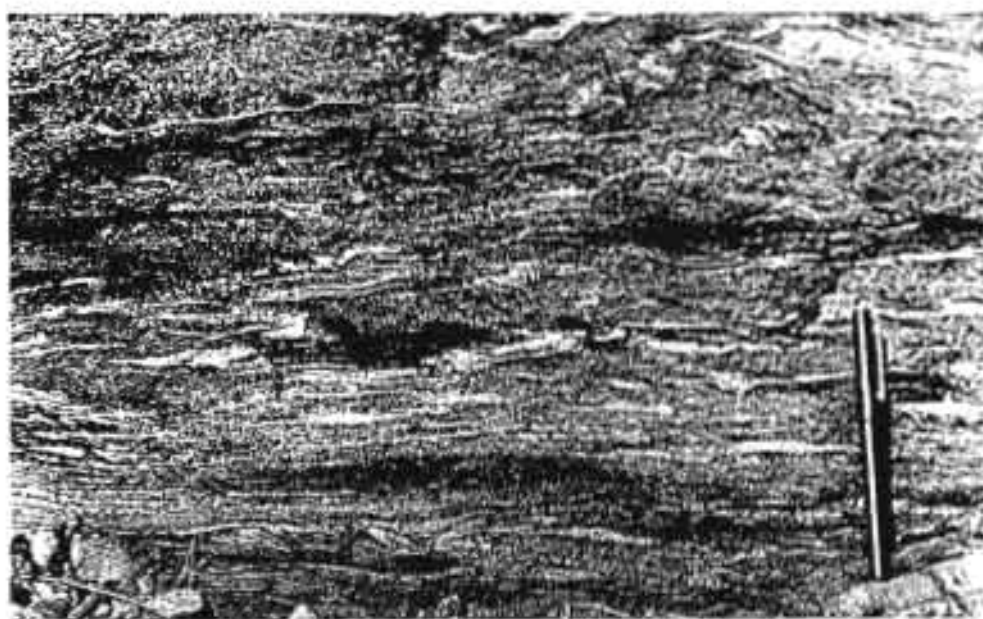


Figure 4.12 Deformed leucosome veinlets from the farm Jobskop in the eastern part of the Mathabatha domain. Structural data from the area shows the small-scale fold axes as subparallel to the  $L_2$  lineation direction. Scale length = 14 cm.

This relationship suggests that leucosomes developed during progressive deformation pre- or very early in the deformation event and that the small intrafolial folds were produced by layer parallel stretching after layer parallel folding. Most veinlets are orientated parallel to the schistosity but a few cross-cut the schistosity, suggesting a post- $S_{2a}$  veining event, resulting in various timing relationships being present at a single outcrop. Sharpe and Chadwick (1982) reported similar features from the Zaaikloof area, where quartzofeldspathic neosomes are developed parallel to bedding, folded with the bedding, and cross-cutting schistosity. These timing relationships indicate that metamorphism and deformation were closely linked. They either represent discrete deformation events or are the result of a single progressive tectonometamorphic event.

The latter interpretation seems most likely as it is supported by porphyroblast-matrix relationships at lower grades where only a single  $D_2$  event is recorded. This is further supported by the work of McLellan (1982), who cautions at interpreting timing relationships in migmatites due to numerous distinct events. This is due to the extreme viscosity contrasts between leucosome and melanosome, and the often non-Newtonian behaviour of the materials. The complex timing relationships seen in relatively simple single phase tectonometamorphic cycles, such as represented in contact aureoles, thus provide a valuable insight into the development of migmatites in more complex regional migmatitic terranes where standard structural techniques and timing criteria may result in misinterpretations.

### *$F_{2b}$ folds*

Occasional open, metre-scale folds were observed in the Magaliesberg Quartzite Formation in the Malips area on the farm Inkomst (Appendix 1A and 1F). The folds plunge towards the south at between  $30^\circ$  and  $40^\circ$  subparallel to the boudin axes and the fold axis of the Katkloof Fold. The fact that these folds were only observed at this locality, close to the western limb of the Katkloof Fold, suggests that they are minor, second order folds related to the development of the  $F_{2b}$  Katkloof Fold structure. Locally the folds deform the earlier  $D_{2a}$  age structures, which suggests that the  $F_{2b}$  folds developed during E-W directed layer-parallel shortening as opposed to E-W directed layer-parallel extension.

### *D<sub>3</sub> thrusting*

In the eastern part of the area, within the upper pelitic unit of the Timeball Hill Formation on the farm Copper, an approximately 5 m wide high-strain zone, characterised by a pronounced schistosity is associated with a brittle-ductile shear with a reverse, top towards north displacement of about 20 cm. The structure is interpreted as a late top to north D<sub>3</sub> thrust in which the earlier S<sub>2a</sub> foliation has been reactivated. Thrusting is associated with retrograde metamorphism and is not the same as the prograde S<sub>2a</sub> foliation.

### *S<sub>3</sub> crenulation cleavage fabric*

This fabric is not found throughout the area and is restricted to very micaceous rocks with a strong S<sub>2a</sub> cleavage fabric such as the thin micaceous horizons in the lower Dwaalheuwel Quartzite Formation. The earlier dominant S<sub>2a</sub> foliation is deformed into millimetre-scale asymmetrical crenulations in places, in which the S<sub>3</sub> spaced fabric is defined by every alternate limb (Figure 4.13a). The S<sub>3</sub> fabric is generally near flat-lying. The S<sub>3</sub> foliation is associated with a top to north shear component indicating a compressional condition of formation. Structural relationships within these rocks are shown in Figure 4.13b.

The Wonderkop Fault is post-Bushveld Complex in age, displacing both the Rustenburg Layered Suite and the Lebowa Granite Suite (Appendix 1). Thrusting is associated with top to north movement which is compatible with the deformation represented by the late-stage localised development of the S<sub>3</sub> crenulation cleavage. The crenulation cleavage is associated with intense sericitisation and in places with sericitisation of andalusite porphyroblasts. This indicates that Wonderkop, post-Bushveld Complex age deformation may be associated with the retrograde metamorphism in the contact aureole and may represent the final stages in the tectonometamorphic evolution of the contact aureole in the study area.

### *D<sub>3</sub> kink banding*

In the micaceous schists of the Dwaalheuwel Formation, centimetre-sized kink-bands crosscut the D<sub>2</sub> foliations. Individual kink-bands are usually up to two centimetres in width, and generally strike north-south and dip steeply towards the east or west. The fact that they typically have a sinistral displacement sense and are found in the vicinity of left-lateral strike-slip faults, suggests that they were developed during the D<sub>3</sub> deformation event. This is



represented by the NE trending Wonderkop Fault system and the Steelpoort Fault to the southeast of the study area.

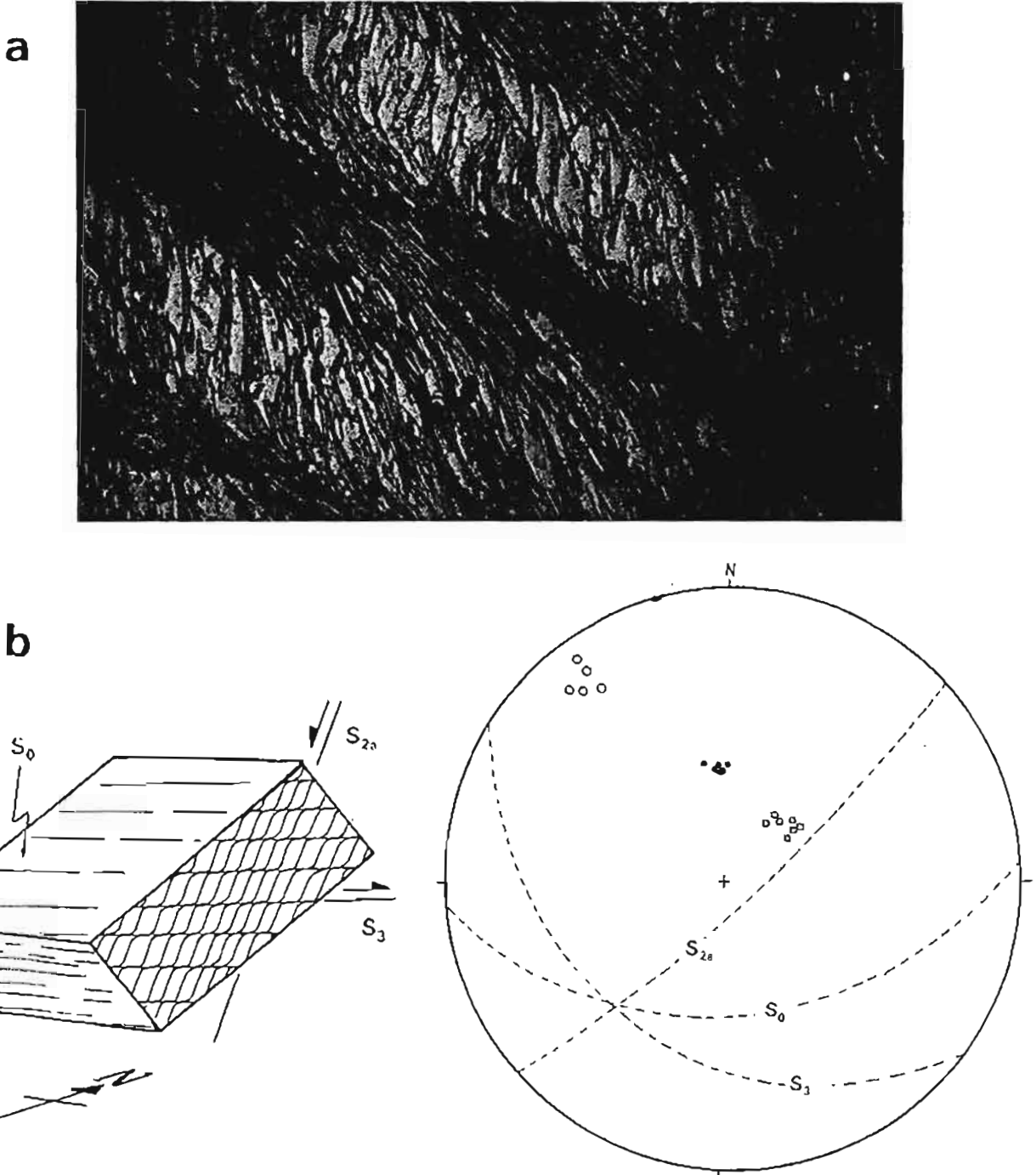


Figure 4.13 a) Photomicrograph of the S<sub>3</sub> crenulation cleavage. The second cleavage (S<sub>3</sub>) deforms the S<sub>2n</sub> transposition foliation. Sample collected on the farm Mathabatha. Section cut normal to the crenulation fold axis. Width of view = 6 mm b) Diagram and orientation data shown on a lower hemisphere equal-angle stereographic projection.

### 4.3.2 The Seropse domain

The area extending westwards from the Wonderkop Fault to the western boundary of the study area comprises the Seropse domain (Appendix 1, map A). Structural fabric data for the area are represented in Figure 4.14. As in the Mathabatha domain, floor-attached contact metamorphosed Pretoria Group rocks are underlain by tightly folded Chuniespoort Group rocks. In comparison to the Mathabatha domain, the pelitic units are not as well exposed, limiting detailed study. The contact with the Rustenburg Layered Suite is considered to be concordant and corresponds approximately with the contact between the Magaliesberg Quartzite Formation and the Vermont Hornfels Formation. The strata dip considerably steeper towards the south than those of the Mathabatha domain. LS-type fabrics are present in most micaceous units in the Dwaalheuwel Formation.

The strata strike approximately east-west and dip towards the south between  $58^\circ$  and  $70^\circ$  with a general increase in dip from east to west. In the eastern part of the area the strike swings towards the SE, a continuation of the eastern limb of the Katkloof Fold structure. This has locally been disturbed by drag folding associated with post-Bushveld left-lateral displacement along the Wonderkop Fault, resulting in a shallowing of the dips and a swing in strike towards the NE. As in the Mathabatha domain, primary sedimentary structures are well preserved in the pelitic sequences, often accentuated by metamorphic mineral growth.

#### *S<sub>2a</sub> cleavage fabric*

The S<sub>2a</sub> fabric is strongly developed in all the micaceous and pelitic units. Cleavage-bedding relationships indicate that the S<sub>2a</sub> cleavage dips consistently more steeply to the south than bedding by between  $10^\circ$  and  $20^\circ$ . Refraction towards the bedding surfaces was observed in very micaceous units in the Dwaalheuwel Quartzite Formation, resulting locally in bedding parallel schistose fabrics. No clear kinematic indicators were found, but it is most likely that the foliation, as in the Mathabatha domain, developed as an extensional shear fabric with a top towards south shear component.

It is also significant that the S<sub>0</sub>-S<sub>2a</sub> intersection angle remains almost constant in similar lithologies as S<sub>0</sub> increases in dip towards the south, from east to west along strike.

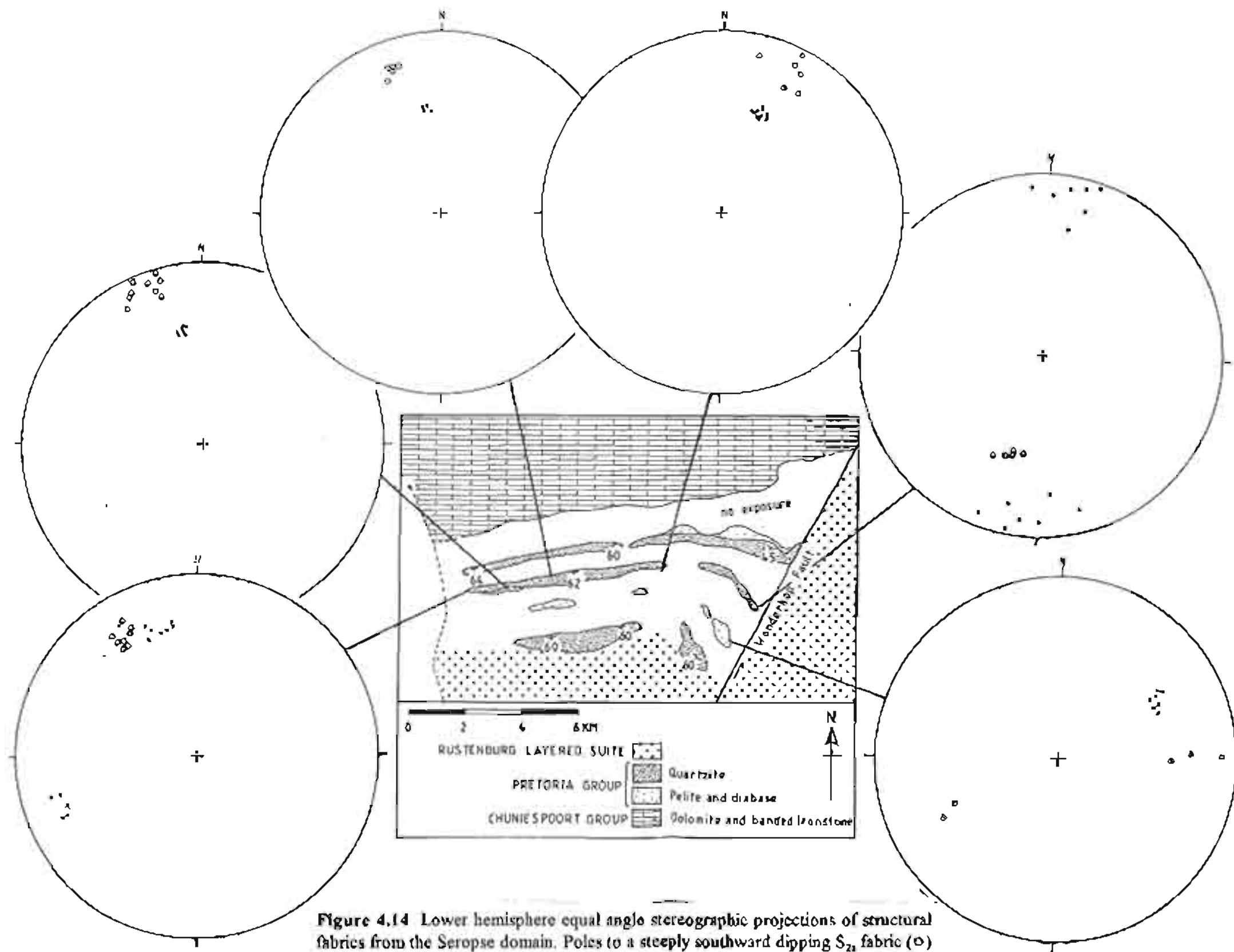


Figure 4.14 Lower hemisphere equal angle stereographic projections of structural fabrics from the Seropse domain. Poles to a steeply southward dipping  $S_{21}$  fabric ( $\circ$ ) and poles to moderately southward dipping bedding ( $\bullet$ ). Mineral lineations ( $\times$ ) have a sub-horizontal orientation.

This suggests that the  $S_{2a}$ -cleavage fabric developed during or prior to the development of the southward tilt in the Pretoria Group strata. The same relationships are true for the Mathabatha domain and provide important timing constraints for the  $D_2$  deformation event.

Chiastolite porphyroblasts in the Silverton Shale Formation, are boudinaged within the enveloping  $S_{2a}$  fabric, with quartz strain shadows defining the extension lineation. The relationships are identical to those described above from the Mathabatha domain.

### *$L_{2a}$ stretching lineations*

Mineral lineation data are limited, but exposures in the western portion of the area indicate a plunge at shallow angles between  $10^\circ$  and  $20^\circ$  towards the west (Figure 4.14). This is in the opposite direction to the lineations observed in the Mathabatha domain. A possible explanation for this is that, post-Bushveld differential subsidence, produced a relative westward rotation of the lineation in the Seropse domain compared to the Mathabatha domain. The other possible explanation is that the  $L_2$  lineations have been deformed by the  $F_{2b}$  Katkloof Fold. The westward-plunging  $L_2$  lineations occur on the extension of the western limb and the eastward-plunging  $L_2$  lineations occur on the eastern limb of the fold. This is discussed in more detail below.

### *$F_{2b}$ folds*

A large open, southerly plunging fold structure is visible in the Timeball Hill Formation quartzite cliff-face on the farm Naaupoort (Appendix 1A and 1F). The fold is developed near the eastern extension of the Katkloof Fold and is interpreted as a second-order  $F_{2b}$  fold structure related to the Katkloof Fold as are the small  $F_{2b}$  folds developed in the Malips area in the eastern Mathabatha domain.

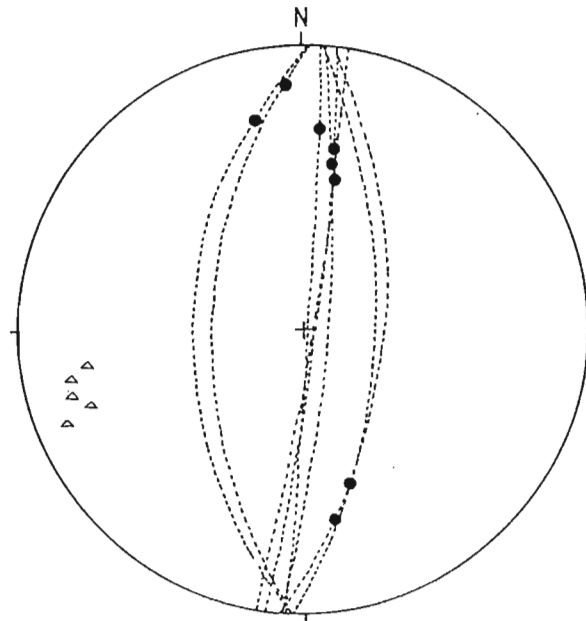
Anatectic veinlets in the Silverton Shale Formation in the eastern part of the area have a predominantly north-south orientation. This direction corresponds to the  $D_{2b}$  axial plane orientation of the Katkloof Fold indicating partial melting was synchronous with folding. Similar axial-planar anatectic veins are also described below from the  $F_{2b}$  Zaaikloof Fold.

### *D<sub>3</sub> kink bands and faults*

At the eastern end of the Seropse domain, 2 to 5 cm wide kink bands are associated with micaceous units in the Dwaalheuwel Quartzite Formation. These strike subparallel to, and have the same shear sense as small left lateral strike-slip faults associated with the Wonderkop Fault (Figure 4.15). Slickenline orientations indicate a dominant strike-slip component on all faults, plunging towards the north and south between 20° and 35°.

### *Brecciation zones*

An extensive part of the quartzite unit of the Timeball Hill Formation in the western part of the Seropse domain is brecciated into blocks varying from 5 to 50 cm in size (Figure 4.16). Compact quartzitic blocks are disrupted within a more friable ferruginous matrix. A possible mechanism for producing this feature may be related to the dewatering of the underlying lower pelitic unit shales as proposed by Matthews (1988) for similar features in Palaeozoic Natal Group sandstones. Hydraulic fracturing occurred when the porewater pressure immediately below the Timeball Hill Quartzite Formation rose above the tensile strength of the quartzites. Unfortunately, no fabrics are developed in the Timeball Hill Formation quartzites, and the development of the regional deformation and metamorphism with respect to the brecciation could not be established.



**Figure 4.15** Lower hemisphere equal-angle stereographic projection of D<sub>3</sub> structures showing the relationship between poles to kink bands (Δ) in micaceous schists and faults with slickenline orientations (●) in more competent quartzite units.



**Figure 4.16** Extensively brecciated Timeball Hill Formation from the western portion of the Seropse domain near Manoge. Paler quartzite blocks occur within a ferruginous matrix. Scale length = 10 cm.

#### 4.3.3 The Katkloof Fold domain

The Katkloof Fold domain (Appendix 1A and 1F) (Figure 4.17) is approximately 7 km in width and is bounded in the west by the post-Bushveld, NE-trending Wonderkop Fault and in the east by a smaller related fault of similar orientation. A continuation of the western limb of the fold partly extends into the Seropse domain (Section 4.3.2).

On the eastern limb of the fold, the strata dip towards the south at between 30° and 40° and steepen from east to west as the fold closure is approached, becoming near vertical in the fold nose. The western limb dips more steeply than the eastern limb, resulting in a slightly asymmetric structure, with an eastward dipping axial plane. The western limbs of second order folds may be locally overturned, dipping steeply to the east, as on the farm Fonteimplaats (Appendix 1). The asymmetry of the fold represents an overall westward-verging structure with a Z-shaped outline when viewed in the down-plunge direction.

The most remarkable feature of this fold, is that the igneous layering of the Rustenburg Layered



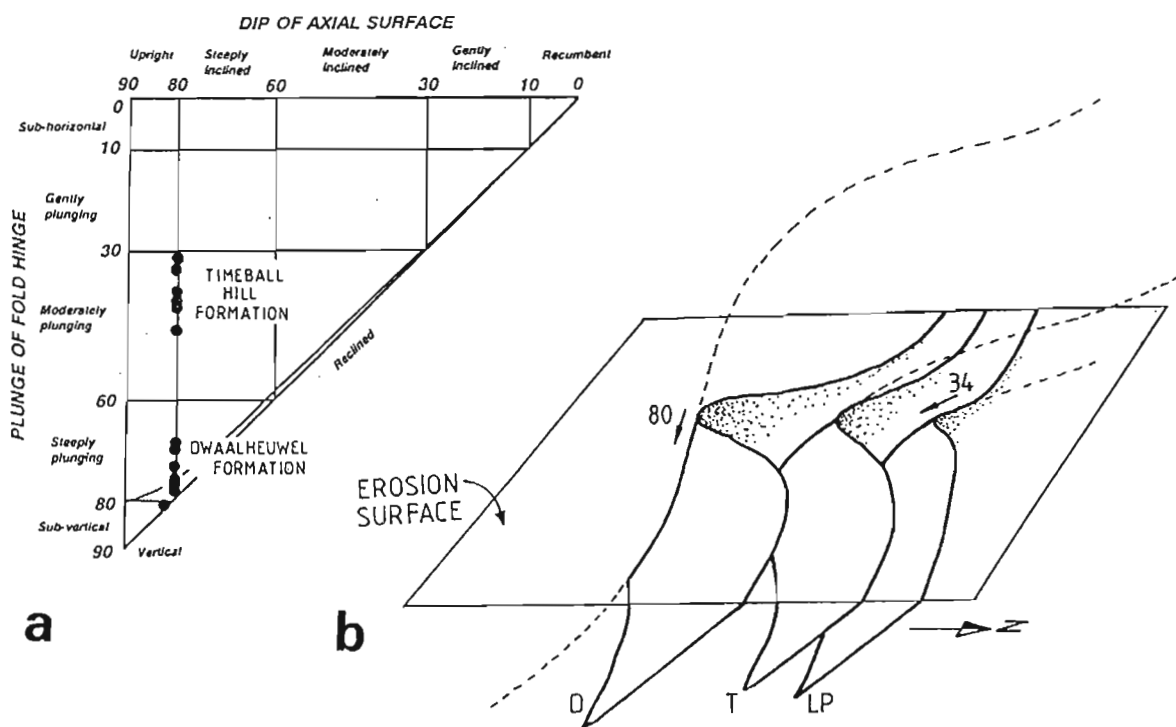
**Figure 4.17** View towards the north from the main zone of the Rustenburg Layered Suite of the fold closure and western limb of the Katkloof Fold. The highest point represents the fold core formed by the Klapperkop Quartzite Member of the Timeball Hill Formation. The lower ridge in the foreground comprises folded Dwaalheuwel Quartzite Formation.

Suite clearly abuts against the eastern limb of the fold. This includes the lower zone, the chromitite seams and Merensky Reef of the critical zone, and the lower portion of the main zone. Schwelnus (1956) interpreted this as being the result of pre-existing floor folds within the Rustenburg Layered Suite. The other possibility is that folding was largely synchronous with the emplacement of the Bushveld magmas. Borehole information and mapping by Johannesburg Consolidated Investments on the farm Leeukop indicates a slight southward swing in strike and a steepening of the igneous layering in the vicinity of the fold which suggests that the folding may still have been active, partially deforming the layering during the late stages of crystallisation of the critical zone.

Structural data from the fold (Figure 4.18) show that at the stratigraphic level of the Dwaalheuwel Quartzite Formation, the fold axis plunges at approximately  $80^\circ$  towards  $165^\circ$ , classifying it as an upright to steeply inclined, steeply plunging to vertical fold (Fleuty, 1964) (Figure 4.19).

**Figure 4.18** Diagram of structural and orientation data shown on lower hemisphere, equal-angle stereographic projections for the Katkloof Fold. Poles bedding (●); poles to planar foliation (○); mineral lineations (x);  $F_{2b}$  fold axes (■); and late stage, near vertical poles to  $D_3$  kinkbands (△).





**Figure 4.19** a) Fleuty (1964) classification for the Katkloof Fold, showing the change in fold plunge with stratigraphic height. b) Sketch showing the proposed geometry of the fold as a domal structure, with the dome culminating point located up-plunge of the exposed fold hinge.

This tight fold closure angle increases into a more open structure with a more moderately plunging fold axis at successively lower stratigraphic levels, thus representing a periclinal structure or non-cylindrical fold with curved fold hinges (Figure 4.19). The present erosional level provides an oblique section through the dome and suggests that most of the structure in the up-plunge direction has been removed by erosion.

The base of the Katkloof Fold is represented by a major decollement surface coinciding approximately with the contact between the Pretoria Group and the Chuniespoort Group (Bastin, 1968; Sharpe and Chadwick, 1981). The decollement zone was later subjected to reactivation during post-Bushveld Complex faulting along the Wonderkop Fault.

#### *S<sub>2a</sub> and axial-planar S<sub>2b</sub> cleavage relationships*

Progressing westwards from the Mathabatha domain into the western limb of the Katkloof Fold, the S<sub>2a</sub> cleavage is increasingly rotated into parallelism with the fold axial-surface, and becomes part of the S<sub>2b</sub> axial-planar fabric (Figure 4.18 and 4.20). Nowhere are the two fabrics observed together. The EW striking S<sub>2a</sub> cleavage in the Mathabatha and Seropse domains and

the N-S striking  $S_{2b}$  axial planar cleavage in the Katkloof Fold core are thus closely linked and form part of the same  $D_2$  syn-Bushveld deformation event, here termed  $D_{2a}$  and  $D_{2b}$  respectively (Section 4.2.1, Table 4.1). The regional expression of the two ( $S_{2a}$  and  $S_{2b}$ ) fabric orientations in relation to the Katkloof Fold is one of an outward diverging fan structure (Figure 4.20).

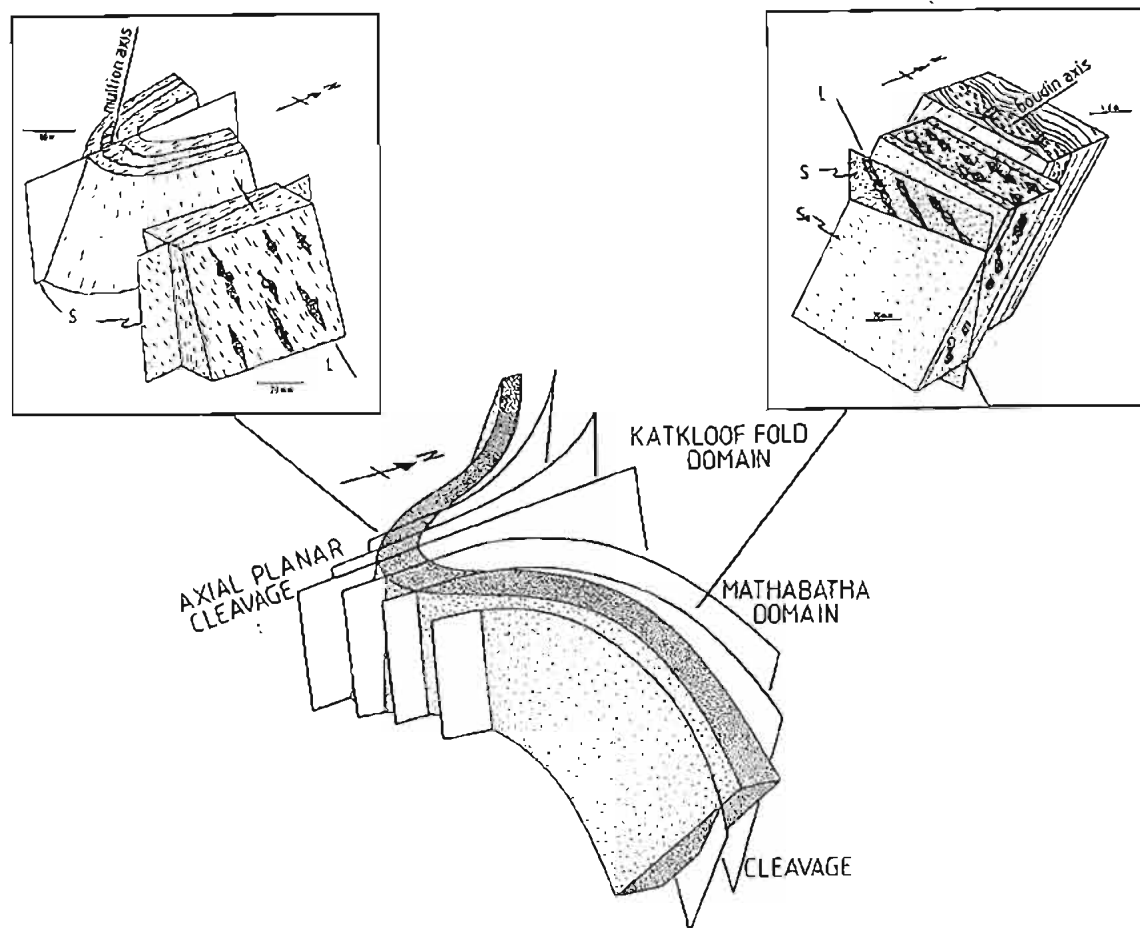


Figure 4.20 Diagram showing the relationship between fabric components in the Katkloof Fold and the adjacent Mathabatha domain.  $S_{2a}$  cleavage in the Mathabatha domain is continuous with  $S_{2b}$  axial planar cleavage in the Katkloof Fold. E-W extension in the Mathabatha domain (boudinage and  $L_2$  mineral lineations) and E-W compression features in the Katkloof Fold (mullion structures and axial-planar cleavage).

The axial-planar  $S_{2b}$  fabric is only developed in the Katkloof Fold core, where it is penetrative through the whole sequence including the most competent rock types, without any evidence of an earlier near bedding-parallel  $S_{2a}$  cleavage fabric (Figure 4.20). Amygdaloidal lavas of the Hekpoort Andesite Formation for example, display a prominent axial-planar  $S_{2a}$  cleavage fabric.

Meta-amygdales of quartz and plagioclase are slightly ellipsoidal in shape and remained more competent than the groundmass during deformation with strain shadows and a cleavage that is partially wrapped around them.

Two possibilities exist as to the relationship between the fabrics,  $S_{2a}$  and  $S_{2b}$ . Firstly, they may represent individual fabrics related to two independent syn-Bushveld Complex deformation events. This argument could be supported by the fact that both fabrics are close to bedding parallel and with intense overprinting would be difficult to distinguish from another. In this situation the  $S_{2a}$  in the Mathabatha domain would have developed during a close to vertical compression with a component of top-to-south shear and associated E-W directed extension event, and the  $F_{2b}$  Katkloof Fold by an E-W directed compression.

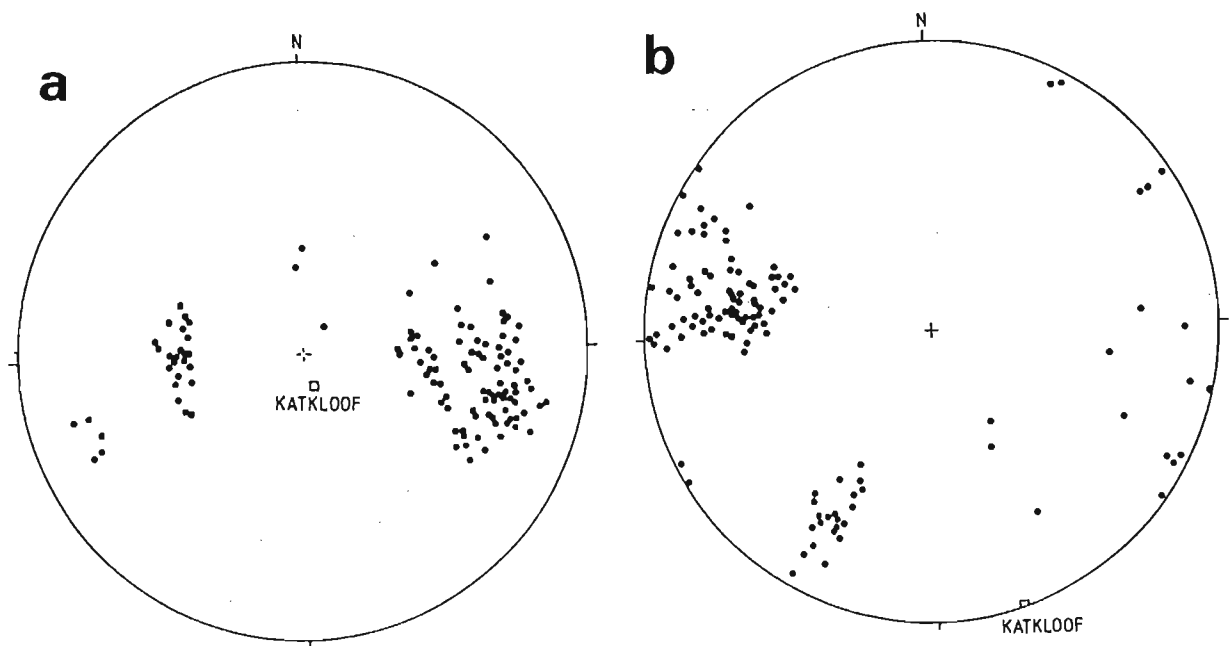
The second possibility, favoured here, is that both fabrics developed synchronously in a single syn-Bushveld Complex progressive deformation event. Further evidence for this is supported by lineation data outlined below.

### ***F<sub>2b</sub> mullion structures***

Large, approximately 1 m wide, mullion rods are developed at the Katkloof Fold closure in coarse-grained quartzite of the Dwaalheuwel Quartzite Formation. They are orientated parallel to the fold axes of second order M-folds and the Katkloof Fold axis (80° towards 165°), and are bounded by the steeply dipping  $S_0$  and the axial-planar  $S_{2b}$  cleavage fabric.

### ***L<sub>2</sub> mineral lineations***

$L_2$  mineral elongation lineations in the Katkloof Fold are best defined by quartz pressure shadows associated with chistolite porphyroblasts in pelitic schists. These are identical to the  $L_2$  lineations developed in the Mathabatha domain (Section 4.3.1) providing an indication of the direction of maximum finite extension. The lineations from the Mathabatha, Seropse and Katkloof Fold domains are widely scattered about the Katkloof Fold axis (Figure 4.21a). Lineations plunge westward on the western fold limb and in the neighbouring Seropse domain, and eastward on the eastern fold limb and the Mathabatha domain.



**Figure 4.21** Lower hemisphere equal angle stereographic plots of lineations from the Katkloof, and adjacent Mathabatha and Seropse domains. a) Unrestored data. b) The same data, with the Katkloof Fold axis restored to the horizontal.

Restored lineations with the fold axis in the horizontal position (Figure 4.21b) indicate that the data do not plot on either a small circle arc, or a great circle arc as would be expected for deformed lineations in a concentric or similar fold respectively.

As shown above, the Katkloof Fold represents an oblique section through a domal structure. In such a structure, lineations associated with flexural slip would tend to be radially distributed about the culmination point and would thus never be normal to the fold axis along an oblique section through the structure. This geometry would explain the eastward-plunging lineations in the Mathabatha domain and the westward plunging lineations in the Seropse domain, with the predicted culmination point of the Katkloof structure in the erosively removed up-plunge direction.

### *F<sub>2</sub> folds*

Second order folds related to the D<sub>2</sub> deformation are most common in the Katkloof Fold core. Metre-scale open to tight M-folds are developed, with a pronounced S<sub>2b</sub> axial-planar cleavage

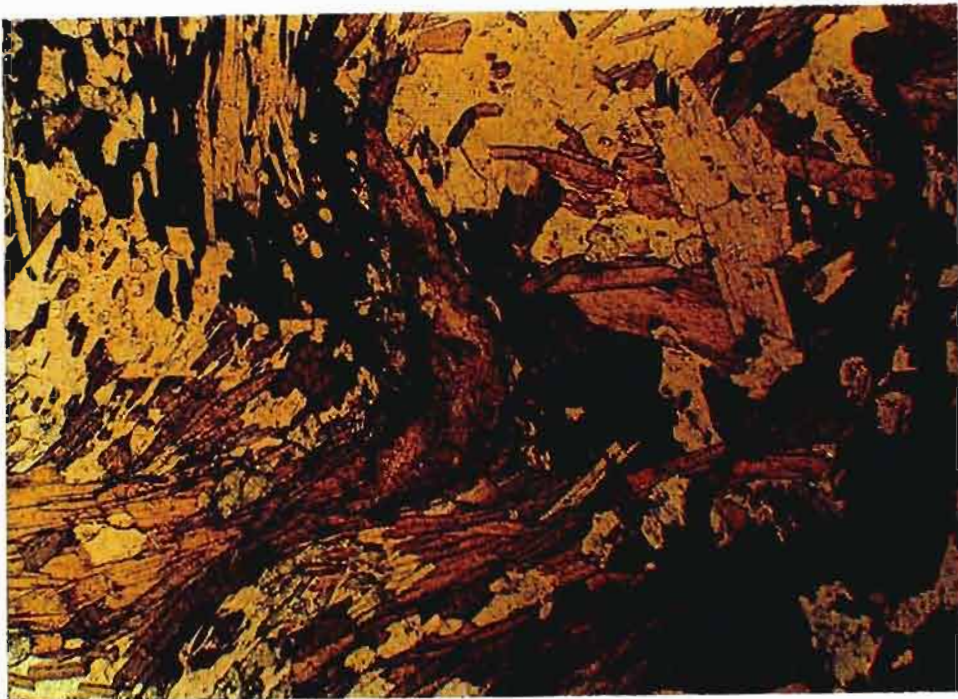
(Figure 4.22) and in the upper pelitic unit of the Timeball Hill Formation, small quartz veins are folded within the axial-planar  $S_{2b}$  foliation, plunging between  $75^\circ$  and  $80^\circ$  towards  $170^\circ$  (Figure 4.18). In places, chialstolite porphyroblasts and fibrolite knots are disrupted and deformed by these folds (Figure 4.23). This indicates that deformation continued after the major porphyroblast-forming event has ceased. The extensional disruption of chialstolite and andalusite porphyroblasts in the Mathabatha domain similarly provides evidence of continued deformation after pophyroblastesis. The age of the  $S_{2a}$  and  $S_{2b}$ -axial planar fabric forming event, relative to porphyroblast development, is thus similar in both domains and provides further evidence that  $S_{2a}$ ,  $L_{2a}$  and  $S_{2b}$ ,  $L_{2b}$  formed synchronously during the  $D_2$  syn-Rustenburg layered Suite deformation. The details of porphyroblastesis and matrix foliation is further discussed in Chapter 6.

### ***D<sub>3</sub> Kink bands and faults***

Numerous 2 to 50 cm wide kink bands are developed in micaceous schist layers throughout the Katkloof domain, usually closely associated with faulting. The kink bands are all steeply dipping with a trend between  $160^\circ$  and  $200^\circ$  (Figure 4.18). They have a left-lateral sense of shear with minor conjugate right-lateral shears.



**Figure 4.22** Down-plunge view of a  $F_2$  second-order fold in andalusite-biotite-garnet-staurolite fels. Fold defined by  $S_0$  and axial planar  $S_{2b}$ . Lower pelitic unit of the Timeball Hill Formation on the farm Katkloof. Scale length = 25 cm.



**Figure 4.23** Photomicrograph of deformed fibrolite knots from the upper pelitic unit of the Timeball Hill Formation, on the farm Tigerpoort. Width of view = 6 mm

Faults have similar orientations to kink bands and are considered to be part of the same  $D_3$  post-Bushveld Complex deformation event. Slickenline orientations indicate a dominant strike-slip component on most fault surfaces (Figure 4.24). NE-trending faults are left-lateral strike-slip structures as indicated by shallow-plunging slickenlines and the displacement of the Pretoria group. The largest horizontal displacement of just over 6 km on the Wonderkop Fault.

The Wonderkop Fault swings eastwards into the Pretoria Group-Chuniespoort Group contact exploiting the  $D_2$  decollement zone at the base of the Katkloof Fold. The change in fault orientation is accompanied by reverse faulting, as is evident by the duplication of the Klapperkop Quartzite Member on the farm Tuimplaats (Appendix 1A and 1F). This relationship suggests that the NE-trending, left-lateral strike-slip faults form lateral ramps to the E-W trending reverse faults which developed as oblique frontal ramps in the restraining bend of the Wonderkop Fault at the base of the Katkloof Fold (Figure 4.25). Minor normal faults, with displacements of a few metres, at high angles to the master Wonderkop Fault were observed on the farm Tuimplaats (Figure 4.24, 4.25). They are considered to represent extension fractures associated with left-lateral simple shear. The pervasive conjugate joint set in the area

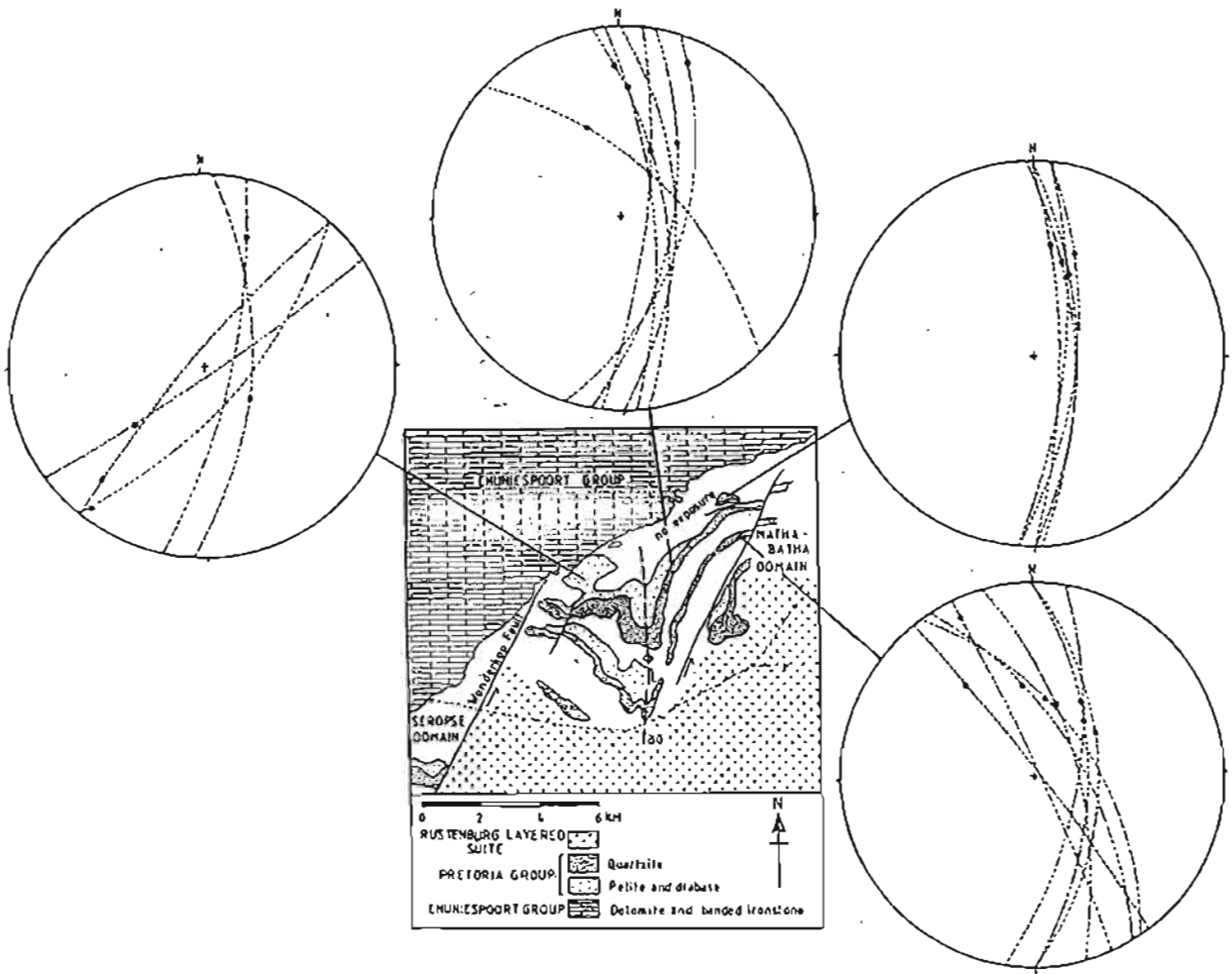
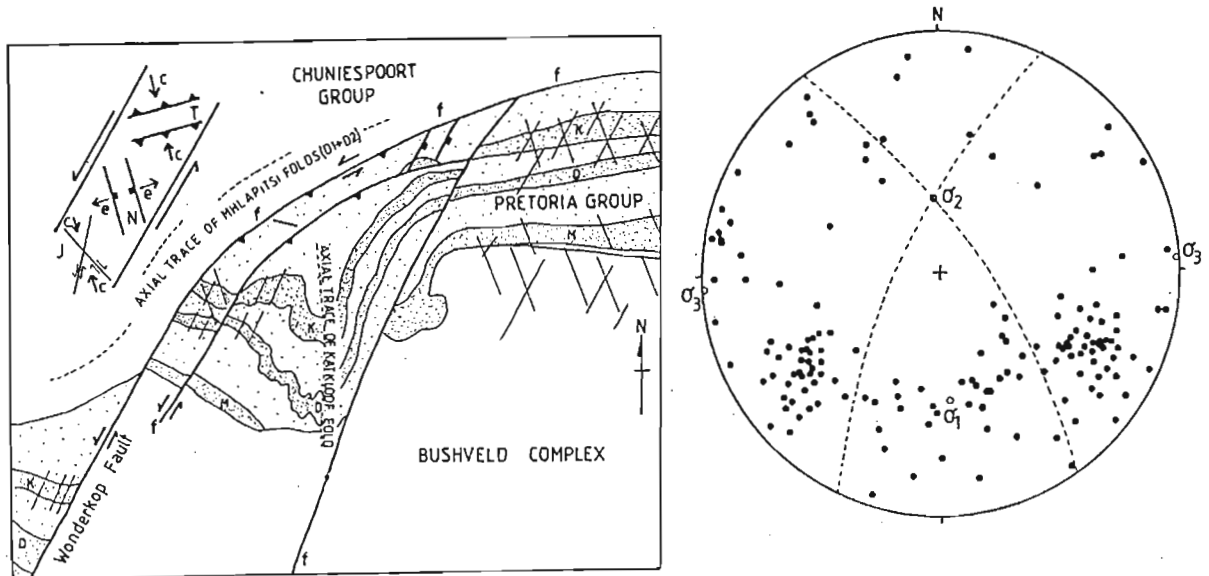


Figure 4.24 Orientation data for  $D_3$  fault traces and slickenline orientations in the Katkloof Fold domain (•). Lower hemisphere equal-angle stereographic projections.

(Figure 4.24, 4.25) may also be explained by left-lateral simple shear. The acute intersection angle between the two dominant joint set orientations, indicate a NS directed compression direction.

Previous studies by Schweltnus *et al.* (1962) and Bastin (1968), had shown that the Wonderkop Fault is not traceable within the Chuniespoort Group to the north of the Katkloof area, although left-lateral strike-slip faults are again observed in the Wolkberg Group and Black Reef Quartzite Formation at the base of the Chuniespoort Group (Figure 2.2). Bastin (1968) suggested that the lower competency calcareous Chuniespoort Group deformed plastically in comparison to the more brittle deformation observed in the Pretoria Group and sub-

Chuniespoort Group formations. This is substantiated by the change in orientation of the  $D_1+D_2$  fold axial traces across the northward extension of the Wonderkop Fault in the Chuniespoort Group (Figure 4.25).



**Figure 4.25** Diagram of the Katkloof area showing the angular relations between normal faults, conjugate joint sets and reverse faults, within a left-lateral simple shear system.  $D_1$  and  $D_2$  fold axial traces in the Chuniespoort Group are deformed into broad S-folds along the western margin of the northward displaced Katkloof block. Lower hemisphere equal angle projection of poles to joints from the Mathabatha domain, showing the orientation of the conjugate joint set and NS-directed compression.

#### 4.3.4 The Schwerin Fold domain

The Schwerin Fold (Figure 4.26) like the Katkloof Fold, is a major 10 km wide floor attached fold structure that penetrates into the Rustenburg Layered Suite. Unlike the Katkloof Fold however, the basal decollement is developed above the stratigraphic level of the quartzite unit in the Timeball Hill Formation, the Klapperkop Member. The sub-decollement, lower Pelitic unit of the Timeball Hill Formation is relatively unaffected by  $F_{2b}$  folding and associated deformation.

From the geological map (Appendix 1) and the structural data represented in Figure 4.27 from various localities in the Schwerin Fold domain, it is clear that the major fold axial trace is



curvilinear and the fold axis varies considerably in plunge. At the stratigraphic level of the Dwaalheuwel Quartzite Formation the Schwerin Fold is an upright, gently plunging fold structure with a plunge of approximately  $15^\circ$  on  $145^\circ$  and a near vertical axial plane in the core area. At higher stratigraphic levels, steeper plunges, up to  $80^\circ$  were recorded on minor fold structures in the Magaliesberg Quartzite Formation. This indicates that the fold has an overall periclinal geometry with a curved axial surface. As in the Katkloof Fold, the change in fold plunge at the various stratigraphic levels is produced by the present oblique topographic section through the periclinal fold structure and results in a range of fold orientations (Appendix 1).

Unlike in the Katkloof Fold, the Magaliesberg Quartzite Formation is still complete in the Schwerin Fold, and partial detachment and xenolith formation by the Bushveld Complex has occurred in post-Magaliesberg Quartzite Formation sequences.



**Figure 4.26** View northwards from the western limb of the Schwerin Fold into the fold core. Folded quartzites of the Dwaalheuwel Quartzite Formation are visible centre right in the Shobaneng gorge which cuts through the fold core. The line of low hills in the foreground consist of the quartz-feldspar porphyry intrusive. Photograph is taken from the ridge formed by the Lydenburg Shale Member of the Silverton Shale Formation. The skyline in the background is formed by the Klapperkop Quartzite Member of the Timeball Hill Formation.

The fold limb discordance with the Rustenburg Layered Suite is not as marked as in the Katkloof Fold. The lower and critical zones thin out towards the Schwerin Fold, and chromite seams within the critical zone are only slightly discordant with the western limb of the fold.

Lower and critical zone magmas vary laterally in thickness, thinning over the floor folds and thickening between the major floor fold structures, such as the Katkloof and Schwerin Folds, giving rise to lateral variations in thickness. This relationship indicates the close relationship between the development of the floor folds and the emplacement and crystallisation history of the Rustenburg Layered Suite.

Intense deformation within the core areas of the Schwerin Fold has resulted in a large spread of the bedding orientations about a NW-SE axis (Figure 4.27). Overtaken cross-stratification structures are associated with intense deformation and folding in the hinge area within the Dwaalheuwel Quartzite Formation.

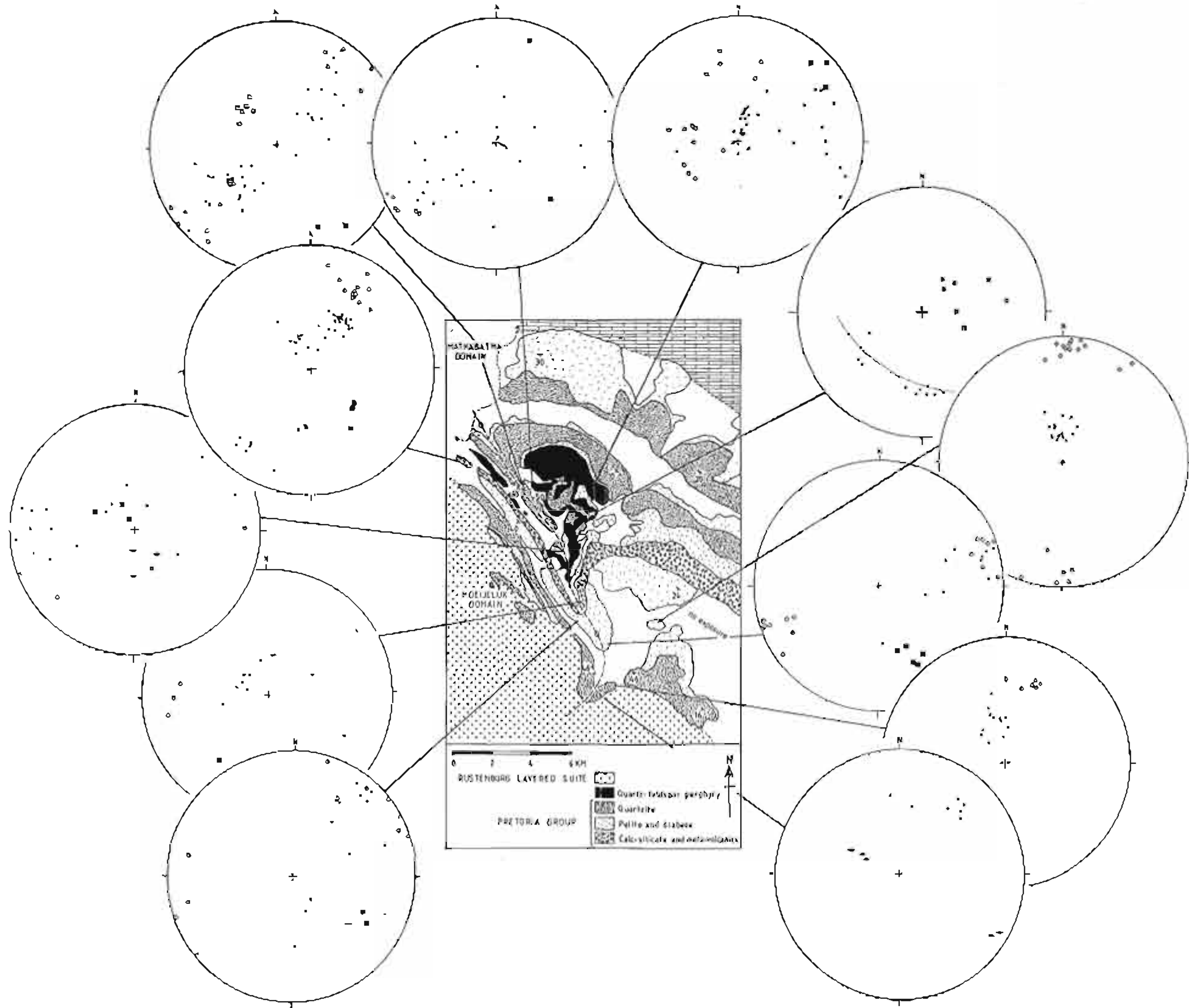
### *S<sub>2</sub> cleavage fabric*

The S<sub>2</sub> cleavage fabric is non-penetrative and is most developed in certain pelitic horizons in the western limb of the fold. As in the Katkloof Fold, nowhere were both S<sub>2a</sub> and S<sub>2b</sub> cleavages observed together, suggesting that they may both be part of the same cleavage forming event, or that the S<sub>2</sub> fabric, being almost bedding parallel, is rotated into parallelism with the later S<sub>3</sub> axial planar cleavage on the fold limbs and will not easily be recognised. In the fold hinges refoliation by S<sub>3</sub> may obliterate the earlier S<sub>2</sub> cleavage.

### *S<sub>2b</sub> axial planar cleavage*

In core of the fold, the S<sub>2b</sub> axial planar cleavage is penetrative in the rock succession above the basal fold decollement. In the Shobaneng gorge on the farm Jobs Kop (Appendix 1B and 1F), axial planar fabrics are associated with concentrically folded Dwaalheuwel Quartzite Formation quartz-mica schists and deformed conglomerates. The fabric is strongly refracted between various lithological units, becoming almost bedding-parallel due to bedding parallel slip. The axial-planar foliation strikes approximately NW-SE and dips steeply towards the SW or NE, within the Dwaalheuwel Quartzite Formation (Figure 4.27, 4.28).

**Figure 4.27** Structural data on lower hemisphere equal angle projections from various stations within the Schwerin Fold domain. Poles to sedimentary stratification (●); poles to planar foliation (○); mineral lineations (x); boudin axes (◆); mesoscale  $F_{2b}$  fold axes (■); flow folds in the Roodekrans Complex quartz-feldspar porphyry (◻); poles to a flat-lying  $S_3$  crenulation cleavage (□).



### ***Boudinage structures***

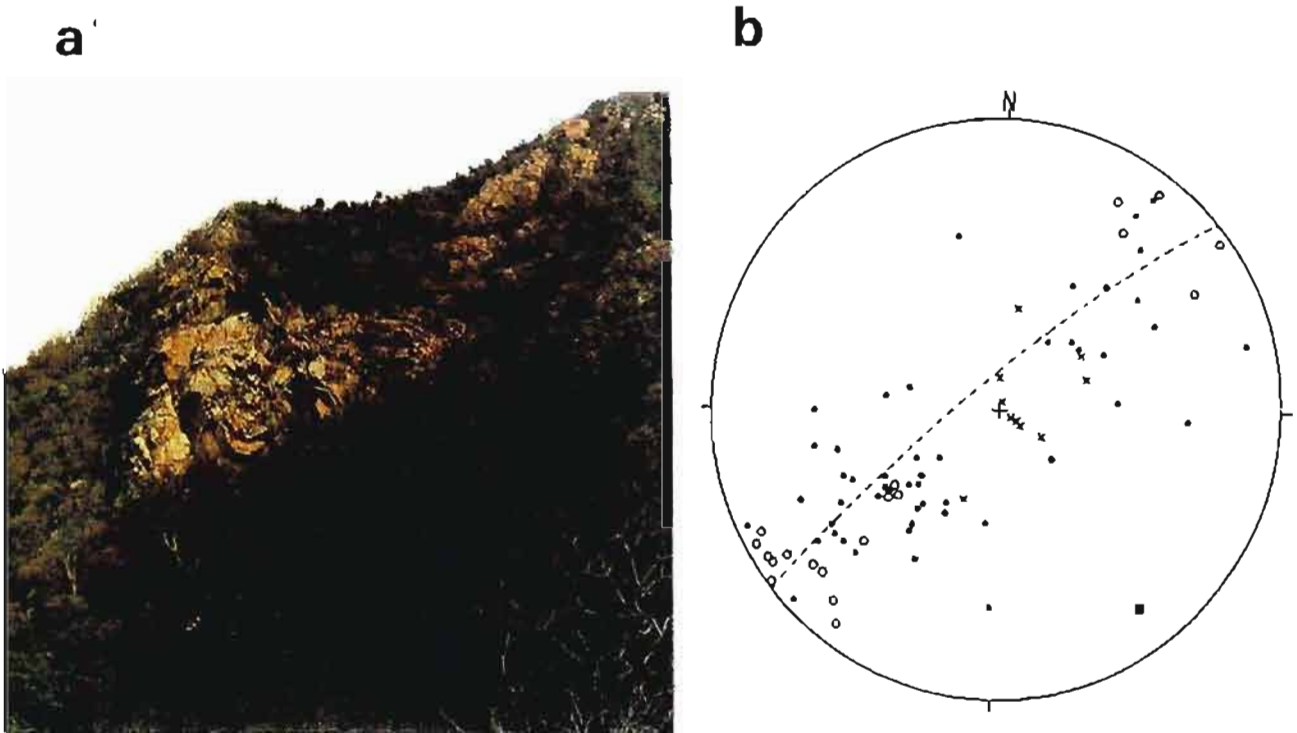
Boudinaged calc-silicate layers in semi-pelites and quartzites of the Vermont Hornfels Formation occur within the upper migmatite zone of the contact aureole and are exposed in the Schwerin Fold closure on the farm Wismar. At lower grades, within the lower fibrolite zone, the calc-silicate unit of the Machadodorp Member typically forms the more ductile component in relation to intercalated semi-pelitic or quartzitic units. This again represents a viscosity switch in these materials in relation to metamorphic grade within the aureole as also described from the Mathabatha domain for quartzite-pelite relationships. In this case the temperature is a little higher, corresponding with the start of migmatitisation in the aureole.

### ***F<sub>2b</sub> folds***

The internal structure of the Schwerin Fold comprises highly deformed and folded strata occurring stratigraphically above the Klapperkop Quartzite Member of the Timeball Hill Formation. F<sub>2b</sub> folds are most apparent in the Dwaalheuwel Quartzite Formation and the Roodekrans Complex quartz-feldspar porphyry. These folds are exposed in the Shobaneng gorge on Jobs Kop (Appendix 1B and 1F) which cuts across large 100 m wavelength second order upright M-type folds in the Dwaalheuwel Quartzite Formation. The low competency contrast between the quartzite layer and overlying semi-pelitic and pelitic unit of the Strubenkop Shale Formation has produced low-amplitude type folds with tight synclinal structures and open rounded anticlines as a series of cusped-lobate style folds (Figure 4.28).

The D<sub>2b</sub> second order fold axes are radially oriented about the main Schwerin Fold axial trace (Appendix 1) In the fold core, in the Shobaneng gorge on the farm Jobs Kop, the folds are the tightest, plunging at between 18° and 20° towards 150° defining the central axis of the Schwerin Fold structure. Eastwards from the axis the folds gradually open, and plunge at more shallow angles, changing their plunge direction. On the farm Stavenhagen for example, the folds plunge at orientations of 10° towards 230°.

Fabrics associated with these folds include a prominent axial-planar cleavage and slickenside lineations that are developed on bedding surfaces. Lineations are normal to the fold axis and form a great circle to the fold axis (Figure 4.27) indicating that folding was controlled largely by flexural slip processes and that these lineations cannot be interpreted as deformed lineations.



**Figure 4.28** a) Northward view of a  $F_{2b}$  fold in the Dwaalheuwel Quartzite Formation in the Shobaneng gorge. b) Lower hemisphere, equal angle stereographic projection of structural data from the area. Poles to bedding ( $\bullet$ ); poles to planar foliation ( $\circ$ ); mineral lineations ( $\times$ ); average  $F_{2b}$  fold axis ( $\blacksquare$ ).

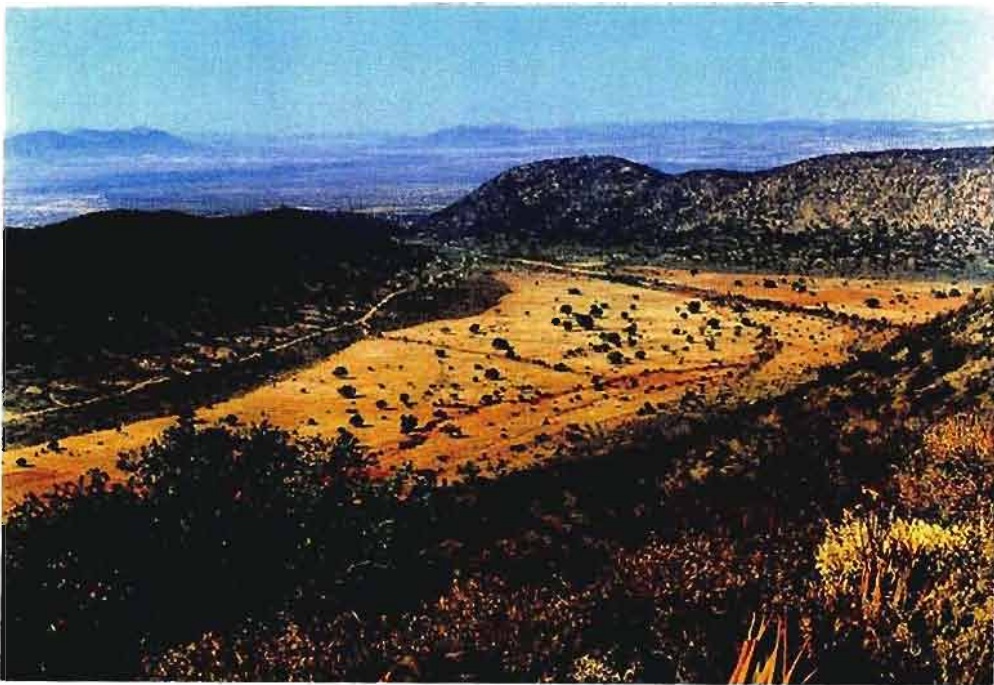
Within the central portion of the Schwerin Fold, on the farm Roodekrans and Stavenhagen (Appendix 1B and 1F), the folds plunge steeper to angles approaching  $60^\circ$ . This is ascribed to fold interference resulting in a Ramsay type 1 dome and basin interference pattern (Ramsay, 1967) where the two interfering fold axes are near orthogonal in orientation. In the intensely deformed fold core on the farm Schwerin, fold hinges are markedly curvilinear with a high degree of non-cylindricity. Non-cylindricity in the folds on an outcrop scale tends to increase with increasing grade and becomes most pronounced within the fibrolite and migmatite zones.

### *$S_3$ crenulation cleavage*

Locally, crenulation cleavages in micaceous units within the folded Dwaalheuwel Quartzite Formation are developed. Fabrics are generally fairly flat-lying. The fabrics are clearly later than the  $D_2$  folding event and are possibly associated with post-Bushveld Complex northward-directed movement.

#### 4.3.5 The Zaaikloof Fold domain

The Zaaikloof Fold structure (Figure 4.29, 4.30) is represented by the fold closure of the upper Pretoria Group, the Magaliesberg Quartzite Formation and remnants of the Vermont Hornfels Formation and the Lakenvalei Quartzite Formation. The fold occurs within the main and upper zone of the Rustenburg Layered Suite and is bounded in the west by the Leeukop Fault which forms the eastern arm of the Wonderkop Fault. Mapping of the area has shown that the fold axis of the Zaaikloof Fold is displaced approximately 2 km left laterally by the Leeukop Fault and can be traced through the Pramkoppies domain which is discussed below in section 4.3.6.



**Figure 4.29** View towards the southeast into the Zaaikloof Fold closure from the fold core underlain by the Machadodorp Member. The folds limbs are formed by the Magaliesberg Quartzite Formation. The alluvium covered plain is underlain by the Lydenburg Shale Member of the Silverton Shale Formation. Hills in the upper left corner are part of the Phepane Fold structure.

On the eastern limb of the fold the rocks are in contact with a thin, up to 600 m wide sliver of granite of the Lebowa Granite Suite that has not been included in any previously published geological maps of the area (1: 125 000 scale, 2429B Chuniespoort, 2430A Wolkberg, 1962 sheet; 1:250 000 scale 2428 Nylstroom, 1978 sheet). The granite is conformable to bedding in the Pretoria Group, cross cutting igneous layering in the surrounding Rustenburg Layered Suite. It was conformably emplaced along the quartzite-Rustenburg Layered Suite contact after

the development of the fold structure and metamorphism.

This is further substantiated by the presence of granite veins within the Zaaikloof structure that cut across all previous fold structures. On the southern limb of the fold, the Pretoria Group strata are in direct contact with the main and upper zones of the Rustenburg Layered Suite.

The Zaaikloof structure is either still attached to the floor (Sharpe and Chadwick, 1981) or represents a large xenolith or raft within the Rustenburg Layered Suite (Schwellnus, 1956). Like the Katkloof and Schwerin Folds, it is an outward-younging anticlinal structure with similar dimensions (about 8 km in width). Steeply dipping quartzite of the Magaliesberg Quartzite Formation and the overlying Vermont Hornfels and Lakenvalei Quartzite Formations form the positive topographic expression of the fold. On the northern part of the eastern limb of the fold, the strata are overturned, dipping steeply between  $60^{\circ}$  and  $85^{\circ}$  towards the west underneath the older Silverton Shale Formation exposed in the fold core. Nearer the fold hinge the strata are not overturned, dipping towards the east at between  $40^{\circ}$  and  $60^{\circ}$ . The southern limb of the fold is not overturned, dipping towards the south at between  $40^{\circ}$  and  $80^{\circ}$ .

Structural data for the fold (Figure 4.30) indicates a plunge of  $58^{\circ}$  towards  $112^{\circ}$  at the stratigraphic level of the Machadodorp Member and in the neighbouring extension of the fold in the Pramkoppies domain (section 4.3.6) the folds plunge at even lower angles towards the southeast (between  $30^{\circ}$  and  $40^{\circ}$ ). This indicates that fold plunges decrease towards lower stratigraphic levels and towards the core of the fold structure. This geometry is also present in the Katkloof Fold domain (section 4.3.3) and indicates the periclinal nature of these structures and the presence of a basal decollement such as exposed in both the Schwerin and the Katkloof Folds.

A feature of the Zaaikloof structure is the very tight to isoclinal nature of the fold in the fold nose area, which widens to a more open structure at lower stratigraphic levels. This geometry corresponds to the Ramsay (1967) Class 3 fold with divergent dip isogons. This fold shape is also typical of cusped-shaped structures developed between two interfaces of differing competency. These features also found in both the Katkloof and Schwerin Folds. These shapes would suggest that during deformation, the Pretoria Group behaved as the relatively



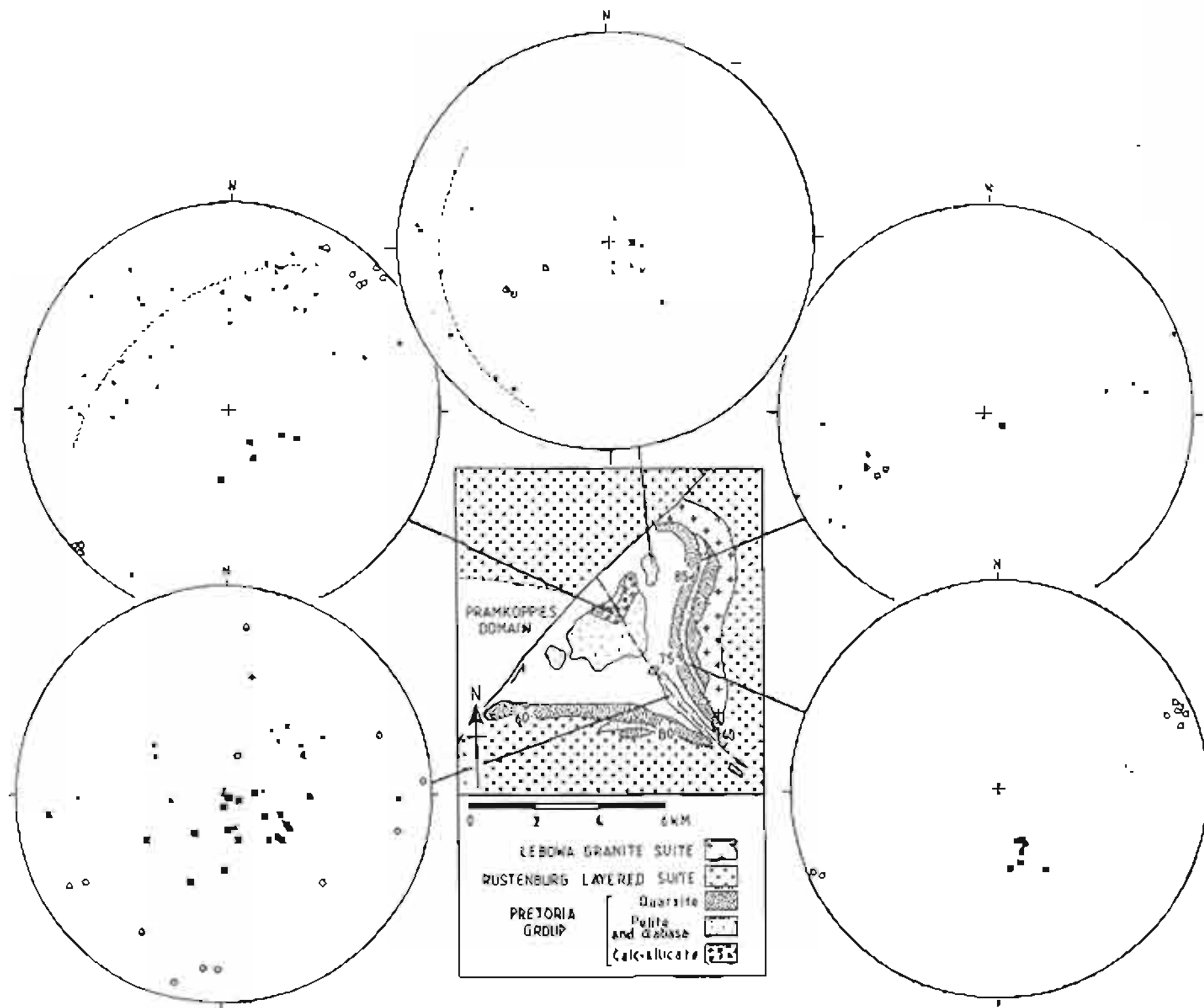


Figure 4.30 Structural map of the Zaikloof Fold showing fabric data from various parts of the fold structure. Poles to bedding ( $\bullet$ ); poles to planar foliation ( $\circ$ ); mineral lineations ( $\times$ ); boudin axes ( $\blacklozenge$ ), mesoscale  $F_1$  fold axes ( $\blacksquare$ ); poles to anatectic leucosome veinlets ( $\circ$ ).

incompetent material compared to the mafic Bushveld magmas. Cusp-like structures can develop either during layer-parallel shortening, or density instability related to layer-normal compression (Price and Cosgrove, 1990). This aspect will be considered in more detail in a later section.

The Zaaikloof Fold is found within the main and upper zones of the Rustenburg Layered Suite. Gently dipping igneous layering, although not as distinct in the main zone, abuts against the steeply dipping quartzite fold limbs. This suggests that the folding was still active during main zone and upper zone times.

Poles to bedding and other structural fabric data from the Zaaikloof Fold are shown in Figure 4.30. Small-scale primary sedimentary structures are generally poorly preserved in outcrop as most of the fold structure falls within upper fibrolite and migmatite zone conditions of metamorphism. The Magaliesberg Quartzite Formation and overlying sequences are generally highly deformed and recrystallised and the pelitic units of the Silverton Shale Formation are migmatized. Bedding is however defined by compositional variations, particularly in the pelitic units and in some cases cross-bedding is preserved and serves as a useful way-up criterion.

### *S<sub>2b</sub> foliation*

Within the lowermost stratigraphic units of the fold structure as defined by the Machadodorp Member and the underlying Boven Shale Member of the Silverton Shale Formation, the foliation in the rocks is axial planar to the main Zaaikloof Fold structure (Figure 4.30).

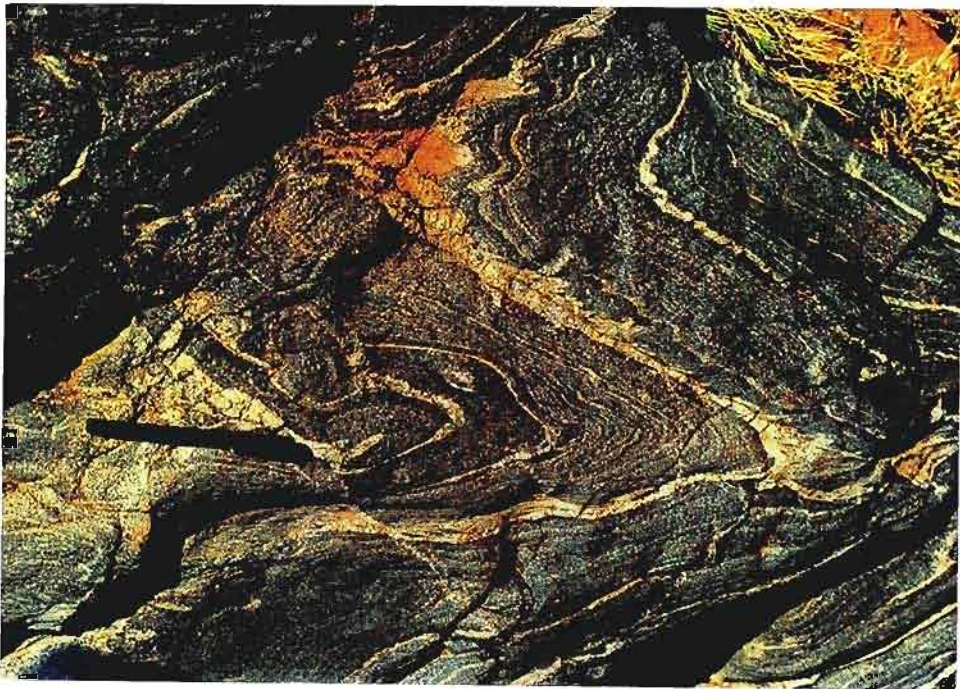
At higher metamorphic grades and higher levels in the stratigraphy, within the Lydenburg Shale Member of the Silverton Shale Formation, the occurrence of small leucocratic melt veinlets are also typically axial planar to second order folds and to the large fold structure. On the eastern limb the axial planar partial melt veinlets define a surface striking approximately 150° and dipping between 70° and 85° towards the east.

Within the intensely deformed core of the fold, S<sub>0</sub> and S<sub>2</sub> becomes increasingly deformed and often does not have an axial planar relationship to the main Zaaikloof Fold structure. This is clearly evident on the stereonet data shown in Figure 4.30. Migmatitic veinlets usually still

define the bedding but also cut across both the bedding and the  $S_2$  foliation (Figure 4.31).

### *$L_{2b}$ lineations*

A linear fabric is dominant within the pelitic units of the Silverton Shale Formation core of the Zaaikloof Fold. Mineral lineations are defined by the stretching directions of boudinaged chialstolite crystals within  $S_{2b}$  (Figure 4.32). These are commonly associated with tight to isoclinal folds and are locally orientated subparallel to the fold axes. The non-cylindrical nature of the folds, with typically curvilinear fold axes, has produced the wide range in lineation orientations. Lineations show no consistent orientation or recognisable deformation pattern (Figure 4.30). This is attributed to a single progressive deformation event, which progressively deformed early tight folds, lineations and the  $S_2$  cleavages by more open folds.



**Figure 4.31** Photograph of migmatized and folded Lydenburg Shale Member of the Silverton Shale Formation in the Zaaikloof fold core. Fold plunges to the right at  $54^\circ$  towards  $130^\circ$ . Leucosomes are mainly bedding parallel but also cut across bedding and foliation. Scale length = 14 cm.



**Figure 4.32** Stretching lineations defined by boudinaged chiastolite crystals in an alternating pelitic and semi-pelitic unit of the Silverton Shale Formation on the farm Zaaikloof. Scale length = 14 cm.

#### **4.3.6 The Pramkoppies Fold domain**

As indicated above, the Pramkoppies domain forms the western extension of the Zaaikloof Fold (Appendix 1C and 1F). The fold axis is displaced by both the Wonderkop Fault in the west and the Leeukop Fault in the east. As in the Zaaikloof Fold, metamorphic grade increases from the core of the fold outwards, with andalusite-fibrolite rocks in the core passing into migmatite zone rocks to the north and south of the fold axis. Way-up criteria in the form of primary sedimentary structures are generally well preserved in the core of the fold.

On Pramkoppies hill, the Daspoort Quartzite Formation of the middle Pretoria Group, defines the intensely deformed fold core (Figure 4.33). To the north of the hill, Machadodorp Member calc-silicates and volcanics are poorly exposed, but can be traced around the base of Pramkoppies hill. The remainder of the Pretoria Group however, is not exposed and is considered to be present under the alluvial cover.



**Figure 4.33** Northeasterly view of the southern slopes of Pramkoppies hill from Grootkop. A tight recumbent fold closure in the Dwaalheuwel Quartzite Formation is shown on the western side of the hill forming the central axes of the Zaaikloof-Pramkoppies Fold structure. The eastern skyline of the hill corresponds approximately to the eastward plunging fold axis. The low-lying ridge and settlement in front of Pramkoppies is underlain by rocks of the Machadodorp Member and Silverton Shale Formation. Hills in the distance are Transvaal Supergroup floor rocks.

This is supported by aeromagnetic data of the area (Appendix 1) which indicates the presence of a considerable extent of low intensity magnetic material to the north of Pramkoppies hill. This suggests that the Pretoria Group contact with the main zone of the Rustenburg Layered Suite is situated almost 2 km further north, and accounts for the presence of upper Pretoria Group stratigraphy under the alluvial cover. Some of the low intensity magnetic material however, may also be an extension of the granite of the Lebowa Granite Suite which forms a narrow sheet along the eastern limb of the Zaaikloof Fold between the Pretoria Group and the Rustenburg Layered Suite.

In either case, this is contrary to the 1:250 000 Nylstroom 2428 Geological Survey Sheet of the area, which shows the quartzite of the Dwaalheuwel Quartzite Formation in direct contact with the upper zone of the Rustenburg Layered Suite.

To the south of Pramkoppies hill, the complete upper succession of the Pretoria Group, from the Dwaalheuwel Quartzite Member to the Magaliesberg Quartzite Formation, is exposed. The Magaliesberg quartzites form a prominent EW-trending ridge and are in contact with the upper zone of the Rustenburg Layered Suite and granites of the Lebowa Granite Suite. Structural data for the Pramkoppies area are represented in Figure 4.34.

### *S<sub>2b</sub> foliation*

The dominant foliation in the area strikes approximately EW and dips towards the south at between 30° and 70° (Figure 4.34). This is considered represent the axial planar foliation of the dominant Pramkoppies anticline. Schistose rocks are generally poorly exposed, particularly in the lower grade core of the fold. In the migmatite zone however, cordierite-biotite-fibrolite rocks of the Lydenburg Shale Member are typified by an anastomosing network of numerous leucosome veinlets. Bedding is often defined by thin, millimetre-scale fibrolite-rich domains that are cross-cut by the veinlets. The veinlets are in turn cut by an S<sub>2</sub> foliation, which is most easily visible within the leucosome veins themselves and suggests that deformation was continued after melt formation and strain was partitioned into the leucosome veins.

On the eastern margin of Pramkoppies, the Roodepoort Complex quartz-feldspar porphyry intrudes the Boven Shale Member of the Silverton Shale Formation. Igneous layering in this exposure is folded and is superimposed by a penetrative S<sub>2</sub> foliation (Figure 4.35 and 4.36) which is generally subparallel to metre-scale folds. In some parts of the exposure however, the foliation deviates markedly from the axial-planar orientation. As discussed earlier in the section on the quartz-feldspar porphyry, the folds in these rocks may represent igneous flow folds. Since the intrusion is correlated with the earliest of the felsic intrusives of the Rashoop Granophyre Suite which is considered to be largely synchronous with the Rustenburg Layered Suite, it is therefore likely that the intrusion is also syntectonic and syn-contact metamorphism. This would explain the common occurrence of flow folding subparallel to the regional tectonic trends in the fold domains and the lack of folding in the interpericlinal domains. Further, the overprint of a marked S<sub>2</sub> foliation slightly discordant to the axial plains of the folds, suggests that deformation continued after the complete crystallisation of the quartz-feldspar porphyry.

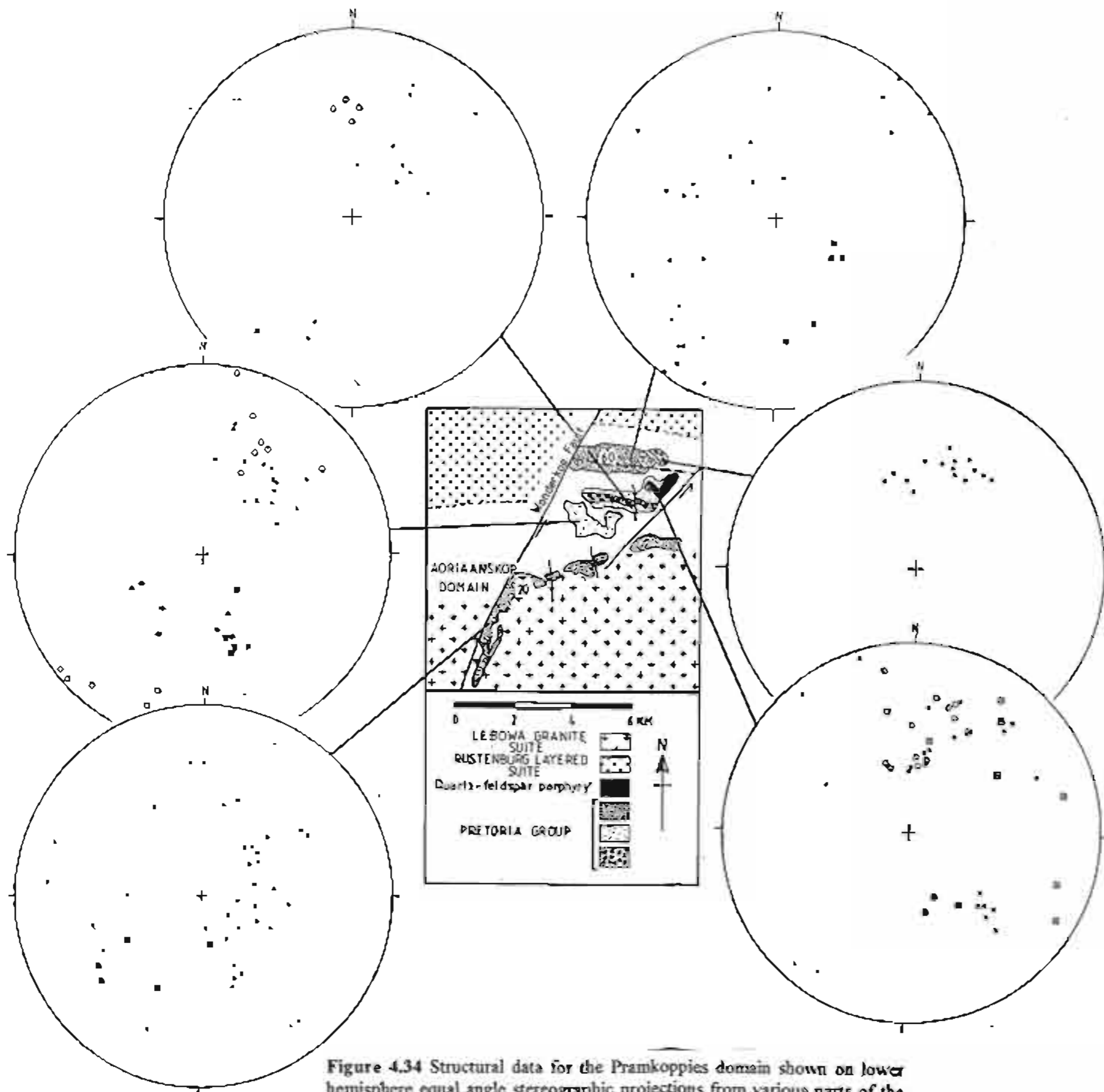
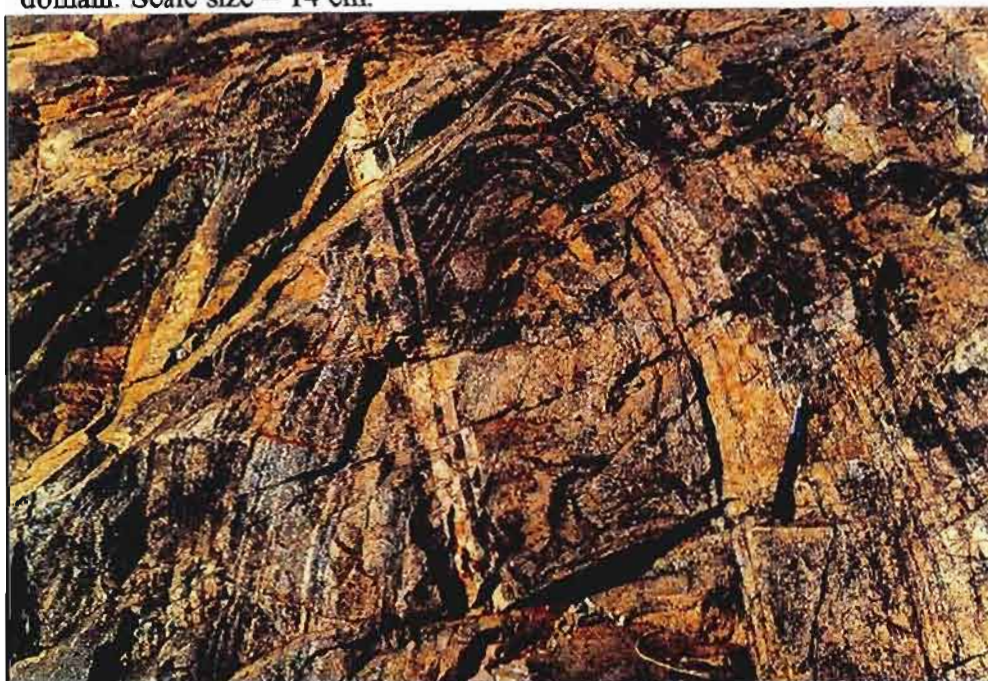


Figure 4.34 Structural data for the Prankoppies domain shown on lower hemisphere equal angle stereographic projections from various parts of the structure. Poles to sedimentary stratification ( $\bullet$ ); poles planar foliation ( $\circ$ ); mineral lineations ( $\times$ ); boudin axes ( $\blacklozenge$ ); mesoscale  $F_2$  fold axes ( $\blacksquare$ ); poles to aplite veins ( $\square$ ).



**Figure 4.35** A steeply dipping and EW-striking  $S_2$  foliation (parallel to pen) in the quartz-feldspar porphyry crosscutting the igneous flow layering. Late left-stepping intrusive aplite veins are unfoliated. Exposure forming the divide between the farms Koppiesdam, Stofpoort and Mphatlele in the Pramkoppies domain. Scale size = 14 cm.



**Figure 4.36** Flow folding in the quartz-feldspar porphyry at the same locality as Figure 4.35.  $S_2$  foliation is parallel to pen. Fold is cut by late-stage unfoliated aplite vein trending NW-SE and small  $D_3$  faults, trending  $160^\circ$ , associated with the Leeukop Fault system. Scale size = 14 cm.



### ***F<sub>2b</sub> folding***

Locally thin siliceous calc-silicate horizons within the Silverton Shale Formation are deformed into metre-scale  $F_{2b}$  folds with axial planes subparallel to the  $S_2$  fabric.

### ***Boudinage***

Boudin axes in the Silverton Shale Formation are oriented both parallel and normal to the fold axes (Figure 4.34). This indicates that significant extension occurred both along the fold hinge orientation as well as normal to the fold hinge in the fold limbs. It could not be established if the two boudin sets were developed at different times during  $D_2$  deformation. The most likely explanation is that the fold-axis normal boudinage developed first, as is found in the interpericlinal domains such as Mathabatha and Seropse. As the folding in the fold domains proceeded, fold axis parallel extension became operative producing the next generation of boudins.

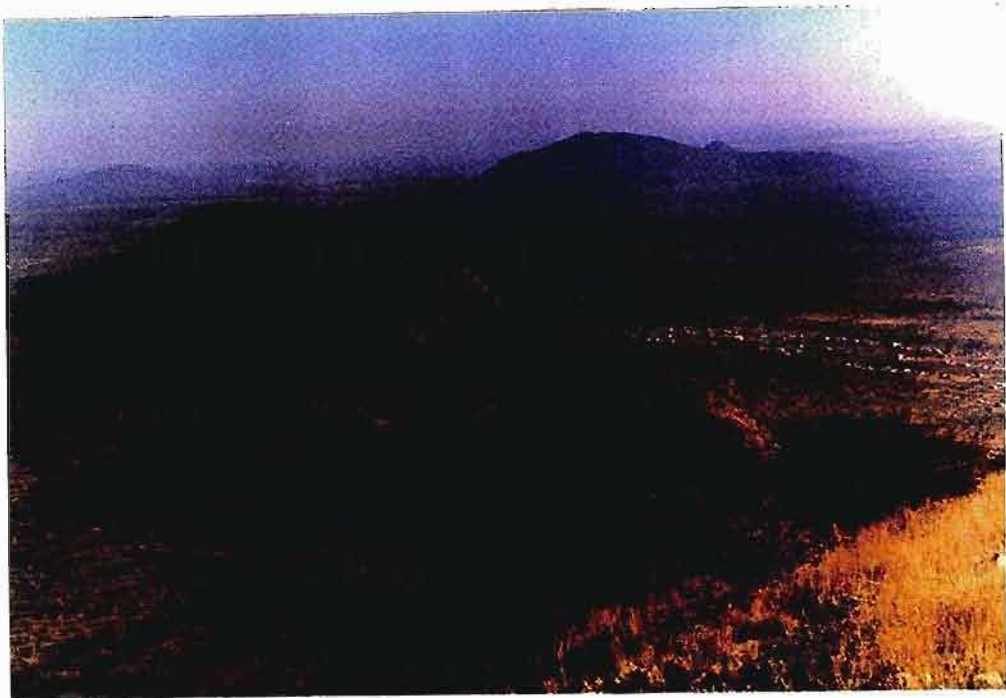
### ***Faulting***

The Pramkoppies area is bounded in the west by the Wonderkop Fault and in the east by the Leeukop Fault. Numerous secondary faults transect the area with displacements ranging from a few metres to tens of metres. These faults generally contain a significant dip slip component. As in the Katkloof domain (Figure 4.25), these faults are oriented at a high angle to the master strike slip system and represent the extensional fractures developed during  $D_3$  deformation.

#### **4.3.7 The Adriaanskop Fold domain**

Adriaanskop is a prominent hill in the southern part of the study area (Figure 4.37) comprising highly deformed quartzites correlated with the Magaliesberg Quartzite Formation and underlain by pelitic rocks of the Silverton Shale Formation (Appendix 1C and 1F). The Adriaanskop structure is surrounded by and in places is intruded by granitic veins of the Lebowa Granite Suite. These are relatively undeformed and clearly post-date the metamorphism and the deformation within the Silverton Shale Formation.

Although the contacts with the Bushveld granite are poorly exposed, the Adriaanskop “fragment” was found to be far more extensive than previously represented. The absence of granitic soils and scattered Pretoria Group outcrops indicates that large parts of the area are



**Figure 4.37** View towards the SSW from Grootkop in the Prankoppies domain towards Adriaanskop. The hill in the foreground comprises deformed quartzite of the Magaliesberg Quartzite Formation. Low lying areas to the immediate left and right are underlain by granite of the Lebowa Granite Suite. Adriaanskop consists of highly deformed quartzite of the Magaliesberg Quartzite Formation and the area immediately in front of Adriaanskop, of deformed pelites of the Silverton Shale Formation. The hill on the far left horizon is part of the Malope Dome.

underlain by Pretoria Group strata contrary to the 1978 geological survey maps (Chuniespoort-Wolkberg, 1:125 000 scale and the 1:250 000 Nylstroom sheet) which show the area to be underlain by granite of the Lebowa Granite Suite.

The relationship with the Rustenburg Layered Suite, although obscured by the granite, must have been similar to the other structures described above to give rise to the typical intense pre-Bushveld Granite deformation and metamorphism. Aeromagnetic data for the area (Appendix 1G) show that area to the west of the Adriaanskop domain is highly magnetic and represents the upper zone of the Rustenburg Layered Suite that immediately underlies the Lebowa Granite Suite rocks. Approximately 5 km south of Adriaanskop lies the Malope Dome described by Marlow and van der Merwe (1977). Here Pretoria Group strata are surrounded by the highly

magnetic upper zone gabbros of the Rustenburg Layered Suite within the granite of the Lebowa Granite Suite. From the aeromagnetic map, the Malope Dome can be traced northwards into the Adriaanskop domain as a continuous trough of low magnetic response, suggesting that Pretoria Group rocks are in some way connected as a continuous domal ridge that is intruded by granite of the Lebowa Granite Suite.

The rocks of the northern margin of the Adriaanskop domain, in the farm Spitskop (Appendix 1C and 1F), comprise highly deformed diamictites (Figure 4.38), conglomerates, quartzites, leptites (Figure 4.39) and minor calc-silicates. This association suggests that the succession correlates with the upper Pretoria Group strata of the Magaliesberg, Vermont and Lakenvalei Formations. This interpretation is also given on the 1978 1:250 000 geological survey map of the area, although the earlier 1962 interpretation was that the rocks correlated with those of the middle Pretoria Group, the Daspoort - Dwaalheuwel Formation.

The structure represents a broad anticline, with the Magaliesberg Quartzite Formation defining both the southern and the northern limbs. This suggests that there is a repetition of the Pretoria Group, excluding the Timeball Hill Formation, between the Seropse domain to the north and the Adriaanskop domain to the south of the Rustenburg Layered Suite.

The rocks in the Adriaanskop domain are deformed into a series of recumbent folds that are overturned to the north. This is similar to the isoclinal style of folding seen in the Dwaalheuwel Quartzite Formation in the Pramkoppies domain. The envelope defined by the deformed strata is in fact overturned, forming the northern limb of the Adriaanskop Fold structure.

To the north of the Kameelbult ridge, the layered mafic sequence dips towards the south at between 70° and 75°, under the Kameelbult-Spitskop quartzite ridge, subparallel to the bedding in the northern limb of the Adriaanskop fold (Figure 4.40). The simplest way to explain this relationship is that the igneous layering is truncated against the overturned northern limb of the Adriaanskop structure in the same way as the igneous layering is truncated by the limbs in the Zaaikloof, Katkloof, Schwerin and Phepane Folds.



**Figure 4.38** Partially feldspathised diamictite from the Lakenvalei Quartzite Formation exposed on the farm Kameelbult. Scale size = 25 cm.



**Figure 4.39** Intensely deformed leptite exposed on the farm Kameelbult on the northern margin of the Adriaanskop domain. Feldspathisation is interpreted as post-dating the deformation. Scale size = 14 cm.

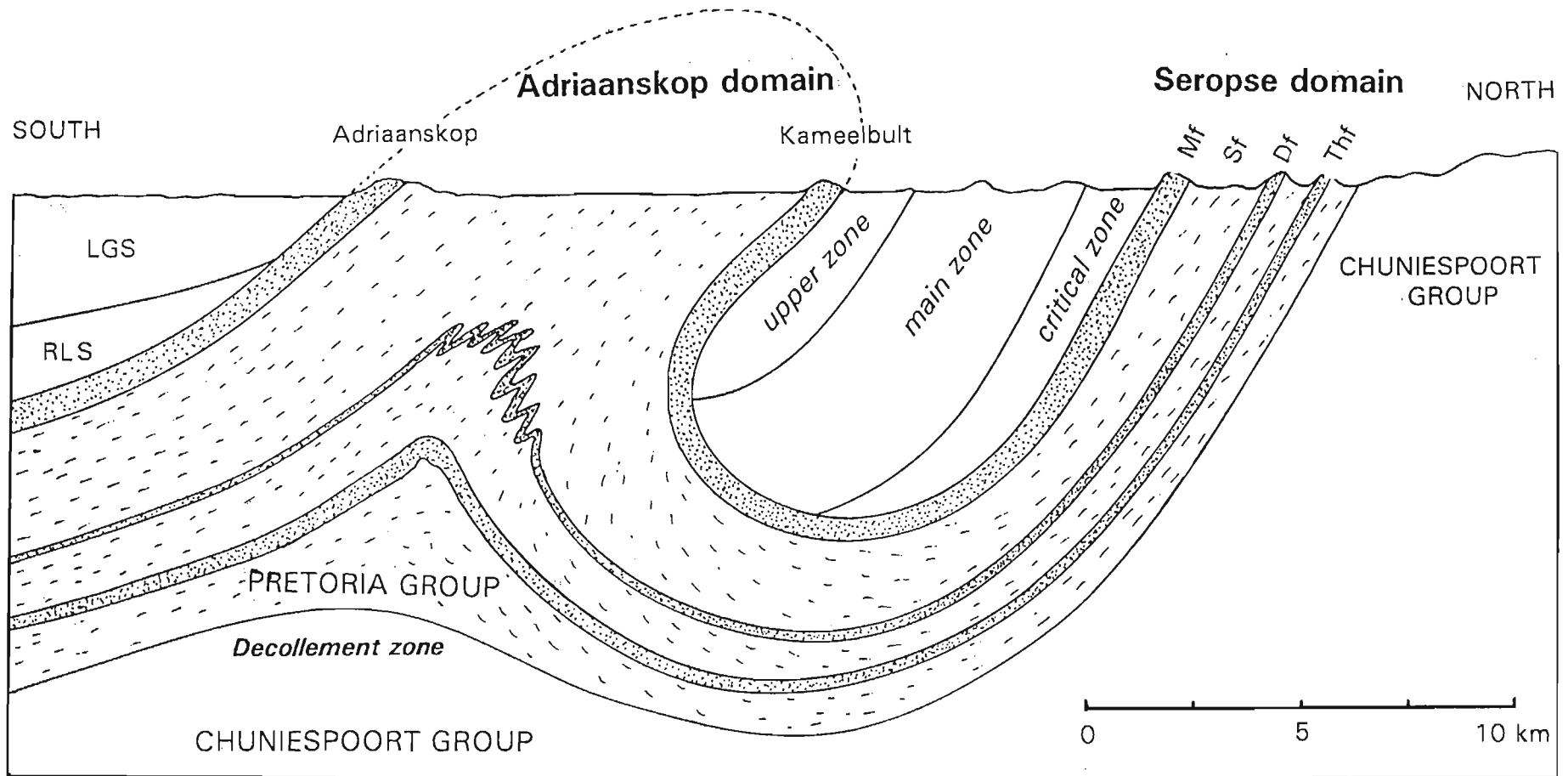


Figure 4.40 Interpretive N-S section across the Adriaanskop and Seropse domains showing the truncation of the Rustenburg Layered Suite (RLS) against the Adriaanskop structure and the proposed decollement zone at the base of the Pretoria Group. The granite of the Lebowa Granite Suite (LGS), which has intruded extensive parts of the Adriaanskop domain, has been omitted for clarity. (Thf) - Timeball Hill Formation, (Df) - Dwaalheuwel Formation, (Sf) - Silverton Shale Formation, (Mf) - Magaliesberg Quartzite Formation.

### *S<sub>2</sub>L<sub>2</sub> foliation*

D<sub>2</sub> fabrics are dominantly linear (Figure 4.41). This is particularly evident in the Magaliesberg Quartzite Formation and in the underlying Silverton Shale Formation in the southern portion of the Adriaanskop domain. Mineral lineations, often defined by chistolite crystals, are locally parallel to mesoscale fold axes. Within a single exposure and across the southern portion of the domain however, these both show a wide range of orientations defining a crude small circle-arc. The southernmost exposures of the Magaliesberg Quartzite Formation are dominated by southerly plunging lineations, whereas northerly plunges are found to the north in the underlying Silverton Shale Formation (Figure 4.41).

This may indicate that the area represents the core of a domal structure, with the lineations and fold axes plunging away from the culmination point. The westerly plunges are in marked contrast to the easterly-plunging lineations and fold axes in the neighbouring Pramkoppies and Zaaikloof domains. Although these orientations may have been affected by the intrusion of the Lebowa Granite Suite, the relatively flat-lying envelope of the Magaliesberg Quartzite Formation and the underlying Silverton Shale Formation, suggests that this area may represent the top of a single broadly periclinal structure defined by the Zaaikloof, Pramkoppies and Adriaanskop domains.

### *F<sub>2</sub> folds*

As described above, fold axes together with fold axis-parallel lineations have a wide range of orientations. In the southern Adriaanskop area, within the Silverton Shale Formation, folds generally have fairly flat-lying axial planes and the fold style is dominated by extreme non-cylindricity. Sheath-like geometry was observed in highly lineated andalusite felses at one locality.

On the northern margin of the Adriaanskop domain feldspathisation of argillites, near the contact with the Lebowa Granite Suite, has produced fine grained leptites. These are intensely deformed on a centimetre scale (Figure 4.39) with fold axes plunging toward the east at between 10° and 20° (Figure 4.41). Feldspathisation post-dates the deformation, and indicates that the granite of the Lebowa Granite Suite was emplaced after the D<sub>2</sub> deformation in the contact aureole.

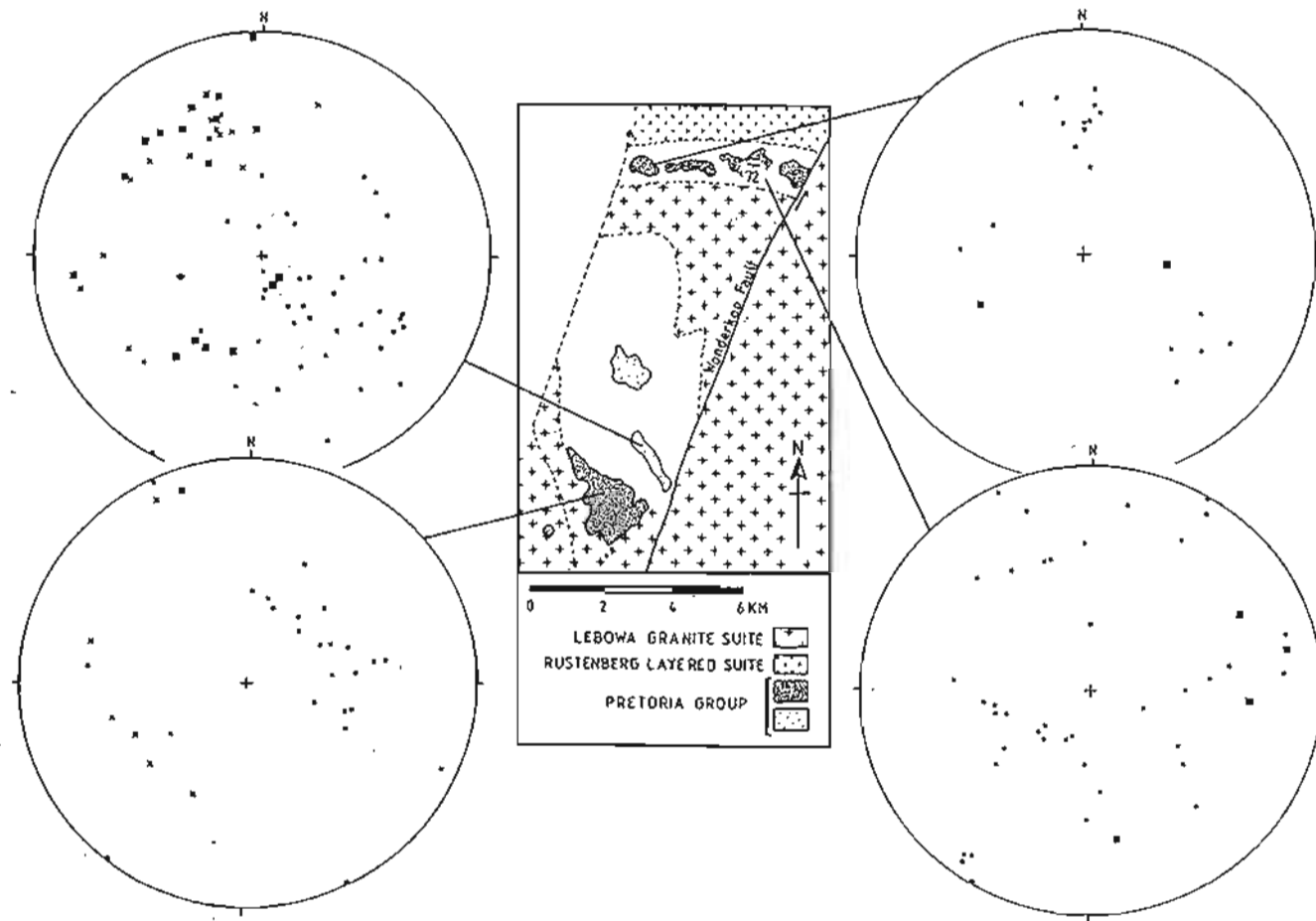


Figure 4.41 Structural data for the Adriaanskop domain. Lower hemisphere equal angle projections. Poles to bedding (●); mineral lineations (x); boudin axes (◆); mesoscale fold axes (■).

### ***Brecciation and leptite formation***

Extensive brecciated zones are found on the northern margin of the Adriaanskop domain. On the farm Zuiping a rheomorphic breccia of quartzite clasts are imbedded in a feldspathic, leptite, matrix. Highly siliceous fragments generally remain unaltered, whereas more arkosic units are more highly recrystallised to leptite (Figure 4.42). Fragments are usually tabular in shape representing original bedding units. These may become rounded due to partial assimilation (Figure 4.42). The origin of these rocks is interpreted as being due to the intrusion of the Lebowa Granite Suite and associated feldspathisation and hydraulic fracturing of the quartzite.



**Figure 4.42** Rheomorphic breccia in quartzite of the Lakenvalei or Magaliesberg Quartzite Formation on the farm Zuiping. Angular and rounded quartzite xenoliths are imbedded in a matrix of leptite. Scale size = 25 cm.

#### **4.3.8 The Phepane Fold domain**

The Phepane or Paradys structure (Sharpe and Chadwick, 1981) forms a prominent closed 8 km by 5 km elliptical feature within the upper zone of the Rustenburg Layered Suite (Appendix 1D). The Machadodorp Member of the Silverton Shale Formation is exposed as a series of low lying hills in the core of the structure (Figure 4.43). The strata young outwards from the core towards the perimeter which is marked by a prominent semi-circular ridge on the western limb, the Phepane hills (Figure 4.43). These hills are formed by the strata of the Magaliesberg





**Figure 4.43** Panoramic view towards the north from the southern margin of the Phepane structure. Ridge on the extreme left consists of overturned eastward-dipping Magaliesberg Quartzite Formation. The three vegetated hills in the centre consist of highly deformed Silverton Shale Formation and Machadodorp Member rocks. The long ridge immediately beyond these hills also consists of inward dipping, overturned Magaliesberg Quartzite Formation strata. The rugged topography in the distance consists predominantly of mafic layered rocks of the main zone of the Rustenburg Layered Suite.

Quartzite, Vermont Hornfels and Lakenvalei Quartzite Formations. Schweltnus *et al.* (1962) and the 1978, 1:250 000 geological survey map of the area indicates that the strata are overturned and dipping inwards at between 80° and as little as 10° on the western limb of the structure. This study however, showed that the southern part of the structure is not overturned and dips steeply outwards at 85°. The overturned strata on the western limb dip inwards at between 86° in the south and 36° in the central area, steepening in the north again to 60°. The eastern limb was found to be overturned, dipping inwards at between 24° and 30° (Figure 4.44).

Geophysical evidence, both gravity and magnetic, for the Phepane structure (Molyneux and Klinkert, 1978) suggests that it is attached to the floor in the same way that the Katkloof and Schwerin Folds are. The similarity in size and geometry and the presence of Machadodorp Member rocks in the core of the Phepane structure further indicates that the structure is situated above a detachment level of similar depth to that of the Schwerin and Katkloof Folds, near the base of the Pretoria Group.

A shallowly dipping magnetite seam of the upper zone of the Rustenburg Layered Suite abuts against the structure on the western and eastern limbs (Appendix 1D). This is confirmed by magnetic data (Appendix 1G) which show that the structure is surrounded by highly magnetic rocks. The discordance with the igneous layering, as seen in the other fold structures, indicates that folding was initiated and developed during the magmatic stage of the Rustenburg Layered Suite. Locally the layering in the upper zone is also disturbed, such as at Malekskraal to the northeast of the structure. This suggests that the same deformation event continued until after the development of igneous layering, or that the igneous layering was folded by a later, unrelated tectonic event.

The distribution of the intrusive Lebowa Granite Suite under the alluvial cover to the west of the Phepane structure is clearly shown on the magnetic map (Appendix 1G). As in the Zaaikloof Fold, the discontinuity formed by the steep limbs of the Pretoria Group folds and the truncated Rustenburg Layered Suite provided a pathway for the emplacement of the granite, which served as feeders to the concordant granite sheets at higher levels.

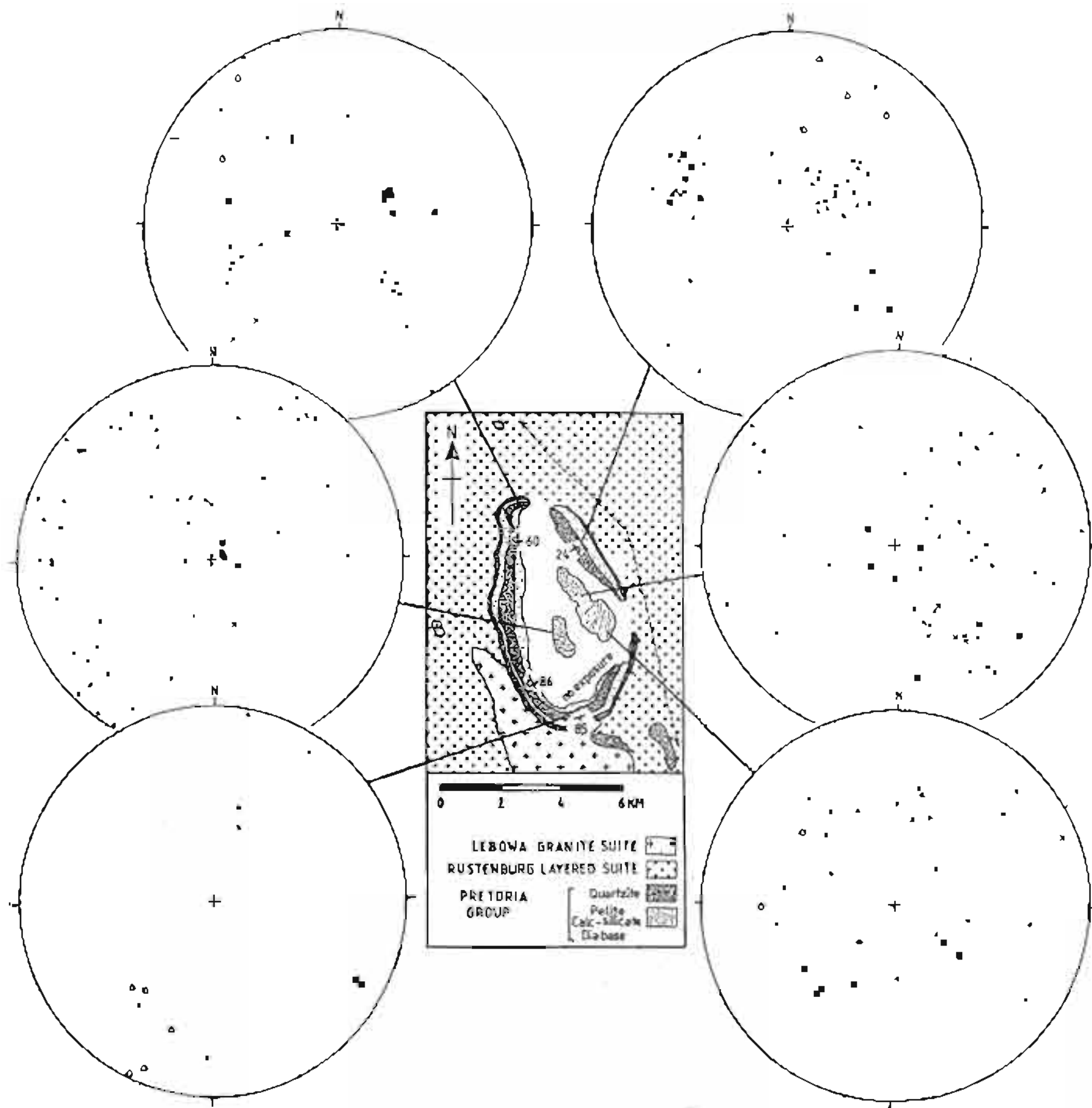


Figure 4.44 Structural orientation data for the Phepane structure. Lower hemisphere, equal angle stereographic projection. Poles to sedimentary stratification ( $\bullet$ ); poles to planar foliation ( $\circ$ ); mineral lineations ( $\times$ ); boudin axes ( $\blacklozenge$ ); mesoscale fold axes ( $\blacksquare$ ).

A zone of low magnetic response shows that the Phepane structure is connected with the Haakdoorndraai structure and extends almost into the Zaaikloof structure. Although no detailed gravity data are available, this may indicate that the Phepane, Zaaikloof, Prankoppies and Adriaanskop structures represent a much larger anticlinal ridge with local culminations and depressions.

Cross-stratification structures in the Magaliesberg and Lakenvalei Quartzite Formations provides further evidence for the overturned nature of the limbs and the outward younging of the structure. Over most of the perimeter, the strata are overturned, dipping at moderate angles inwards beneath the Silverton Shale Formation in the core.

Strata in the core are steeply dipping compared to the overlying and overturned perimeter sequences, suggesting that the geometry of the structure is bulbous in shape rather than a synformal anticline. A general steepening of the dips inwards is also evident from the north to the south of the structure, becoming vertical and dipping steeply southwards at the southern end.

### *S<sub>2</sub> L<sub>2</sub> fabric*

In the core of the structure, fabrics are dominantly linear. Hornblende crystals in metavolcanics of the Machadodorp Member best define the mineral lineations that plunge steeply in the core and at more moderate angles nearer the margins of the structure. Locally, S<sub>2</sub> defines an axial-planar fabric to mesoscale folds.

On the perimeter the S<sub>2</sub> foliation is near bedding parallel and has a broadly tangential distribution around the circumference of the structure. Two lineation directions are present. The first set (L<sub>2b</sub>) plunges down-dip into the centre of the structure. These lineations are deformed in places by folds with fold-axes that are oriented tangentially to the structure (Figure 4.45).



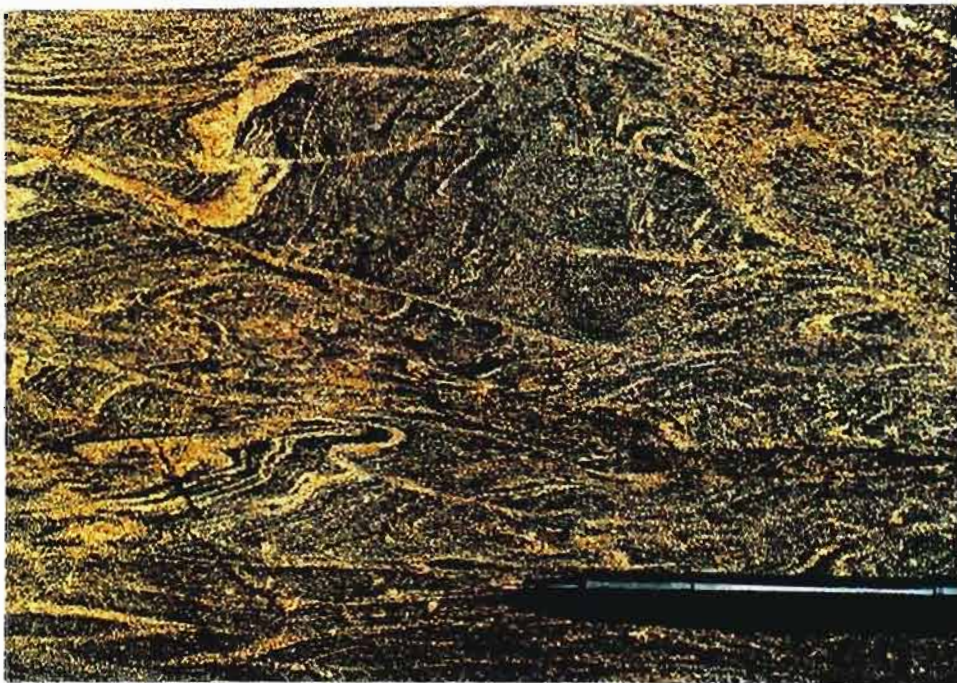
Figure 4.45 Deformed lineations in the Vermont Hornfels Formation on the northern perimeter of the Phepane structure. Early steeply plunging lineations that plunge towards the centre of the structure are deformed by later shallow plunging folds with axes oriented tangentially to the structure. Scale length = 14 cm.

In places, the  $S_2$  foliation strongly transposes the original bedding by a series of spaced ductile shears. These are found in the Magaliesberg Quartzite Formation on the perimeter of the Phepane structure (Figure 4.46) and in the pelites of the Silverton Shale Formation where they are associated with anatectic melts. Melt veins are both bedding parallel and occupy the  $S_2$  shears (Figure 4.47).

On the northern margin of the Phepane structure the dominant shear direction is left lateral. A migmatitic diamictite horizon in the upper Silverton Shale Formation is similarly deformed by left lateral ductile shears. Tails on semi-ductile clasts provide useful kinematic indicators showing left-lateral displacement (Figure 4.48a). Competent vein-quartz clasts, some still showing hexagonal crystal structure, are unaffected by the melting and are scattered within a ductile pelitic matrix (Figure 4.48b).

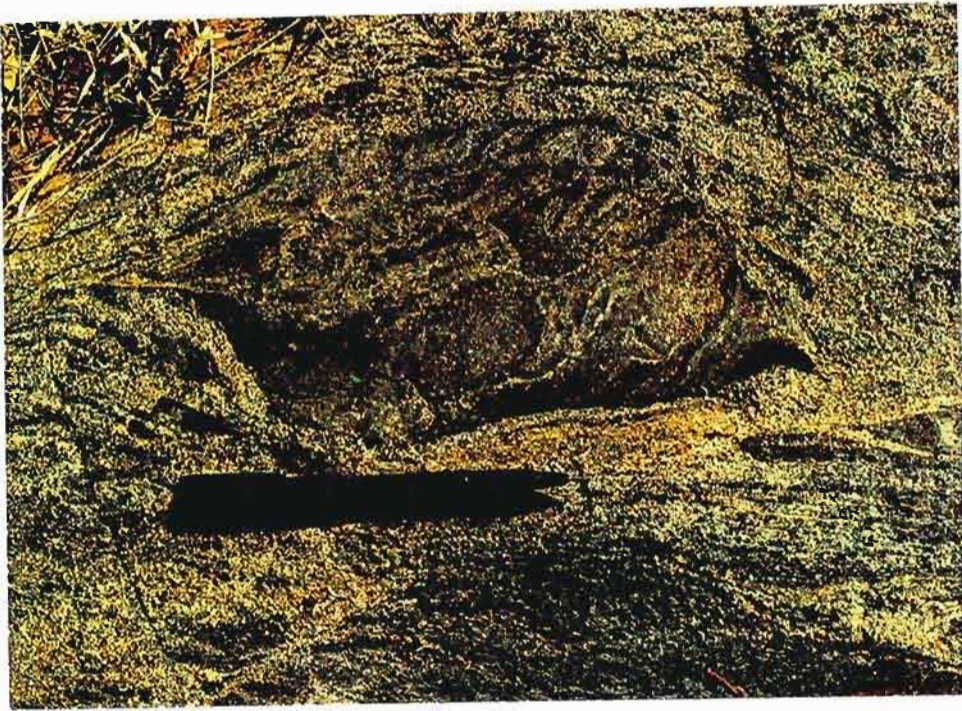


**Figure 4.46** Spaced ductile shears in the Magaliesberg Quartzite Formation on the northeastern limb of the Phepane structure defining the  $S_2$  foliation that transposes the original bedding. Scale length = 14 cm.



**Figure 4.47** The  $S_2$  transposition fabric in migmatitic Vermont Hornfels Formation in the northern part of the western limb of the Phepane structure. Shears are consistently left lateral in this part of the structure. Scale length = 10 cm.

**a**



**b**



**Figure 4.48** a) Semi-ductile clast in a diamictite unit in the upper part of the Silverton Shale Formation showing left lateral kinematic shear sense. Northern margin of the Phepane structure on the farm Driekop. b) More competent vein quartz clast with draped  $S_2$  foliation. Scale sizes 14 and 12 cm respectively.

### *F<sub>2</sub> folds*

Mesoscale fold axes, together with mineral lineations, are steeply plunging in the core of the structure (Figure 4.49). Around the perimeter of the structure however, fold axes and mineral lineations are plunge at more shallow angles, defining both tangential and radial orientations (Figure 4.44). The tangential oriented folds deform earlier steeply plunging lineations (Figure 4.45).



Figure 4.49 Steeply plunging fold of Machadodorp Member calc-silicate in the core of the Phepane structure. Scale size 20 cm.

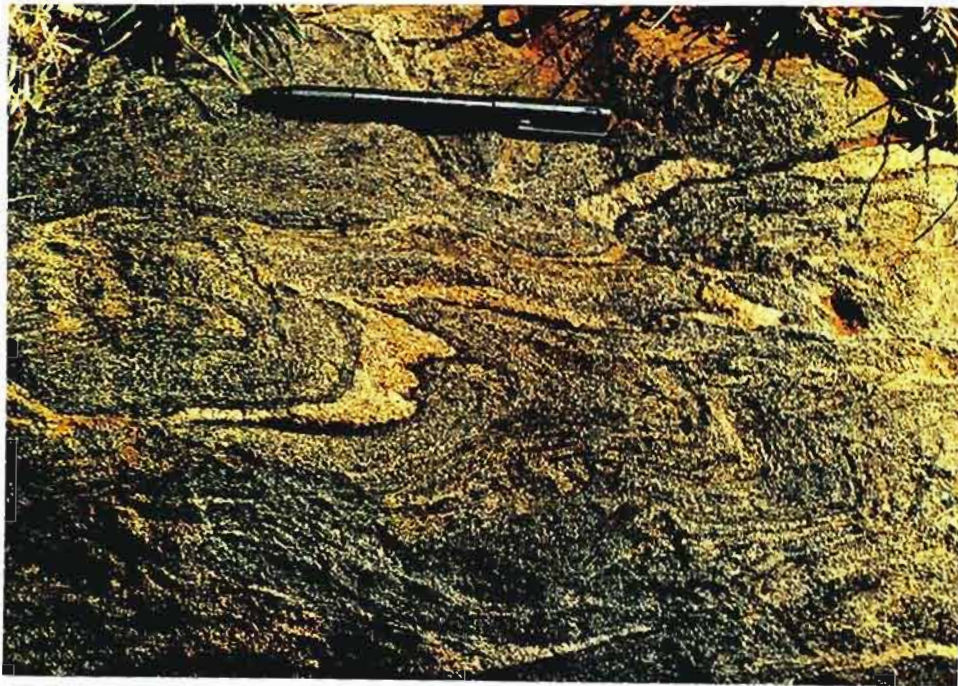
The typical association of spaced ductile shears with the  $D_2$  deformation in the Phepane structure, results in the development of incipient “fish-hook type” folds. These are particularly common in the migmatites in the core of the Phepane structure (Figure 4.50). The folds are considered to be produced by a single progressive  $D_2$  deformation. For dextral shears, maximum incremental shortening rotated clockwise from an initially layer parallel to a layer oblique orientation. During the final stages, right lateral leucosome-filled shears resulted in extreme limb attenuation.

In places, more symmetrical tight folds are developed within the  $S_2$  transposition fabric. These are defined by early bedding parallel leucosomes that form small folds with highly attenuated, often rootless limbs (Figure 4.51).



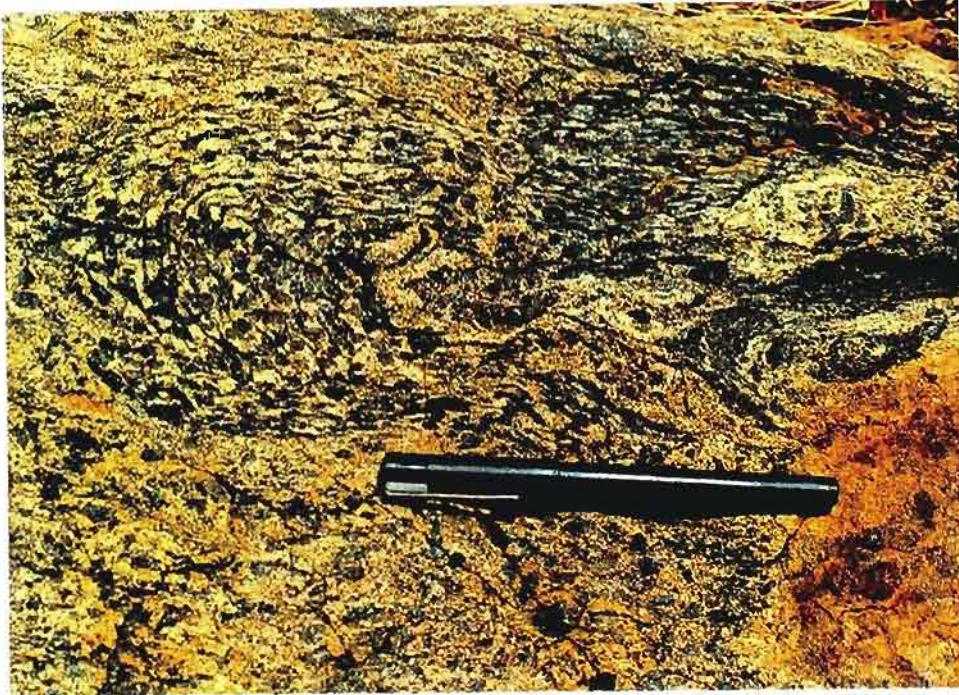


**Figure 4.50** Incipient “fish-hook type” folds developed by right lateral ductile shears. Migmatite from the core of the Phepane structure in the Silverton Shale Formation. Scale size = 14 cm.



**Figure 4.51** Folded bedding-parallel leucosomes in a migmatite from the core of the Phepane structure, Silverton Shale Formation. Scale size = 14 cm.

In folded cordierite-rich migmatites, cordierite porphyroblasts define strain markers (Figure 4.52). Low strains are found within the cores of the folds, with slightly flattened axial planar cordierite porphyroblasts. In the limbs these become extremely flattened within the  $S_2$  foliation.

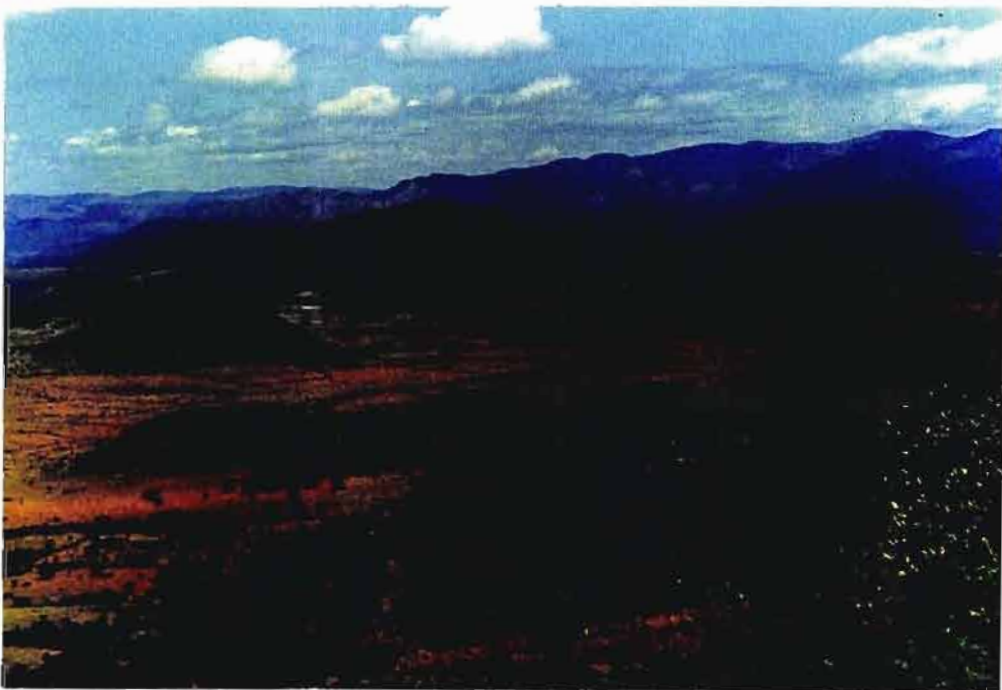


**Figure 4.52** Folded cordierite gneiss in the Silverton Shale Formation on the northern margin of the Phepane structure. Transposition of  $S_0$  or early near bedding parallel  $S_2$  layering during progressive deformation. Flattened cordierite porphyroblasts define the  $S_2$  foliation on the limbs of the fold but are almost spherical in the low strain fold core. Scale size = 14 cm.

#### 4.3.9 Xenoliths

Numerous small xenoliths may be found throughout most of the Rustenburg Layered Suite. The lower contact of the lower zone with the Pretoria Group floor (Cameron' (1978) basal subzone, which is correlated with the marginal zone elsewhere) is rich in xenoliths. Other important localities in the eastern Bushveld Complex have been described by Willemse and Bensch (1964), Willemse and Viljoen (1970), Wallmach (1986) and Wallmach *et al.* (1989). These are mostly calc-silicates characterised by extremely high grade metamorphic mineral assemblages with peak temperatures between 1200 and 1300°C.

The most prominent and more significant xenoliths in the study area are found between the Katkloof and the Schwerin Folds. The xenoliths outcrop as a series of hills that form an EW-striking zone within the lower zone of the Rustenburg Layered Suite. The rocks comprise migmatitised upper Pretoria Group strata, correlated with the Vermont Hornfels Formation. Ten small localities occur on the farm Winterveld, and three on the farm Moeijelyk (Figure 4.53) (Appendix 1).



**Figure 4.53** View towards the west from the eastern Moeijelyk xenolith exposed in the foreground to the right. The lower ridge immediately beyond that is part of the central Moeijelyk xenolith, and the isolated hill beyond that, the western Moeijelyk xenolith. The Winterveld xenoliths are exposed at the Winterveld residence, visible as a small white dot beyond the Moeijelyk west xenolith. The cuesta ridge dip slope is formed by erosively resistant lower zone pyroxenites that overlie norites of the basal subzone (marginal zone) of the Rustenburg Layered Suite. The high-lying area in the distance comprise contact metamorphosed rocks of the Transvaal Supergroup.

#### *Internal structure of xenoliths*

The least deformed xenolith is the Moeijelyk East xenolith which is only slightly detached from the underlying Pretoria Group. The strata are near-concordant with the western limb of the Schwerin Fold and are intruded by numerous Bushveld norite sills. The internal structures are characterised by near-bedding-parallel leucosomes.

The Moeijelyk Central xenolith comprises more highly folded Vermont Hornfels Formation strata in contact with norite. Folds are truncated by the intrusions suggesting that deformation occurred before or during the incorporation of the strata into the lower zone as a xenolith. The fold axes show a wide range of orientations that approximate a small-circle arc (Figure 4.54). This suggests that the early folds, of  $F_{2b}$  age, have been deformed about an approximately NS trending axis.

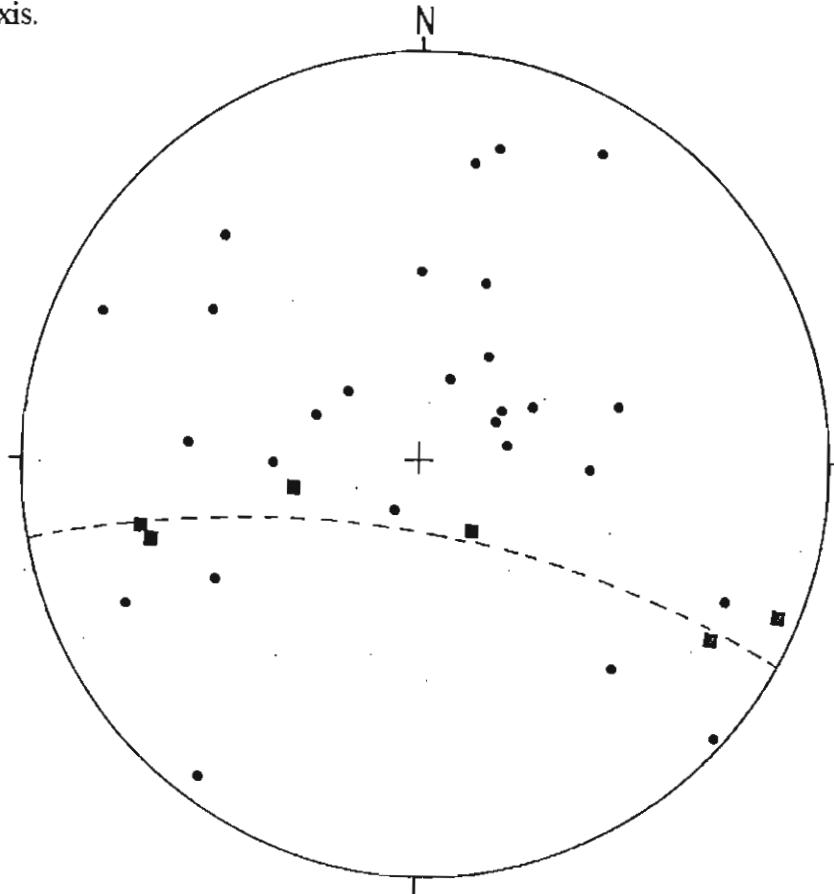


Figure 4.54 Structural data from the Moeijelyk Central xenolith showing the wide scatter of bedding orientations and fold axes that define a small circle arc. Lower hemisphere equal angle projection. Poles to sedimentary stratification (●); mesoscale fold axes (■).

The Moeijelyk West xenolith forms a thin deformed capping of Vermont Hornfels Formation quartzite, semi-pelite and minor calc-silicate to the hill which is mainly underlain by norite. The southern portion of the xenolith contains tight to isoclinal folds that plunge towards the southwest at  $10^\circ$  with an associated near vertical axial planar foliation.

The xenoliths on Winterveld are more poorly exposed and mainly comprise massive recrystallised quartzite without any internal fabric.

If the line of xenoliths is extended along strike to the Katkloof Fold, it intersects the fold where the Magaliesberg Quartzite Formation is partially detached from the underlying Pretoria Group. A similar structure is developed on the western flank of the Schwerin Fold, where the Moeijelyk-east xenolith is only just separated from the floor. This relationship indicates that most of the lower zone in this area was emplaced at the contact between the Magaliesberg Quartzite Formation and Vermont Hornfels Formation.

#### **4.3.8 Conclusions**

The four large fold structures studied all have a periclinal geometry with similar diameters of approximately 8 km. The metamorphic grade as well as the internal structures are also very similar, suggesting that they are closely related in time and developed by similar deformation mechanisms. Reconstruction of the folds by axial planar sections shows that shape variations on the map are due to the differing erosional levels and erosional orientations relative to the culmination axis of the periclinal folds. All four large fold structures studied are thus considered to have been initiated at the same time with very similar growth histories and  $D_2$  deformation paths. From the above field evidence, deformation is considered in each of the structures to have been initiated during lower zone times and continued into Lebowa Granite Suite time. More precise timing constraints will be explored in subsequent chapters. These conclusions are in contrast to previous interpretations. Schweltnus (1956) concluded that the folding of the Katkloof Fold ceased before the crystallisation of the critical zone. Sharpe and Chadwick (1981) suggested that each structure evolved independently, each initiated during pre-lower zone times and each terminating at different times from between critical zone times to pre-upper zone times.

#### ***Erosional level***

The lowest erosional section seen is in the Schwerin Fold, which is in contact with the lower and critical zones of the Rustenburg Layered Suite. The erosional section is oblique to the culmination axis and the northern periclinal fold closure has been removed by erosion. Reconstruction of the fold shows that the structure probably did extend upwards into the upper zone of the Rustenburg Layered Suite.

The erosional level in the Katkloof Fold is slightly higher, showing that the structure is in

contact with the lower, critical, and main zone of the Rustenburg Layered Suite. Upper zone rocks are exposed approximately two kilometres to the south of the fold nose and a simple pre erosion reconstruction shows that the upper part of the fold was in contact with the upper zone. As in the Schwerin structure, the northern periclinal closure has been removed by erosion.

The Zaaikloof-Pramkoppies-Adriaanskop structure is in contact with the main and upper zones of the Rustenburg Layered Suite and represents an erosional level slightly higher than the Katkloof Fold. The true geometry of the pericline is obscured by post-Bushveld Complex strike-slip faulting, but reconstruction indicates that the complete structure represents a floor attached anticlinal ridge with a curving axial trace. The Rustenburg Layered Suite is truncated by the anticlinal ridge on both the northern and southern sides.

The Phepane structure represents an erosional section that is stratigraphically the highest and that is almost normal to the culmination axis of the pericline. It is completely surrounded by upper zone rocks.

### *Overturning*

The degree of overturning in the limbs of all the structures also increases with stratigraphic height. For example no overturning is found in the Schwerin Fold. The western limb of the Katkloof Fold is locally overturned. The eastern limb of the Zaaikloof Fold is largely overturned and in the Pramkoppies and Adriaanskop area the complete northern limb of the structure is overturned. At the highest erosional level seen in the Pramkoppies structure, almost the entire outer rim of the fold structure is overturned.

The geometry of these fold structures is thus consistent with bulbous shapes at the highest levels and more cusped shapes at lower structural levels. These shapes are consistent with diapiric geometries. The origin of these structures as diapirs will be explored in more detail in Chapter 7.

### *Metamorphic grade*

Metamorphic grade also increases with structural height within the structures. Erosional sections through the lower levels of the structures, such as the Schwerin and Katkloof Folds

show grades from the upper andalusite zone to migmatite zone. In the Zaaikloof Fold only the fibrolite and migmatite zone are represented. At the highest erosional section, in the Phepane structure, all the rocks are migmatites and show the presence of high temperature spinel-bearing assemblages (Chapter 6). The possible reasons for this will also be discussed in a later chapter.

#### **4.4 SYN-BUSHVELD ( $D_2$ ) DEFORMATION OF THE CHUNIESPOORT GROUP**

##### **4.4.1 Introduction**

Although this study concentrated on the  $D_2$  syn-Bushveld Complex deformation in the Pretoria Group, the occurrence of  $D_2$  structures in the underlying Chuniespoort Group is briefly investigated. As discussed in the introductory sections, the age and origin of the deformation events in the Chuniespoort Group, forming the Mhlapitsi Fold Belt, are not well established (Table 4.1). The complexity has resulted from repeated reactivation of the Thabazimbi Murchison Lineament (TML) which produced multiple post-Transvaal Supergroup deformation events (Good and De Wit, 1997). The recognition of syn-Bushveld Complex deformation is therefore an important time marker in unravelling the structural history of this fold belt.

The 20 km wide Mhlapitsi Fold Belt defines the northern margin of the eastern Bushveld Complex and is considered to form part of the TML (Good and De Wit, 1997). The orogenic belt is characterised by intensely deformed sub-Pretoria Group sequences of the Chuniespoort Group, Black Reef Formation and Wolkberg Group (Bastin, 1968; Button, 1973; Dreyer, 1982; Potgieter, 1988; 1991). Banded ironstones and dolomites of the Chuniespoort Group are characterised by short wavelength, tight to isoclinal folds (Figure 4.55) compared to the more open, longer wavelength folds in the underlying Black Reef Quartzite Formation and the volcanosedimentary Wolkberg Group (Schwellnus *et al.*, 1962). Chuniespoort Group dolomites and banded ironstones are considered to have been less competent than the underlying arenaceous and volcanic rocks of the Wolkberg Group and thus show a higher degree of fold development.

##### **4.4.2 $D_2$ structures**

In the Mathabatha area, moderately inclined sub-horizontal isoclinal folds in the banded ironstones of the upper Chuniespoort Group (immediately underlying the Pretoria Group) are

generally slightly overturned towards the north, with the southern limbs consistently more highly attenuated than the northern limbs (Figure 4.55). Dip isogon construction of the thicker more competent beds reveal slightly convergent dip isogons characteristic of class 1C folds. Ptygmatic folds developed in chert bands within dolomite (Figure 4.56) are typical of the high viscosity contrast fold structures developed in the Malmani Subgroup of the Chuniespoort Group.



**Figure 4.55** Westward down plunge view of an isoclinal fold in the banded ironstones of the Penge Formation, on the farm Hoogenoeg. Note the more attenuated southern limbs of the folds. Scale size = 14 cm.

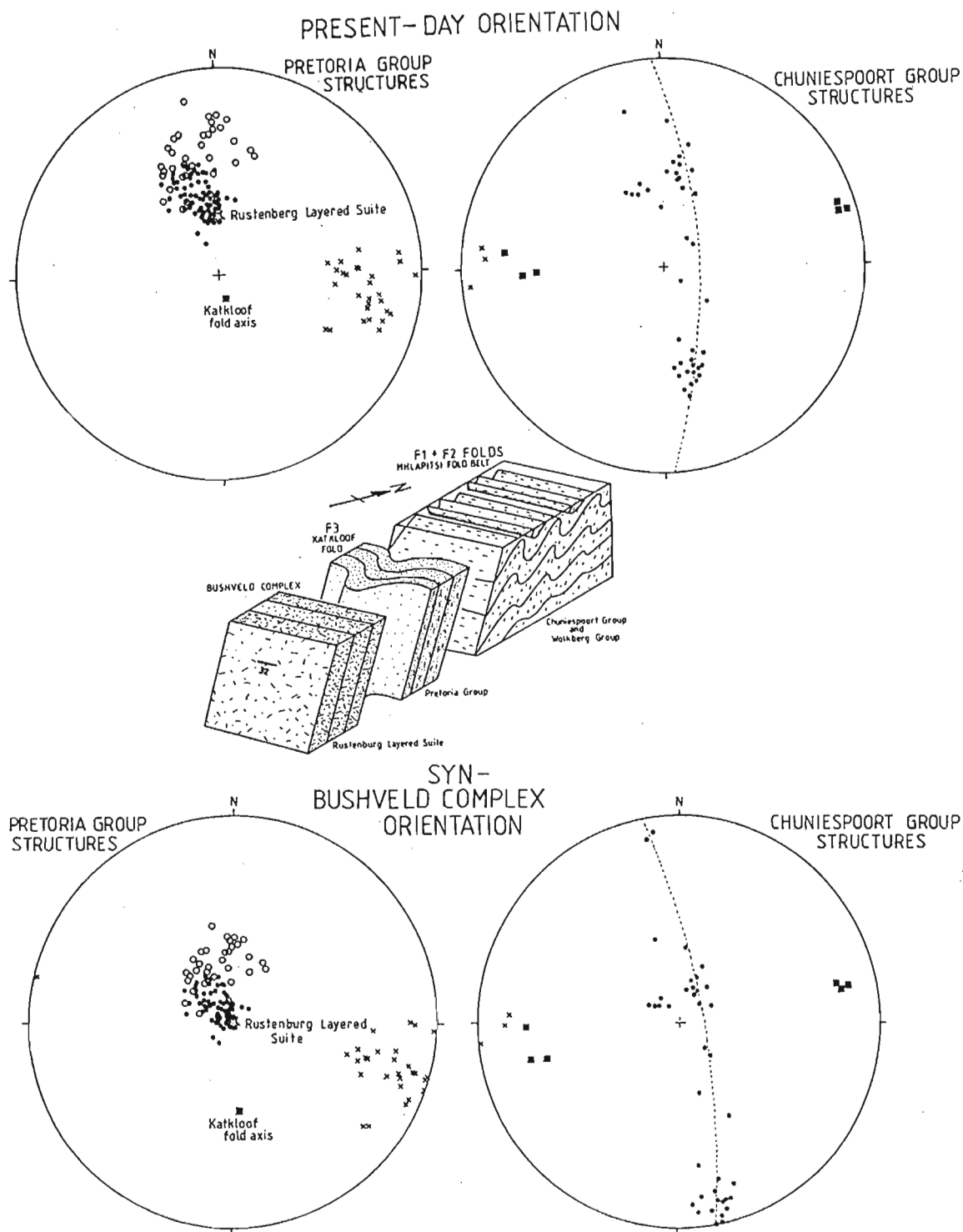




**Figure 4.56** Second order ptygmatic folds in a chert layer within dolomite of the Chuniespoort Group at Donkerkloof. Scale size = 25 cm.

On a regional scale the folds are truncated by the sub-Pretoria Group unconformity. This would correspond to the  $D_1$  pre-Pretoria Group deformation of Potgieter (1991). Locally however, no direct evidence of refolding of  $F_1$  by  $F_2$  could be found. This may be due to the fact that  $F_1$  and  $F_2$  are almost coaxial and that the syn-Bushveld Complex  $D_2$  event would have resulted only in a tightening of the pre-Pretoria Group  $F_1$  fold structures as suggested by Potgieter (1991).

Structural data from tightly folded Chuniespoort Group banded ironstones and from the immediately overlying Pretoria Group (Figure 4.57), indicate that the axial planar cleavage orientations of the Chuniespoort Group folds are identical to the  $S_2$  fabric developed in the overlying Pretoria Group. Fold axes in the Chuniespoort Group are however, generally slightly oblique to the stretching lineations in the Pretoria Group, with folds plunging towards the west at between  $10^\circ$  and  $30^\circ$  (Figure 4.57) compared to the between  $20^\circ$  and  $40^\circ$  easterly plunging mineral lineations in the Pretoria Group.



**Figure 4.57** Diagram and lower hemisphere, equal angle stereographic projections of  $D_2$  syn-Bushveld structures from the Chuniespoort and Pretoria Groups in the Mathabatha area. The cleavage fabric in the Pretoria Group is axial planar to isometric  $F_2$  folds ( $\pi$ -circle) in the Chuniespoort Group. Mineral lineations in the Pretoria Group are also subparallel to  $F_2$  fold axes and mineral lineations in the Chuniespoort Group. Poles to sedimentary stratification ( $\bullet$ ); poles to foliation ( $\circ$ ); mineral lineations ( $\times$ ); boudin axes ( $\blacklozenge$ ); mesoscale fold axes ( $\blacksquare$ ).

Microstructural evidence from these folds shows that the initial asbestiform fibres developed normal to layering, and are overprinted by later amphiboles that define an axial planar foliation (Figure 4.58). The axial planar fabric is parallel to the  $S_2$  foliation in the overlying Pretoria Group in the Mathabatha domain. This suggests that asbestiform growth may have been associated with the  $D_1$  pre-Pretoria Group deformation and that the tightening and recrystallisation of the fibres was associated with the  $D_2$  syn-Bushveld tectonothermal event. This is supported by field evidence where silicified asbestos is found immediately below the pre-Pretoria Group unconformity (G.Cawthorn pers. comm. 1996).

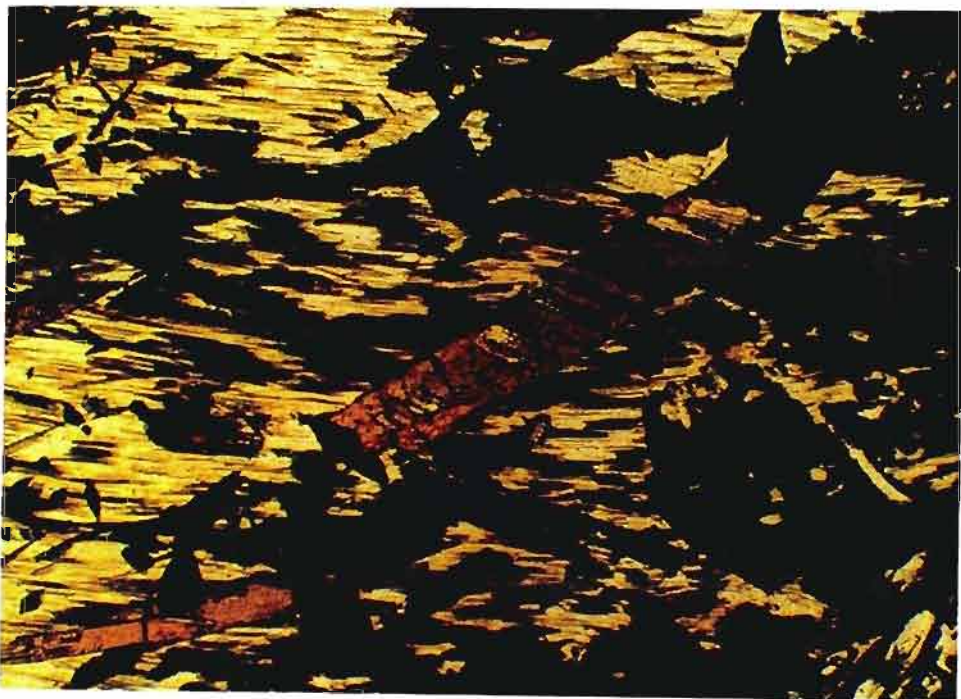


Figure 4.58 Microphotograph showing early asbestiform orthoamphibole fibres overgrown by later axial planar amphibole porphyroblasts, that are parallel to the  $S_2$  foliation in the overlying Pretoria Group. Plane polarised light. Width of view = 4 mm.

#### 4.4.3 $D_3$ structures

Low-angle decollement surfaces, with northward-directed movement accompanied by intense folding in the overriding thrust sheet were found within banded ironstones of the Chumiespoort Group (Figure 4.59).

These structures may be of  $D_2$  syn-Bushveld age, but are more likely related to later, post-

Bushveld ( $D_3$ ) northward-directed thrusting associated with the Wonderkop Fault strike-slip system.

As indicated by Bastin (1968), tightening and local reorientation of the ENE-trending Mhlapitsi folds had occurred during post-Bushveld left-lateral strike-slip faulting along the Wonderkop Fault. He concluded that the eastern block of the Wonderkop Fault was transported northwards against the Chuniespoort Group rocks which, due to competency contrasts deformed plastically, resulting in the tightening of the Mhlapitsi fold structures. For this to occur the Pretoria Group and underlying Chuniespoort Group must have already been dipping at close to the present day orientations during  $D_3$  deformation. Brittle deformation is again present in the underlying Black Reef Quartzite Formation forming the Mount Welkom Fault on strike to the northeast of the Wonderkop Fault (Figure 4.1).



**Figure 4.59** Low angle decollement surface in banded ironstones of the Penge Formation in the Mhlapitsi Fold Belt on the farm Stylkop. Ironstones are intensely folded above the thrust surface and relatively undeformed below it. Thrusting is represented by top towards the left movement. View is towards the east. Scale size = 25 cm.

#### 4.4.4 Conclusions

The  $D_2$  syn-Bushveld Complex deformation is mainly restricted to the Pretoria Group of the Transvaal Supergroup and is closely associated with the development of large periclinal fold structures. Most of the deformation is restricted to the strata above the decollement zones which define the base of the periclinal structures. In the Mathabatha domain however, the complete Pretoria Group is affected and the deformation can be traced to below the Pretoria Group into the upper parts of the Chuniespoort Group.

Earlier Pre-Pretoria Group  $F_1$  folds were modified by the  $D_2$  syn-Bushveld Complex deformation. In the Mathabatha area, extensional reactivation of the folds resulted in the reorientation of the folds into parallelism with the main extensional  $S_{2a}$  foliation in the overlying Pretoria Group. This is supported by the more attenuated southern limbs of these folds indicating a top-towards-south extension. This is consistent with the top towards south extensional foliation given by kinematic indicators in the overlying Pretoria Group.

Further support for a syn-Bushveld age for the deformation is provided by intensely deformed diabase sills within the Chuniespoort Group which are generally accepted to be precursors to the emplacement of the main mafic phase of the Bushveld Complex (Sharpe, 1984; Von Gruenewaldt *et. al.*, 1985). If the deformation seen in the Chuniespoort Group rocks was all of pre-Pretoria Group age, then chert and banded ironstone clasts in the Bevets Conglomerate Member of the Rooihogte Formation should contain pebbles with small-scale folds and a cleavage fabric of the type commonly seen in present day pebbles and outcrops of the Penge and Deutschland Formations. This was never observed during this investigation, neither has it been reported from previous investigations.

#### 4.5 SYN-BUSHVELD ORIENTATION OF $D_2$ STRUCTURES

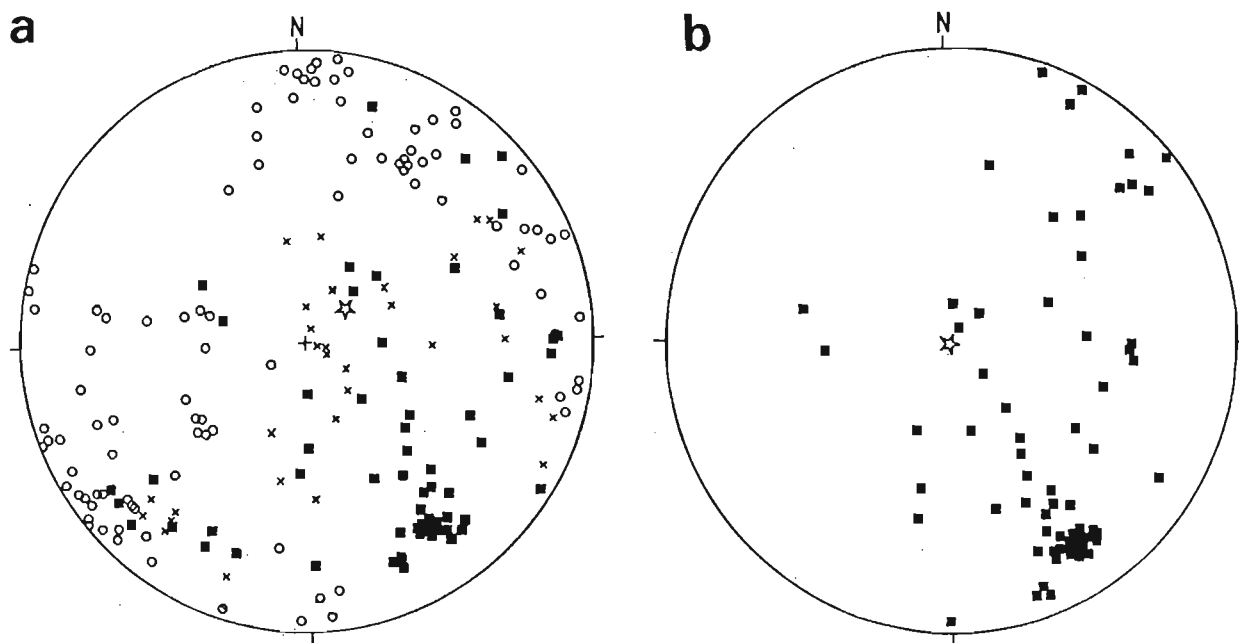
The present erosional remnant of the Transvaal Supergroup forms a basin-shaped structure dipping inwards beneath the Bushveld Complex. Dips progressively steepen from the southern eastern Bushveld Complex to up to  $80^\circ$  along the northern margin. A slight increase in dip is also evident as the contact with the Bushveld Complex is approached (Button, 1976). Igneous layering in the Rustenburg Layered Suite similarly dips inwards suggesting that the basin-shaped structure is a post-Bushveld feature. This is substantiated by palaeomagnetic studies

(Gough and Van Niekerk, 1959; Hattingh, 1986) which showed that the igneous layering in the Bushveld cooled through 650°C while in a near horizontal position. The age of the tectonic subsidence is further considered to post-date the  $^{40}\text{Ar}/^{39}\text{Ar}$  Merensky Reef biotite age of about 2010 Ma, as the closing temperature of the Ar system in biotite is similar to the Curie point of remnant magnetism (Walraven *et al.*, 1990).

In the Mathabatha and Serpose domains, the Pretoria Group and the layering in the Bushveld Complex have a present tectonic dip ranging between 20° and 80° towards the south from east to west across the area. Restoration of the Rustenburg Layered Suite layering to the horizontal simultaneously restores the underlying Transvaal Supergroup and associated structures represented to their original syn-Bushveld Complex emplacement orientation (Figure 4.57). The Katkloof Fold axis becomes more shallow in plunge towards the south and fold plunges in the core of the fold become close to horizontal.

In the Schwerin Fold domain the sub-decollement Pretoria Group strata (Timeball Hill Formation) dip towards the south at between 22° and 30°. The strata immediately above the decollement (Dwaalheuwel Quartzite Formation) dip less steeply towards the south at between 12° and 15° (Appendix 1). Restoration of the Schwerin Fold structures to syn-Rustenburg Layered Suite time rotates the sub-decollement strata to the horizontal and the deformed Dwaalheuwel Quartzite Formation from a southern dipping orientation to a northerly dipping orientation (Figure 4.60). The multiple second order folds in the Dwaalheuwel Quartzite Formation also change their plunge from the present southward plunge to a northerly plunge (Figure 4.60). The fold nose of the Schwerin Fold (Magaliesberg Quartzite Formation) still plunges towards the south, but at a much lower angle. This geometry is consistent with a periclinal structure with the second order fold axes projecting towards the culmination point of the pericline.

From Figure 4.57 it is also clear that the folds immediately underlying the Pretoria Group are similarly restored to their syn-Rustenburg Layered Suite orientation, which shows that the folds were near recumbent during this time.



**Figure 4.60** a) Structural data from the Schwerin Fold domain showing the doubly plunging and radial nature of the fold axes. b) Fold axes restored to syn-Rustenburg Layered Suite time. Equal angle stereographic projection. Poles to planar foliation ( $\circ$ ), mineral lineations ( $\times$ ), mesoscale fold axes ( $\blacksquare$ ), pole to igneous layering in the Rustenburg Layered Suite and the sub-decollement Pretoria Group strata ( $\star$ ).

The near-vertical  $D_2$  maximum strain orientation, that produced the near bedding-parallel foliation is consistent with magmatic loading stress by the Rustenburg Layered Suite. Although the  $D_2$  deformation had a large pure shear (loading) component, there is considerable evidence for an associated extensional simple shear component. This is seen in the consistent top-to-south shear sense associated with the  $S_{2a}$  foliation in the Mathabatha domain and in the south-verging folds in the Chuniespoort Group folds immediately underlying the Pretoria Group. The most likely explanation for this is that simple shear in the Mathabatha area was a product of progressive subsidence and southward tilting of the floor. This must have occurred soon after the development of the igneous layering in the Rustenburg Layered Suite.

# CHAPTER 5

## PORPHYROBLAST-MATRIX RELATIONSHIPS

### 5.1 INTRODUCTION

The nucleation and growth of various porphyroblasts in relation to fabric-producing events are crucial in unravelling the metamorphic and deformational history within various parts of the Bushveld Complex contact aureole. As indicated by Paterson *et al.* (1991), these relationships provide information on the timing of metamorphism and deformation, kinematics, and the nature and orientation of older foliations. Unfortunately, porphyroblast inclusion geometries and fabric formation are still poorly understood. The earliest classical models for interpreting evidence of pre-tectonic, syntectonic and post-tectonic porphyroblastic growth were developed by Zwart, (1962). This was followed by an intense discussion on the subject of "replacement" versus "displacement" porphyroblast growth (Spry, 1969, 1972, 1974; Misch, 1971; Saggerson, 1974).

More recently, a lively debate was initiated by the suggestion that porphyroblasts are all syntectonic, even in contact aureoles where static growth had been the accepted process (Bell, 1981, 1985, 1986; Bell *et al.*, 1986; Bell and Rubenach, 1983 and Bell and Johnson, 1989, 1992; Johnson, 1990; 1992). This work further suggested that porphyroblasts nucleate only in low-strain, quartz-rich (Q) domains during the sequential development of a crenulation foliation and are dissolved in active high-strain, non-coaxially deformed, mica-rich (M) domains. The generally accepted notion that porphyroblasts underwent rotation with respect to geographical coordinates during deformation (Zwart, 1962; Spry, 1969; Schoneveld, 1977) was also questioned in favour of a hypothesis whereby porphyroblasts that do not undergo any internal deformation, do not rotate, preserving the shapes of earlier foliations and their orientations.

The rotation versus non-rotation controversy remains the subject of intense discussion (Passchier *et al.*, 1992; Busa and Gray, 1992; Bell *et al.*, 1992; Vernon *et al.*, 1993b; Johnson 1993a, 1993b; Barker, 1994; Bell *et al.*, 1997) and has important implications for resolving



geological histories in metamorphic terrains. Porphyroblast rotation, interpreted from S-shaped inclusion trails (Schoneveld, 1977) or even straight inclusion trails (Barker, 1994) would imply that deformation and metamorphism was a single event and that porphyroblasts are useful kinematic indicators. However, an apparent opposite shear sense would result if porphyroblasts developed S-shaped inclusion trails during changes in foliation orientation (Wilson, 1971). In the Bell (1985) and Bell *et al.* (1986) model, the same S-shaped inclusion trails would be interpreted as fold remnants overgrown by non-rotating porphyroblasts. This model provides a more complex tectonometamorphic history, with inclusion trails representing 'snapshots' of earlier foliations and their orientations.

In the most recent overview of porphyroblast-matrix relations, Passchier and Trouw (1996), present a modified version of the Zwart (1962) scheme. The main timing relations between porphyroblast and matrix are subdivided into pre-, syn-, inter- and post- tectonic with a system of mathematical symbols (Figure 5.1). Although porphyroblast-matrix relationships from the Bushveld Complex aureole are investigated within the context of this ongoing debate, for the purposes of this thesis, the classification scheme of Passchier and Trouw (1996) is used as a general guideline for interpretations.

## 5.2 PREVIOUS WORK

Porphyroblast-matrix relationships from the northeastern Bushveld Complex aureole were first used by Saggerson (1974) to support the crystal displacement theory of Misch (1971) assuming that the aureole developed by pure static-type metamorphism. Vernon and Powel (1976) cautioned at this interpretation as local deformation during intrusion can always be expected. They also suggested that bulk volume changes due to expansion, cooling and volume changes during metamorphic reactions could produce a deflection of matrix foliation around porphyroblasts. They further suggested that the porphyroblasts in the Bushveld aureole developed by a process of replacement rather than displacement.

Lapinsky (1981) working in the same area, reported sparsely developed foliation in the aureole and described some porphyroblast-matrix relationships with disturbed S-surfaces. She suggested bulk-rock volume change during recrystallisation as an important process. She



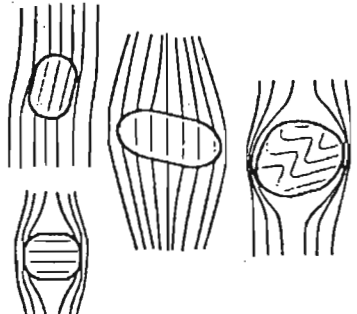

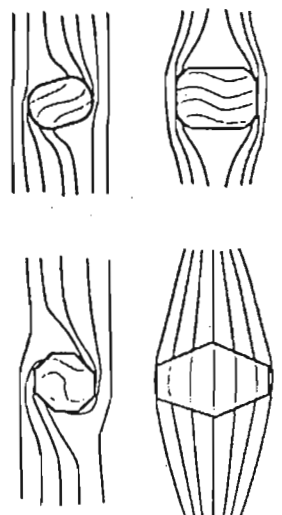
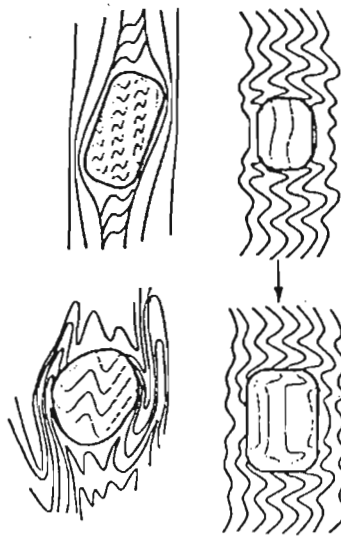
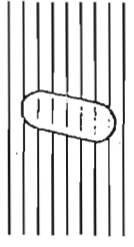
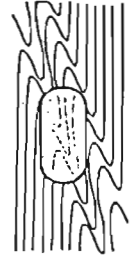
<p>pre-tectonic</p> <p><math>P &lt; D_1</math></p>		
<p>inter-tectonic</p> <p><math>D_n &lt; P &lt; D_{n+1}</math></p>		
<p>syn-tectonic</p> <p><math>D_n &gt; P</math></p>		
<p>post-tectonic</p> <p><math>D_n &lt; P</math></p>		
	<p>deformation does not cause folding of matrix foliation</p>	<p>deformation causes folding of matrix foliation</p>

Figure 5.1 Classical microstructural classification and abbreviated system for porphyroblast-matrix relationships after Passchier and Trouw (1996).

further considered early formed biotite forming an S-fabric, to have developed during initial heating of the aureole. As heating continued, stress was dissipated and later porphyroblasts developed a random orientation. Cooling and contraction then produced draping of the early-formed fabric over porphyroblasts.

Hartzer (1989, 1995) interpreted the PMR relationships in andalusite schists in the Crocodile River Fragment to indicate that deformation preceded porphyroblast growth and used this relationship to suggest that the fragment deformed before the intrusion of the Bushveld Complex and the growth of andalusite. Courtnage *et al.* (1995) described complex porphyroblast-matrix relationships from the Bushveld Complex metamorphic aureole in an area northwest of Johannesburg. These were identified as representing pre-, syn-, and post- tectonic textures and interpreted as being related to a number of pre-, syn- and post-Transvaal Supergroup deformations.

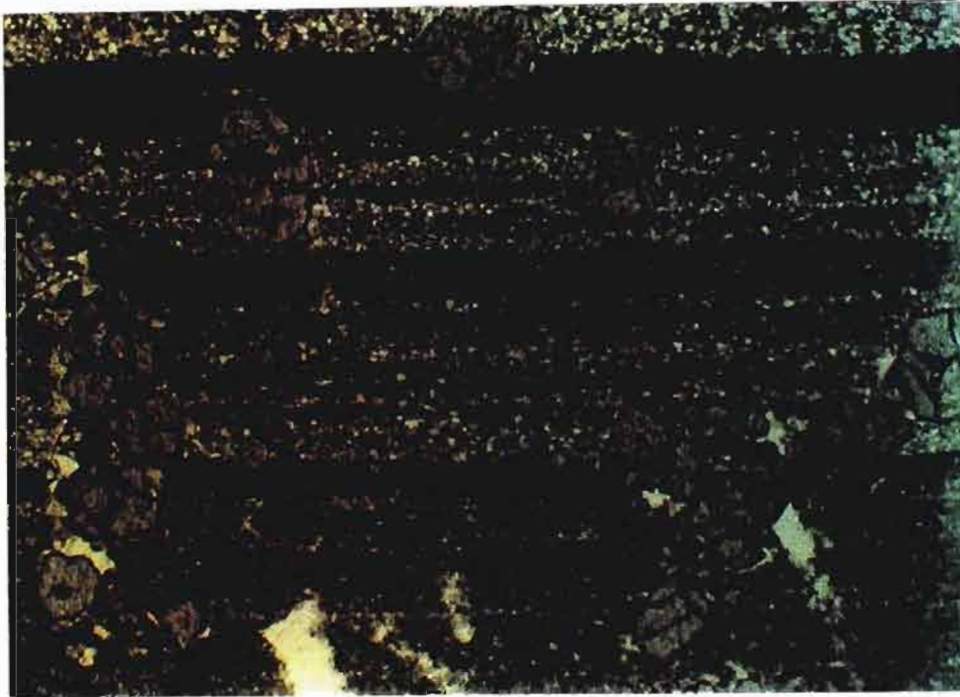
### 5.3 SAMPLE PREPARATION

Ideally a large number of orientated thin sections are required from a single sample at a complete range of orientations to determine the three dimensional geometry of inclusion trails and their relationship with the matrix. For this study, orientated samples were collected in the field from various pelitic and semi-pelitic units. From each sample, thin sections were cut a) approximately perpendicular to the foliation (usually near bedding parallel) and parallel to the stretching lineation, which in most cases also approximates the bedding-foliation intersection; b) perpendicular to the foliation and normal to the stretching lineation and c) normal to foliation but oblique to the lineation direction.

### 5.4 INTERPERICLINAL DOMAINS

#### 5.4.1 Pretectonic porphyroblast growth ( $P < D_{2a}$ )

In the interpericlinal domains (Mathabatha and Seropse) the dominant fabric ( $S_{2a}$ ) in the pelitic rocks is formed by the alignment of sericite and biotite, commonly deflecting around porphyroblasts of biotite, staurolite, garnet, cordierite and chiastolite. The intensity of the matrix foliation varies considerably from foliation absent, low strain areas (Figure 5.2), to areas where an intense schistosity is developed.



**Figure 5.2** Garnet porphyroblasts in a foliation-absent low strain domain from the lower pelitic unit of the Timeball Hill Formation on the farm Hoogenoeg. Sample 2021. Plane polarised light. Width of view = 6 mm.

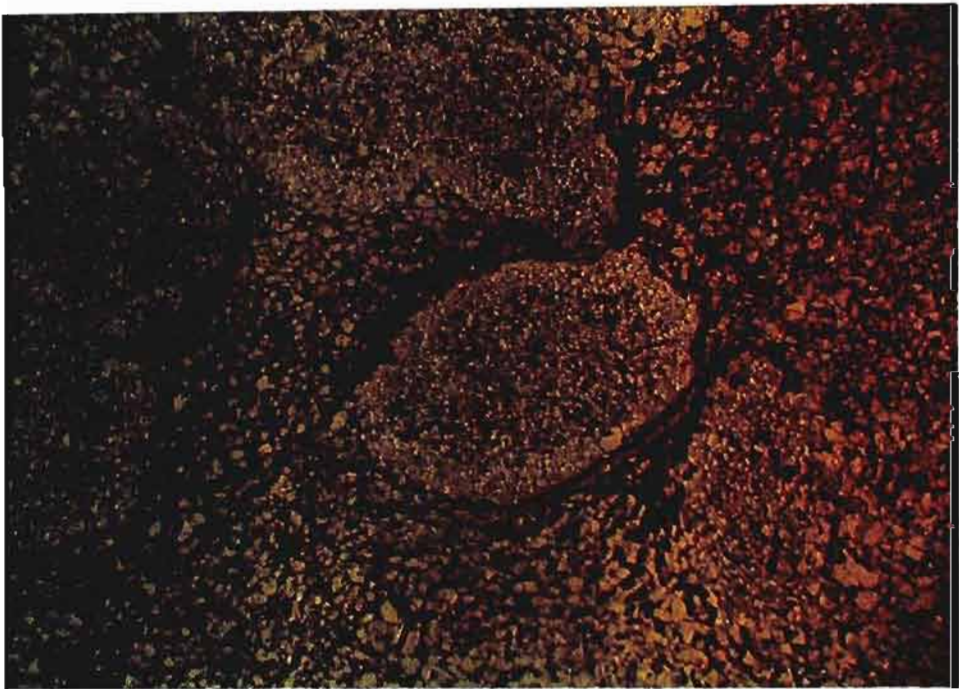
Evidence for pre- $S_{2a}$  fabric growth is seen by the common occurrence of randomly oriented porphyroblasts. Chistolite crystals for example, lack a visible preferred orientation, except in the highest strain zones and in thinly bedded rocks where the crystals have tended to grow along bedding surfaces.

Porphyroblasts also commonly lack an internal foliation fabric (Figure 5.3), except for original bedding laminations that remain preserved in many of the larger porphyroblasts (helicitic texture) (Figure 5.4). The presence of randomly oriented internal inclusions, further indicates that no foliation was present in the vicinity of the growing porphyroblast (Zwart, 1962; Vernon *et al.*, 1993a, 1993b) and that porphyroblast growth was initiated under conditions preceding local fabric development. This is also seen in staurolite porphyroblasts, which contain relatively clear non-poikilitic domains of randomly oriented replaced biotite, whereas biotite in the groundmass is often sheared with a preferred orientation (Figure 5.5).

**a**



**b**



**Figure 5.3 a)** Poikilitic andalusite with randomly oriented biotite inclusions. Matrix contains primary randomly oriented pre-tectonic biotite and secondary syntectonic oriented biotite. Sample DDH 80.5. Upper pelitic unit, Timeball Hill Formation from the farm Copper. Plane polarised light. Width of view = 6 mm. **b)** Cordierite poikiloblast with randomly oriented biotite inclusions compared to external oriented biotite. Sample 16/9. Lower pelitic unit, Timeball Hill Formation on the farm Hoogenoeg. Plane polarised light. Width of view = 6 mm.



**Figure 5.4** Pre-tectonic porphyroblasts of biotite and staurolite showing primary sedimentary laminations preserved as inclusion trails within the porphyroblasts. Sample 1819 from the andalusite zone, lower pelitic unit of the Timeball Hill Formation on the farm Hoogenoeg. Plane polarised light. Width of view = 6 mm.



**Figure 5.5** Porphyroblast of staurolite with laths-shaped clear domains pseudomorphing randomly oriented biotite porphyroblasts and partially enclosing garnet. Sample M4. Andalusite zone, lower pelitic unit, Timeball Hill Formation on the farm Hoogenoeg. Plane polarised light. Width of view = 6 mm.

Carbonaceous rocks, with a poorly or moderately developed  $S_{2a}$  foliation, typically have cleavage domes associated with sector zoned staurolite porphyroblasts (Figure 5.6), as well as chiastolite and garnet. Where the  $S_{2a}$  fabric is more intense, such as towards the western part of the Mathabatha and Seropse domains and towards the Bushveld Complex contact, cleavage domes are generally absent, but the porphyroblasts are strongly sector zoned.



Figure 5.6 Carbonaceous cleavage domes associated with sector zoned staurolite porphyroblast from the lower pelitic unit. Sample HAPL. Timeball Hill Formation on the farm Hoogenoeg. Plane polarised light. Width of view = 2 mm.

Rice and Mitchell (1991) describe the development of cleavage domes and sector zoning as closely related and the result of growth in a near-hydrostatic stress field. If this relationship is correct, then the presence of chiastolite or sector zoned porphyroblasts in strongly foliated rocks indicates that the porphyroblasts grew in previously near-hydrostatic conditions prior to matrix foliation. It can be argued that cleavage domes would have been present but were destroyed during the subsequent matrix foliation event.

Provided the deformation intensity is low enough, cleavage dome formation may still develop syntectonically. Evidence for this is provided below in the section on syntectonic porphyroblasts.

Chiastolite crystals have Rice and Mitchell (1991) Type-2 intergrowths which consist of fine quartz rods and graphite trails. These are not relicts of the matrix but formed simultaneously during porphyroblast growth (Andersen, 1984) and are indicators of growth normal to the crystal faces (Rice and Mitchell, 1991). Type-2 inclusions are crystallographically controlled, radiating outwards from the crystal nucleus along growth prongs separated by re-entrants (Figure 5.7).

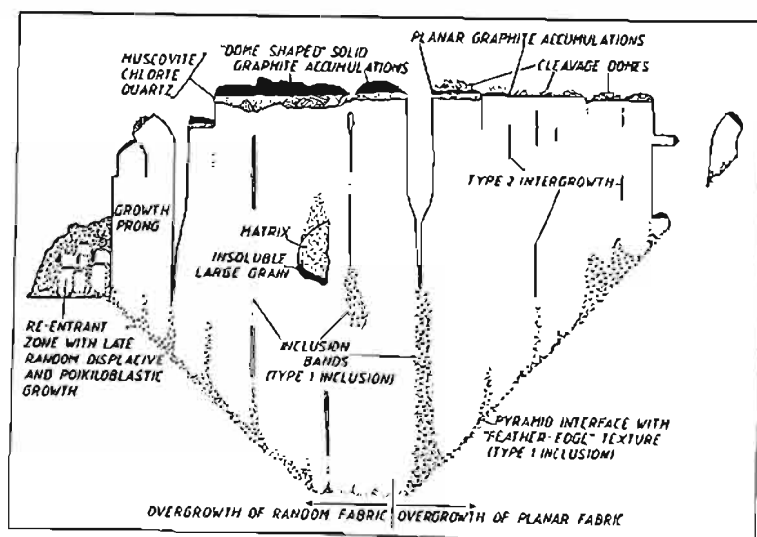
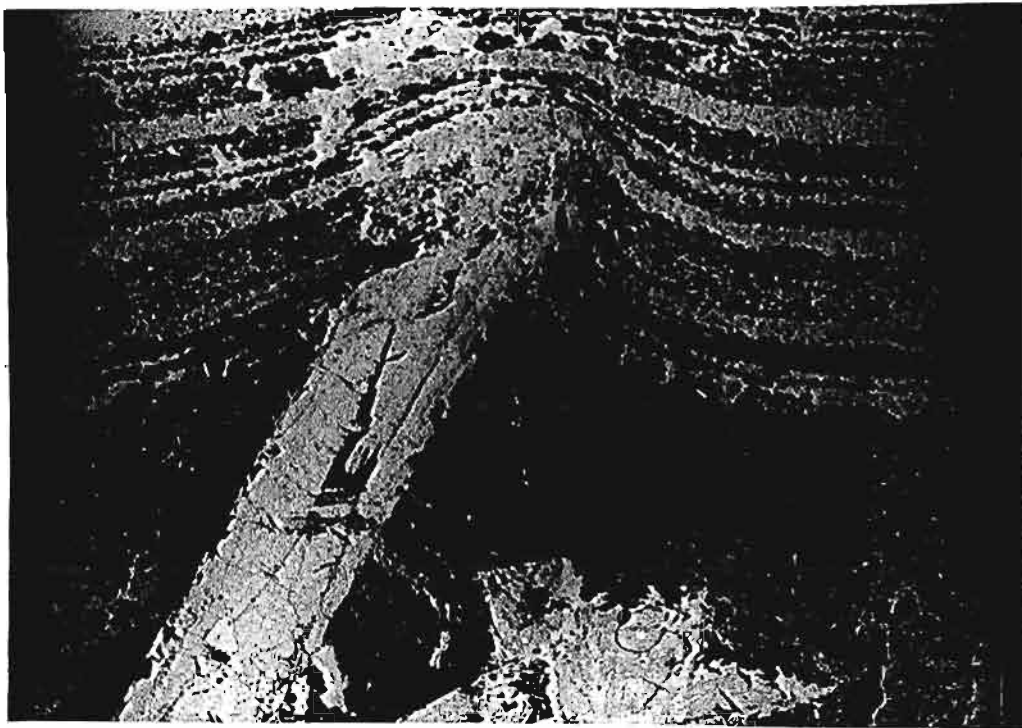


Figure 5.7 a) Typical pre-tectonic sector-zoned chiastolite crystal from the Mathabatha domain on the farm Uitkyk. Plane polarised light. Width of view = 6 mm. b) Diagram showing the textures associated with displacement growth (from Rice and Mitchell, 1991).



In some cases, sedimentary laminations surrounding porphyroblasts show significant deflection, especially in association with large chiasmolite crystals (Figure 5.8). This texture is particularly intriguing as there is no evidence of a secondary post-porphyroblast foliation.

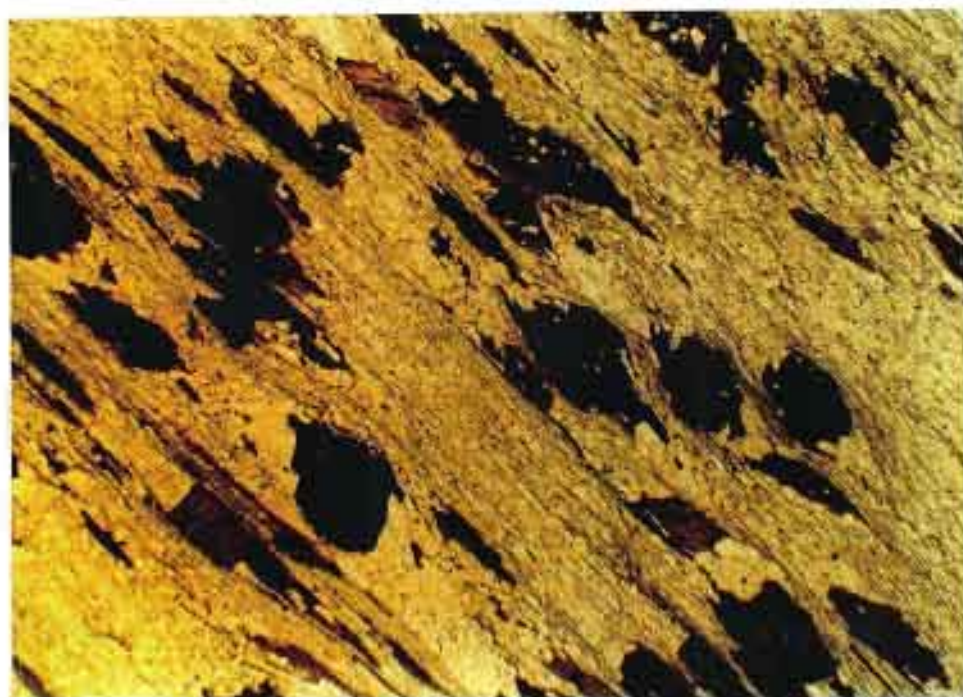
The orientation of the strain cap on the rigid chiasmolite crystals indicates a stress system with a near bedding-normal maximum compression orientation. Asymmetry in the disturbed laminations further suggests that the strain ellipse orientation conforms to the  $S_{2a}$  fabric, dipping slightly steeper to the south than bedding in the Mathabatha domain. The most likely explanation therefore is that the chiasmolite crystal grew essentially under pre-tectonic conditions in near-hydrostatic conditions. Subsequent  $D_2$  deformation produced the disturbance of primary sedimentary laminations around the large rigid chiasmolite crystals but was locally not intense enough to generate a secondary foliation in the rock matrix.



**Figure 5.8** Strongly deflected sedimentary lamination around a porphyroblast of chiasmolite with partial inclusions of staurolite, in a matrix that shows no visible secondary fabric development. Sample 7/99. Andalusite zone, Hoogenoeg Andalusite Mine on the farm Hoogenoeg. Plane polarised light. Width of view = 15 mm.

Biotite porphyroblasts in strongly foliated rocks from high strain domains within the aureole, have well developed strain shadows of quartz and form lozenge-shaped mica-fish within an anastomosing sericite foliation (Figure 5.9). These structures are interpreted as products of

pre-tectonic porphyroblastesis followed by a combination of basal plane slip, rigid-body rotation, boudinage and recrystallisation, as described by Lister and Snoke (1984). Sections viewed parallel to the stretching lineation and normal to the S-fabric provide useful kinematic shear-sense indicators. From the western Mathabatha domain within the fibrolite zone, mica-fish consistently show a top-to-south shear sense. Deformation partitioning into M- and Q-domains of Bell (1985) are well represented. Asymmetric biotite tails extend into adjacent M-domains (high non-coaxial shear strain) whereas the biotite porphyroblasts, together with quartz form low strain Q-domains within anastomosing M-domains.



**Figure 5.9** Pre-tectonic biotite porphyroblasts with quartz strain shadows forming Q-domains within anastomosing sericite M-domains that define the S<sub>2</sub> fabric. Progressive shortening and top-to-south shear within the M-domains has produced biotite mica-fish. Sample MAL08048. Boven Shale Member, Silverton Shale Formation. Fibrolite zone, on the farm Mathabatha. Plane polarised light. Width of view = 6 mm.

In some chistalite schists lath-shaped biotite-quartz clusters, that have clearly pseudomorphed an earlier porphyroblastic mineral, are deformed into a range of geometrical shapes depending on their original orientation. Graphite remains concentrated as partially preserved cleavage domes adjacent to the pseudomorphs - strong evidence that they represent pseudomorphs after crystals that grew by matrix displacement processes (Figure 5.10).

Flattened hourglass shapes are developed where the long axis of the pseudomorph assemblage is oriented at a high angle to the matrix foliation. Where the original orientation coincided with the extension direction, the pseudomorphs form highly elongate shapes. Although the pseudomorphs have strain caps and strain shadows they deformed almost homogeneously with the matrix, which has a similar composition. This is in contrast to chialstolite crystals that are disrupted by brittle deformation mechanisms within the same rock. Chialstolite crystals are boudinaged, usually on the crystallographic 001-cleavage surfaces and between adjoining crystals. The spaces between the separated chialstolite segments are infilled with quartz and in higher grade rocks, fibrolite is usually present (Figure 5.11).

#### 5.4.2 Syntectonic porphyroblast growth ( $D_{2a} \rightarrow P$ )

In highly foliated rocks from the andalusite zone, andalusite and staurolite may show typical syntectonic growth characteristics (Figure 5.12). In these zones porphyroblasts are usually poikilitic, have an absence of sector zoning, and have an internal fabric that mimics the external matrix foliation due to replacement of matrix sericite. A strain cap is invariably present and extensional fractures normal to the foliation, are developed within porphyroblasts.

In some rocks a combination of sector zoning, cleavage dome development and syntectonic inclusion geometries are present. For example, staurolite porphyroblasts (Figure 5.13) show well developed cleavage dome foliations that are continuous with the matrix foliation. The internal foliation is curved and continuous with the external foliation, becoming increasingly curved from the centre of the crystal towards the margin. This texture shows that cleavage dome and sector zoning can develop syntectonically contrary to the observations of Rice and Mitchell (1991). It is possible that at a certain strain intensity this may breakdown, with cleavage domes and sector zoning no longer developing.

Biotite which predates and is included in both andalusite and staurolite, has randomly oriented inclusions and is strongly sheared by the S-fabric. This further suggests that biotite nucleated early, predating fabric development and syntectonic staurolite and andalusite. Further evidence for syntectonic growth is seen in some samples where chialstolite is rimmed by poikilitic andalusite that partly overgrows adjacent foliated mica domains defined by sheared and



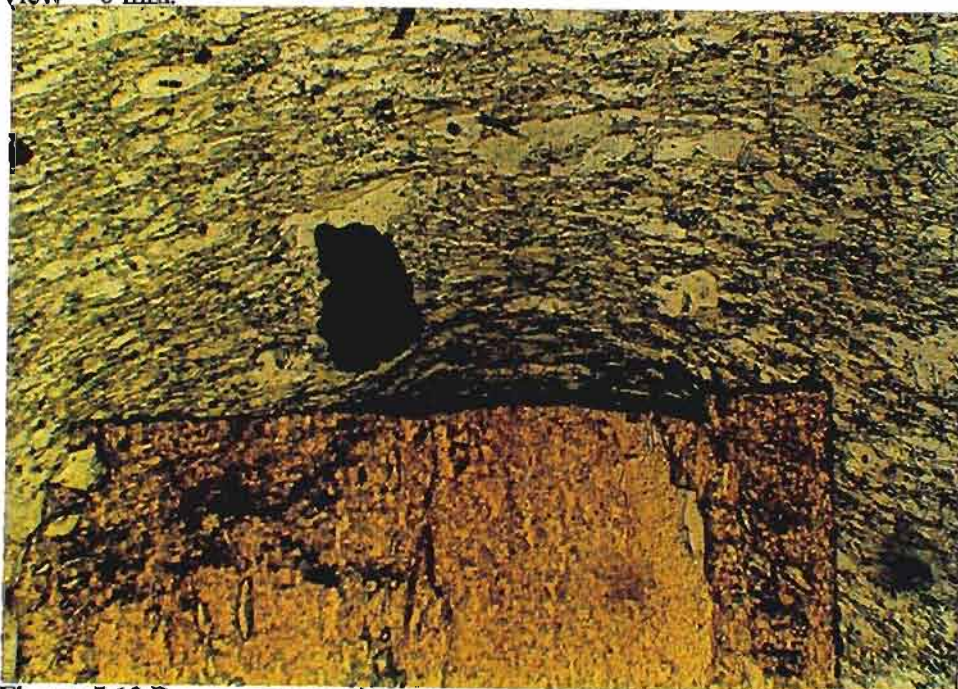
**Figure 5.10** Hourglass-shaped biotite and quartz intergrowths pseudomorphic after a preexisting pseudo hexagonal porphyroblast. The pseudomorph long-axis is oriented at a high angle to the plane of flattening. Note that biotite in the pseudomorph domains is unoriented. Biotite in the groundmass is foliated with secondary asymmetric overgrowths giving a dextral shear sense (see Figure 5.15). Sample MAL06652 from the fibrolite zone, Boven Shale Member, Silverton Shale Formation on the farm Mathabatha. Plane polarised light. Field of view = 10 mm.



**Figure 5.11** Two previously joined pretectonic chiasolite crystals separated by a quartz strain shadow that contains syntectonic fibrolite showing microboudinage. Sample MAL06652a. Same locality as Figure 5.10. Plane polarised light. Field of view = 13 mm.



**Figure 5.12** Syntectonic andalusite and staurolite from the lower pelitic unit of the Timeball Hill Formation on the farm Hoogenoeg (Sample THF1A). Biotite nucleated early with respect to fabric development and is also included in syntectonic staurolite and andalusite. Compare this sample to the pre-tectonic textures from the same locality in Figure 5.7. Plane polarised light. Width of view = 6 mm.



**Figure 5.13** Pre- to syntectonic, sector zoned staurolite porphyroblast showing deflected matrix foliation that is continuous with the internal foliation. The cleavage dome fabric is continuous with the  $S_{2a}$  matrix foliation. Sample HAPL. Plane polarised light. Width of view = 0.8 mm.

orientated biotite (Figure 5.14). Sections cut through overgrowths only clearly show that the internal foliation is oblique, continuous and sigmoidal with the external foliation.



Figure 5.14 Thin syntectonic andalusite rim on a chiastolite core, overgrowing foliated mica-rich domains and expelled carbon. Sample MAL6652 from Lot 235, Boven Shale Member, Silvertown Shale Formation. Crossed polarised light. Width of view = 6 mm.

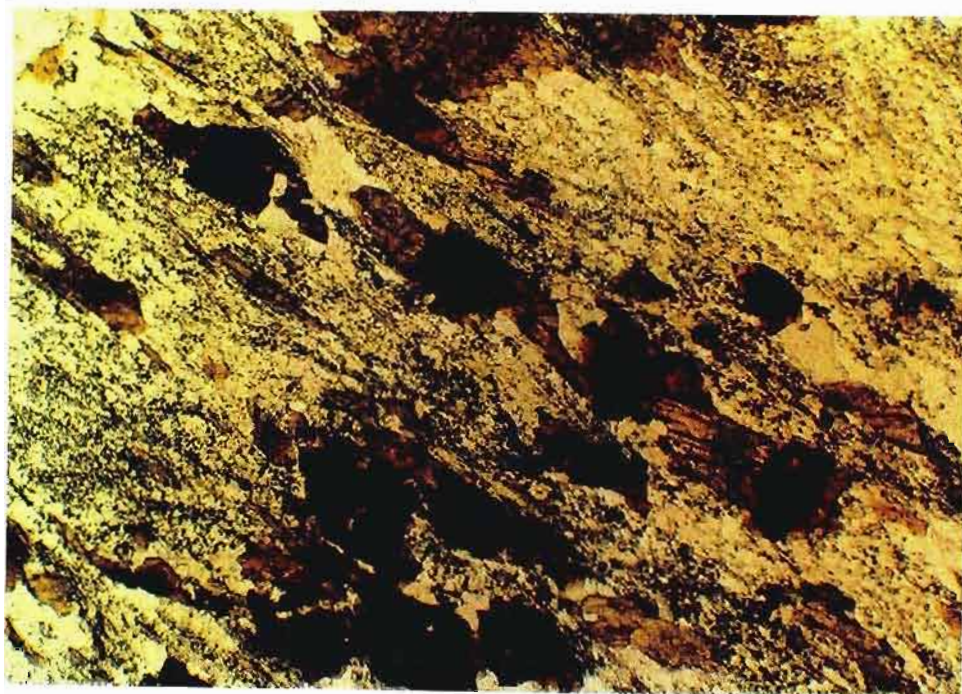
Within the fibrolite zone, fibrolite needles associated with boudinaged chiastolite crystals form part of the extension lineation and are interpreted as syntectonic. These needles may themselves be slightly boudinaged, suggesting that deformation continued after cessation of their growth (Figure 5.11) and provide evidence that the temperature and deformation intensity increased on the prograde metamorphic path. In this interpretation, strain partitioning around the chiastolite porphyroblast results in the porphyroblast becoming a zone of progressive shortening (Q-domain), whereas the matrix takes up the progressive shearing component (M-domain). Localised strain on the edges of the porphyroblasts promotes dissolution by chemical potential gradients.

Pressure shadow recrystallisation zones associated with porphyroblasts are elongated, producing a prominent  $L_2$  lineation within the  $S_{2a}$  fabric. In cases where chiastolite crystals are fractured and fibrolite is developed as a fracture fill, the texture could be interpreted as the first

stage of reaction softening (White *et al.*, 1980) brought about by a change in metamorphic conditions during deformation. In this case dissolution may also have been further facilitated by destabilisation due to increased temperature.

This association of syntectonic fibrolite with pre-tectonic chiasmolite indicates a close link between deformation and metamorphism. Similar observations were made by Vernon *et al.* (1993b) in the central Sierra Nevada, California. They suggested that the deformation probably represented a continuation of the same metamorphic/deformation event responsible for the main cleavage in the area. In most areas of the northeastern Bushveld Complex contact aureole, the earliest stages of porphyroblast development occurred under near-hydrostatic conditions, without the development of a visible foliation. As the D<sub>2</sub> deformation phase progressed, areas of low strain were progressively incorporated into the S<sub>2</sub> foliation domains.

Biotite may also show evidence for syntectonic growth. In highly foliated rocks, pre-tectonic biotite cores, rich in fine carbon inclusions, are commonly overgrown by clear syntectonic rims forming the tails of biotite-fish (Figure 5.15).



**Figure 5.15** Pre-tectonic biotite cores identified by graphite-rich inclusions overgrown by syntectonic clear oriented biotite tails in a garnet-staurolite-chiasmolite schist. Biotite tail geometry suggests a dextral shear sense. Sample (COP11440), upper pelitic unit, Timeball Hill Formation, upper andalusite zone on the farm Copper. Plane polarised light. Width of view = 2 mm.



These invariably indicate a dextral shear sense to the  $S_{2a}$  foliation within the Mathabatha domain. In other samples little evidence remains of a pre-tectonic growth phase and biotite laths form part of the mica foliation.

#### 5.4.3 Post-tectonic porphyroblast growth ( $D_{2a} < P$ )

Large porphyroblasts of muscovite commonly show post-tectonic relationships. They have a random orientation and cross-cut the dominant foliation of sericite (Figure 5.16). There is also no visible deflection of  $S_c$  around the porphyroblasts as a strain cap, suggesting that they grew during a post-tectonic retrograde alteration event after the  $D_2$  deformation had ceased. This is considered to be synchronous with the partial and often complete pseudomorphism of andalusite by coarse-grained muscovite, with or without chloritoid, and the minerals garnet and staurolite by chlorite.



**Figure 5.16** Post-tectonic retrograde chlorite (Chl) and chloritoid (Cld) in a staurolite-biotite fels from the Hoogenoeg Andalusite Mine (Sample HAPL). Chlorite and chloritoid overgrow the  $S_{2a}$  strain caps on earlier biotite porphyroblasts without any sign of matrix deflection. Plane polarised light. Width of view = 2 mm.

## 5.5 PERICLINAL DOMAINS

### 5.5.1 Pre-tectonic porphyroblast growth ( $P < D_{2a}$ and $D_{2b}$ )

Pre-tectonic porphyroblast-matrix relationships are common in all the large periclinal structures. Of these, chiasolite, staurolite, garnet, and cordierite from the andalusite zone are the most obvious. They show sector zoning, randomly oriented inclusion trails, strain shadows and boudinage structure within the dominant fabric. Cordierite has a randomly oriented internal fabric with an external foliation. Early-formed, pre-tectonic chiasolite crystals may be broken around the hinges of mesoscale folds in the cores of periclinal structures. Hornblende crystals from the Phepane Fold domain are also bent around fold hinges.

### 5.5.2 Syntectonic porphyroblast growth

$$D_{2a} \supset P$$

Chiasolite porphyroblasts from the andalusite zone in the lower pelitic unit of the Timeball Hill Formation on the eastern limb of the Katkloof Fold have epitaxial overgrowths of andalusite. The overgrowths are typically poikilitic and overgrow a matrix foliation (Figure 5.17).

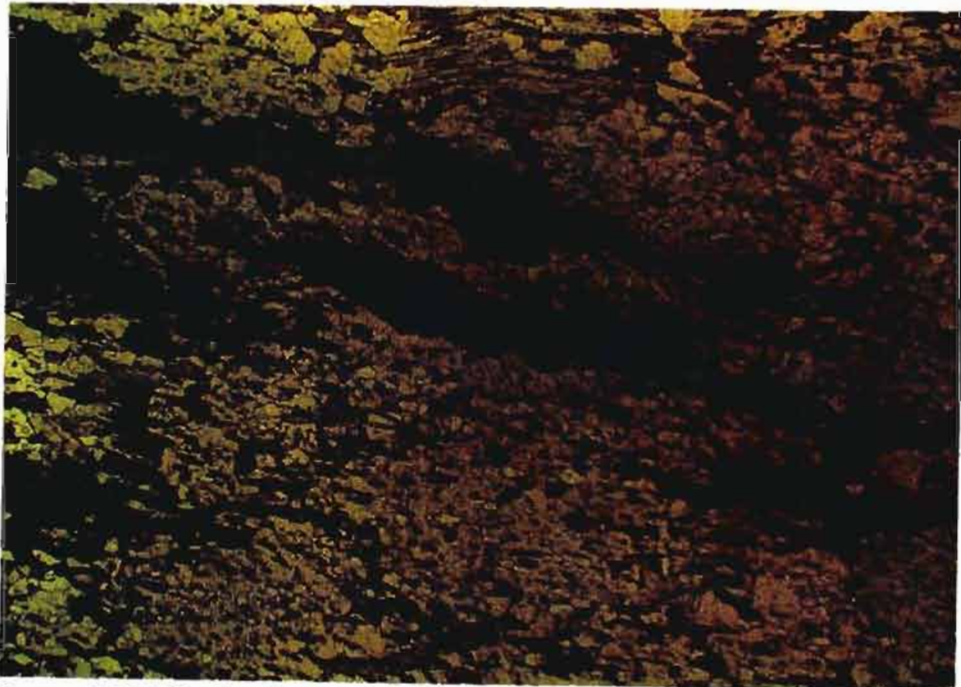


Figure 5.17 Porphyroblast-matrix relationships from the eastern limb of the Katkloof Fold on the farm Tuimplaats. Cleavage domes associated with the pre-tectonic chiasolitic stage of growth are preserved within the poikilitic syntectonic andalusite overgrowths. Sample 16/8A. Plane polarised light. Width of view = 6 mm.

In places, cleavage domes associated with chiastolite growth prongs are preserved within the poikilitic epitaxial overgrowths (Figure 5.18). The early chiastolitic growth is thus interpreted as a pre-tectonic growth phase, which proceeded under relatively static conditions. Progressive deformation during the same metamorphic event was accompanied by the growth of a syntectonic poikiloblastic andalusite phase which nucleated onto the earlier chiastolite.

Deformation continued after andalusite growth had ceased as is evident by boudinaged andalusite (5.17). Since this sample is from the eastern limb of the Katkloof Fold, the foliation is not axial planar, but corresponds to and is considered almost synchronous with the foliation in the adjacent interpericlinal Mathabatha domain ( $S_{2a}$ ).

At higher grades within eastern limb of the Katkloof Fold, fibrolite bundles have interiors of randomly oriented fibres, but have tails that form part of the foliation together with biotite (Figure 5.18). This suggests that fibrolite grew early or before the development of the foliation and continued growing during deformation, producing syntectonic tails. The foliation is identified as the near bedding parallel  $S_{2a}$  fabric which is deformed into mesoscale folds during  $D_{2b}$  deformation.



**Figure 5.18** Fibrolite knots with oriented tails forming part of the  $S_{2a}$  fabric. Sample 1713 from the eastern limb of the Katkloof Fold, Silverton Shale Formation, on the farm Tigerpoort. Plane polarised light. Width of view = 6 mm.

### $D_{2b} \supset P$

As described in Chapter 4, the cores of the folds are characterised by an axial planar  $S_{2b}$  fabric. In these areas, andalusite crystals are generally pre-tectonic but may show evidence of syntectonic overgrowth of, or boudinage by, the  $S_{2b}$  foliation. In the core of the Katkloof Fold for example, poorly aligned chiasolite crystals are contained within a strongly developed axial planar foliation. The crystals are boudinaged with quartz filling the interboudin areas and fibrolite developed along fractures (Figure 5.11). This textural relationship is identical to that developed in the interpericlinal areas between andalusite porphyroblasts and the  $S_{2a}$  near bedding-parallel fabric. This suggests that both the  $S_{2a}$  and the  $S_{2b}$  foliation developed almost synchronously by similar processes in differing orientations. Some of the rocks from the core of the Schwerin pericline, in the Boven Member of the Silverton Shale Formation, were found to contain only syntectonic andalusite that had not nucleated on pre-tectonic chiasolite cores (Figure 5.14). In these areas, a weakly developed crenulation, axial planar to the Schwerin Fold, is overgrown by andalusite porphyroblasts (Figure 5.19). A well preserved internal foliation ( $S_i$ ) within andalusite porphyroblasts is curved and continuous with the external fabric ( $S_e$ ). This texture indicates that andalusite overgrew the earlier  $S_{2a}$  fabric during the development of the  $S_{2b}$  axial planar fabric ( $D_{2a} < P \leq D_{2b}$ ).



Figure 5.19 Poikilitic andalusite overgrowing a well developed fabric ( $S_{2a}$ ) and a secondary weakly developed axial planar crenulation ( $S_{2b}$ ). Sample W88110. Plane polarised light. Width of view = 6 mm.

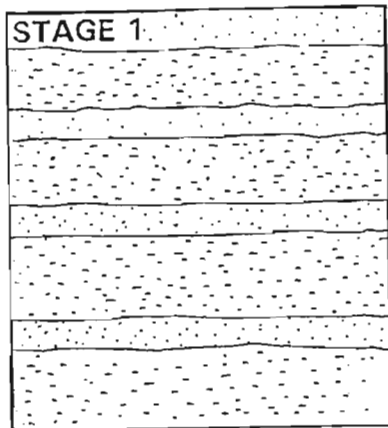
## 5.6 SEQUENTIAL PORPHYROBLAST AND MATRIX GROWTH

Based on the above microstructural relationships and inclusion mineralogy, a sequential order of porphyroblast growth can be established for the andalusite and fibrolite zones: biotite-garnet-staurolite-andalusite-fibrolite. This corresponds to the regional zonation: biotite-chloritoid, staurolite-andalusite; sillimanite-cordierite within the northeastern Bushveld Complex contact aureole (Blain, 1975), and suggests that the temporal growth sequence is related to the spatial sequence along the metamorphic field gradient. Similar relationships have been described from a number of other metamorphic provinces, particularly low-pressure, magmatically heated terrains (Bell and Rubenach, 1983; Yardley *et al.*, 1987; Lang and Dunn, 1990; Gibson, 1992).

In sample THF1A from the andalusite zone (Figure 5.12) for example, biotite is pre- or early with respect to the  $S_{2a}$  foliation, whereas staurolite and andalusite are syntectonic. This is supported by the fact that biotite is always found as inclusions or is replaced by both staurolite and andalusite. Garnet is also included in both staurolite and andalusite and is always found to be pre-tectonic with respect to the  $S_{2a}$  foliation in the andalusite zone. At higher grades, syntectonic fibrolite postdates pre-tectonic chiasmolite indicating that sequential porphyroblast growth is related to a sequential growth of progressively higher grade metamorphic minerals which may or may not be associated with foliation development.

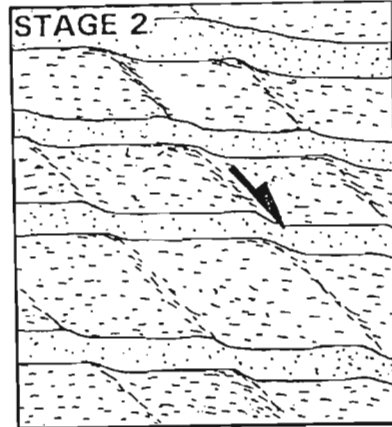
Bell and Rubenach (1983) distinguished six sequential stages of crenulation cleavage development, whereby an initial homogeneous  $S_1$  fabric deforms to a new homogeneous  $S_2$  fabric by a process of progressive inhomogeneous deformation. Any of these stages may be preserved as inclusion trails within porphyroblasts. This model is generally used to establish relationships between porphyroblast growth and deformation in multiply deformed terrains (Reinhardt and Rubenach, 1989; Lang and Dunn, 1990; Gibson, 1992).

The range of foliation intensities across the contact aureole allows for similar observations of systematic foliation development (Figure 5.20). Initially unfoliated rocks became highly foliated with increasing deformation and metamorphic grade. Where the foliation is poorly developed, original sedimentary laminations are weakly crenulated by a spaced secondary foliation ( $S_2$ ) with top-to-south (downdip) shear. Since this is the first foliation to



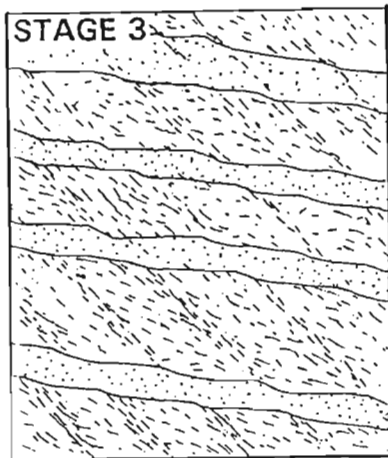
STAGE 1

bedding parallel mimitic growth



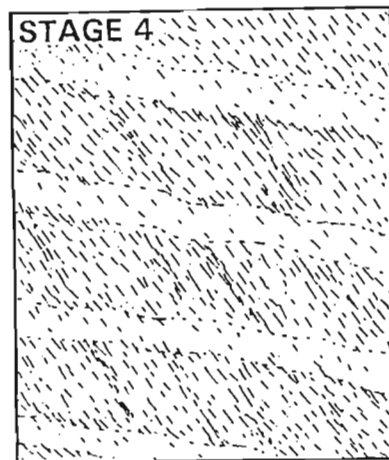
STAGE 2

gentle extensional crenulations  
 $S_0$  is dominant fabric



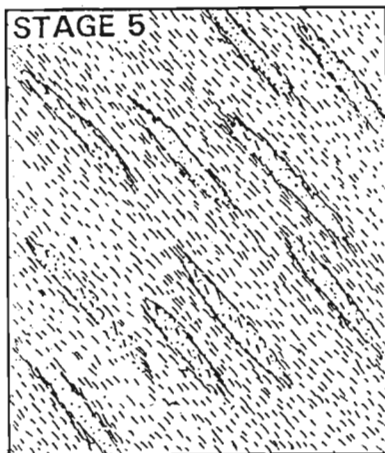
STAGE 3

closely spaced extensional shears  
 $S_2$  fabric becomes dominant



STAGE 4

continuous  $S_2$  foliation  
 $S_0$  becomes obliterated



STAGE 5

strongly transposed  $S_0$

**Figure 5.20** Diagram illustrating five stages of secondary foliation development as observed in the andalusite and fibrolite zones of the contact aureole. Successive stages approximate conditions of increasing deformation and metamorphic grade.

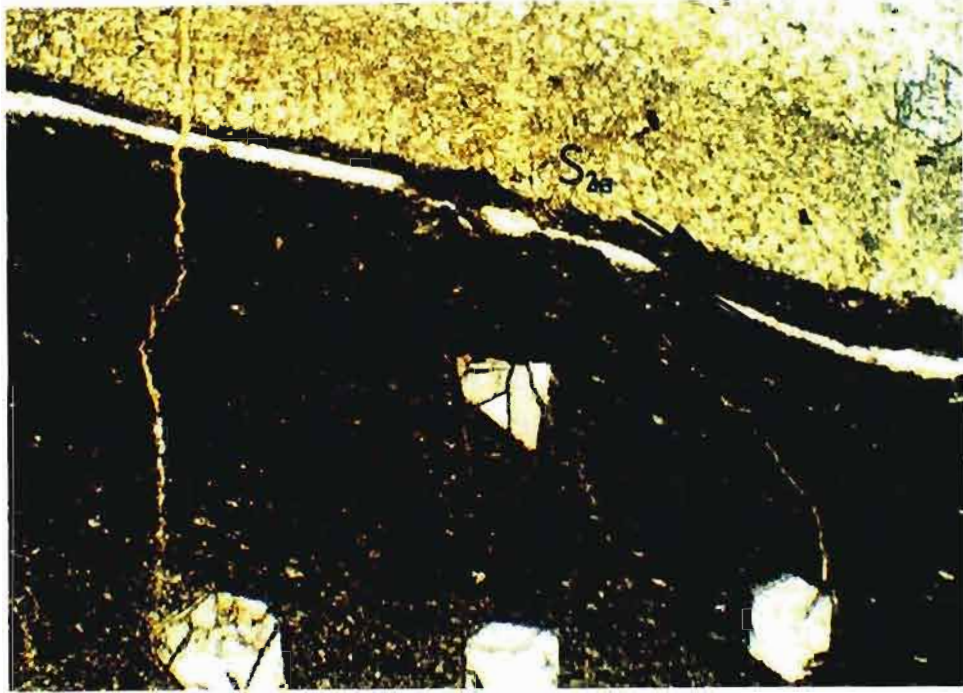
develop in the rock mass, micas between the crenulations are randomly oriented. As this foliation becomes more intense, the fabric becomes continuous and in highly sheared rocks,  $S_0$  is successively transposed into parallelism with the secondary foliation.

The stages of foliation formation can provide a framework for determining the sequence of porphyroblast growth in a single thin section or regionally if the foliation develops synchronously within a given rock mass. As Gibson (1992) emphasises, the development of a fabric during progressive inhomogeneous deformation implies that different parts of a deforming rock mass may follow different strain paths with the result that two or more porphyroblasts containing different microstructures, need not necessarily have formed at different times. This is supported by porphyroblast-matrix relationships observed in the study area. Within the andalusite zone of the Mathabatha domain, the same sequential porphyroblast order is observed in both high and low strain zones. In relation to the porphyroblast sequence, the earliest record of fabric development occurred after biotite and garnet growth. At the other end of the spectrum, a well developed fabric is absent yet porphyroblast relationships indicate the same sequential growth history. This implies that foliation development is not predictably sequential, and is also not synchronous over the area, and therefore cannot be used as a reliable time marker within the aureole. In this case, strain partitioning has produced a highly differentiated foliation, which is diachronous with respect to porphyroblast development.

## 5.7 RELATIVE ROTATION OF PORPHYROBLASTS

In the andalusite zone of the interpericlinal areas (Mathabatha domain), primary sedimentary lamination, preserved both as  $S_i$  and  $S_e$ , is consistently disrupted in a top-to-south sense along micro-shears within the S-fabric (Figure 5.21). In more highly foliated rocks shear movement is often found on the immediate margins of pre-tectonic porphyroblasts, forming zones of contact strain. Porphyroblasts flanked by these zones, give an apparent antithetic rotation sense (anticlockwise) with respect to  $S_0$  and  $S_2$  (Figure 5.22).

Apparent porphyroblast rotation can be interpreted in three different ways (Figure 5.23) (a) The porphyroblasts have rotated in a dextral sense during dextral non-coaxial flow in which the  $S_0$  primary layering underwent less rotation than the porphyroblasts; (b)  $S_0$  has been deformed

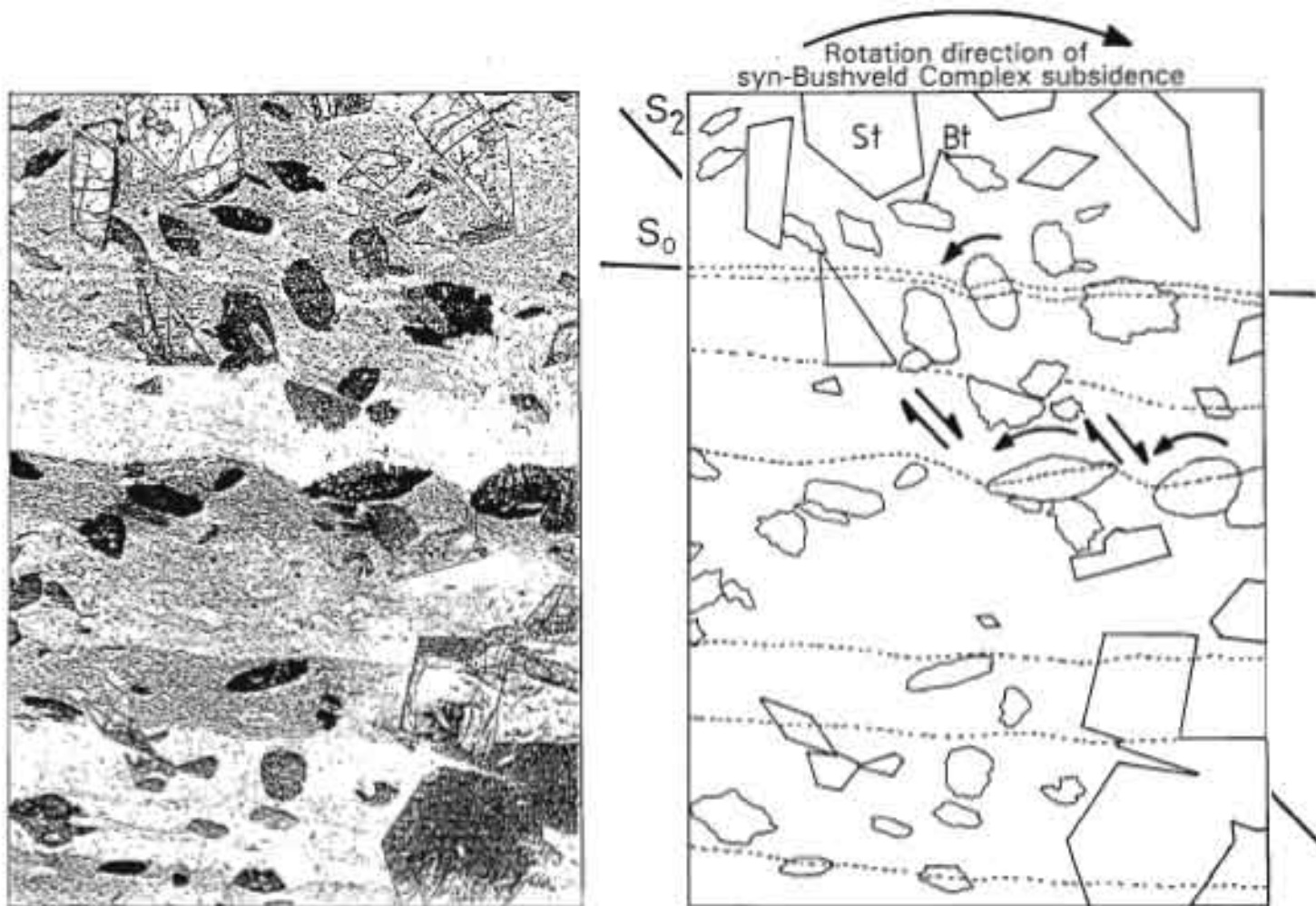


**Figure 5.21**  $S_{2a}$  foliation in a thin shear zone in an otherwise unfoliated garnet fels shows extensional top to south shear. Note extensional boudinage of the thin quartz lamination. Sample Q1B4 from the lower pelitic unit of the Timeball Hill Formation, Hoogenoeg Andalusite Mine. Plane polarised light. Width of view = 6 mm.

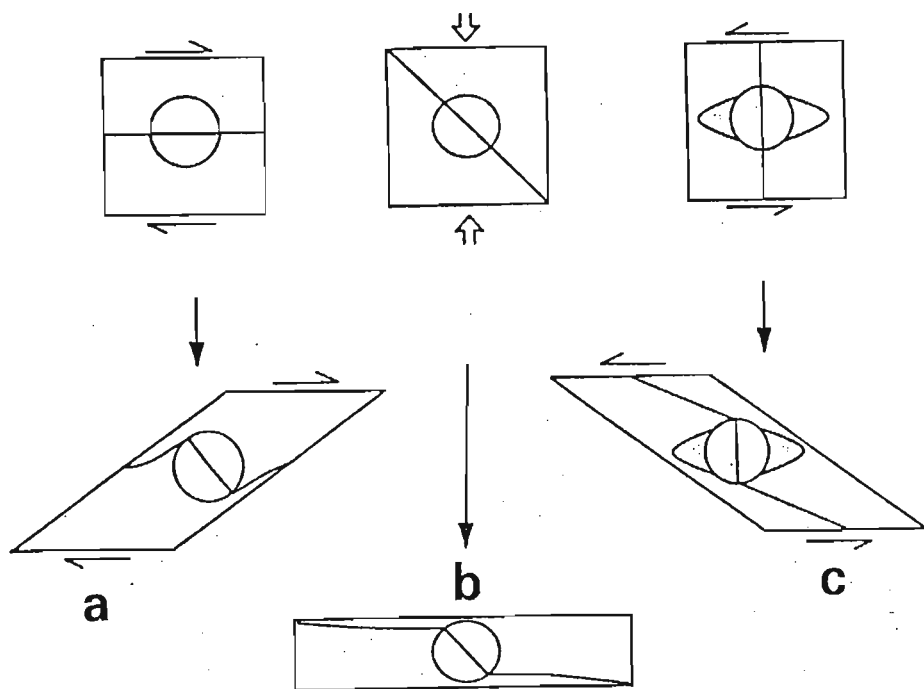
around a stationary porphyroblast during coaxial flow; and (c) sinistral rotation of the foliation ( $S_e$ ) with respect to a stationary porphyroblast in dextral non-coaxial flow.

Where shears are not developed adjacent to porphyroblasts ( $S_{oi} = S_{oc}$  orientation), rotation of porphyroblasts has been synthetic with respect to the tilt axis of the strata. Where porphyroblasts are flanked by shears ( $S_{oi} \neq S_{oc}$ ) however, porphyroblasts have a antithetic rotation sense with respect to the tilt axis of the strata (Figure 5.22). For non-rotation to occur matrix deformation must be totally decoupled from the porphyroblasts. In this example, of the initial stages of foliation development, decoupling between matrix and each porphyroblast is not complete, resulting in a continuum of rotational situations for each porphyroblast. Only once the matrix becomes completely differentiated into zones of non-coaxial high-strain and coaxial low-strain, with complete decoupling between these zones, can non-rotation occur. This observation may explain why inclusion trails in a population of porphyroblasts are often not parallel across the entire thin section.





**Figure 5.22** Microfiche image of staurolite-biotite fels normal to bedding and  $S_2$  fabric. Top-to-south shears define an early stage of  $S_2$  foliation development. Decoupling of matrix and biotite porphyroblasts results in an apparent antithetic rotation with internal  $S_0$  inclusion trails preserving the original bedding orientation. Incomplete decoupling results in synthetic porphyroblast rotation during Bushveld Complex subsidence. Sample HAPL, lower pelitic unit, Timeball Hill Formation, Hoogenoeg farm. Width of view = 14mm.



**Figure 5.23** Origin of apparent rotation of porphyroblasts: a) Dextral rotation of porphyroblast during dextral simple shear. b) Rotation of foliation around non-rotating porphyroblast during pure shear. c) Sinistral simple shear and relative non-rotation of porphyroblast if it lies in and is coupled with a non-deforming microlithon (Passchier and Trouw, 1996).

Vernon *et al.* (1993b) reported wide domains greater than a few porphyroblast widths, in which inclusions trails in porphyroblasts had similar orientations. In the model of Bell and Rubenach (1983), these would represent originally wide Q-domains that existed early in the deformation history that then became narrower to approximate porphyroblast width.

The interesting aspect of this scenario is that the original bedding orientation in helicitic staurolite and biotite porphyroblasts which are flanked by shears (shear decoupling) may remain preserved. In Figure 5.22 for example, the  $S_{0i}$  in the staurolite porphyroblast suggests that the strata had an almost horizontal dip when metamorphic porphyroblast growth proceeded. This is obviously only possible if fabric development can be linked to the tilting event. Evidence for this is provided by the fact that fabric development was a progressive extensional shearing event (dextral-top-to-south shear), recording Bushveld Complex subsidence. Further evidence

supporting syn- to post-Bushveld intrusion subsidence is confirmed by palaeomagnetic studies on the Rustenburg Layered Suite (Hattingh, 1986). These observations have important implications for the development of the aureole structure and magma emplacement mechanisms.

In areas of higher strain and metamorphic grade, such as represented by stages 4 and 5 of foliation development (Figure 5.20), chiasolite porphyroblasts associated with syntectonic fibrolite, often show evidence of collision interference with adjacent porphyroblasts. Vernon *et al.* (1993b) suggested that this may lead to porphyroblast rotation. Individual chiasolite crystals also often have curved or sigmoidal-shaped Rice and Mitchell (1991) Type-1 and Type-2 intergrowths (Figure 5.24).



**Figure 5.24** Chiasolite crystal in the fibrolite zone showing bent and sigmoidal Type-1 and Type-2 intergrowths suggesting syntectonic growth. Sample SF1-2324. Plane polarised light. Width of view = 6 mm.

Although Rice and Mitchell (1991) report that these intergrowths can be slightly curved, sigmoidal intergrowth geometries may indicate that crystallographic-controlled growth may also develop in a deviatoric stress field whereby individual growth prongs are deformed during growth. This texture further suggests that the sigmoidal inclusion trails did not simply

overgrow a pre-existing crenulation, but are syntectonic with respect to matrix foliation development and underwent a certain amount of rotation during growth.

The rotation versus non-rotation debate (Bell, 1985, 1986; Bell and Johnson, 1989, 1992; Vernon, 1988; Passchier *et al.*, 1992; Bell *et al.*, 1992; Busa and Grey, 1992; Vernon *et al.*, 1993b; Johnson 1993a, 1993b) has shown that it is both difficult to determine which process operated and also that a continuum of processes is the most likely and that both rotation and non-rotation of porphyroblasts can occur (Passchier and Trouw, 1996).

## 5.8. CONCLUSIONS

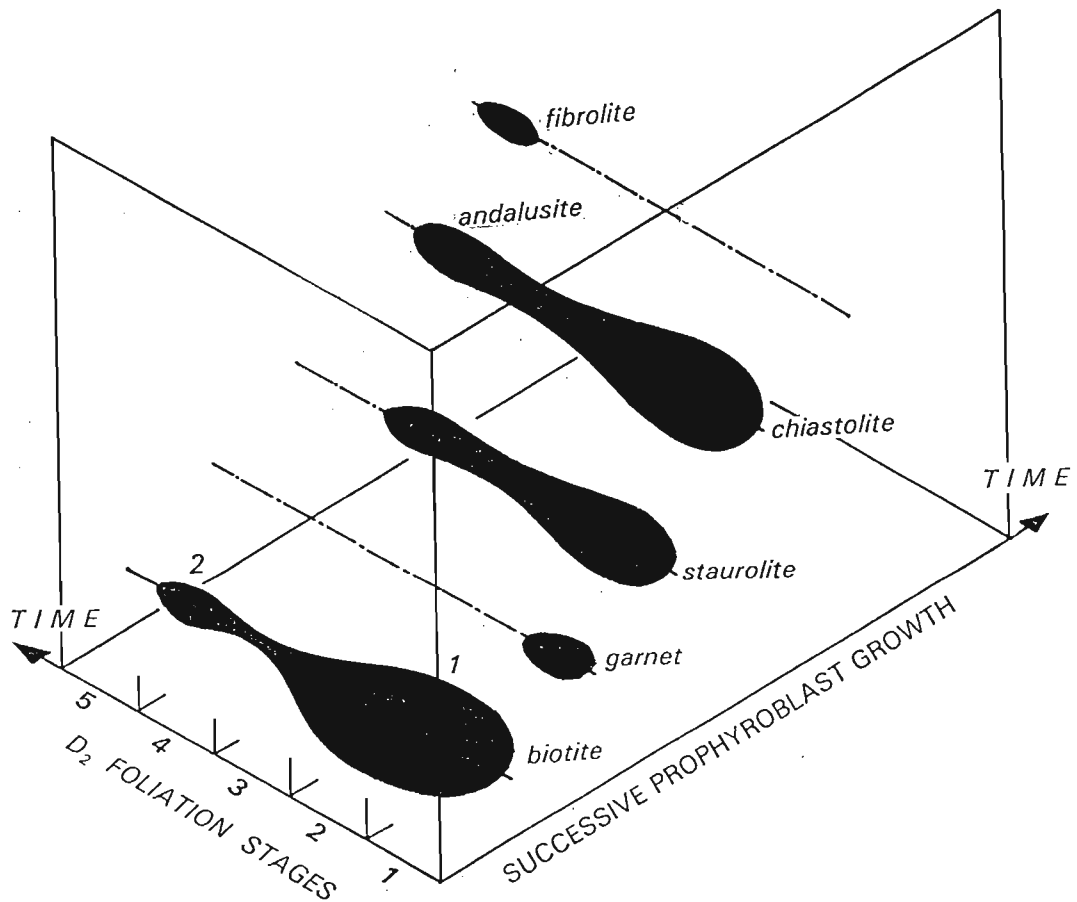
The northeastern Bushveld Complex aureole was affected by widespread syn-Bushveld deformation. The interpretation of the relative timing of fabric formation with respect to porphyroblastesis varies from sample to sample, and with the intensity of the matrix fabric. In zones of lowest strain where only a faint foliation is discernable, delicate cleavage domes adjacent to chistolite are preserved. The development and preservation of these textures requires an absence of, or a very low intensity deformation (Rice and Mitchell, 1991; Vernon *et al.*, 1993a) and are therefore reliable indicators of growth in a near hydrostatic stress field.

This effect is however very localised, and in adjoining areas of higher strain, characterised by a more pronounced fabric, evidence of syntectonic porphyroblast growth with respect to the same fabric is observed. These porphyroblasts are usually anhedral and poikilitic and show an absence of crystallographic-controlled growth. These two "end-member" situations must have developed contemporaneously during the same metamorphic event, and indicate that the local interpretation of PMR's in the area is governed by the inhomogeneous nature of the fabric-forming event that accompanied the deformation.

In areas where porphyroblast growth proceeded under near-hydrostatic conditions, porphyroblastesis was followed by the expansion of the fabric outwards from smaller localised higher strain zones as the deformation event evolved. This was accompanied in some cases by continued syntectonic porphyroblastic growth as shown by epitaxial overgrowths of andalusite on chistolite and at higher grades by the growth of syntectonic fibrolite. These observations all indicate that deformation intensity increased on the prograde metamorphic path.

Deformation then ceased before the growth of retrograde minerals such as muscovite and chloritoid which are post-tectonic and overgrow the  $S_2$  fabric (Figure 5.16).

In comparison to the interpericlinal domains, the periclinal domains have a strongly developed axial planar foliation which is highly discordant to the dominant foliation. As described in Chapter 4, field evidence indicates that the foliation trace from interpericlinal areas into the periclinal cores is continuous, having the basic geometry of an outward fanning structure. Comparing interpericlinal with periclinal timing of porphyroblast growth shows almost the identical porphyroblast-matrix relationships, suggesting that the two fabrics ( $S_{2a}$  and axial planar  $S_{2b}$ ) developed almost synchronously during  $D_2$  progressive deformation (Table 5.1). Localised evidence for refoliation of  $S_{2b}$  in the cores of the periclinal domains during porphyroblast growth (Figure 5.19) suggest that the  $S_{2a}$  foliation preceded the  $S_{2b}$  foliation, but as periclinal growth proceeded,  $S_{2a}$  remained active in the interpericlinal areas (Figure 5.25).



**Figure 5.25** Sequential foliation-porphyroblast-time diagram illustrating the sequence of porphyroblast growth in relation to the 5-stage  $S_{2a}$  fabric evolution shown in Figure 5.20. Most porphyroblasts developed early with respect to foliation with some growth during later stages of foliation development.

**Table 5.1** Summary of porphyroblast-matrix relationships in the andalusite zone of the interpericlinal and periclinal areas.

**ANDALUSITE ZONE**

	<b>Interpericlinal areas</b> <b>S<sub>2a</sub> fabric</b>	<b>Periclinal cores</b> <b>S<sub>2b</sub> axial planar fabric</b>
biotite	$P < D_{2a} ; P \supset D_{2a}$	$P < D_{2b} ; P \supset D_{2b}$
garnet	$P < D_{2a}$	$P < D_{2b}$
staurolite	$P < D_{2a} ; P \supset D_{2a}$	$P < D_{2b} ; P \supset D_{2b}$
chiastolite	$P < D_{2a} ; P \supset D_{2a}$	$P < D_{2b} ; P \supset D_{2b} ; D_{2a} < P \leq D_{2b}$
plagioclase	$P < D_{2a}$	
cordierite	$P < D_{2a}$	$P < D_{2b} ; P \supset D_{2b}$
sericite	$P \supset D_{2a}$	$P \supset D_{2a}$
muscovite	$D_{2a} < P$	$D_{2b} < P$
chloritoid	$D_{2a} < P$	$D_{2b} < P$

**FIBROLITE ZONE**

biotite	$P < D_{2a} ; P \supset D_{2a}$	$P < D_{2a} ; P \supset D_{2a}$
garnet	$P < D_{2a}$	$P < D_{2a}$
andalusite	$P < D_{2a} ; P \supset D_{2a}$	$P < D_{2a} ; P \supset D_{2a}$
cordierite	$P < D_{2a} ; P \supset D_{2a}$	$P < D_{2a} ; P \supset D_{2a}$
fibrolite	$P \supset D_{2a}$	$P \supset D_{2a}$
K-feldspar	$P \supset D_{2a}$	$P \supset D_{2a}$
muscovite	$P \supset D_{2a} ; D_{2a} < P$	$P \supset D_{2a} ; D_{2a} < P$

Fabric development during subsidence was accommodated predominantly in the matrix. This followed a general progression from relatively wide zones of coaxial strain (Q-domains) that narrowed as deformation proceeded. Porphyroblasts within these domains were in some cases decoupled from the deforming matrix and preserved the original pre-D<sub>2</sub> deformation bedding orientations. These are preserved as inclusion trails and support palaeomagnetic data that indicates that metamorphism was initiated when bedding was in a near-horizontal orientation. Where porphyroblasts were not entirely decoupled from the matrix foliation, during early stages of foliation development, porphyroblasts have rotated. Inclusion trails in the porphyroblasts do not preserve the original pre-foliation bedding orientation.

In the interpericlinal areas (Mathabatha domain) a more steeply southward dipping  $D_2$  foliation is superimposed on a moderately southward dipping bedding. The kinematics of this fabric forming event is consistent with a dextral top-to-south sense of shear. This implies that the foliation records an extensional event that is synchronous with contact metamorphism. This would be related to Rustenburg Layered Suite subsidence soon after intrusion.

# CHAPTER 6

## METAMORPHISM

### 6.1 METAMORPHIC ZONES

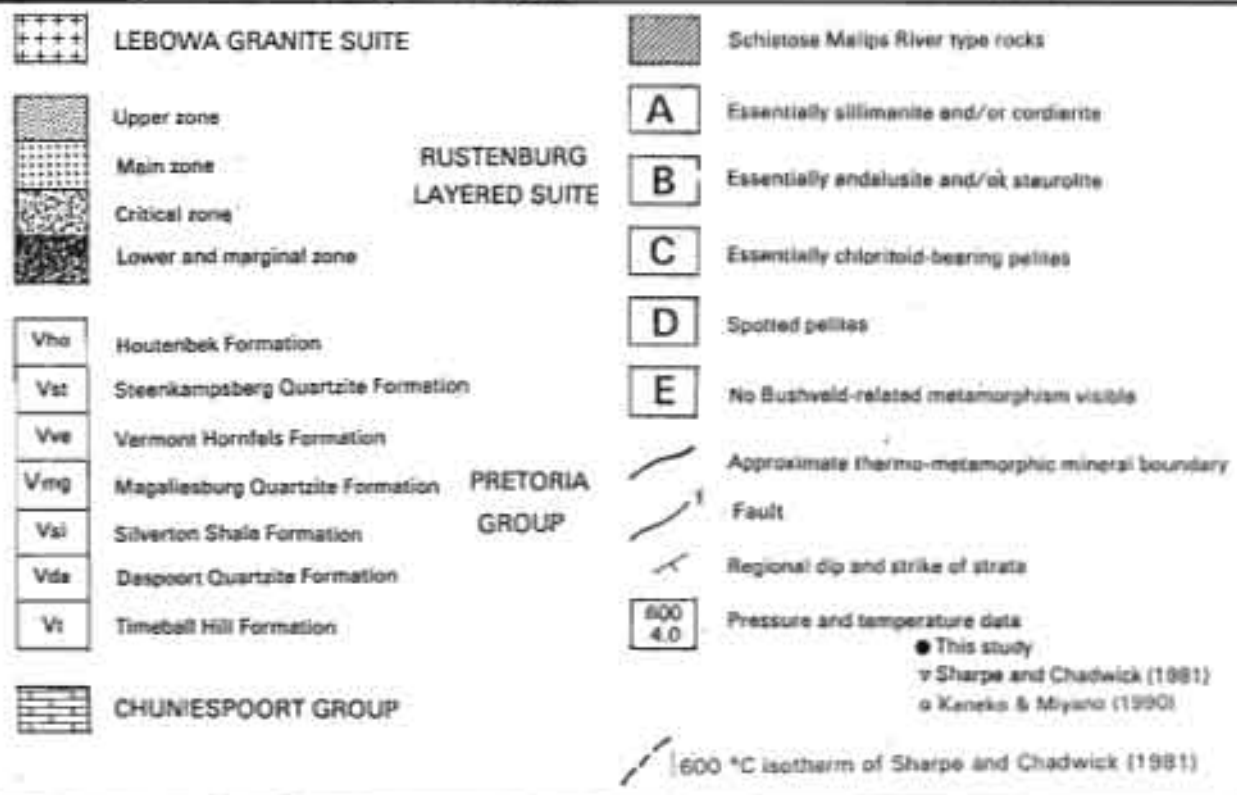
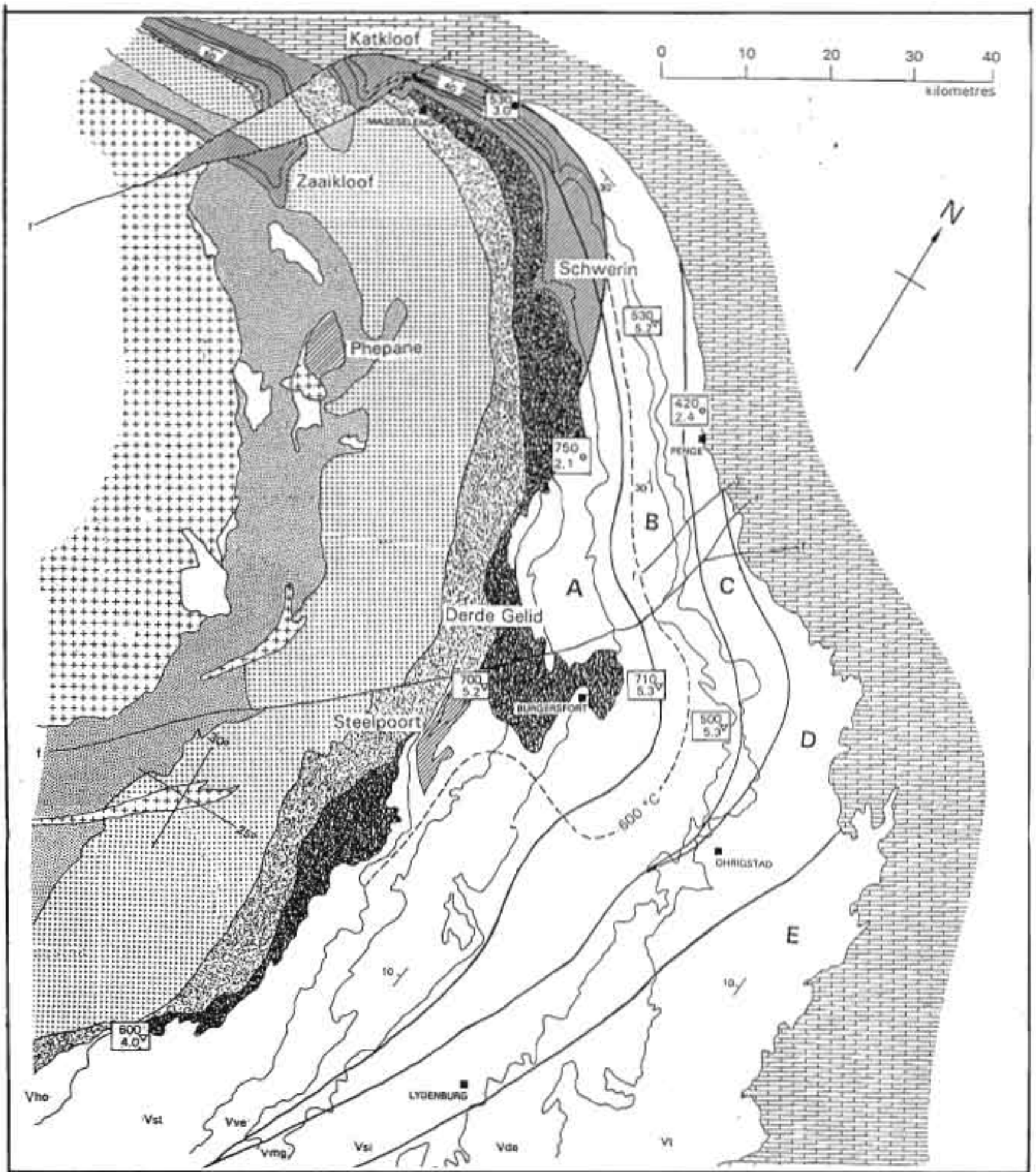
The metamorphic zones of the Bushveld Complex aureole are based primarily on pelitic mineral assemblages from the argillaceous formations of the Pretoria Group (Saggerson and Turner, 1995). Although these zones relate broadly to a metamorphic zonation, they also reflect stratigraphic-dependant bulk-rock compositional changes. This is because the Rustenburg Layered Suite is approximately sill-shaped with a lower contact that in most areas is only slightly discordant with the underlying Pretoria Group floor. In the undeformed parts of the aureole, metamorphic grade decreases with depth below the intrusion contact. Isograds tend to parallel the bathograds with the highest metamorphic grades equilibrated under the lowest pressures and the lowest grades under the highest pressures. The resulting metamorphic field gradient is thus not an isobaric section, as commonly described from aureoles surrounding steep-sided granitic plutons (Pattison and Tracy, 1991) but represents a negative slope in PT space. This gradient varies for different parts of the contact aureole and is dependant on the dip of the floor sequence, a result of syn-and post-Bushveld Complex deformation.

In the northeastern Bushveld Complex the lowest grade metamorphic zones are defined by spotted slates followed by chloritoid-chlorite assemblages (Figure 6.1). This is followed up grade by an extensive zone dominated by andalusite-cordierite or andalusite-staurolite assemblages. Sillimanite-cordierite assemblages usually form the innermost zone with sillimanite-cordierite-orthopyroxene assemblages preserved at the highest grades at the immediate contact and in pelitic xenoliths (Blain, 1975; Saggerson and Turner, 1995).

In the study area three distinct zones, easily identified in the field, characterise the contact metamorphic facies series: an outer andalusite (mainly chiastolite) zone, a fibrolite zone and an inner migmatite zone (Figure 6.2 and 6.3). All three are exposed in the perimeter of Bushveld Complex whereas only the fibrolite and migmatite zones are represented in the periclinal structures exposed within the Bushveld Complex.



**Figure 6.1** Regional map of the eastern Bushveld Complex and the distribution of the main metamorphic subdivisions after Blain (1975). Geothermobarometry results and the proposed 600 °C isotherm of Sharpe and Chadwick (1981) is also shown.



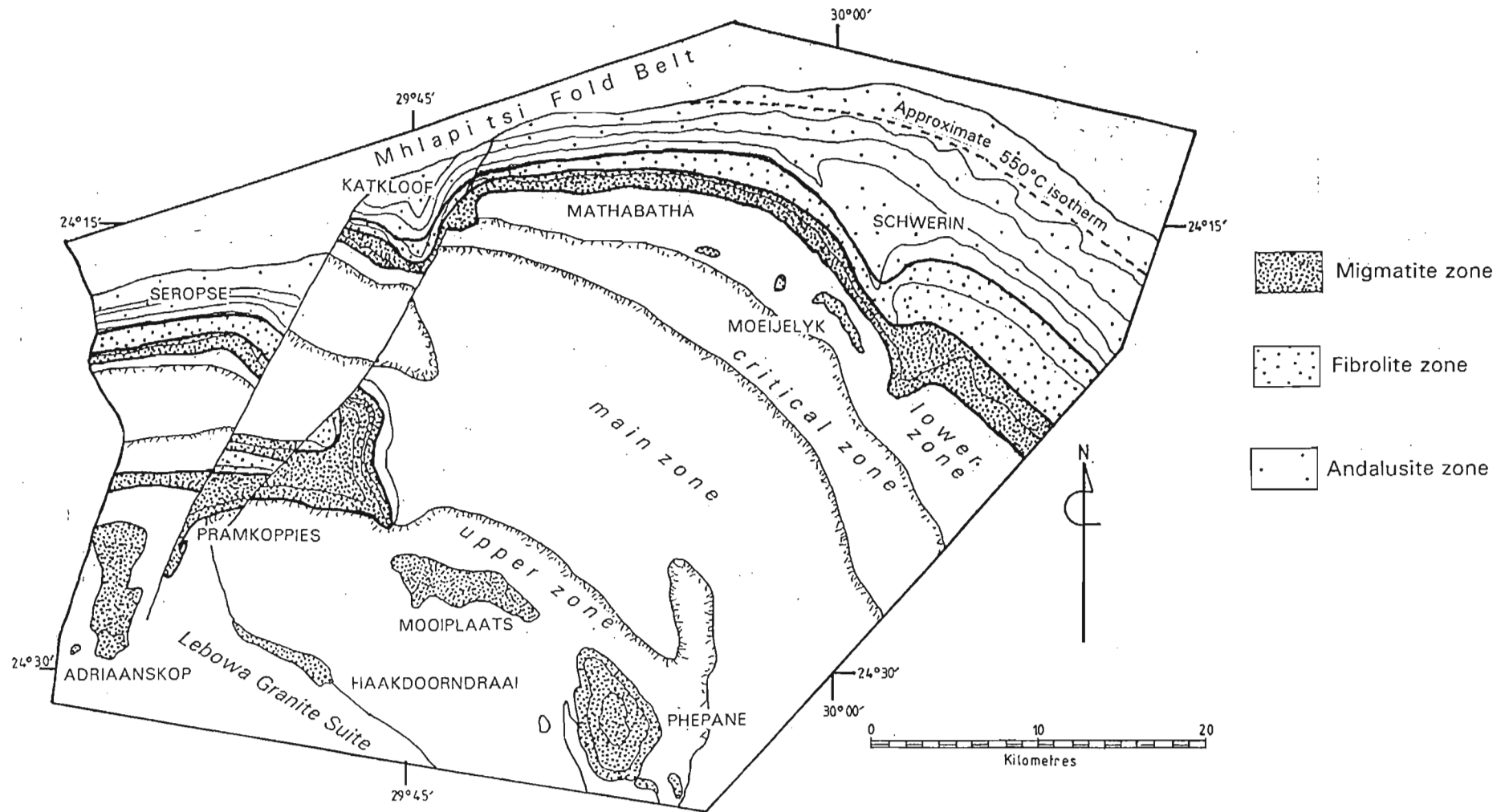
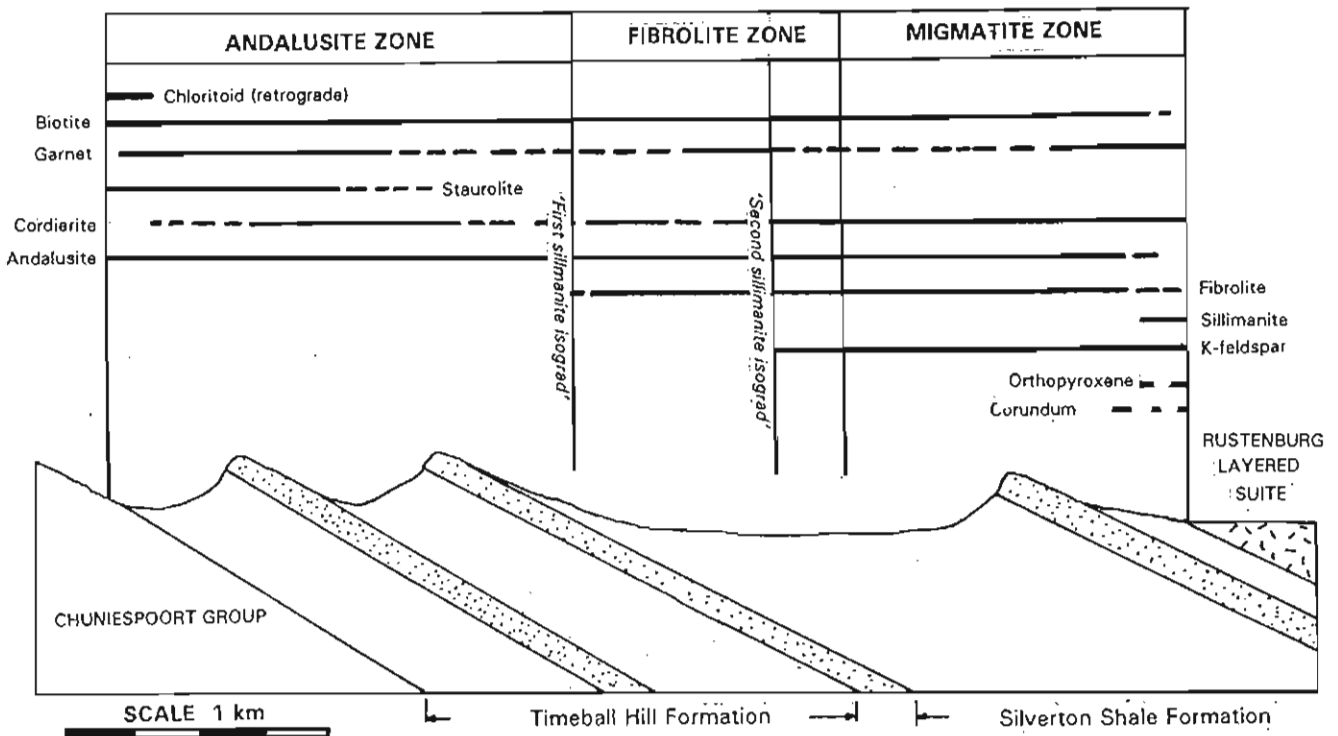


Figure 6.2 Map of the study area showing the distribution of the three main metamorphic zones recognised in the field within the pelitic units of the Pretoria Group.



**Figure 6.3** Schematic diagram showing the distribution of porphyroblastic minerals typical of the contact aureole in the Mathabatha area.

Across the study area within the interpericlinal domains (Mathabatha and Seropse domains), metamorphic zone boundaries closely follow the lithological contacts. Within the periclinal domains however, the zones transgress the lithological contacts into lower stratigraphic units (Figure 6.2). For example in the Katkloof Fold, fibrolite is found within the upper pelitic unit of the Timeball Hill Formation. In the adjacent interpericlinal areas, such as the Mathabatha area and Seropse areas, the first appearance of fibrolite is only found at the base of the Silverton Shale Formation. Rocks of the Phepane structure are intensely deformed and migmatized and this zone is expected to continue to well below the Silverton Shale Formation. The same is seen in the Zaaikloof-Pramkoppies-Adriaanskop structure, where all the rocks are metamorphosed to fibrolite and migmatite zone conditions.

This downward transgression of higher grade zones indicates that the periclinal domains were subjected to a higher heat flow, being completely surrounded by the Rustenburg Layered Suite magmas. It also implies that the periclinal folds must have developed before or during contact metamorphism as post-contact metamorphic deformation would simply have resulted in folded isotherms without any transgression across lithological contacts.

## 6.2 THE ANDALUSITE ZONE

The largest part of the aureole is characterised by the presence of chiasolitic andalusite in pelitic units from the lowermost Pretoria Group, the Rooihogte Formation, to the lower part of the Silverton Shale Formation. Since the entire Pretoria Group in the study area has been metamorphosed upwards from medium grade conditions, the transition from low grade (albite-epidote facies) to medium grade (amphibolite facies) is not located within the Pretoria Group but within the underlying Chuniespoort Group.

Typical mineral associations of the andalusite zone are presented below in Table 6.1. Staurolite coexists with andalusite over most of the andalusite zone, and disappears before the incoming of fibrolite at the fibrolite zone (Figure 6.3). Cordierite is more dominant in the higher grade parts of the andalusite zone and extends to the highest grades within the aureole. Most of the mineral assemblages are associated with muscovite, plagioclase and quartz although some muscovite-poor and muscovite-absent assemblages are found interbedded with the more common muscovite-bearing assemblages.

### *Andalusite*

Prismatic andalusite porphyroblasts are usually the largest with a diameter of up to 20 mm and often reaching 200 mm in length. Most crystals are idioblastic chiasolites showing marked textural and chemical sector zonation with graphite concentrated along sector boundaries extending as diagonals from a central inclusion-rich and/or red coloured (001) core sector. Microprobe analyses from andalusite in the Burgersfort area show that the red-coloured (001) sector has the highest iron content (Lapinsky, 1981). Preferential absorption of iron and inclusions onto the growing terminal ends of the (001) sectors is believed to be related to a combination of processes involving variations in ion exchange, atomic configuration, growth rates and roughness between different sectors (Kouchi *et al.*, 1983). Graphite, biotite and ilmenite are common inclusions and are preferentially concentrated in the (001) sector and along sector zone boundaries whereas inclusions of staurolite and garnet may occur in any of the sectors. Included staurolite may form complex symplectic intergrowths with vermiform quartz (Figure 6.4) a texture not developed in staurolite outside the andalusite porphyroblasts.

**Table 6.1** List of common pelitic mineral associations of the andalusite zone.  
Mineral abbreviations after Kretz (1983).

**MUSCOVITE-PRESENT ASSEMBLAGES**

+ quartz + muscovite ± plagioclase

	PROGRADE PHASES	RETROGRADE PHASES
1)	Ad + Bt	Ms + Chl
2)	Ad + Bt + St	Ms + Chl
3)	Ad + Bt + Grt	Ms + Chl
4)	Ad + Bt + St + Grt	Ms + Chl + Cld
5)	Ad + Bt + Crd	Ms + Chl
6)	Ad + Bt + St + Crd	Ms + Chl
7)	Ad + Bt + Grt + Crd	Ms + Chl
8)	Bt + St	Ms + Chl
9)	Bt + Grt	Ms + Chl
10)	Bt + St + Grt	Ms + Chl
11)	Bt + St + Grt + Crd	Ms + Chl
12)	Bt + St + Crd	Ms + Chl

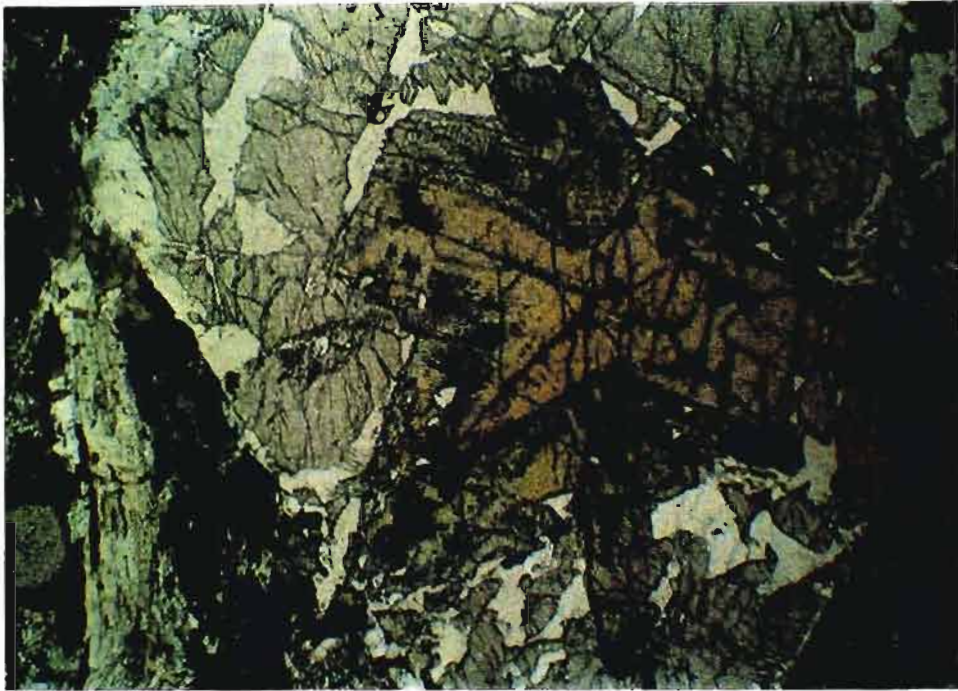
**MUSCOVITE-ABSENT ASSEMBLAGES**

+ quartz ± plagioclase

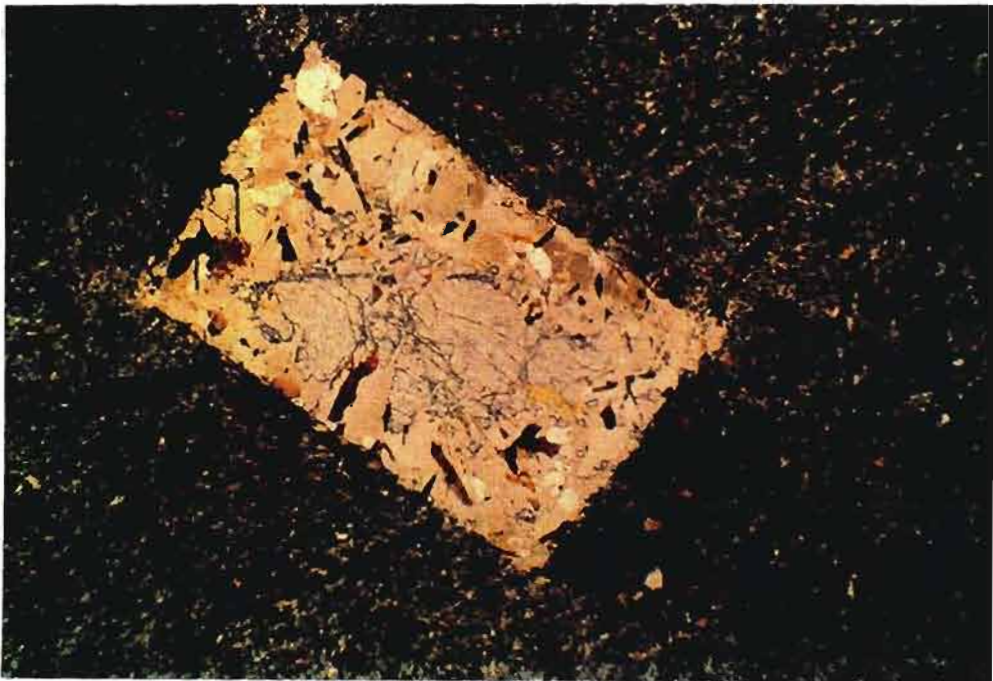
13)	Ad + Bt + Grt	Chl
14)	Ad + Bt + St + Grt + Crd	Chl
15)	Ad + Bt + St + Grt + Crd + Oam	Chl
16)	Bt + St	
17)	Bt + St + Grt	Chl
18)	Bt + St + Grt + Oam	Chl
19)	Bt + Grt	Chl
20)	Bt + Grt + Crd	Chl

As discussed in Chapter 5, cleavage domes are invariably associated with chiastolite crystals and are best preserved in low strain zones where a matrix foliation is poorly developed, or preserved in epitaxial overgrowths (Figure 5.17 in Chapter 5).

Late stage replacement of andalusite by plagioclase is often seen in rocks from the base of the lower pelitic unit of the Timeball Hill Formation (Figure 6.5). More widespread is the alteration of andalusite to muscovite which also is also found to be more prevalent towards the lower part of the andalusite zone. Replacement is usually only confined to crystal margins but in some cases complete pseudomorphism produces a schimmer aggregate texture.



**Figure 6.4** Staurolite inclusion in chiastolite with a rim of vermiform quartz inclusions. Sample HOEG MAH. Lower pelitic unit, Timeball Hill Formation. Hoogenoeg farm. Plane polarised light. Width of view = 4.5 mm.

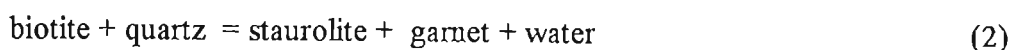
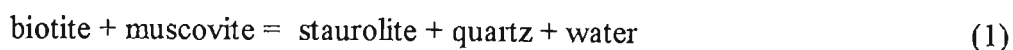


**Figure 6.5** Plagioclase replacing chiastolite. Note the cleavage domes developed during chiastolite growth. Sample C7. Plane polarised light. Width of view = 6 mm.

### *Staurolite*

Staurolite is always twinned and occurs as up to 20 mm sized porphyroblasts. The crystals are usually idioblastic, particularly in rocks with a fine-grained carbonaceous matrix. In a coarser matrix the staurolite is xenoblastic and poikiloblastic. This produces helicitic textures in finely laminated rocks, preserving the layering within crystals as contrasting clear and poikiloblastic zones. Sector zoning is common with small quartz inclusions defining sector boundaries and the associated development of graphite cleavage domes in the matrix of graphite-rich rocks. Almost all staurolite crystals display an aggregate pseudomorph texture (Spry, 1969) which was first described from the Bushveld Complex aureole by Schweltnus (1956) and subsequently by Lapinsky (1981). In sericite-rich assemblages larger lath-shaped inclusion-free areas represent “ghosts” of replaced or partially replaced biotite laths with a finer-grained texture that mimics the sericite-quartz groundmass (Figure 6.6). This indicates that both biotite and sericite were consumed during the growth of staurolite such as represented in reaction (1).

The same textures are also seen in muscovite-absent, garnet-staurolite assemblages (assemblage group 17) (Figure 6.7). The lack of sericite in these rocks may have resulted from complete muscovite consumption such as represented by reaction (1) or, since no recognisable sericite pseudomorphs are visible in the staurolite, sericite may not have been directly involved in staurolite production. Such a process is represented by reaction (2) in the staurolite-garnet assemblages:



In some samples, such as HOEG STZ2 (Figure 6.8) the aggregate pseudomorph texture bears little resemblance to the groundmass and indicates that an earlier texture and paragenesis has been replaced and that the subsequent groundmass has been texturally modified. In this case one can only speculate as to the nature and mineralogy of the original paragenesis. The most likely mineralogy is one that represents any one of the staurolite producing phases such as chlorite, muscovite, chloritoid or biotite. These are represented by the reactions such as (3), (4) and (5).





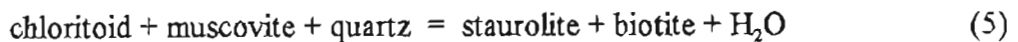
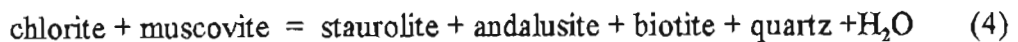
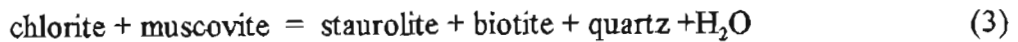
**Figure 6.6** Aggregate pseudomorph or ghost texture in staurolite. Biotite is partially replaced. Smaller lath shapes may represent replaced chlorite or chloritoid. The groundmass texture is perfectly preserved within the staurolite mimicking the groundmass aggregate of muscovite and quartz. Sample SC from Hoogenoeg farm. Plane polarised light. Width of view = 6 mm.



**Figure 6.7** Aggregate pseudomorph or ghost texture in staurolite in the muscovite absent, assemblage group 17. Clear lath-shaped areas in the poikiloblastic staurolite represent replaced biotite. Garnet forms inclusions in staurolite. Sample M4 from the lower pelitic unit of the Timeball Hill Formation on the farm Hoogenoeg. Plane polarised light. Width of view = 6 mm.

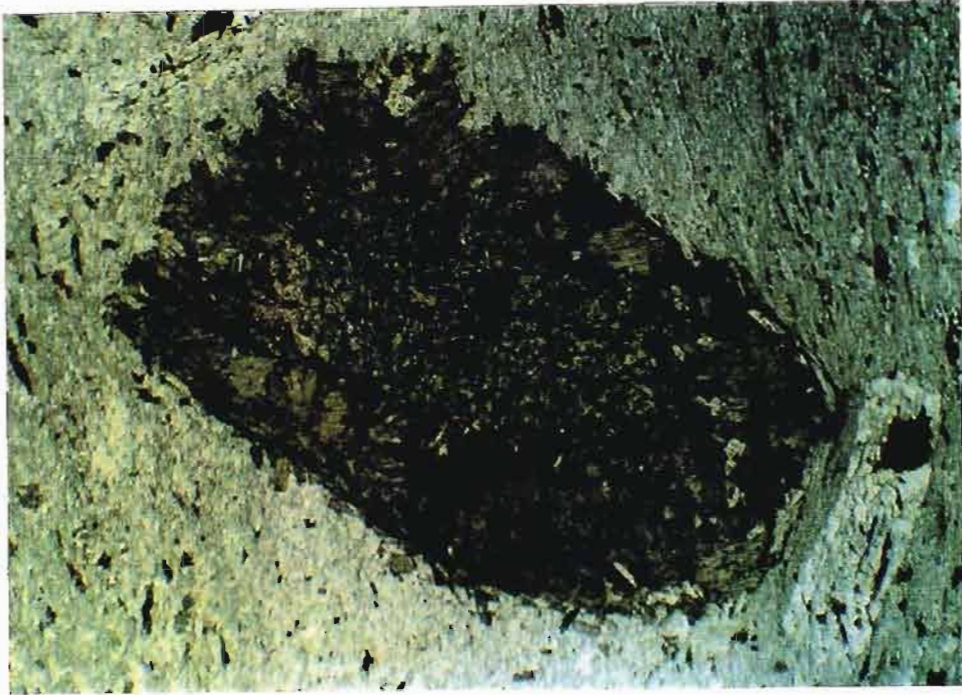


**Figure 6.8** Aggregate pseudomorph replacement texture in staurolite *not* mimicking the groundmass texture. Lath-shaped inclusion-free zones thus represent an earlier paragenesis and texture. Larger biotite porphyroblasts are only partially replaced by staurolite. Lower pelitic unit, Timeball Hill Formation on the farm Hoogenoeg. Sample HOEG STZ2. Width of view = 6 mm.



Inclusions in staurolite commonly consist of quartz, ilmenite and remnants of partially replaced biotite. Garnet is the only other porphyroblast that is commonly partially included or included in staurolite (Figure 6.7).

Retrograde alteration of staurolite may be seen as small chlorite laths within the staurolite poikiloblasts, or more substantial almost complete replacement of staurolite by chlorite (Figure 6.9).



**Figure 6.9** Staurolite replacement by green chlorite. Sample XII from the lower pelitic unit of the Timeball Hill Formation on the farm Hoogenoeg. Plane polarised light. Note small lath-shaped grain of quartz aggregate, possibly after biotite. Width of view = 6 mm.

### ***Biotite***

Biotite ranges considerably in size from 0.2 mm to 5.0 mm in length. It is developed as subidioblastic to xenoblastic laths forming the matrix together with quartz and sericite to larger staurolite and andalusite porphyroblasts. Biotite in this zone of the contact aureole is typically dark brown in colour. In areas of low strain, thin sedimentary lamellae are preserved as alternations of quartz-poor, graphite-rich and quartz-rich, graphite-poor inclusion trains giving rise to helicitic textures. As described in Chapter 5, in areas of high strain, biotite often defines a lepidoblastic fabric together with sericite. In these rocks, biotite cores are preserved as clouded cores containing numerous inclusions of fine graphite. These are overgrown by clear optically continuous biotite tails that form part of the foliation together with sericite in the groundmass.

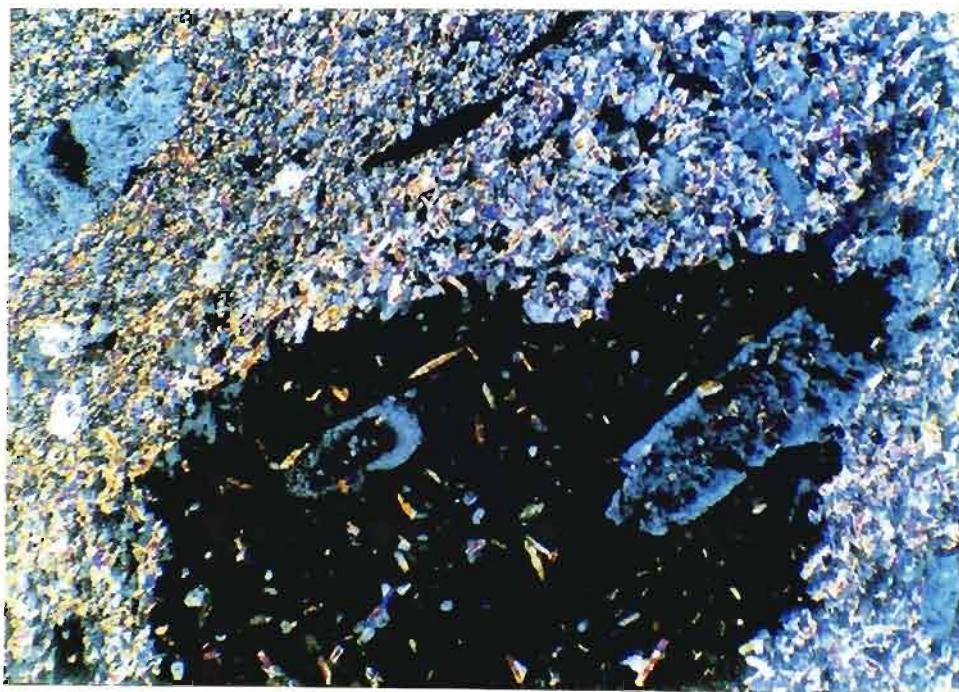
In the muscovite-bearing assemblages, biotite typically has included muscovite, ilmenite and plagioclase porphyroblasts if present. Large pleochroic halos surrounding included zircons are common. Biotite represents one of the earliest phases in these rocks and is found as inclusions in andalusite and cordierite as well as replaced by garnet and staurolite. The most likely biotite

forming reaction therefore is a continuous reaction in which the muscovite becomes less phengitic as the reaction proceeds:



### *Plagioclase*

Plagioclase usually occurs as small near ellipsoidal to lath-shaped microporphyroblasts of approximately 0.5 mm to 2.0 mm in size displaying both optical zonation and textural zonation, with inclusion-rich cores and inclusion-free rims (Figure 6.10). Lapinsky (1981) showed that the zoning is normal with anorthite-rich cores and albite-rich rims. Plagioclase porphyroblasts nucleated early as they are commonly enclosed in the biotite and may end up within large staurolite porphyroblasts that replace biotite. As mentioned above, plagioclase is also found replacing andalusite in some horizons, particularly near the base of the Pretoria Group, suggesting that plagioclase may in some instances be a product of late-stage alkali-metasomatism.



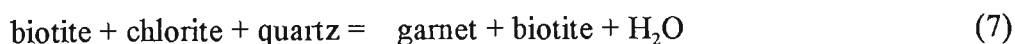
**Figure 6.10** Plagioclase porphyroblasts showing both textural and optical zonation found in the groundmass and as inclusions in biotite porphyroblasts. Sample HAPL from the lower pelitic unit of the Timeball Hill Formation, on the farm Hoogenoeg. Crossed polarised light. Width of view = 2 mm.

### ***Garnet***

Garnet occurs as subidioblastic and idioblastic dodecahedral crystals ranging in size from 0.5 mm to 2.0 mm in diameter. Single layers within stratified rocks tend to have the same sized garnets which are generally unsieved if associated with a fine-grained groundmass. These become both poikiloblastic and xenoblastic in association with a coarse-grained quartz matrix.

Garnets may show sector zonation (Figure 6.11) with associated graphite cleavage domes preserved in the surrounding groundmass. As the microprobe results show (Appendix 3), all garnets from the andalusite zone were found to be strongly chemically zoned (growth zoning) and in some cases were found to also show a textural zonation with a poikiloblastic core and clear rims.

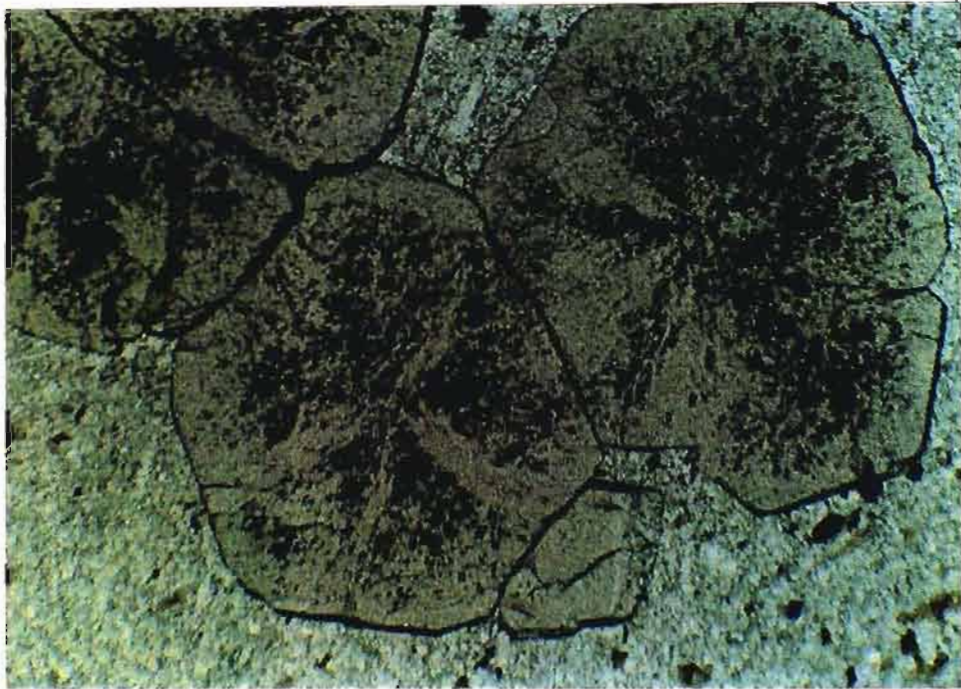
Larger porphyroblasts of staurolite, andalusite and cordierite usually partially or totally enclose garnet, suggesting that garnet is an early phase in the reaction sequence. Garnets are usually closely associated with biotite and in some cases garnet may overgrow and replace biotite. This reaction relationship suggests that biotite was part of the garnet-forming reaction such as:



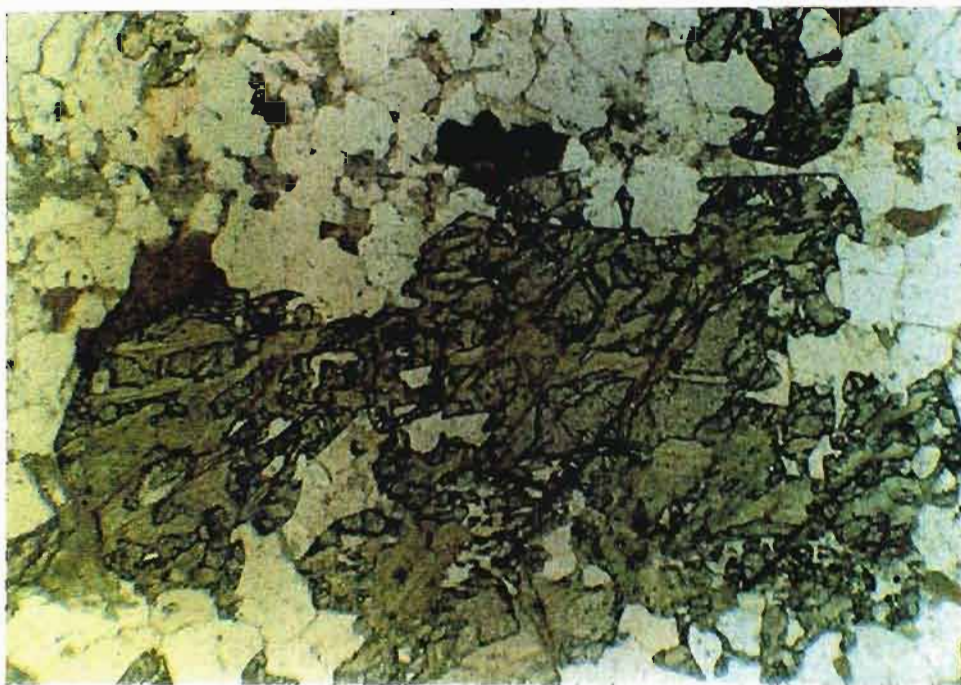
Garnets may be partially altered or in some cases completely pseudomorphed by chlorite due to retrograde metamorphism (Figure 6.12).

### ***Cordierite***

Cordierite assemblages become more common towards the upper part of the lower pelitic unit of the Timeball Hill Formation whereas staurolite assemblages are dominant in the lower part of the unit. This is best explained by bulk-rock chemical controls that limit the equilibrium coexistence of both staurolite and cordierite (Winkler, 1979; Bucher and Frey, 1994). Coexisting staurolite and cordierite assemblages are however, found (assemblages 11, 24 and 15). This is rare if staurolite and cordierite forms a stable assemblage with muscovite (assemblage 11). This has only been reported from a few contact aureoles, notably from the Bushveld Complex aureole (Hall, 1932). The association of staurolite and cordierite without muscovite is however, relatively common (Pattison and Tracy, 1991).

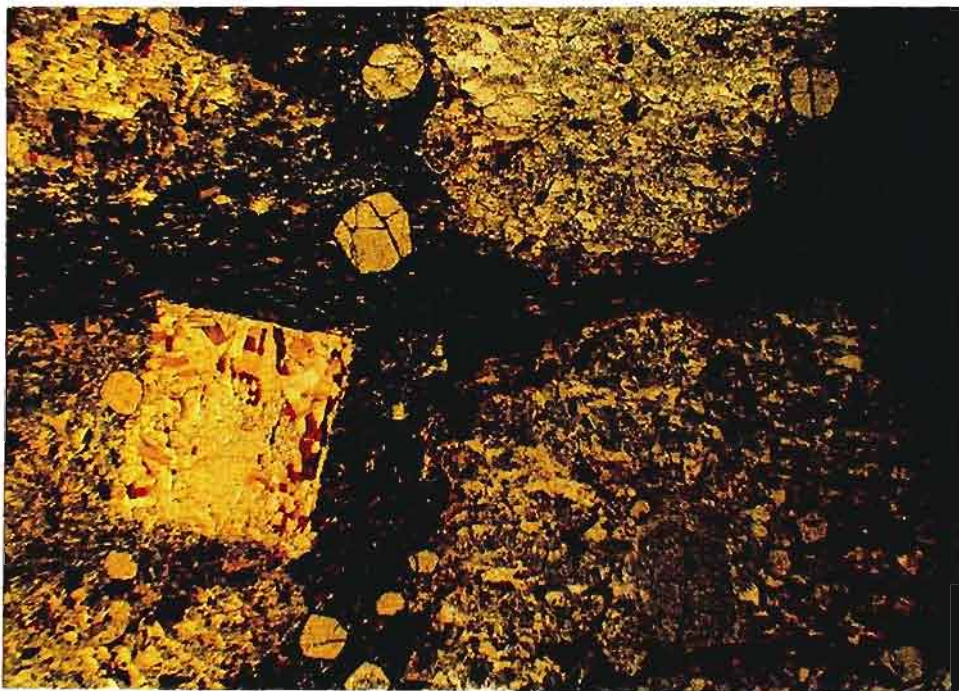


**Figure 6.11** Sector zonation in garnets from the upper pelitic unit of the Timeball Hill Formation on the farm Copper. Sample GTS/HFS. Plane polarised light. Width of view = 2 mm.



**Figure 6.12** Retrograde alteration of garnet to chlorite. Sample TH 16/4 from the lower pelitic unit of the Timeball Hill Formation on the farm Tuimplaats. Plane polarised light. Width of view = 2 mm.

Cordierite forms large xenoblastic and elongate-shaped poikiloblasts up to 10 mm in diameter sieved with quartz and biotite inclusions. Garnet, orthoamphibole, ilmenite and to some degree staurolite are often included or partially included in cordierite. Cordierite may also have an aggregate pseudomorph texture (Figure 6.13). As in staurolite, clear patches represent original replaced reactant mineral phases. Biotite inclusions are not affected suggesting that the texture may have resulted from the replacement of chlorite or muscovite such as represented by reaction (8). Cordierite is commonly also zoned with a central inclusion-rich area surrounded by a relatively inclusion-free rim (Figure 5.3 in Chapter 5).



**Figure 6.13** Large zoned cordierite porphyroblasts with an internal foliated aggregate pseudomorph texture. Inclusions are of graphite, garnet, ilmenite and biotite. Andalusite is partially replaced by biotite and quartz. Chlorite is replacing cordierite along the andalusite - cordierite contact. Sample 16/7. Lower pelitic unit, Timeball Hill Formation on the farm Tuinplaats. Plane polarised light. Width of view = 6 mm.

Andalusite and cordierite porphyroblasts are closely associated in a number of assemblages, and texturally appear to have grown simultaneously. The most likely reaction producing both cordierite and andalusite is represented by reaction (9).



Reaction (9) is also observed as a retrograde reaction involving cordierite, andalusite and biotite inclusions associated with the (001) chiasolite sector and the alteration of cordierite to chlorite. Late stage pinitization is also a common retrograde feature in many of the cordierite porphyroblasts.

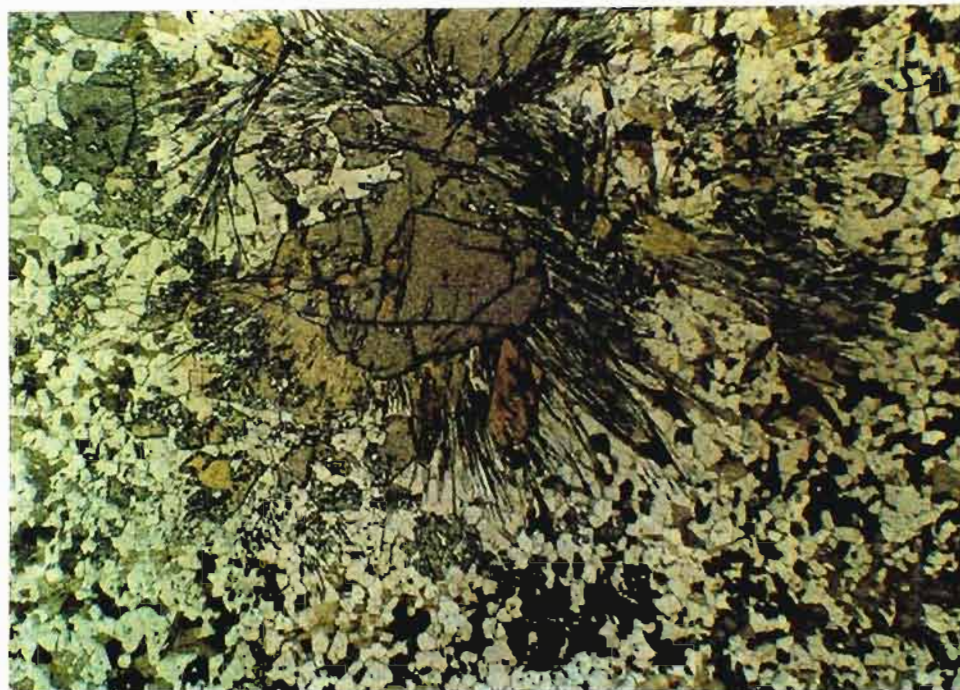


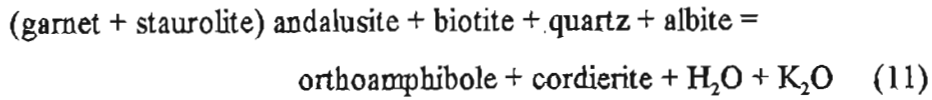
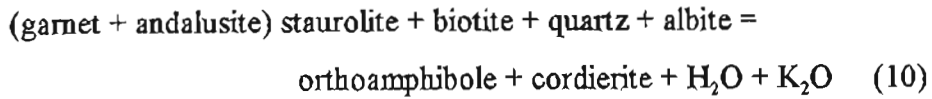
Figure 6.14 An orthoamphibole, garnet and staurolite cluster in a groundmass of quartz and biotite. Sample UP/TH. From the farm Copper. Plane polarised light. Width of view = 6 mm.

### *Orthoamphibole*

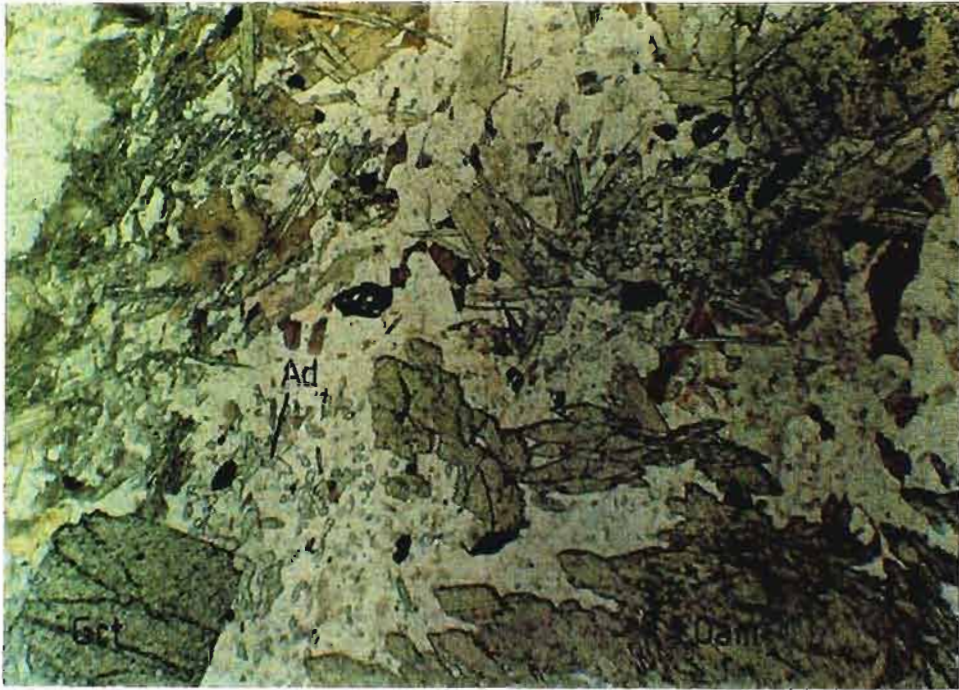
Orthoamphibole assemblages are found in thin bands interbedded with the more common orthoamphibole-free assemblages in both the upper and lower pelitic units of the Timeball Hill Formation (Figure 6.14 and 6.15). These rocks are muscovite-free suggesting a more restricted bulk chemical composition. Orthoamphiboles occur as long acicular porphyroblasts up to 20 mm in length often with a pseudo-bow tie structure. Textural relationships suggest that orthoamphibole formed early involving chlorite and/or biotite-consumption without the growth of  $\text{K}_2\text{O}$  product phases. Arnold and Sandiford (1990) found that consumption of staurolite and/or andalusite was an important step in stabilizing a cordierite-orthoamphibole assemblage involving open system behaviour with metasomatic  $\text{K}_2\text{O}$  depletion. This is represented by the



following reactions:



In sample H9 orthoamphibole and cordierite grew at the expense of biotite and andalusite as represented by reaction (11). This is indicated by the biotite-absent reaction halos surrounding the orthoamphibole clusters and the embayed margins and small remnants of andalusite in optical continuity (Figure 6.15).



**Figure 6.15** Reaction relationship showing orthoamphibole growth at the expense of andalusite and biotite. Sample H9. Lower pelitic unit, Timeball Hill Formation on the farm Hoogenoeg. Plane polarised light. Width of view = 6 mm.

### *Chloritoid*

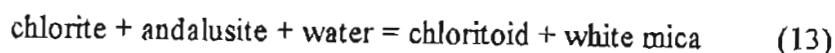
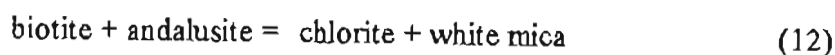
Chloritoid is usually between 0.5 to 1.0 mm in length and is found either associated with sericite and quartz in the groundmass or forms clusters in the cores of large retrogressed (shimmer aggregate) andalusite porphyroblasts (Figure 6.16). Chloritoid is most commonly

found in the lower part the lower pelitic unit of the Timeball Hill Formation. As shown in Chapter 5, the groundmass chloritoid is typically post-tectonic overgrowing the sericite-quartz matrix foliation. The randomly orientated chloritoid porphyroblasts within the cores of shimmer texture andalusite together with chlorite are also considered to be a product of retrograde growth as no chloritoid was found within any unaltered andalusite crystals.

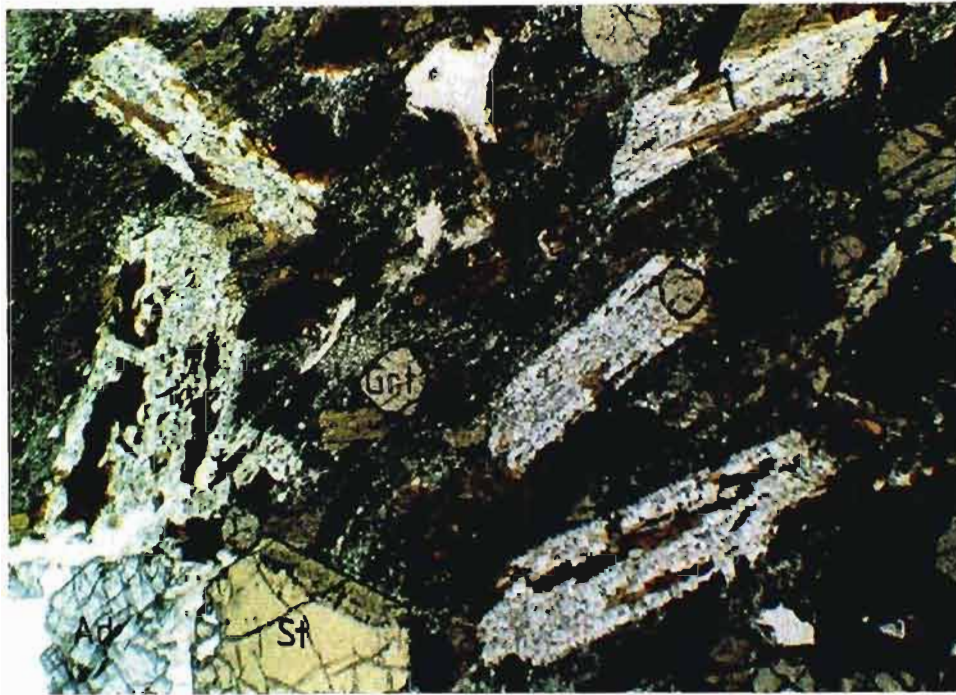


Figure 6.16 Retrograde chloritoid, shimmer aggregate and chlorite replacing a large 15 mm diameter andalusite porphyroblast from the lower pelitic unit, Timeball Hill Formation on the farm Uitkyk. Sample H4. Plane polarised light. Width of view = 2 mm.

This is in contrast to the interpretation of Lapinsky (1981) who considered the chloritoid in the area to be part of the prograde assemblage. The tendency for chloritoid to concentrate only in the andalusite cores may be due to the higher iron content of the 001 core sector of the chiastolite crystal and the often greater abundance of iron-rich inclusions. The most likely chloritoid, white mica and chlorite producing reaction in the andalusite cores suggests a combination of the following reactions:



A common feature of the andalusite zone pelitic assemblages is the occurrence of lath-shaped quartz aggregates intergrown with biotite either with or without muscovite (Figure 6.17). The laths are usually idioblastic with a pseudo hexagonal shape, typically 2 to 5 mm in length, and commonly show an hourglass internal structure defined by a single optically continuous biotite crystal. This texture may represent a pseudomorph of biotite and quartz after early phase of biotite or chloritoid.



**Figure 6.17** Lath-shaped quartz-biotite intergrowths possibly pseudomorphic after an earlier phase of chlorite or biotite in an andalusite-biotite-staurolite-garnet assemblage. Sample HOEG MAH from Hoogenoeg farm. Plane polarised light. Width of view = 6 mm.

This is supported by the fact that the texture is only present in rock compositions characterised by assemblages of staurolite, with or without garnet and andalusite.

### 6.3 THE FIBROLITE ZONE

The first appearance of fibrolite in the Mathabatha area is found at a distance of approximately 2000 m from the contact with the Bushveld Complex. The distinction between fibrolite and sillimanite used here is based on the classification of Kerrick and Speer (1988) in which fibrolite has a grain size diameter below 10  $\mu\text{m}$ . The appearance of fibrolite marks the transition from the andalusite zone to the fibrolite zone. Typical mineral assemblages are listed below in Table

## 6.2.

The fibrolite zone is nowhere greater than approximately 600 m in thickness and passes immediately up grade into the migmatite zone. In the Mathabatha domain fibrolite first appears in the Boven Member of the Silverton Shale Formation immediately above the Dwaalheuwel Quartzite Formation. The fibrolite zone is subdivided into a lower zone, in which fibrolite coexists with andalusite without K-feldspar, and a narrow upper zone marked by the incoming of K-feldspar in the absence of melting. In the Mathabatha area, the K-feldspar reaction-isograd is located within the lower part of the Lydenburg Shale Member of the Silverton Shale Formation. The appearance of fibrolite coincides with a marked increase in deformation intensity and the appearance of schistose rocks compared to the more weakly foliated rocks of the andalusite zone. Although fibrolite is the dominant sillimanite growth form, true sillimanite occurs only in a few isolated samples from the higher grade parts of the migmatite zone.

Staurolite is also absent from this zone. This may in part be due to composition effects and metamorphic grade. Nell (1984) showed that pelites of the Silverton Shale Formation are significantly lower in iron than those of the Timeball Hill Formation. It is also known that staurolite disappears from muscovite - quartz pelites at these grades although it may still be preserved in muscovite-absent assemblages.

**Table 6.2** List of common pelitic mineral associations of the fibrolite zone. Mineral abbreviations after Kretz (1983).

### MUSCOVITE-PRESENT ASSEMBLAGES

+ quartz + muscovite ± plagioclase

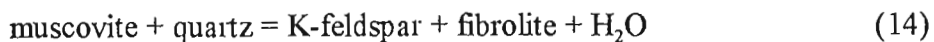
	PROGRADE PHASES	RETROGRADE PHASES
1)	Ad + Fib + Bt + Crd	Ms + Chl
2)	Ad + Fib + Bt + Grt + Crd	Ms + Chl
3)	Fib + Bt + Grt	Ms + Chl
4)	Ad + Fib + Bt + Kfs	Ms + Chl

### *Andalusite*

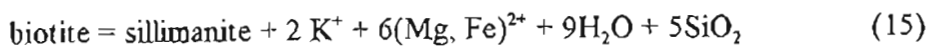
Compared to the very large crystals found in the andalusite zone, crystals in the fibrolite zone seldom exceed 5 mm in width. Fibrolite may partially replace andalusite (Figure 6.18) or nucleate on the margin of the crystals. In schistose rocks andalusite remnants are overprinted by orientated biotite and fibrolite knots (Figure 6.19). Andalusite may be found well up grade of the first appearance of fibrolite, a feature reported from many contact aureoles (Kerrick, 1990). The most favoured explanation is that of sluggish reaction kinetics in the aluminosilicate polymorphic transitions (Fyfe, 1969). Other explanations have suggested the metastable persistence of andalusite to higher grades (Kerrick and Woodsworth, 1989) as well as several unique mechanisms for the growth of fibrolite involving metasomatism, deformation and recrystallisation (Kerrick, 1990).

### *Fibrolite*

As indicated above, the first appearance of fibrolite may be seen as small matted aggregates replacing andalusite (Figure 6.18), nucleating on andalusite or more commonly intergrown with biotite. The absence of K-feldspar in these rocks suggests that this is a polymorphic transition and represents the “first sillimanite isograd”. Only at higher metamorphic grades is fibrolite found as globular or lenticular aggregates forming part of the foliation together with biotite and K-feldspar (Figure 6.19). This association represents the growth of fibrolite at the “second sillimanite isograd” a term originally suggested by Evans and Guidotti (1966) involving the melt-absent dehydration reaction:



The occurrence of fibrolite-andalusite intergrowths suggest that fibrolite was in part formed by a polymorphic transformation reaction below the K-feldspar isograd (first sillimanite isograd). This reaction is considered sluggish, due to very small free energy differences, difficulties in nucleation and slow growth rates (Fyfe, 1969). The growth of fibrolite on biotite (fibrolization of biotite) however, is far more common and documented from many areas (Harker, 1950; Kerrick, 1987; Kerrick and Woodsworth, 1989). Vernon (1979, 1987) suggested that the most likely process is one involving base-leaching reactions such as:



**Figure 6.18** Andalusite replaced by fibrolite within a biotite-quartz-cordierite-K-feldspar assemblage. Sample 27/10. Silverton Formation, Koedoeskop farm. Plane polarised light. Width of view = 6 mm.



**Figure 6.19** Remnants of andalusite in a strongly foliated assemblage of biotite-fibrolite-K-feldspar-quartz. Sample 17/13. Silverton Formation, Tigerpoort farm. Plane polarised light. Width of view = 6 mm.

Kerrick (1987) suggested that the influx of acidic (HC1) volatiles from intrusions can cause fibrolization and that this process may therefore not be indicative of a polymorphic reaction. Vernon (1987) also suggested that fibrolite growth was strain induced. This is supported here by the growth of syntectonic fibrolite in the strain shadows of chiastolite and in small shear fractures within some chiastolite crystals (Figure 5.11 in Chapter 5). Wintsch and Andrews (1988) suggested that stress destabilized feldspar, forming fibrolite and releasing alkalis and silica into the fluid phase. The incoming of fibrolite at the “first sillimanite isograd” is for these reasons not a reliable indicator of metamorphic conditions.

### ***K-feldspar***

K-feldspar is first seen forming xenoblastic microporphyroblasts up to 2 mm in size with numerous graphite inclusions. The absence of melting and the association with fibrolite indicates that K-feldspar was produced by the muscovite dehydration reaction (14) at the “second sillimanite isograd”. The appearance of K-feldspar in the Mathabatha domain occurs approximately 800 m up grade from the first appearance of fibrolite. This corresponds to a vertical stratigraphic distance of approximately 500 m.

### ***Biotite***

Compared to lower grade parts of the aureole, biotite is more highly pleochroic and is typically fox-red in colour rather than dark brown. This change was noted to coincide with the incoming of fibrolite and was also reported by Lapinsky (1981). These changes are also accompanied by marked chemical changes with grade as reported from the Penge area by Kaneko and Miyano (1990).

## **6.4 MIGMATITE ZONE**

The innermost zone of the contact aureole is defined by the migmatite zone. In the Mathabatha domain the first migmatites encountered occur approximately 100 m up grade of the “second sillimanite isograd” - a vertical distance of approximately 60 m. In other parts of the study area this distinction is not clear and suggests that the “second sillimanite isograd” is very closely associated with the onset of melting. Mineral associations from this zone are diverse and are listed below in Table 6.3.

The first indication of melting is seen as minute leucocratic segregations, often forming thin millimetre-scale bedding-parallel veinlets of quartz and feldspar. If these veins become larger they are often accompanied by a melanocratic biotite selvage.

Rocks of the migmatite zone can be subdivided broadly into three subzones: a lower zone characterised by sillimanite (fibrolite) + K-feldspar assemblages; a middle zone which is dominated by a cordierite + K-feldspar  $\pm$  garnet assemblages; an upper zone characterised by cordierite + orthopyroxene assemblages

**Table 6.3** List of pelitic and semi-pelitic mineral associations of the migmatite zone. Mineral abbreviations after Kretz (1983).

**QUARTZ - PRESENT ASSEMBLAGES**

+ quartz  $\pm$  plagioclase

	PROGRADE PHASES	RETROGRADE PHASES
1)	Ad + Fib / Sil + Bt + Kfs	$\pm$ Ms $\pm$ Chl
2)	Bt + Crd $\pm$ Kfs	$\pm$ Ms $\pm$ Chl
3)	Bt + Crd + Grt $\pm$ Kfs	$\pm$ Ms $\pm$ Chl
4)	Ad + Bt + Crd $\pm$ Kfs	$\pm$ Ms $\pm$ Chl
5)	Ad + Fib / Sil + Bt + Crd $\pm$ Kfs	$\pm$ Ms $\pm$ Chl
6)	Ad + Bt + Crd + Hc $\pm$ Kfs	$\pm$ Ms $\pm$ Chl
7)	Ad + Fib / Sil + Bt + Crd + Hc $\pm$ Kfs	$\pm$ Ms $\pm$ Chl
8)	Ad + Bt + Crd + Hc + Grt $\pm$ Kfs	$\pm$ Ms $\pm$ Chl
9)	Bt + Crd + Hc $\pm$ Kfs	$\pm$ Ms $\pm$ Chl

**QUARTZ-ABSENT ASSEMBLAGES**

$\pm$  plagioclase

10)	Ad + Bt + Crd $\pm$ Kfs	$\pm$ Ms $\pm$ Chl
11)	Ad + Bt + Crd + Hc $\pm$ Kfs	$\pm$ Ms $\pm$ Chl
12)	Ad + Crn + Sill / Fib + Bi + Crd + Kfs	$\pm$ Ms $\pm$ Chl
13)	Sill / Fib + Bt + Crd + Opx + Kfs	$\pm$ Ms $\pm$ Chl
14)	Sill / Fib + Crd + Opx + Kfs	$\pm$ Ms $\pm$ Chl

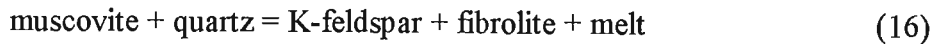


### *Andalusite*

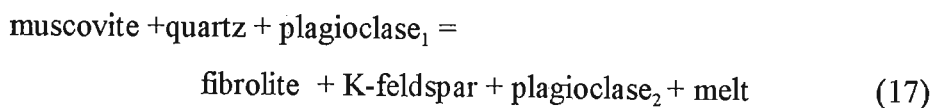
Andalusite occurs throughout the lower migmatite zone, and is particularly prevalent within the fold structures. In the Mathabatha domain, andalusite as both chistolite and xenoblastic poikilitic crystals is found mainly within the lower part of the migmatite zone in the Lydenburg Member of the Silverton Shale Formation. Crystal sizes in general are still smaller than in the underlying fibrolite zone and seldom exceed 3 mm in diameter. At higher grades, such as found within the fold structures, andalusite may be completely pseudomorphed by an intergrowth of hercynitic spinel, cordierite and plagioclase. This is discussed in more detail below. Remnants of andalusite also form part of assemblage (12). Here andalusite is in places partially replaced by corundum, fibrolite and plagioclase.

### *K-feldspar*

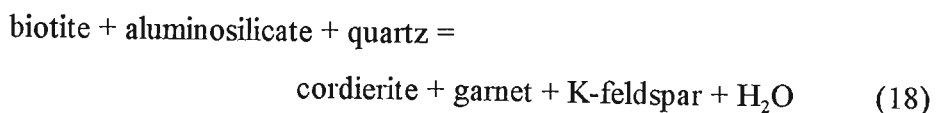
The growth of K-feldspar in the K-feldspar + fibrolite zone in the presence of a leucosome suggests that dehydration melting occurred by the following reaction:



The appearance of K-feldspar plus plagioclase leucosomes suggests that this reaction is also accompanied by the continuous reaction:

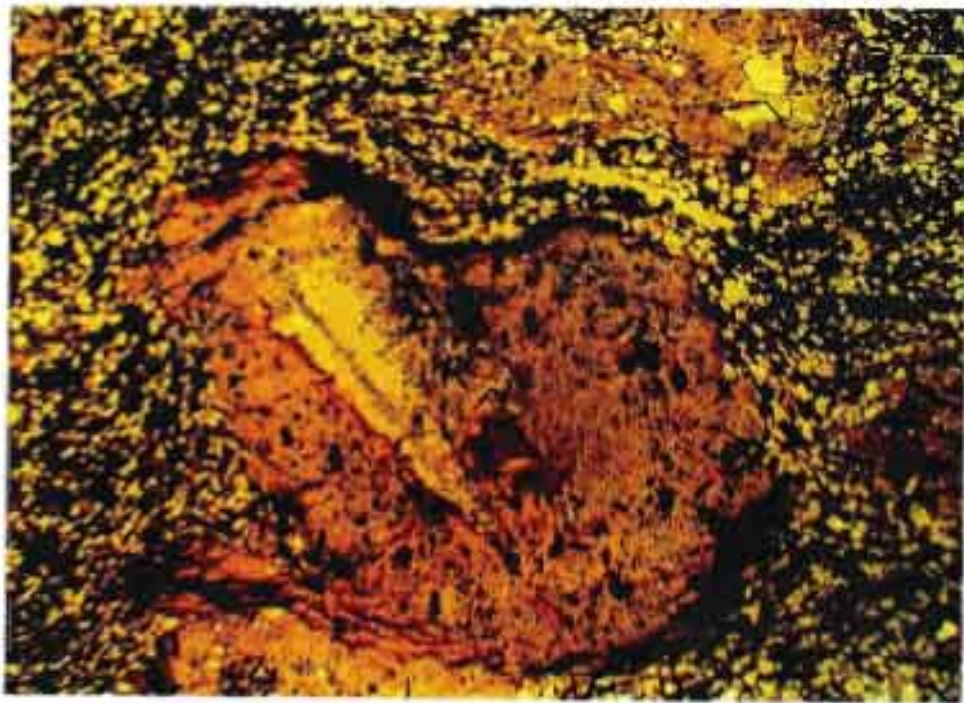


Although no textural evidence was found to indicate the development of the widespread occurrence in the migmatite zone of the characteristic assemblage cordierite + K-feldspar + biotite ± garnet ± aluminosilicate, the most probable reaction is a dehydration reaction such as:



### *Cordierite*

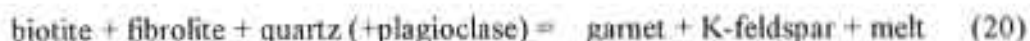
Cordierite is common throughout the pelites of the migmatite zone except in the zone near the onset of melting. Porphyroblasts generally range in size between 1 mm and 5 mm and are almost always anhedral and poikilitic with numerous inclusions mostly of biotite and quartz. In some cases cordierite porphyroblasts may have a pseudo hexagonal outline displaying sector zonation. If present, andalusite porphyroblasts may also be partly or completely included and partially replaced by large cordierite crystals (Figure 6.20). Andalusite replacement by cordierite is usually also accompanied by varying amounts of hercynite. The probable cordierite producing reaction involving melting and andalusite is:



**Figure 6.20** Pinitized cordierite porphyroblast overgrowing and replacing a chistolite crystal. Sample PHOS 1023 B1 from the migmatite zone in the Zaaikloof Fold on the farm Zaaikloof. Plane polarised light. Width of view = 6 mm.

### *Garnet*

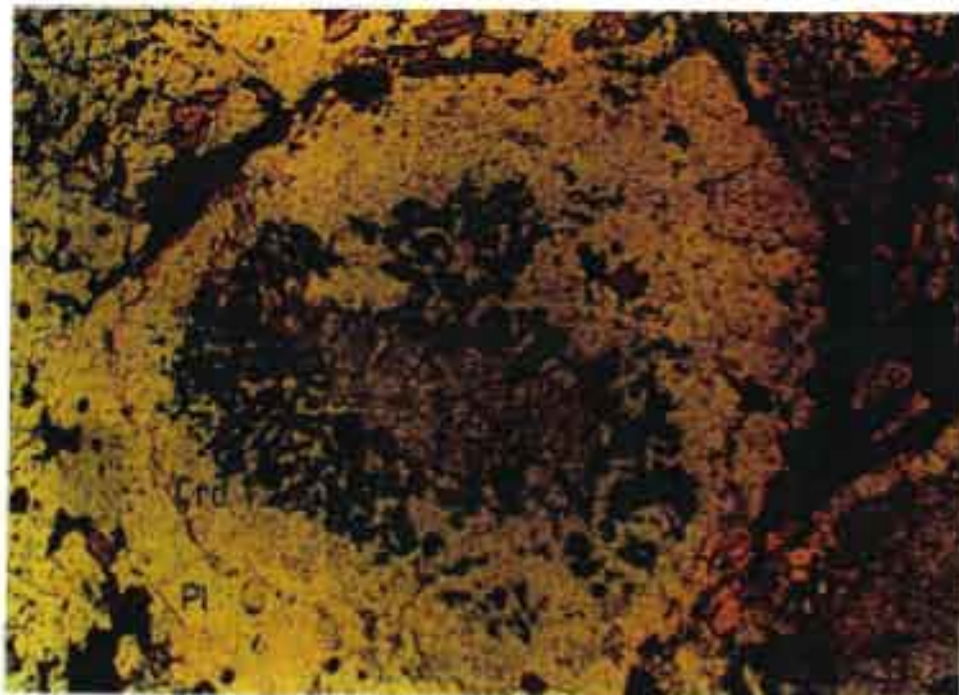
As in the andalusite zone, garnets are usually 1-2 mm in diameter. They form the stable assemblage garnet + cordierite + K-feldspar. The presence of leucocratic segregations within these rocks suggests the reaction:



Compared to the garnets of the andalusite zone, these garnets are generally poorly zoned and do not show any evidence of textural zoning as is often the case in the andalusite zone.

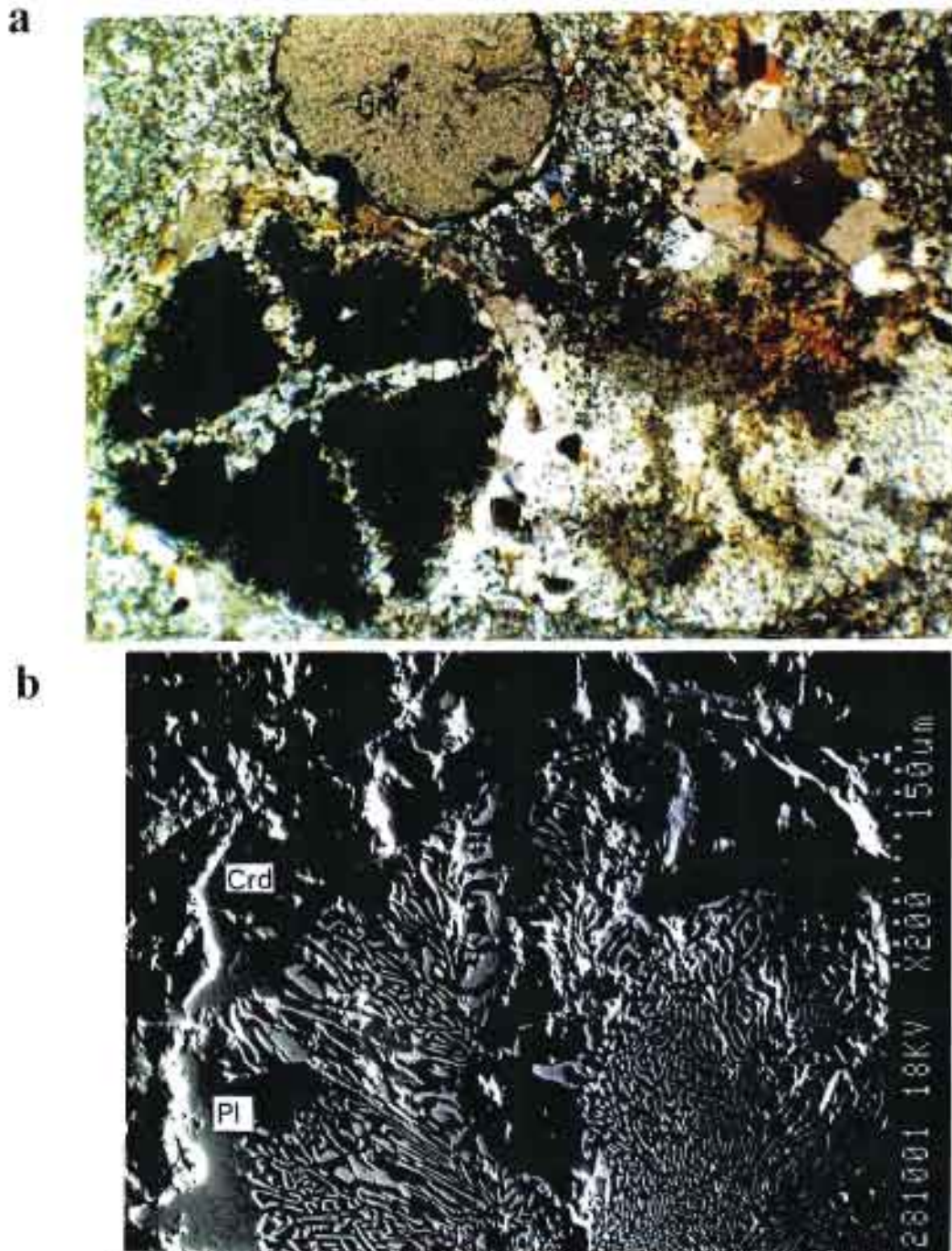
### *Spinel*

A symplectic replacement of andalusite by either hercynitic spinel and cordierite or hercynitic spinel and plagioclase is common in the pelitic cores of the Zaaikloof-Prankoppies, Katkloof and Phepane structures. In many cases no andalusite remains but an outline of the chialstolite cross is still preserved. The most common type is an intergrowth of hercynite with cordierite that is replacing andalusite (Figure 6.21). This is always accompanied by a rim of granular plagioclase.



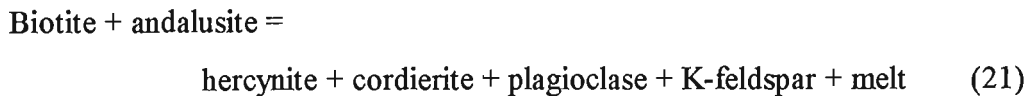
**Figure 6.21** Replacement of andalusite by a symplectic intergrowth of cordierite and hercynite. This is surrounded by a clear rim of plagioclase. Sample PAR 3 from the core of the Phepane structure, Silverton Shale Formation. Plane polarised light. Width of view = 3 mm.

Where an intergrowth of hercynite and plagioclase replace andalusite, a rim of cordierite is always present (Figure 6.22).



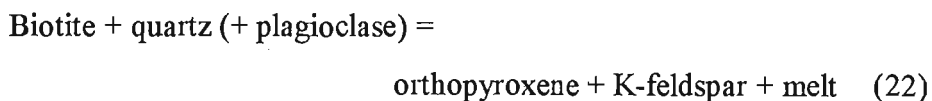
**Figure 6.22** Pseudomorphism of chiastolite by an intergrowth of hercynite and plagioclase with a rim of cordierite. Sample PHOS 1023 C. Zaaikloof Fold core, Lydenburg Shale Member of the Silverton Shale Formation. a) Microphotograph in plane polarised light. Width of view = 2.5 mm. b) SEM back-scattered image of the same sample showing the details of the intergrowth and the plagioclase rim.

These textures have now also been recognised in the Marble Hall Fragment (P. Pitra pers. comm., 1998). The intergrowth is often also surrounded by a biotite-poor halo suggesting that biotite is also consumed in the reaction. Quartz may be present in the groundmass but is shielded from the spinel by either the plagioclase or cordierite rim. The following reaction is suggested:



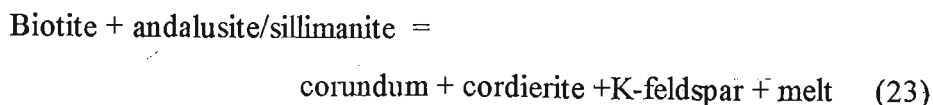
### *Orthopyroxene*

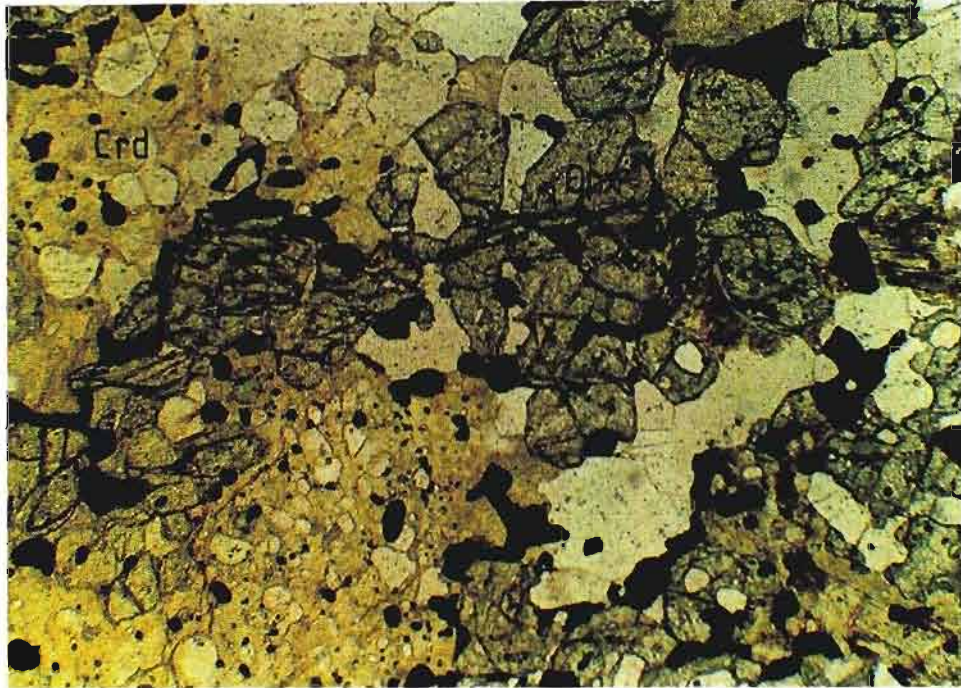
Orthopyroxene (hypersthene) assemblages are found at the immediate contact with the Rustenburg Layered Suite (Figure 6.23, 6.24). These rocks are generally poorly exposed and were found at only a few isolated localities. These include exposures on the northeastern limb of the Phepane Fold structure, the northern margin of the Pramkoppies domain, the nose of the Katkloof Fold, and in the Haakdoendraai exposure. A sample was also collected from a small pelitic xenolith on the farm Driekop. These assemblages are all characterised by the absence of quartz and are often biotite free. Dehydration melting of biotite is generally responsible for the production of orthopyroxene by the reaction:



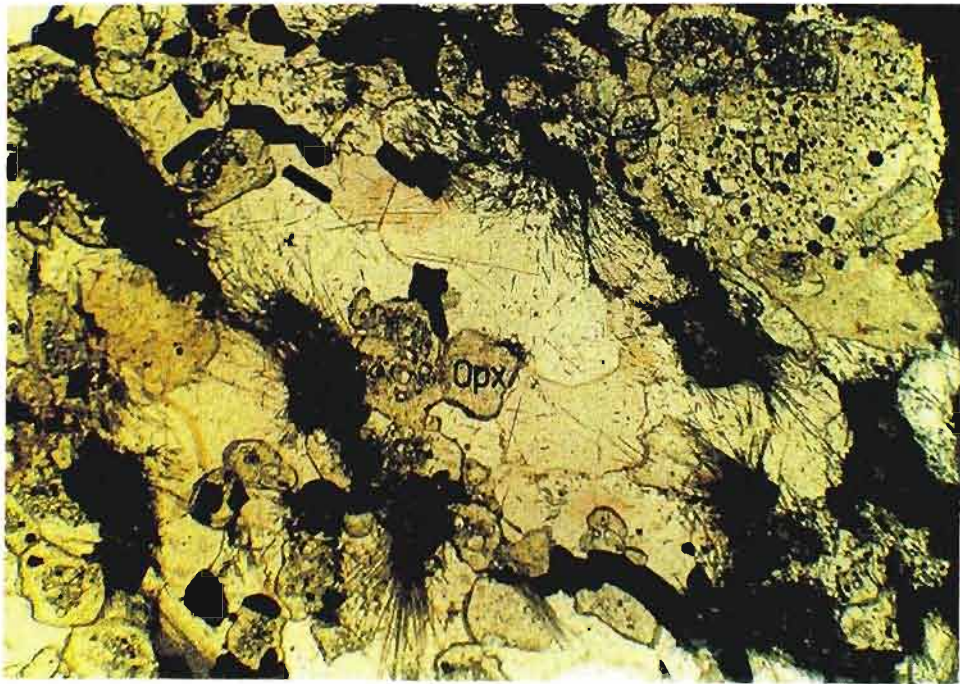
### *Corundum*

Corundum-bearing pelites were found in the Vermont Hornfels Formation on the northeastern limb of the Phepane structure. Corundum occurs as small subhedral crystals, often with a hexagonal outline (Figure 6.25). The crystals are closely associated with cordierite, sillimanite or fibrolite. In these same rocks, corundum is also seen replacing andalusite together with fibrolite and plagioclase in assemblage (12) (Figure 6.26). This texture suggests a reaction similar to the dehydration melting involving hercynite (reaction 21):

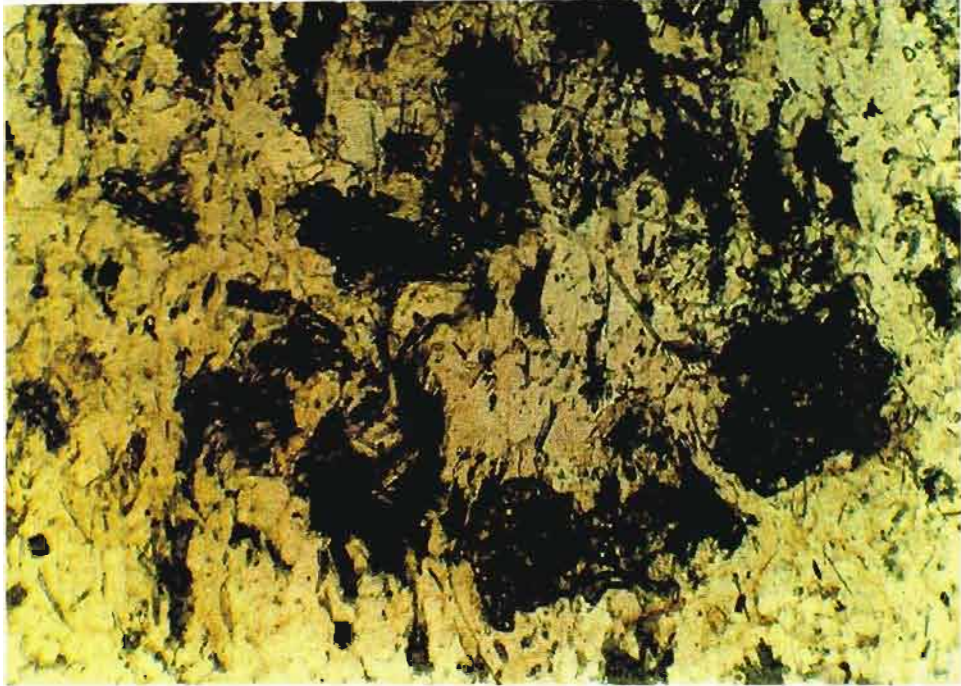




**Figure 6.23** Orthopyroxene + cordierite + K-feldspar + plagioclase assemblage. Cordierite is pinitized and K-feldspar altered. Opaque mineral is magnetite. Sample MASET 2 collected from the northern margin of the Prankoppies domain. Plane polarised light. Width of view = 2 mm.



**Figure 6.24** Orthopyroxene + cordierite + fibrolite + K-feldspar + plagioclase assemblage. Cordierite forms large pinitized grain in the top right. Opaque phase is magnetite. Sample KRG from the Katkloof Fold nose, Silverton Shale Formation on the farm Tigerpoort. Plane polarised light. Width of View = 2 mm.



**Figure 6.25** High relief corundum crystals associated with sillimanite in an assemblage of corundum + sillimanite + cordierite + plagioclase. Sample PAR 1128 from the northeastern limb of the Phepane structure on the farm Paradys. Plane polarised light. Width of view = 2 mm.



**Figure 6.26** Detail of corundum and fibrolite replacing large grain of andalusite. Clear groundmass is plagioclase. Note also the presence of biotite. Sample PAR 1123 from the northeastern limb of the Phepane structure on the farm Paradys. Plane polarised light. Width of view = 0.8 mm.

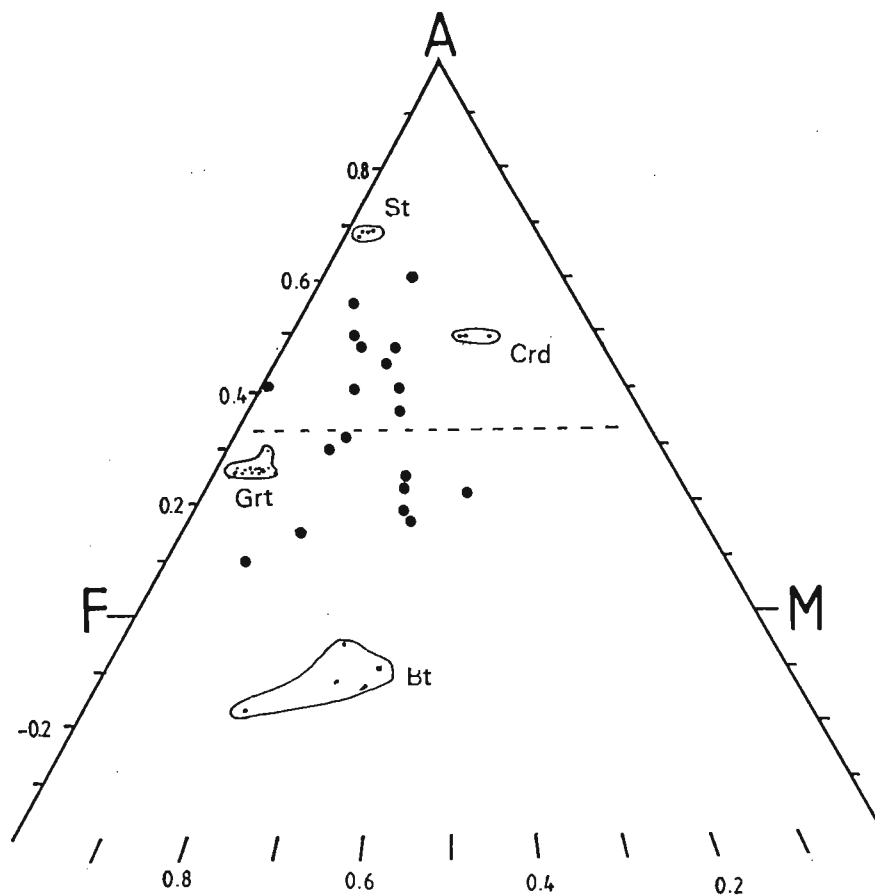
## 6.5 PELITE COMPOSITION

Samples selected for bulk rock analysis were taken from the lower and upper pelitic units of the Timeball Hill Formation, and the Silverton Shale Formation in the Mathabatha domain. The mineralogy of these samples is shown in Appendix 2. Major element microprobe analyses of minerals used for temperature and pressure calculations are presented in Appendix 3. The chemistry of minerals is briefly outlined below.

All samples contain excess quartz. Muscovite is present as either sericite in the groundmass or as larger retrograde grains in all samples except sample B/1. Pelite compositions are generally high in  $\text{Al}_2\text{O}_3$  and FeO. Most samples contain negligible CaO except for samples 16/7, 3/4 and 26/9A which contain up to 1.5% CaO. MnO is low with molar ratios against  $\text{MgO} + \text{FeO} + \text{MnO}$  being  $< 0.02$ . The average  $X_{\text{Fe}} = 0.7$ , with a considerable range between 0.45 and 1.0 (Appendix 3). The pelite compositions can be subdivided into three groups based on the alumina content when compared to the average shale of Shaw (1956), an aluminous intermediate and a sub-aluminous group. The aluminous compositions have  $A'$  values above the chlorite join ( $A' = 0.2 - 0.3$ ) when compared to the average shale ( $A' = 0.326$ ) on the Thompson (1957) AFM projection. The intermediate group has  $A'$  values that approximate the AFM chlorite field and the sub-aluminous group plots below the AFM chlorite field with  $A'$  values as low as 0.1 (sample AQ/X).

As a first approximation, the pelitic rock compositions can be represented by the component model system  $\text{K}_2\text{O}-\text{FeO}-\text{MgO}-\text{Al}_2\text{O}_3-\text{SiO}_2-\text{H}_2\text{O}$  (KFMASH) with rocks dominated by assemblages in which quartz and muscovite are in excess and  $\text{H}_2\text{O}$  is considered to have been in excess. These assemblages are therefore representable on the AFM muscovite projection diagram of Thompson (1957) (Figure 6.27), except for sample B/1 which is muscovite absent. This assemblage is more accurately modelled against the system  $\text{FeO}-\text{MgO}-\text{Al}_2\text{O}_3-\text{SiO}_2-\text{H}_2\text{O}$  (FMASH). The more recent development of calculated petrogenetic grids using internally consistent thermodynamic data sets (Spear and Cheney, 1989; Powell and Holland, 1990; Wang and Spear, 1991; Dymoke and Sandiford, 1992; Xu *et al.*, 1994; Mahar *et al.*, 1997) has provided a means of predicting reaction sequences as well as the effects of additional components to the model KFMASH system.





**Figure 6.27** Thompson (1957) AFM projection of whole rock compositions for pelites from the Pretoria Group.  $A' = 0.326$  for an average shale (Shaw 1956) is shown as a dotted line which corresponds approximately to the chlorite join.

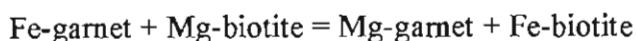
Mineral analysis used for geothermometry and geobarometry (Appendix 3) are also plotted on the AFM projection (Figure 6.27). Biotite compositions have  $X_{Fe}$  ranging between 0.59 and 0.78 with individual grains within a sample being homogeneous in composition. Staurolite has  $X_{Fe}$  ranging between 0.92 and 0.83. Staurolite crystals are sector zoned with slightly higher Mg in the cores compared to rim compositions. ZnO was found to be low, ranging between 0.17 and 0.39 percent. Garnet crystals are all normally zoned with high MnO cores compared to rim compositions. Core MnO compositions range between 3.99 and 0.92 percent and rim compositions range between 2.06 and 0.19 percent.  $X_{Mg}$  values from core to rim for all garnets analysed show both an increase and a decrease from core to rim. CaO generally decreases from core to rim. Cordierite grains analysed were found to be homogeneous with  $X_{Fe}$  values ranging between 0.35 and 0.45. The general sequence of  $X_{Fe}$  values for these minerals is  $Grt > St > Bt > Crd$ .

## 6.6 THERMOBAROMETRY

Metamorphic pressures were determined using garnet-cordierite and garnet-staurolite equilibria from the andalusite zone in the lower pelitic unit of the Timeball Hill Formation. Rim and core compositions of grains in contact were analysed to determine growth and temperature relationships, constraining temperatures for the peak of metamorphism and for the closure of exchange reactions. It is assumed that the garnet rim, but not necessarily the garnet core is in chemical equilibrium with the adjacent biotite or cordierite grain (Hollister, 1966). Garnet cores should give the temperatures realised at the onset of metamorphic crystallisation of the mineral pair if no later homogenisation of the garnet has taken place and if the compositions of the coexisting minerals remained constant.

### 6.6.1 The garnet - biotite geothermometer

Garnet and biotite are commonly associated in pelitic rocks with a wide range of metamorphic conditions, proving a very useful geothermometer in most metamorphic terrains. The thermometer is based on the exchange reaction:



The cation exchange reaction has been calibrated empirically as a geothermometer by Thompson (1976) and Holdaway and Lee (1977) by determining the linear relationship between  $\ln K_D^{\text{gt-bi}}$  to reciprocal temperature based largely on comparisons of natural assemblages with experimental phase equilibria. The Ferry and Spear (1978) calibration is experimentally derived and is based on experiments in the purely binary Fe-Mg system using synthetic annite-phlogopite micas and almandine-pyrope garnets between 550°C and 800°C at 2.07 kb pressure. Field application of the Ferry and Spear calibration can be hampered by significant deviations from the idealised binary system (Ferry and Spear, 1978). The Thompson (1976) and the Holdaway and Lee (1977) calibrations probably minimise compositional effects since they are based on natural assemblages (Hodges and Spear, 1982).

Ferry and Spear (1978) estimate the precision of their calibration to be  $\pm 50^\circ\text{C}$  for the geothermometer which corresponds to the error in temperature that results when  $\pm 0.001$  error in  $X_{\text{annite}}$ ,  $X_{\text{phlogopite}}$ ,  $X_{\text{almandine}}$  and  $X_{\text{pyrope}}$  are propagated through the various equations. The

above only applies to rocks containing garnet and biotite that are close to the binary Fe-Mg compounds since  $K_D$  is also a function of the Ca and Mn content of the garnet and the Ti and  $Al^{VI}$  content of the biotite (Dallmeyer, 1974; Saxena, 1969).

Certain compositional limits have been suggested for other components for reliable results for the application of the geothermometer without correction (Ferry and Spear, 1978):

$$(Ca + Mn) / (Ca + Mn + Fe + Mg) \text{ up to } 0.2\text{-garnet}$$
$$(Al^{VI} + Ti) / (Al^{VI} + Ti + Fe + Mg) \text{ up to } 0.15\text{-biotite}$$

Caution should therefore be taken if applying the data to systems containing significant amounts of Ca, Mn and Ti. The three calibrations (Thompson, 1976; Holdaway and Lee, 1977; Ferry and Spear, 1978) used here to calculate temperatures all assume ideal mixing in the garnet and biotite solid solutions, although the Fe-Mg solid solution is probably non-ideal. Müller (1972) however, suggested that the Fe-Mg solid solution in biotite is nearly ideal although this has been questioned by other workers such as Wones and Eugester (1965) and Dallmeyer (1974). Biotite non-ideality increases where Ti is a major biotite component (Hodges and Spear, 1982). Non-ideality in garnet increases with increasing grossularite and spessartine components (Ganguly and Kennedy, 1974). As the garnets from the study area are relatively low in Ca and Mn, it is believed that no serious errors in the temperature calculations will arise from omitting activity coefficients which are included in more recent calibrations. Another problem may be the effect of  $Fe^{3+}$  in biotite which cannot be determined with the electron microprobe. Many workers use total iron for  $Fe^{3+}$  in biotite which can significantly lower the temperature estimate. This becomes a problem at higher metamorphic grades (upper amphibolite to granulite facies) where biotites are increasingly rich in Ti, F and Cl (Bohlen and Essene, 1980).

The three calibrations each produce a surface whose position in P-T- $\ln K_D$  space is slightly different resulting in different estimates of T. The temperatures calculated according to the calibrations of Holdaway and Lee (1977), are consistently higher than those of Thompson (1976) (Table 6.4).

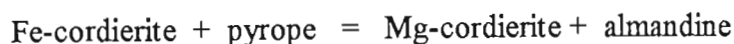
**Table 6.4** Metamorphic temperatures calculated from garnet-biotite geothermometers of Thompson (1976), Holdaway and Lee (1977) and Ferry and Spear (1978). Samples from the Mathabatha domain, Andalusite zone, lower pelitic unit of the Timeball Hill Formation. Microprobe analyses are presented in Appendix 3.

Sample	OB5	AQ/X	M/1	HWU	16/7
Grt <sub>core</sub> X <sub>mg</sub>	0.0711	0.0418	0.0619	0.1041	0.0970
Grt <sub>rim</sub> X <sub>mg</sub>	0.0798	0.0411	0.0690	0.1007	0.0997
Bi X <sub>mg</sub>	0.3430	0.2194	0.3493	0.4087	0.3874
K <sub>D core</sub>	0.1467	0.1552	0.1229	0.1681	0.1699
K <sub>D rim</sub>	0.1662	0.1525	0.1381	0.1620	0.1751
<b>Thompson (1976)</b>					
T <sub>core</sub> (°C)	514	527	476	546	549
T <sub>rim</sub> (°C)	544	523	501	538	556
<b>Holdaway and Lee (1977)</b>					
<b>2 kbar</b>					
T <sub>core</sub> (°C)	528	539	493	557	528
T <sub>rim</sub> (°C)	554	537	515	548	554
<b>3 kbar</b>					
T <sub>core</sub> (°C)	531	548	496	560	531
T <sub>rim</sub> (°C)	552	540	518	552	557
<b>4 kbar</b>					
T <sub>core</sub> (°C)	534	546	499	563	534
T <sub>rim</sub> (°C)	561	543	522	555	561
<b>Ferry and Spear (1978)</b>					
<b>2 kbar</b>					
T <sub>core</sub> (°C)	507	524	460	549	552
T <sub>rim</sub> (°C)	545	519	490	537	562
<b>3 kbar</b>					
T <sub>core</sub> (°C)	511	528	462	553	556
T <sub>rim</sub> (°C)	549	522	494	541	566
<b>4 kbar</b>					
T <sub>core</sub> (°C)	515	531	466	556	560
T <sub>rim</sub> (°C)	553	526	497	545	570

The major reasons for the variation in the temperatures calculated may be due to disequilibrium between garnet and biotite, analytical uncertainty, retrograde metamorphism and re-equilibration and the influence of minor elements in garnet and biotite participating in the Fe-Mg exchange reaction. Erroneous values can also result from the presence of a third Fe-Mg mineral coexisting with biotite and garnet, even temporarily could influence K<sub>D</sub>.

### 6.6.2 The garnet-cordierite geothermometer

The temperature dependence of the exchange reaction:



was determined empirically by Thompson (1976) and Perchuk (1977) and experimentally by Holdaway and Lee (1977). Wells (1979) calibrated a geothermometer based on the experimental work of Holdaway (1976), Henson (1977), Henson and Green (1971, 1973) and Currie (1971). This is a modification of the Wells (1976) thermometer. The Fe, Mg distribution between the two phases is little affected by compositional variations although the Ca content of garnet may markedly affect the stability relations (Henson and Green, 1973). Almandine low in Mn and Ca does not participate in cordierite reactions where muscovite is present (Holdaway and Lee, 1977). Garnets used are relatively low in Ca and Mn and solid solution is assumed to behave ideally.

The temperatures calculated using various calibrations of the garnet - cordierite geothermometer are listed below in Table 6.5. The temperatures calculated by the Wells (1976) calibration show substantially higher temperatures than other calibrations which were all in fairly close agreement. Differences in temperature estimates may occur due to variations in the slope and positions of the equilibria and the extent by which the H<sub>2</sub>O content in cordierite, Al in biotite and minor components - Mn, Ca, Ti and Fe<sup>3+</sup> modify the equilibria.

**Table 6.5** Metamorphic temperatures calculated from garnet-cordierite equilibria. Calibrations after Thompson (1976), Wells (1976), Holdaway and Lee (1977) and Wells (1979). Samples from the Andalusite zone, Mathabatha domain. Lower pelitic unit of the Timeball Hill Formation.

Sample	16/7	19/12	HWU
Grt <sub>core</sub> X <sub>mg</sub>	0.0970	0.1132	0.0104
Grt <sub>rim</sub> X <sub>mg</sub>	0.0967	0.1312	0.0977
Crd X <sub>mg</sub>	0.5505	0.6520	0.5677
K <sub>D core</sub>	11.4351	14.6790	11.2410
K <sub>D rim</sub>	11.4395	12.4060	12.1090
<b>Thompson (1976)</b>			
T <sub>core</sub> (°C)	545	488	548
T <sub>rim</sub> (°C)	545	525	531

**Wells (1976)**

<b>2 kbar</b>			
$T_{\text{core}}$ (°C)	615	560	619
$T_{\text{rim}}$ (°C)	615	596	602
<b>3 kbar</b>			
$T_{\text{core}}$ (°C)	611	556	615
$T_{\text{rim}}$ (°C)	611	595	598
<b>4 kbar</b>			
$T_{\text{core}}$ (°C)	607	553	611
$T_{\text{rim}}$ (°C)	607	589	594

**Holdaway and Lee (1977)**

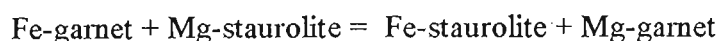
<b>2 kbar</b>			
$T_{\text{core}}$ (°C)	552	501	555
$T_{\text{rim}}$ (°C)	552	534	539
<b>3 kbar</b>			
$T_{\text{core}}$ (°C)	556	504	559
$T_{\text{rim}}$ (°C)	556	538	543
<b>4 kbar</b>			
$T_{\text{core}}$ (°C)	560	508	563
$T_{\text{rim}}$ (°C)	560	542	547

**Wells (1979)**

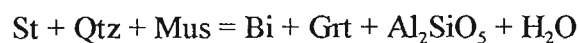
<b>2 kbar</b>			
$T_{\text{core}}$ (°C)	550	493	554
$T_{\text{rim}}$ (°C)	540	530	536
<b>3 kbar</b>			
$T_{\text{core}}$ (°C)	545	488	549
$T_{\text{rim}}$ (°C)	545	526	531
<b>4 kbar</b>			
$T_{\text{core}}$ (°C)	541	484	545
$T_{\text{rim}}$ (°C)	541	521	527

**6.6.3 The garnet-staurolite geobarometer**

This geobarometer is based on the two staurolite equilibria:



and



The first of the two equilibria depends only on temperature and mineral composition and the second on temperature, pressure and the chemical potential of  $\text{H}_2\text{O}$ . Perchuk (1977) established the relationship of  $\ln K_D$  Mg in the first equilibria to inverse temperature from known mineral compositions in biotite + garnet + staurolite paragenesis by using established isotherms for the Mg distribution between biotite and garnet. From the compositions of the associations in the

second equilibria coexisting with staurolite a relationship between  $\ln K_D$  Mg to pressure and temperature was established for the first equilibria. The results are presented below in Table 6.6.

**Table 6.6** Metamorphic pressure calculated from staurolite-garnet pairs from the Perchuk (1977) geobarometer. Samples from the Andalusite zone, Mathabatha domain, lower pelitic unit of the Timeball Hill Formation.

Sample	AQ/X	HWU	OB5	M/1
Grt <sub>core</sub> X <sub>mg</sub>	0.0408	0.0983	0.0672	0.0590
Grt <sub>rim</sub> X <sub>mg</sub>	0.0409	0.0931	0.0839	0.0679
St X <sub>mg</sub>	0.0854	0.1681	0.1384	0.0956
Ln K <sub>D core</sub>	0.7383	0.5365	0.7219	0.4826
Ln K <sub>D rim</sub>	0.7383	0.5365	0.5005	0.3420
<b>Perchuk (1977)</b>				
P <sub>core</sub> (kbar)	3.2	4.1	3.3	4.3
P <sub>rim</sub> (kbar)	3.2	3.8	4.2	4.8

## 6.7 P-T CONDITIONS AND THE KFMASH GRID

The contact aureole in the study area contains pelitic assemblages that typify the low pressure high temperature (Buchan-type) metamorphism. Reactions involving the minerals andalusite, garnet, staurolite, biotite, chlorite, muscovite, quartz and H<sub>2</sub>O can be modelled in the simplified chemical system K<sub>2</sub>O - FeO - MgO - Al<sub>2</sub>O<sub>3</sub> - SiO<sub>2</sub> - H<sub>2</sub>O (KFMASH). A variety of petrogenetic grids have been constructed for this system (Pattison and Harte, 1985; Spear and Cheney, 1989; Powel and Holland, 1990; Dymoke and Sandiford, 1992; Xu et al., 1994). Petrogenetic grids such as these have proven useful in determining mineral changes along the metamorphic reaction path.

### 6.7.1 Andalusite zone

Within the andalusite zone of the Timeball Hill Formation, the assemblages andalusite-staurolite are characteristic. This system was analysed in detail by (Dymoke and Sandiford, 1992) for similar rocks in the Mount Lofty region of Australia. They developed a petrogenetic grid, P-T and T- X<sub>Fe</sub> sections for these rocks using the internally consistent data set of Holland and Powel (1990) in the system KFMASH and assuming a(H<sub>2</sub>O) ~ 1. The grids and pseudosections are

calculated for the assemblage chlorite, aluminosilicate, staurolite, cordierite and/or garnet with biotite+muscovite +quartz +H<sub>2</sub>O in excess.

The quantitative estimates of temperature and pressure conditions (Figure 6.28) for the andalusite zone in the lower pelitic unit of the Timeball Hill Formation are generally slightly lower than the temperature conditions predicted by the grid. This is indicated by the important assemblage cordierite + staurolite (+biotite + muscovite + quartz + H<sub>2</sub>O in the calculated P-T grid of Dymoke and Sandiford (1992) (Figure 6.29). The assemblage is restricted to a very small triangular field to pressures between 2.8 kb and 3.2 kb and temperatures between 535 °C and 563 °C. In the absence of cordierite, staurolite is shown to exist only above approximately 3.5 kb. The stability of staurolite below about 3 kb has also not been observed in natural pelitic systems (Pattison and Tracy, 1991). This is the only part of the Bushveld Complex contact aureole where staurolite is found (Figure 6.1) and can be classified as the Pattison and Tracy, (1991) facies type 2b, hence the interpretation of a greater depth of metamorphism compared to other parts of the contact aureole (Chapter 2).

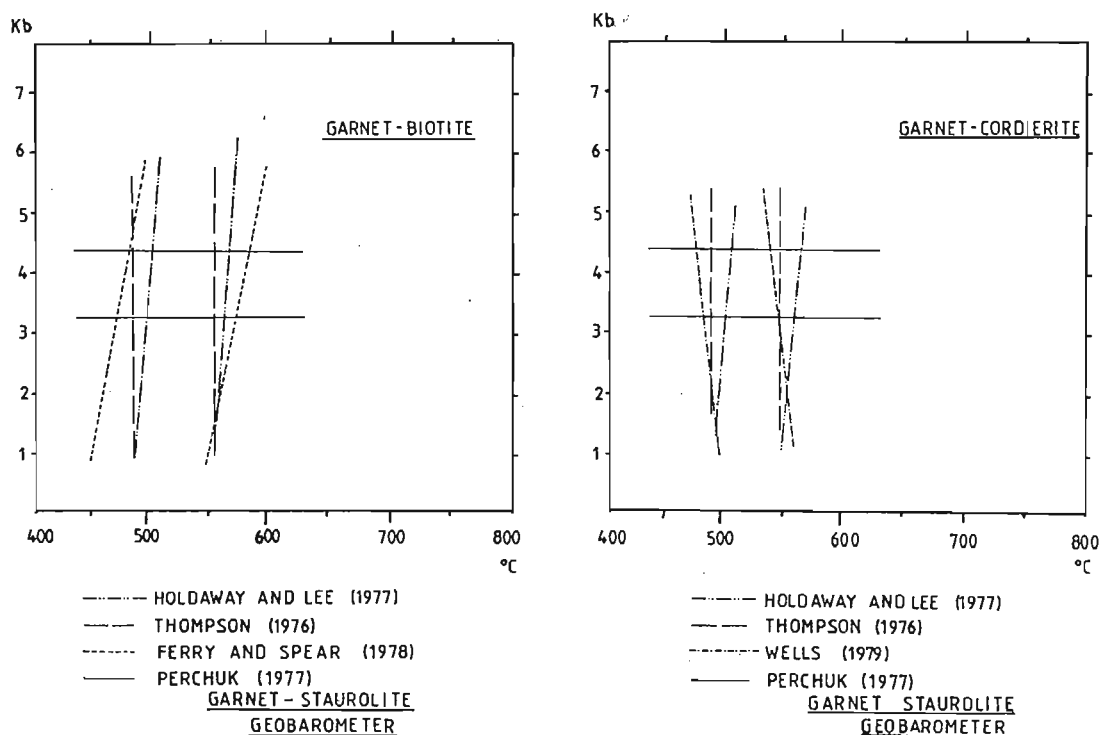
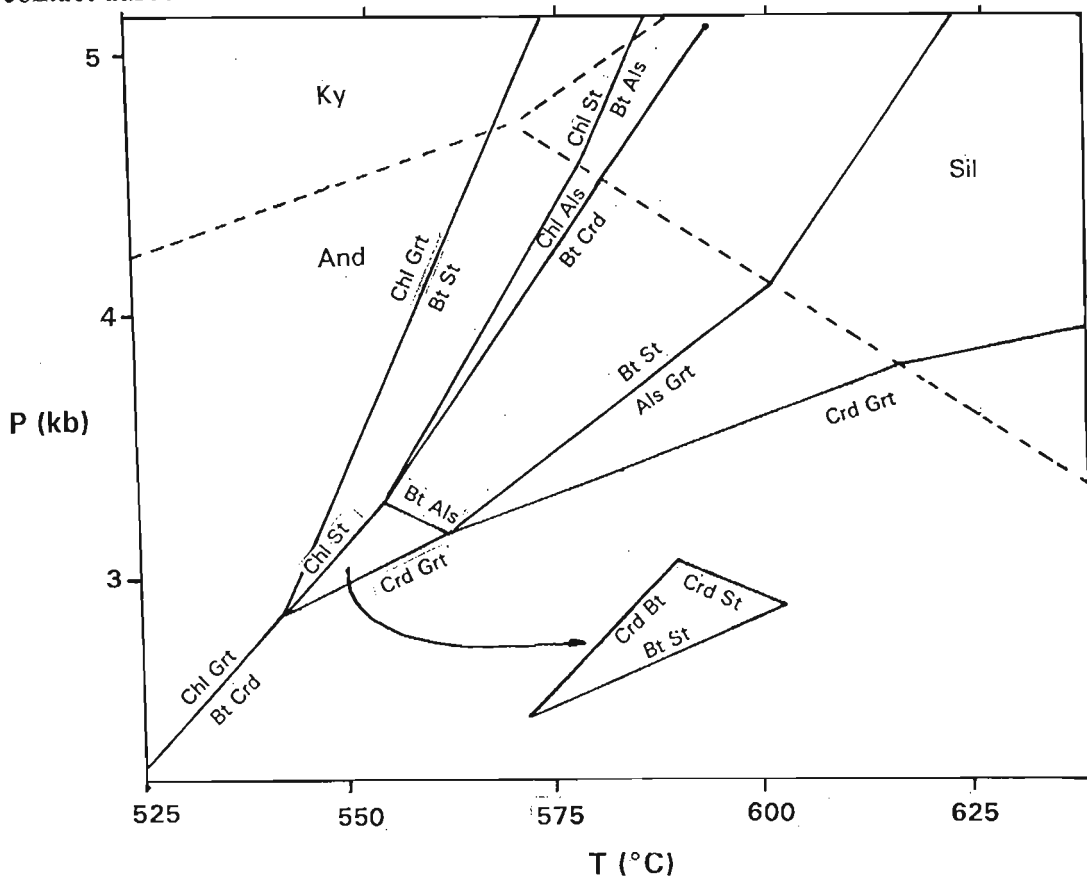


Figure 6.28 Plotted calculated pressure and temperature fields for the andalusite zone in the lower pelitic unit of the Timeball Hill Formation, Mathabatha domain.

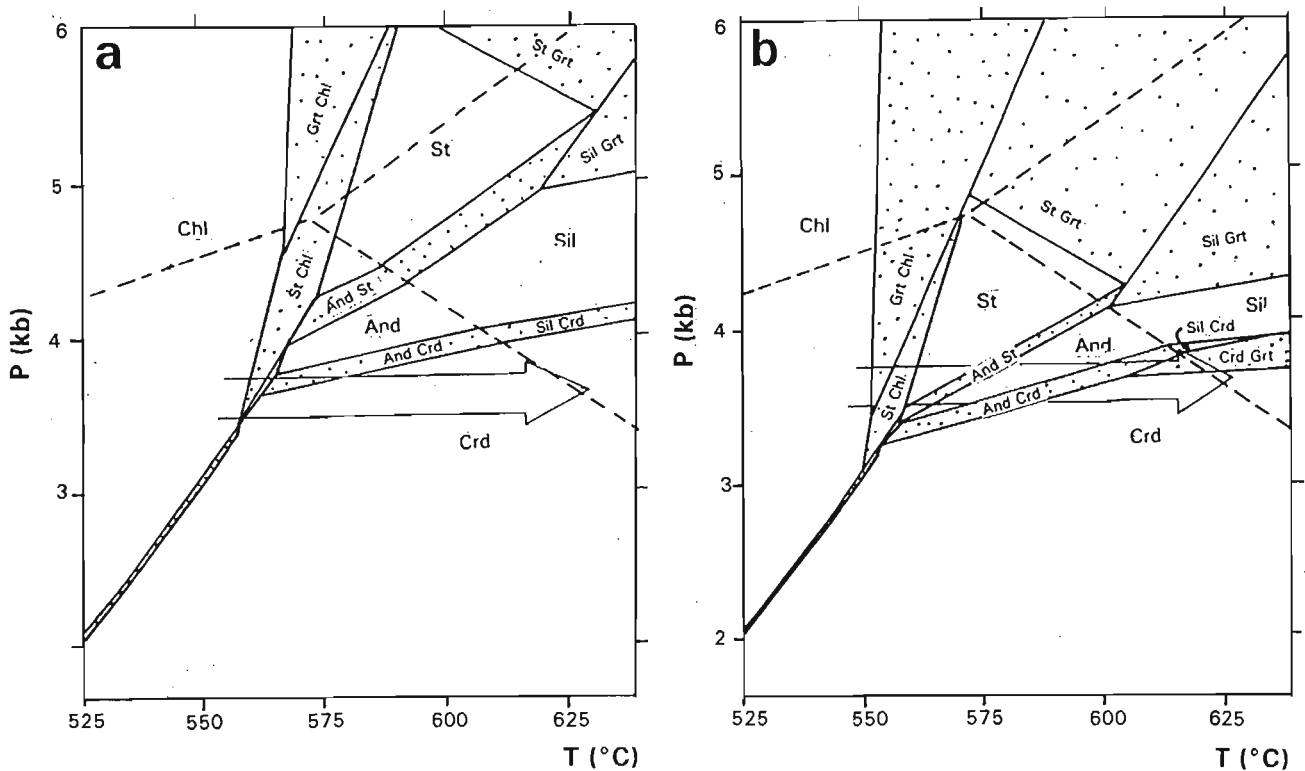


A combination of the grid and the calculated temperature and pressure results constrain the temperature in this part of the contact aureole to approximately 550 °C. This is an important horizon in the contact aureole, coinciding approximately with the decollement zone for the periclinal structures and marks the transition from the essentially poorly deformed zone of the contact aureole to the deformed zone.



**Figure 6.29** The Dymoke and Sandiford (1992) calculated P-T grid for reactions for the phases staurolite + cordierite + garnet + chlorite + andalusite + sillimanite + kyanite (biotite + muscovite + quartz + H<sub>2</sub>O in excess).

Calculated P-T pseudo-sections for compositions  $X_{Fe} = 0.7$  and  $X_{Fe} = 0.8$  by Dymoke and Sandiford (1992) (Figure 6.30), are useful to provide a qualitative interpretation on the zonal sequence recognised in the aureole and the P-T path for the rocks. The reaction sequence in the andalusite zone is compatible with an isobaric prograde reaction path at a pressure between 3 kb and 4 kb on the grid of Dymoke and Sandiford (1992) (Figure 6.30). Important reaction textures showing this are the occurrence of andalusite either overgrown by or partially replaced by cordierite in low  $X_{Fe}$  bulk compositions. These textures would suggest that the P-T path for the Mathabatha domain is isobaric or has a negative slope in P-T space.



**Figure 6.30** The Dymoke and Sandiford (1992) pseudo-sections for  $X_{Fe} = 0.7$  and  $X_{Fe} = 0.8$  bulk-rock compositions. The observed sequence of staurolite before andalusite and cordierite replacing andalusite is consistent with an isobaric or a negative P-T path slope in the andalusite zone of the Mathabatha domain.

### 6.7.2 Migmatite zone

No calculated thermobarometry results are made for the migmatite zone. Migmatites in pelites are produced by two main types of reactions hydrous melting and vapour absent reactions. Hydrous melting may occur at temperatures as low as 670 °C at 2 kb pressure (Tuttle and Bowen, 1958). Vapour-absent melting occurs at higher temperatures and is fluxed by H<sub>2</sub>O released by biotite decomposition. Petrogenetic grids based on experimental data and theoretical models indicate that vapour-absent melting is initiated at temperatures around 700 °C at low pressures. The KFMASH grid of Pattison and Harte (1991) (Figure 6.31) indicates that the assemblages of the migmatite zone are compatible with pressure conditions that stabilised garnet in quartz-bearing assemblages. Preliminary THERMOCALC results have suggest that the pseudomorphism of andalusite by hercynitic spinel and cordierite occurs at low pressures, below 2 kb at temperatures in the order of 700 °C (P. Pitra pers. comm., 1998).

Other than this, no metamorphic evidence has been found to suggest any decompression during the growth of the floor domes. Metamorphic assemblages relate broadly to an isobaric P-T path as indicated on Pattison and Harte (1991) KFMASH grid for high grade reactions (Figure 6.31).

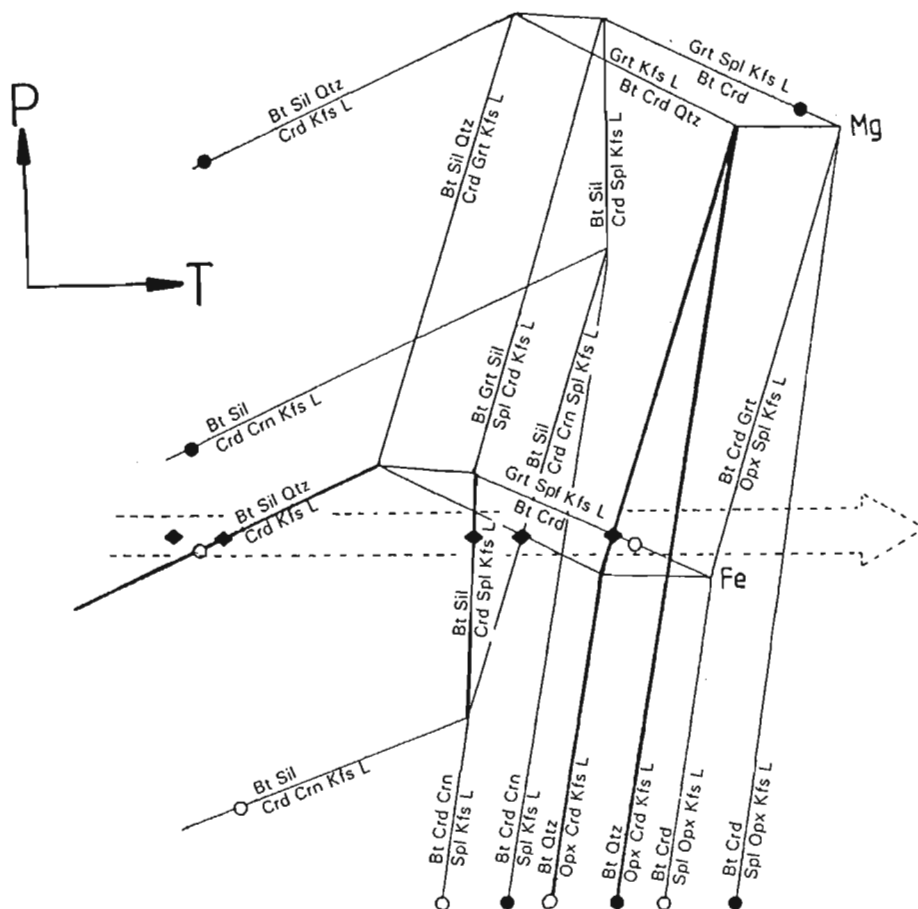


Figure 6.31 The schematic KFMASH petrogenetic grid of Pattison and Harte (1991) for the high grade portion of contact aureoles involving cordierite. The assemblages developed in the migmatite zone (◆) from the study area are compatible with an isobaric P-T path as shown. Fe-rich (○) and Mg-rich (●) bounding end-member curves are represented.

## 6.8 DISCUSSION AND CONCLUSIONS

As indicated in the introduction to this chapter, the essentially sill-shaped intrusion of the Rustenburg Layered Suite has produced a contact aureole in which the highest grades would have equilibrated under the lowest pressures and the lowest grades under highest pressures. The rate of magma intrusion relative to heating is critical in establishing a P-T path for the contact aureole. An intrusion rate that is slow, comparable to the heating rate, would produce an anticlockwise PT path in the floor if deformation is negligible. It has however, recently been

realised that Bushveld Complex magmatism was a relatively fast, plume related event, (Hatton and Schweitzer, 1995; Schweitzer and Hatton, 1997) and that the Rustenburg Layered Suite was emplaced rapidly (Cawthorn and Walraven, 1997). These aspects are further discussed in more detail in Chapter 7. Fast emplacement relative to deformation and metamorphism implies that loading on the Pretoria Group floor was almost instantaneous in terms of the metamorphic P-T path and if no deformation occurs during metamorphism then a simple isobaric prograde and retrograde P-T path can be expected for the aureole.

These conditions would correspond approximately to a load thickness (Rustenburg Layered Suite and volcanic roof rocks) of between 9 and 12 km at the contact and between 12 and 15 km at the base of the Pretoria Group. Assuming that lithostatic pressure approximates the total confining pressure, this would correspond to a pressure of between 2.4 kb and 3.1 kb at the contact and a maximum of between 3.1 kb and 3.9 kb at the base of the Pretoria Group in the study area. These lithostratigraphic controls suggest that the original high P estimates published in Sharpe and Chadwick (1981) are exaggerated. Much lower results were obtained more recently by Kaneko and Miyano (1990) in the Penge area of between  $2.1 \pm 0.4$  kb at 5.4 km and  $2.4 \pm 0.9$  kb at 8.9 km distance from the contact with the Bushveld Complex. These values suggest that stratigraphic overburden thickness at the contact may have been as little as 6 km. As discussed above, the ubiquitous presence of staurolite in this region is more compatible with pressures of above 3 kb and for this reason the Kaneko and Miyano (1990) results may be on the low side.

The presence of syn-Bushveld Complex extensional deformation (maximum stress was vertical), suggests that the metamorphic P-T path may be more complex and not simply isobaric. If the domes existed prior to the emplacement of the Rustenburg Layered Suite, as suggested by Hartzer (1995), then metamorphic assemblages in the highest portions of the domes should record an isobaric P-T path of lower pressure than the interpericlinal areas. Isobaric paths could however, also result if the regional subsidence, due to magma additions occurs at the same rate as the growth or uplift rate of the domes, representing a closely balanced isostatic situation.

Evidence outlined in Chapters 4 and 5 however, show firstly that the domes grew during

metamorphism and were not present before emplacement of the Rustenburg Layered Suite. Secondly, rapid intrusion rates followed by a longer period of heating and deformation would result in non-isobaric P-T paths particularly if intrusion rates are an order of magnitude faster than heating and deformation. In a purely isostatic situation local subsidence of the Rustenburg Layered Suite with isostatic uplift in the periclinal would produce a situation where the interpericlinal areas should record an anticlockwise PT path and the periclinal a clockwise PT path.

The isobaric or possible decompression paths indicated on the Dymoke and Sandiford (1992) grid for the andalusite zone in the interpericlinal Mathabatha domain, are not the compression paths as expected for the interpericlinal domains. This suggests that the northern margin of the Bushveld Complex also underwent uplift associated with tilting immediately after Rustenburg Layered Suite emplacement. This uplift is considered to have given rise to the Chuniespoort dome or arch to the north of the study area. This has important implications for the origin of the other large basement domes surrounding the Bushveld Complex and these probably formed in response to Bushveld Complex subsidence and extension.

Regional crustal extension during the emplacement of the Bushveld Complex has recently been advocated by Gibson and Stevens (1998) to explain the P-T path in the Vredefort Dome. They propose that impingement of a mantle plume beneath the Kaapvaal Craton resulted in heterogeneous thinning of the crust along thin spots. Thermal weakening of the crust then led to further thinning to accommodate magmatic over-thickening. One of the most obvious weaknesses in the Kaapvaal Craton would have been the Thabazimbi-Murchison-Lineament, forming the northern margin of the eastern Bushveld Complex. Extension was focussed along this zone producing the extensional fabrics in the contact aureole and the Chuniespoort arch to the north.

Unfortunately, the results from this metamorphic study are not conclusive and more detailed metamorphic studies would be necessary to place more rigorous constraints on the metamorphic P-T path from various parts of the Bushveld Complex contact aureole.

# CHAPTER 7

## TECTONOMETAMORPHIC MODEL

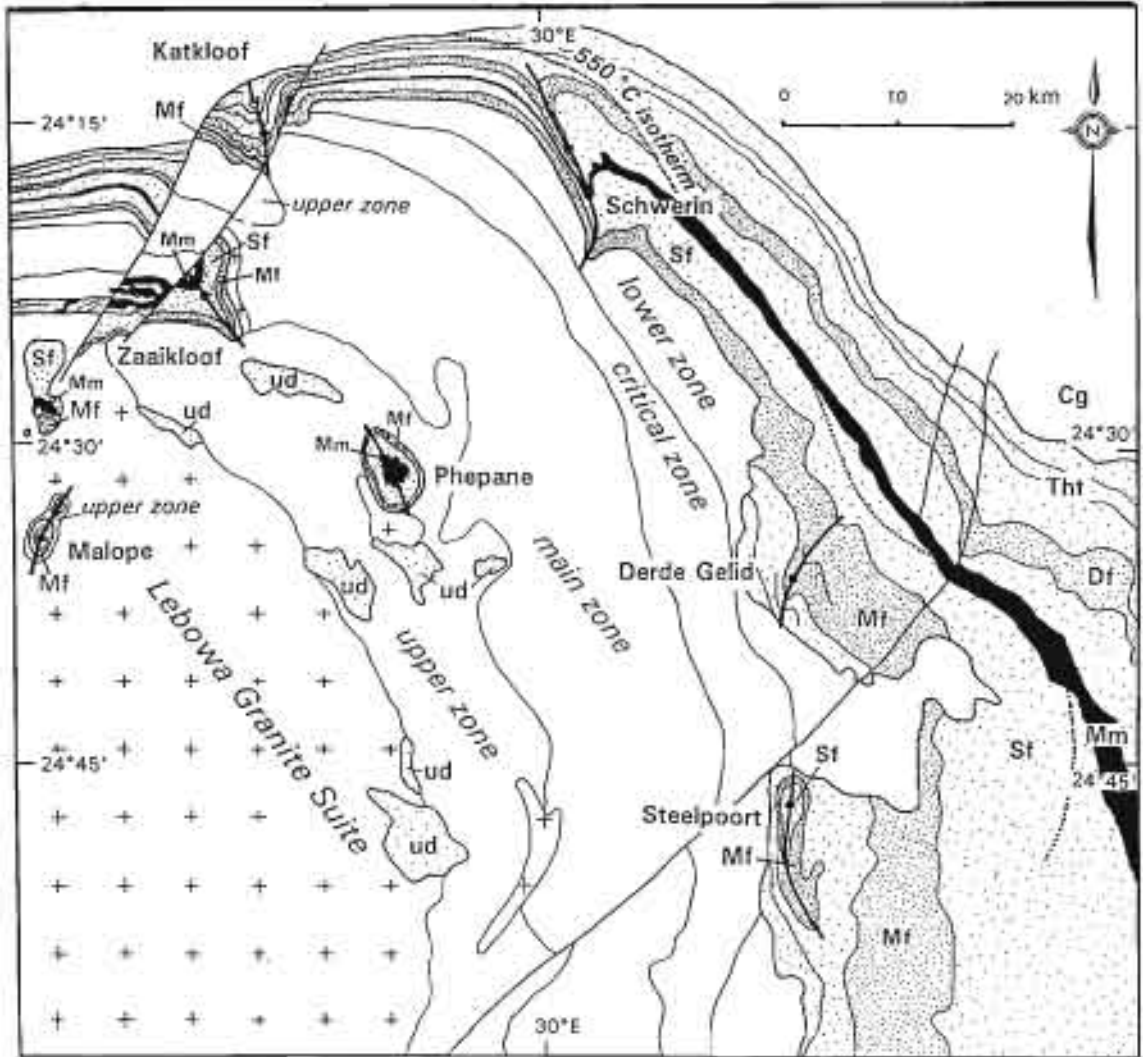
### 7.1 INTRODUCTION

As discussed previously, the domes or periclinal folds of contact metamorphosed Transvaal Supergroup rocks within the northeastern Bushveld Complex (Figure 7.1) have been attributed to a number of mechanisms. These include pre-Bushveld age folding and doming, syn-Bushveld xenolith development or doming; and post-Bushveld thrusting models (Hartzer, 1995 and references therein). A diapiric mechanism was first proposed by Button (1978). Sharpe and Chadwick (1982) although accepting that diapirism may have played a part in the deforming mechanism, reinterpreted the structures as a result of compressional folding produced by the emplacement of the Rustenburg Layered Suite into a subsiding basin as modelled by Sharpe and Snyman (1980). More recently, du Plessis and Walraven (1990) suggested that folding developed in response to a left-lateral strike-slip system aided by diapiric mechanisms.

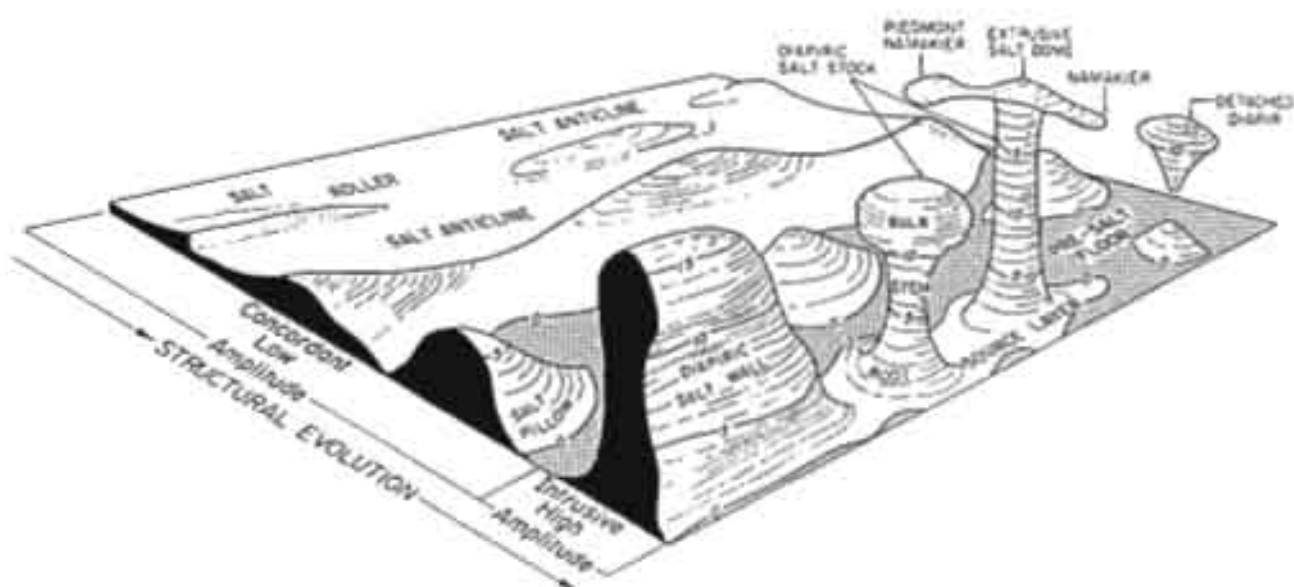
In this chapter, the structural and metamorphic observations are combined and shown to be most compatible with a dominantly diapiric model, with diapirism initiated by magma intrusion processes in a regionally extensional tectonic framework.

### 7.2 DIAPIRISM

The term diapir indicates piercing or intrusion from the Greek *diapirein* implying a crosscutting relationship with the layering of the overburden. The term diapir has however also become synonymous with the term dome, relating to structures that have resulted from gravity-generated processes. The best and most studied examples are salt diapirs, as they commonly occur in Phanerozoic petroleum-bearing basins and are associated with oil traps. The most important examples are those of northern Germany, the North Sea, the Gulf Coast, southern Iran and the Canadian Arctic (Trusheim, 1960; Talbot and Jackson, 1987; Jackson and Talbot, 1989). Salt structures have a range of geometries (Figure 7.2) that indicate a progression from concordant, low-amplitude structures to discordant, high-amplitude intrusions and extrusions (namakiers).



**Figure 7.1** Simplified map of the northeastern Bushveld Complex showing the distribution of the major floor periclines (Katkloof, Schwerin, Zaaikloof, Malope, Phepane, Derde Gelid and Steelpoort) within the Rustenburg Layered Suite and their relationship to the 550 °C isotherm. Contact metamorphosed Transvaal Supergroup: Cg - Chuniespoort Group; Thf - Timeball Hill Formation; Df - Dwaalheuvel Quartzite Formation; Sf - Silverton Shale Formation; Mm - Machadodorp Member; Mf - Magaliesberg Quartzite Formation; ud - undifferentiated Pretoria Group xenoliths.



**Figure 7.2** Compilation of the geometries of salt structures from Jackson and Talbot (1986).

Although controversial, diapiric mechanisms have also been suggested for both the ascent and emplacement of many granite plutons and batholiths (Ramberg, 1981; Bateman, 1985; Paterson, 1988). Diapir-like emplacement of mafic magma into a granitic host is also possible during horizontal crustal shortening (Watkeys, 1996). Observations from salt diapirs and particularly the discussions arising from the granite ascent and emplacement controversy have provided a useful comparative background for investigating the origin and mechanisms of the Bushveld Complex aureole structures.

The most important magma ascent processes are considered to be dominated either by dyke-transport mechanisms (Clemens and Mawer, 1992; Petford, 1996) or diapiric ascent mechanisms (Paterson and Vernon, 1995). Both are end-member situations and the relative importance of each of these processes is often controversial. Emplacement mechanisms, the mechanisms by which magma is accommodated at its final resting place, are similarly controversial with a number of processes suggested (Turcotte, 1982; Bateman, 1984). These include, (1) domal uplift, (2) stoping, (3) ring-dyke intrusion, (4) granitisation, (5) zone melting, (6) diapirism and (7) ballooning. The first three mechanisms are associated with late-stage brittle intrusion whereas the last four are ductile processes. Of the ductile processes,



diapirism and ballooning are the most widely accepted and the relative importance of each has been intensely debated. This has produced a host of criteria by which to identify diapirism in granitoid intrusions (Coward, 1981; England, 1990; Clemens *et al.*, 1997). It is to these criteria, and the characteristics of salt diapirs, that the structures in the Bushveld Complex aureole are compared, and the diapiric hypothesis is tested.

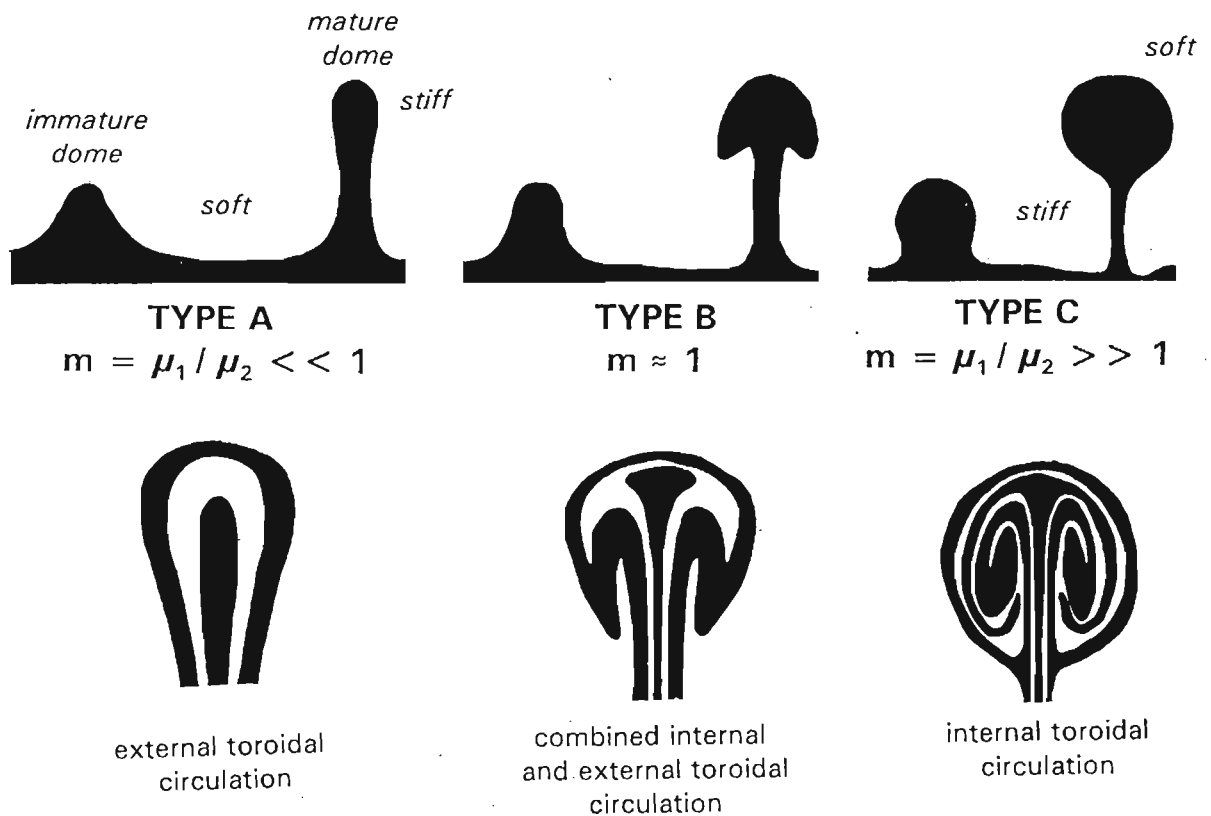
### 7.2.1 Pericline geometry and effective viscosity

*Less dense material should occupy circular or oval-shaped complexes surrounded by more dense material.*

Due to oblique erosional sections of all the periclinal structures, except for the Phepane pericline, typical circular or oval shapes are not developed on the geological map (Figure 7.1). It is however, clear that in sections normal to the pericline axis, oval cross-sections similar in size and shape to that of the Phepane will be produced for the other major floor structures. In each case the floor structures, having a density of approximately  $2.7 \text{ g.cm}^3$ , are surrounded by higher density mafic layered rocks of the Rustenburg Layered Suite having a density of approximately  $3.1 \text{ g.cm}^3$ .

The floor structure geometries are comparable to those of salt structures (Figure 7.2). The Phepane dome is interpreted as being an almost completely preserved mature diapiric structure with a bulb and stem-type geometry. The other structures (Katkloof, Schwerin, Zaaikloof) probably had similar bulb-like geometries, but the deep and oblique erosional sections now only provide sections showing anticlinal geometries with some limb overturn. Although not necessarily a requirement for diapirism, geophysical evidence for the Malope (Marlow and Van der Merwe, 1977) and Phepane domes (Molyneux and Klinkert, 1978), suggests that both structures are attached to the floor in the same way as the perimeter periclinal structures. As indicated in Chapter 5, deformed Machadodorp Member rocks exposed in the core of the Phepane and Zaaikloof periclinal structures imply that the decollement level in both structures is similar in depth to that of the Schwerin and Katkloof periclinal structures. The Malope dome represents a shallow dipping pericline with limbs dipping at an average of  $30^\circ$  (Marlow and Van der Merwe, 1977). The geometry of the structure may represent either the top of a bulbous shape similar to the Phepane pericline, or a simple low amplitude domal structure as represented by the Derde Gelid and Steelpoort periclinal structures.

In systems where diapir growth involves only the interaction of the buoyant layer with the overburden layer, diapir geometry is related to the viscosity contrast ( $m = \mu_1/\mu_2$ ) where the overburden viscosity is  $\mu_1$ , the buoyant layer viscosity is  $\mu_2$ , and  $m$  is the viscosity ratio (Selig, 1965; Whitehead and Luther, 1975; Whitehead and Helfrich, 1990). Unfortunately, the effective viscosities of natural materials are very poorly constrained. Salt, being the most studied is estimated to range in effective viscosity from  $10^{14}$  to  $10^{20}$  Pa s (Jackson and Talbot, 1986). From experimental studies (Whitehead, 1988; Whitehead and Luther, 1975; Talbot and Jackson, 1987; Jackson and Talbot, 1989; Zaleski and Julien, 1992) it was found that where the viscosity ratio ( $m$ ) is less than unity ( $m \ll 1$ ), the diapirs are found to have only slightly bulbous shapes and have a simple internal structure (Figure 7.3).



**Figure 7.3** Diagram showing the relationship between shape, spacing and viscosity contrast for both immature and mature diapirs. Overburden viscosity is  $\mu_1$ , buoyant layer viscosity is  $\mu_2$ , and  $m$  is the viscosity ratio. After Jackson and Talbot (1986, 1989).

These have been termed type A diapirs (Jackson and Talbot, 1986; 1989). Type B diapirs are produced where  $m \approx 1$ . These are characterised by mushroom-heads. Type C diapirs result where  $m \gg 1$ . Mature Type C diapirs have balloon and tail shapes and are characterised by the most complex internal structure (Figure 7.3). With an increase in effective viscosity, the toroidal circulation progressively moves inwards from the surrounding material towards the diapir. Where  $m \ll 1$ , toroidal circulation is found only in the surrounding material. Where  $m \approx 1$ , toroidal circulation involves both the diapir and the surrounding material. When  $m \gg 1$ , toroidal circulation is restricted to the diapir (Figure 7.3).

The overall geometry of the Phepane dome is one in which the diapir has a bulbous asymmetrical head typified by an overhang and a near vertical side. No skirt or entrained mafic rocks of the Rustenburg Layered Suite were found within the structure, suggesting that a mushroom-shaped Type B diapir geometry is unlikely. The overall internal structure is also simple, with no repetition of stratigraphy as expected for Type C diapirs. The most likely viscosity contrast for the generation of the Phepane and the other domes is thus one in which  $m = \mu_1/\mu_2 \ll 1$ , indicating that the deforming contact aureole was more viscous than the mafic magmas.

Type A diapirs should have an internal structure dominated by steeply plunging folds and lineations. As shown in Chapter 4, lineations and fold axes in the core of the the Phepane structure are indeed steeply plunging as expected with both the lineations and fold axes defining a radial pattern and the folds displaying a “curtain-type” geometry. In contrast however, around the periphery of the structure, the folds are shallowly plunging, concentric-type folds which deform an earlier lineation which is represented by the lineation seen in the core of the structure. This suggests that some degree of internal toroidal flow did occur, suggesting effective viscosity contrasts greater than unity ( $m \gg 1$ ) This is discussed in more detail below.

Other evidence suggesting that an effective viscosity contrast greater than unity may have existed is seen in the Katkloof and Schwerin structures. The fold hinges of these folds are markedly cusp-shaped into the Rustenburg Layered Suite. Cusp-lobate geometries are produced by a number of processes at junctions between two materials of contrasting viscosity (Talbot and Sokoutis, 1992). In all examples, the low competency material forms the cusp

protruding into the higher competency material. The cusp-like geometry of the Katkloof Fold is an indication that the wall rocks had a lower viscosity in their final stages of growth than the overlying Rustenburg Layered Suite in which  $m \gg 1$ . This is in contradiction to the effective viscosity contrasts displayed by the geometry of the fold structures.

This apparent contradiction may be explained by fact that deformation occurred during a continuously changing effective viscosity contrast between the wall-rocks and the Rustenburg Layered Suite magma. The floor diapirs would initially have grown into a low viscosity magma ( $m \ll 1$ ). Growth continued as the Rustenburg Layered Suite crystallised and even continued once the mafic magma had reached the critical melt fraction (CMF) of 50%. Compared to the contact aureole, the Rustenburg Layered Suite would increase in viscosity more rapidly, while the floor rocks retained or even decreased in viscosity with time, becoming relatively less viscous than the lower parts of the Rustenburg Layered Suite. Proof of this on an outcrop scale is the common occurrence of rheomorphic veins of felsic material derived from partially molten Pretoria Group within the lowermost parts of the Rustenburg Layered Suite.

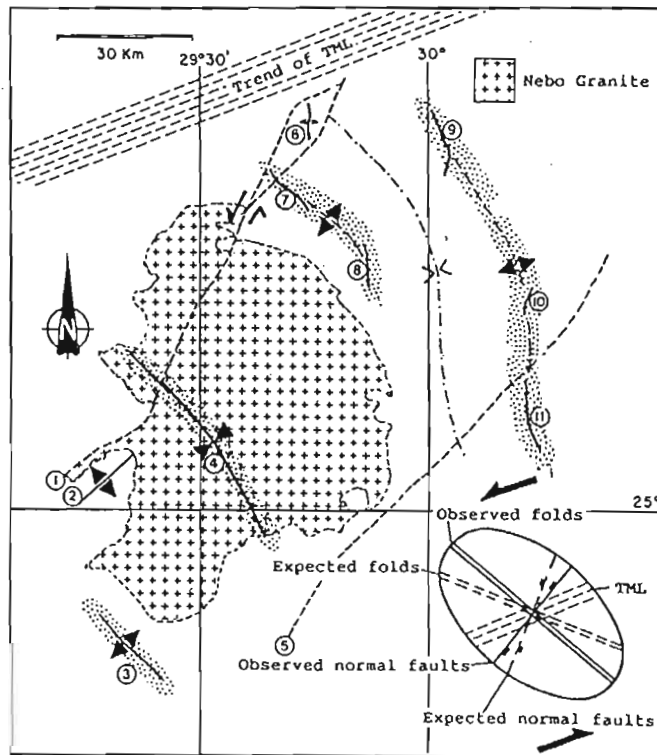
Time dependent effective viscosity contrasts were also suggested for salt diapir evolution by Jackson and Talbot (1989). As diapir growth progressed, newly deposited overburden near diapir caps would increase in effective viscosity by compaction. This would result in an effective viscosity contrast that progressively increased with time. In some circumstances early formed Type A diapirs could be modified to Type B geometries then progress to Type C geometries as the effective viscosity contrast changed with time.

### 7.2.2 Pericline arrangement

*The domes should not conform to a regular array such as produced by fold interference.*

Many previous workers have attempted to explain the periclinal structures as a series of dome and basin interference patterns from two near-orthogonal fold axes (Hunter, 1975; Hartzler, 1995) or as a systematic fold system related to strike-slip deformation (Du Plessis and Walraven, 1990). The problem with this interpretation is that widely separated individual periclinal structures are incorrectly joined to form a single fold axis. For example in the Du Plessis and Walraven (1990) interpretation, the fold axes of the Steelpoort-Derde Gelid periclinal structures are joined with that

(1990) interpretation, the fold axes of the Steelpoort-Derde Gelid periclinal axes are joined with that of the Schwerin Pericline, that parallels the main synformal axis in the Rustenburg Layered Suite (Figure 7.4). According to this model, the folding would also post-date the emplacement of the Nebo Granite of the Lebowa Granite Suite which is not the case as has been shown in Chapter 4.



**Figure 7.4** A strike-slip model to explain the origin of the floor structures in the northeastern Bushveld Complex. After du Plessis and Walraven (1990). (1) Wonderkop Fault, (2) Marble Hall dome, (3) Dennilton dome, (4) Nebo Granite syncline, (5) Steelpoort Fault, (6) Katkloof pericline, (7) Zaaikloof pericline, (8) Phepane dome, (9) Schwerin pericline, (10) Derde Gelid pericline, (11) Steelpoort pericline, (TML) - Thabazimbi Murchison Lineament.

The alternative diapiric model does not require such a regular array of fold orientations and can also explain the existence of domes with diapiric geometries and diapiric walls, linking the Phepane structure with the Zaaikloof structure and isolated smaller periclinal structures such as the Katkloof and Schwerin structures.

### 7.2.3 Pericline spacing

*A fairly even spacing between individual diapirs.*

Static state experiments with immiscible and incompressible Newtonian dyed fluids of various viscosities, have shown that a lower density fluid underlying a higher density fluid is prone to develop fluid dynamic instabilities (Strutt and Rayleigh, 1900; Taylor, 1950; Chandrasekhar, 1955). These manifest themselves as evenly spaced protrusions of optimum wavelength (spacing). With time, these progressively amplify, becoming channel ways allowing the lower viscosity material to buoyantly pass upward through the overlying material of higher viscosity. This phenomenon is known as the Rayleigh-Taylor instability. Natural systems are far more complex and few rocks behave as homogenous Newtonian fluids. In the case of the Bushveld Complex floor structures, growth also occurred under changing thermal conditions.

Attempts to simulate geological conditions, using analogue experiments with non-Newtonian fluids in a centrifuge (Ramberg, 1963, 1970), have in general shown that the wavelength of the protrusions is proportional to the viscosity ratio of the materials to the one-third power. The physical interpretation for this is that it is more efficient for the low-viscosity fluid to flow large lateral distances up a gradual slope, accumulating in diapirs, than it is to push straight up through a stiffer overburden. The Rayleigh-Taylor instability also results in a direct relationship between diapir spacing and the depth to the buoyant layer. The greater the overburden thickness the greater the spacing.

When applied to the salt diapirs of northern Germany, Turcotte and Schubert (1982) showed that the average spacing of salt diapirs ( $D$ ) is related to the depth to the salt layer ( $z$ ) by the expression  $D = 2.568z$ . The spacing between individual Bushveld Complex floor periclinal structures has an average of approximately 33 km, varying from 23 km for the Katkloof, Zaaikloof-Pramkoppies-Adriaanskop and Malope structures in the west, to a distance of 44 km between the Phepane and Steelpoort-Derde Gelid periclinal structures in the eastern part of the study area (Figure 7.1). The irregular array and distribution of the domes is similar to that of salt dome spacing in northern Germany. If the Turcotte and Schubert (1982) relationship is applied to the Bushveld Complex periclinal structures,  $D = 3.67z$  for the thinner and more closely spaced structures in the west and  $D = 4.49z$  for the areas of greater Rustenburg Layered Suite thickness in the east, where ( $z$ ) represents 6 and 8 km respectively.

Diapir spacing also relates to the viscosity ratio ( $m = \mu_1/\mu_2$ ), whereby the wavelength of fastest growth (diapir spacing) is proportional to the viscosity ratio ( $m$ ). Experimental studies (Selig, 1965; Whitehead, 1988; Whitehead and Luther, 1975; Whitehead and Helfrich, 1990; Talbot and Jackson, 1987; Jackson and Talbot, 1989; Zaleski and Julien, 1992) have shown that as the viscosity ratio ( $m$ ) increases, diapir spacing increases. Diapirs with simple mature shapes ( $m \ll 1$ ) are most widely spaced and diapirs showing intense internal vorticity or toroidal flow ( $m \gg 1$ ) are the most closely spaced (Figure 7.3).

#### 7.2.4 Pericline - Rustenburg Layered Suite relationship

*There should be conformable structures such as foliation, cleavage and lineations in the diapir and in the surrounding rocks.*

This generally accepted relationship is documented from a number of granite plutons and their country rocks where diapirism has been inferred as the emplacement process (Bateman, 1984, 1985; Cruden, 1990; Schwerdtner, 1990; Paterson and Fowler, 1993; Paterson and Vernon, 1995). Although no detailed structural fabric data exist for the Rustenburg Layered Suite cumulates, most of the cumulates are foliated with a shape preferred orientation (SPO). In this study, in the Mathabatha domain, pyroxenites approximately 1600 m above the floor contact, were found with well developed foliations. The pyroxene cumulates are strongly lineated with a consistently down-dip L-fabric or shape-preferred orientation that plunges at, or plunges marginally steeper to the south than the igneous layering (Appendix 1). This magmatic fabric does not conform to the subhorizontal stretching lineation in the underlying contact schists of the Mathabatha domain suggesting that a complex relationship between the magma and wall rocks must have existed.

The down-dip lineation in the magma is either a product of northward magma flow involving top-to-north shear or a result of top-to-south extensional shear. Since the foliation in the Mathabatha domain is an extensional top to south S-fabric, the most likely cause of the magmatic foliation is due to a top-to-south shear. The extensional lineation in the contact aureole, at almost 90° to the magmatic lineation, represents flow towards the periclinal culminations on either side of the Mathabatha domain (Chapter 4). This relationship can be considered analogous to that suggested by Clemens *et al.* (1997) for a model granitic diapir in which lineations on the contact may be either steeply plunging, due to diapir ascent, or

horizontal if radial pluton expansion becomes the most important process.

Quandling and Cawthorn (1994) showed that a down dip lineation is also a common fabric defined by plagioclase laths in gabbro-norites from the main zone to the east of the Phepane pericline. They suggested that the fabric is a result of density currents within the magma chamber. Although magmatic fabrics may be of primary origin, the fact that the foliation is so widespread and coherent across the eastern Bushveld Complex (down-dip lineations) strongly supports a more regional tectonic control on SPO fabric development.

The most likely interpretation favoured here is that the SPO fabrics are related to secondary tectonic processes. Compaction combined with non-coaxial flow with a top-to-south sense of shear resulted in the development of the dominant down-dip SPO lineation. This is consistent with tectonic subsidence of the Rustenburg Layered Suite throughout the submagmatic stage into the solid-state stage and is compatible with fabrics and kinematic indicators in the contact aureole.

Further evidence for a tectonic origin of the SPO fabrics is found in the Malope dome. The Rustenburg Layered Suite is highly attenuated over the dome and the layered mafic rocks show intense fabric development (Marlow and Van der Merwe, 1977). This is most likely a product of viscous drag during pericline growth into a partially crystallised stratified magma, analogous with the country rock structure above a rising non-piercement type salt dome or granite plug (Ramberg, 1981; Cruden, 1988).

On the northwestern and southern margins of the Phepane and Zaaikloof periclinal structures, a broad synclinal structure is developed in the layering of the Rustenburg Layered Suite. Within the synclinal structure, magnetite seams of the upper zone are folded into open folds that verge away from the floor periclinal structures (Appendix 1). Since these folds are confined to the upper parts of the Rustenburg Layered Suite, and closely associated with the floor periclinal structures, they are probably a direct result of lateral spreading or ballooning in the upper portion of the periclinal structures. Similar structures have been simulated in analogue models adjacent to diapir bulbs (Ramberg, 1981).



### 7.2.5 Internal pericline structures

*Strain distributions should be extensional, sub-horizontal and tangential in the crestal regions. Strains should be vertical in the trunks associated with radial axial planes.*

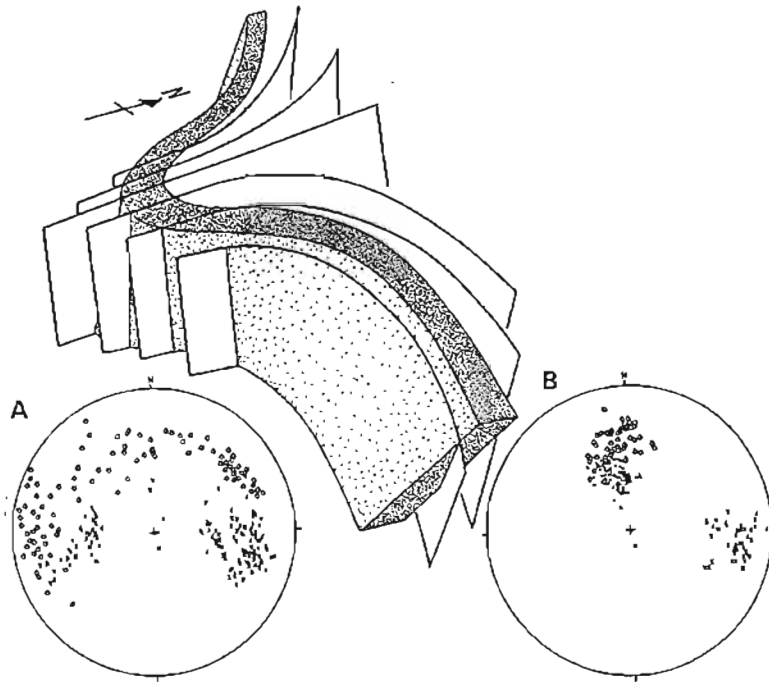
In the contact metamorphic rocks exposed around the perimeter of the Rustenburg Layered Suite, each of the periclinal structures is developed above a decollement surface that is situated between 3.8 km and 2.3 km below the contact with the Rustenburg Layered Suite. The deepest exposed decollement level is located below the Katkloof pericline, coinciding with the contact between the Chuniespoort Group and the Pretoria Group. Further east in the Schwerin pericline, the decollement is developed immediately above the quartzites of the Timeball Hill Formation. The shallowest decollement is found below the Derde Gelid and Steelpoort periclinal structures, where it is located within the Silverton Shale Formation corresponding approximately to the level of the Machadodorp Member.

In each of the structures the decollement is located at a major lithological contact within the lower part of the andalusite zone, corresponding approximately to the depth of the 550° C isotherm in the contact aureole (Figure 7.1). The eastward rise of the decollement level below the periclinal structures follows the eastward and southward thinning of the contact aureole from the Katkloof pericline to the Derde Gelid and Steelpoort periclinal structures and a concomitant rise of the Rustenburg Layered Suite floor contact.

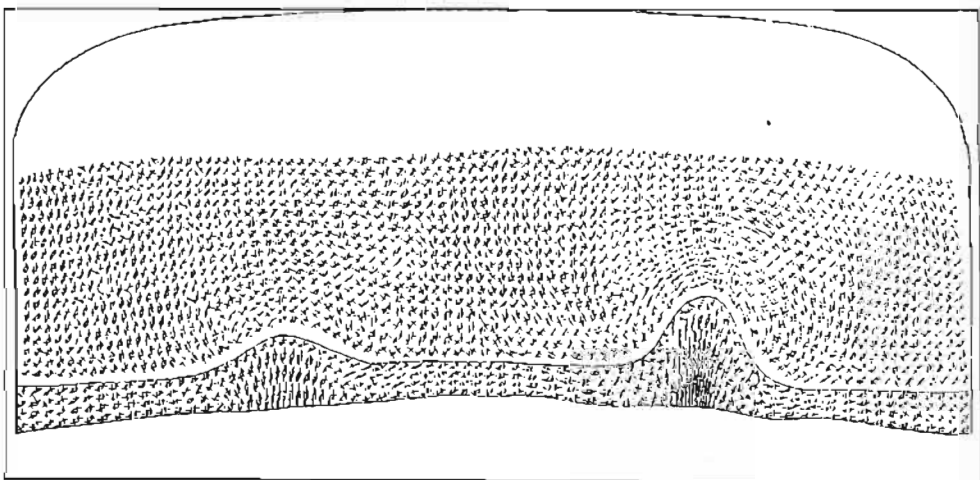
As shown in Chapter 4, the cores of the Katkloof and Schwerin periclinal structures are characterised by a marked axial planar cleavage which fans outwards and is continuous with the fabric in the interpericline areas (Figure 7.5). A similar relationship is represented in the analogue diapir models of Dixon and Summers (1985) (Figure 7.6). The strain distributions produced in the models match the observed foliation orientations in the interpericline and pericline cores of the Bushveld Complex floor structures.

In three dimensions, the planar fabric should define a conical shape fanning outwards into the decollement surface at the base of the periclinal structures. Lineations contained within this fabric on the limbs of the Katkloof structure radiate outwards from the predicted pericline culmination, plunging towards the east on the eastern side of the fold and towards the west on the western limb (Figure 7.5). Sections through higher levels within periclinal structures, as represented by the

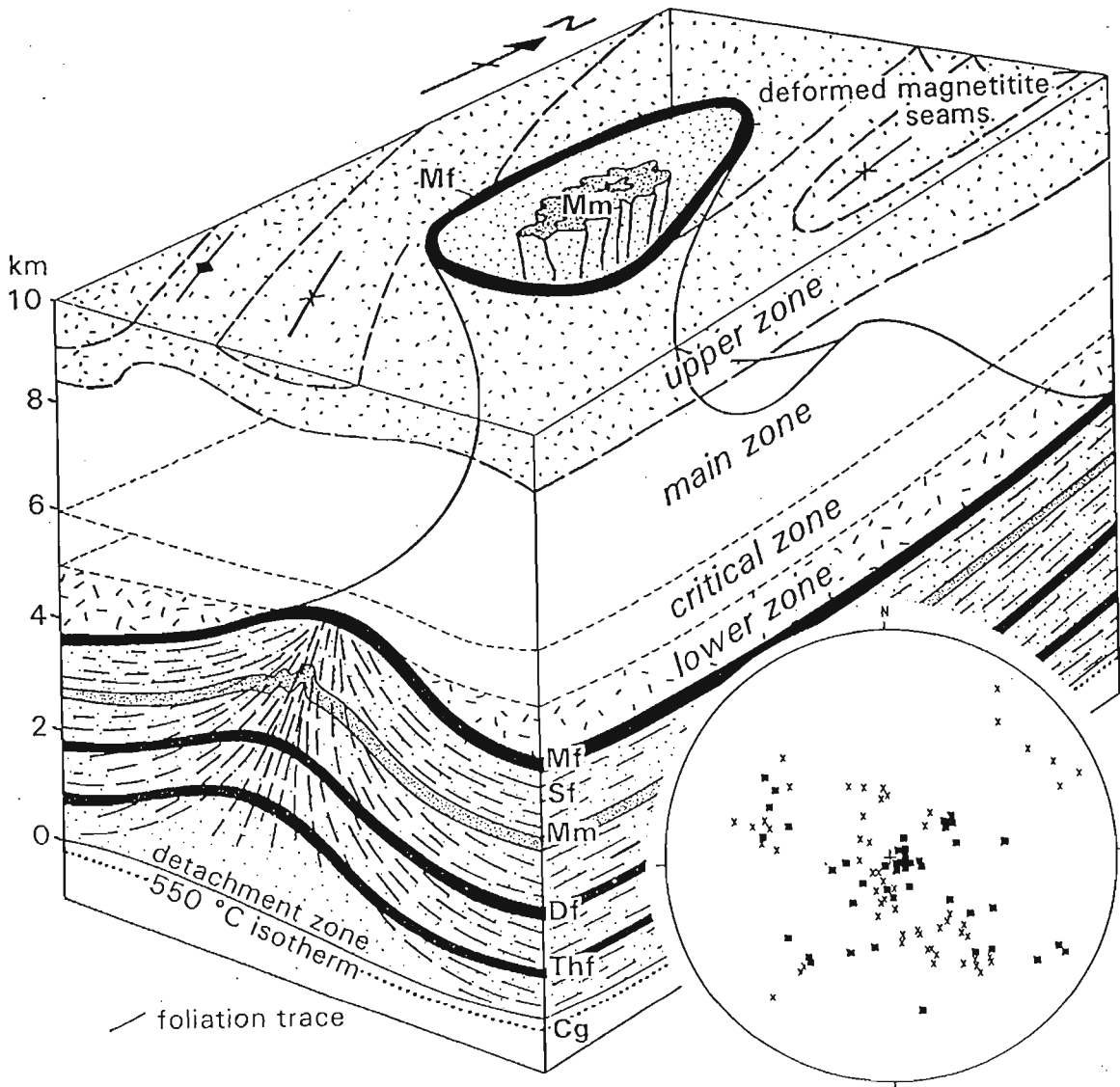
Phepane pericline, are represented in the core by steeply plunging radial curtain folds and lineations (Figure 7.7).



**Figure 7.5** Diagrammatic representation of outward-fanning cleavage associated with the Katkloof pericline A: Fabric orientation data from within dome. B: Orientation data from adjacent eastern interpericlineal area. Equal-angle, lower-hemisphere projections of poles to bedding (●), foliation (○) and stretching lineations (x) in relationship to Katkloof Fold axis plunge (■).

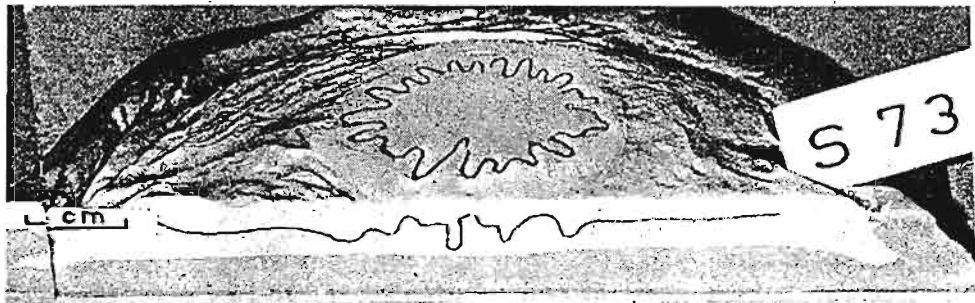


**Figure 7.6** Strain map profile of an analogue centrifuge model of two diapirs by Dixon and Summers (1985). The long axes of the crosses correspond to the orientation and relative magnitude of the minimum stress axis of the strain ellipse. The width of the model is approximately 250 mm.



**Figure 7.7** Diagram showing bulbous Phepane dome within deformed upper zone of Rustenburg Layered Suite. Internal structure of dome is characterised by an outward fanning cleavage developed above a sub-domal detachment at the Pretoria/Chuniespoort Group contact and the 550 °C isotherm. Steeply plunging, radially oriented curtain folds are represented by a lower-hemisphere, equal-angle stereoplots of lineations (x) and fold axes (■) from dome core. Stratigraphic symbols as for Figure 7.1.

Within the core of the Phepane structure the folds have diversely orientated axial surfaces radiating outwards from the central part of the dome, and steeply plunging fold axes. Folds are characterised by a high degree of noncylindricity with strongly arcuate curvilinear geometries and widely ranging plunges within a single outcrop. These structures are considered to represent interfering folds associated with a single phase of constrictional deformation similar to those produced experimentally (Figure 7.8) (Ramberg 1981, Ghosh *et al.*, 1995).



**Figure 7.8** Analogue model diapir from Ramberg (1981) showing the internal radial curtain folds. Buckled sheet of modelling clay was originally imbedded as a thin straight sheet in the buoyant layer. The overburden layer has been removed and the buoyant layer has been cut both vertically and horizontally to reveal the internal structure.

More shallowly plunging, concentrically orientated folds and lineations are confined to the outer shell of the structure. Folds in this part of the pericline have axial surfaces parallel to the dome margins with shallowly plunging fold axes. Similar relationships are also described from the Barrow Dome, Melville Island, Canadian Arctic (Tozer and Thorsteinsson, 1964). Jackson and Talbot (1989) reinterpreted the structure as a near horizontal section through a mushroom structure in which the shallowly plunging folds around the outer margins of the structure represent the skirt of the mushroom. This is separated from the central steeply plunging folds in the core by a screen of entrained country rocks.

No mafic rocks of the Rustenburg Layered Suite were found *within* the floor domes, suggesting that mushroom development did not take place. The internal fold geometries however, do suggest that some refolding has occurred to produce the shallowly plunging folds on the margins of the structures. This may have resulted from internal toroidal circulation during the final stages of growth, when the effective viscosity contrast was such that the floor domes were less viscous than the surrounding mafic magmas of the Rustenburg Layered Suite. --

### 7.2.6 Interpericlinal structures

*Interdomal areas or source layers should conform to strain distributions which show horizontal flow and attenuation.*

Between the Katkloof and Schwerin periclinal structures, contact metamorphosed strata strike approximately E-W and dip moderately towards the south. As described in Chapter 4, at all metamorphic grades, the rocks are characterised by a pronounced planar foliation, ranging in orientation from near bedding parallel to more steeply southward dipping, and an associated shallow plunging linear fabric. The most prominent lineation is represented by quartz stringers elongated in the direction of maximum finite extension. Chistolite porphyroblasts are boudinaged within the lineation direction while quartz fills the boudin necks, often accompanied by fibrolite in the fibrolite zone.

Large metre-scale boudins are common in competent coarse-grained arenaceous and conglomeratic units in the Dwaalheuwel Formation. Boudin axes trend approximately north-south, plunging sub-parallel to the bedding dip direction. Within the partial melt zone of the aureole, extension is associated with conjugate ductile shears that produce asymmetrical boudinage and sigmoidal pinch and swell structures.

Aureole fabrics within the interpericlinal areas correspond to a syn-metamorphic E-W directed extension during the emplacement of the Rustenburg Layered Suite, normal to the long axis orientation of the adjacent periclinal structures. Removal of the post-Bushveld Complex dip indicates a flat lying planar foliation and a near horizontal stretching lineation as shown in Chapter 4.

Model diapirs all show that the interdiapir zones are extended with thinning of the buoyant layer as the material migrates into the rising diapir (Ramberg, 1981). This produces a range of extensional deformation structures. Analogue models show that extension and thinning of a heterogeneous source layer results in boudinage in layers of contrasting competency (Figure 7.9). In areas of extension rock salt becomes foliated and lineated. Boudinage, flow breccias and anastomosing bedding parallel shears are commonly reported (Talbot and Jackson, 1987; Talbot, 1992; Smith, 1996).

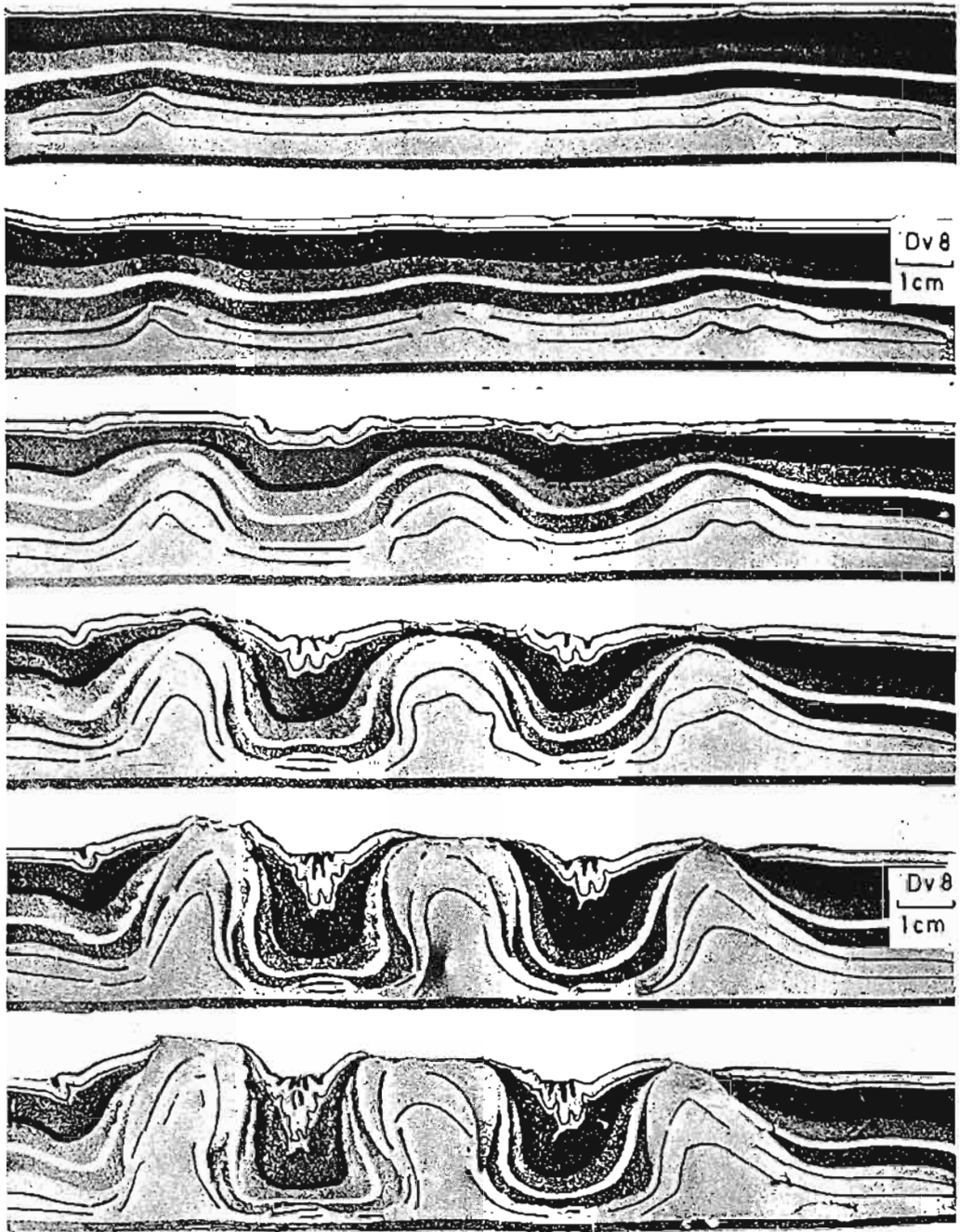


Figure 7.9 Analogue model of Ramberg (1981) showing the sequential cuts through three diapirs of silicone putty that have ascended into an overburden of multilayered painters putty with a top complex consisting of thin sheets of competent modelling clay. Thinning of the interdiapir zones has produced boudinage of more competent modelling clay layers within the buoyant silicone putty.

## **7.3 RATES OF PROCESSES**

### **7.3.1 Magma accumulation rates**

Jaeger (1957, 1959, 1961, 1964, 1968) produced a series of mathematical models to predict the cooling history of magma bodies and the temperatures that would be attained in the surrounding country rocks. Although a number of assumptions and approximations have to be made, these calculations are generally accepted as providing a good estimate of the time spans involved in conductive cooling of igneous intrusions. Further refinements were made by Irvine (1970) to include convection and crystal settling processes in large layered intrusions. Based on these models, Irvine (1970) predicted that for a single injection model the entire Rustenburg Layered Suite magma would have accumulated within a period of 200 000 years. In a more recent analysis of accumulation rates, Cawthorn and Walraven (1997) showed that the magma chamber could have been filled within an even shorter time of 60 000 years involving average magma emplacement rates of 6 km<sup>3</sup> per year.

Complete crystallisation of a mafic magma involves a relatively small temperature drop from an original liquidus temperature of 1300°C (Cawthorn and Bigger, 1993) to temperatures of approximately 900°C (Cruden, 1988). Given the fast emplacement rates, complete crystallisation of the Rustenburg Layered Suite is considered to have occurred within a time of 150 000 years (Cawthorn and Walraven, 1997).

At the high solidus temperatures for the mafic magmas, the felsic contact aureole rocks would still be subjected to a high heat flow. The migmatite zone under these conditions would remain in a viscous or semi-viscous state in which the percentage melt exceeds the critical melt fraction. This for most rocks is approximately 30-35% (Arzi, 1978, Van der Molen and Paterson, 1979) corresponding to the change from rigid to viscous behaviour.

### **7.3.2 Aureole deformation rates**

As shown above, floor dome geometries and internal dome structures are consistent with a positive viscosity contrast, in which initially at least, the aureole had a higher relative viscosity than the overlying mafic magma. The maximum uplift of exposed periclinal cores relative to the floor was approximately 8 km. Since all the observed deformation is part of the metamorphic event, and occurred at temperatures above 550° C (deformation is confined to

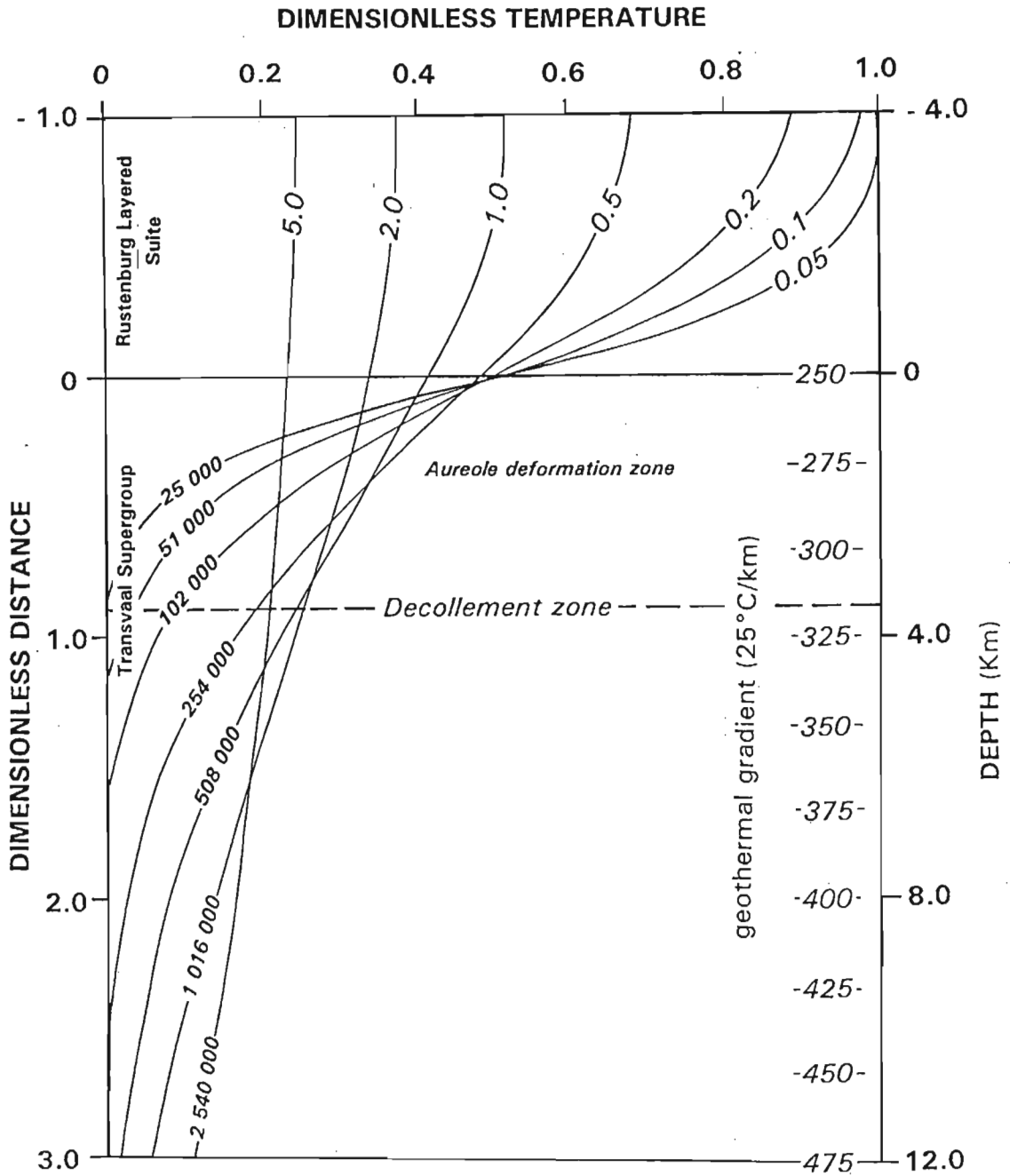
the zone above the 550° C isotherm), uplift rates and strain rates can be determined from model cooling histories.

The standard one dimensional cooling curves for a sheet intrusion (Jaeger, 1968) are shown in Figure 7.10. These indicate that temperatures outside the intrusion never exceed the midpoint of the country rock and intrusion temperatures. Using this model, calculations for the Rustenburg Layered Suite show that the time required to heat the floor rocks to peak temperatures at the Katkloof Fold decollement would take approximately 1 Ma. This assumes that the Rustenburg Layered Suite is sill shaped, 8 km in thickness, and emplaced into wall rocks with a temperature of 250° C and a thermal diffusivity  $31.5 \text{ m}^2.\text{yr}^{-1}$ . This is compatible to conditions at a depth of approximately 10 km and a geothermal gradient of  $25 \text{ }^\circ\text{C.km}^{-1}$ .

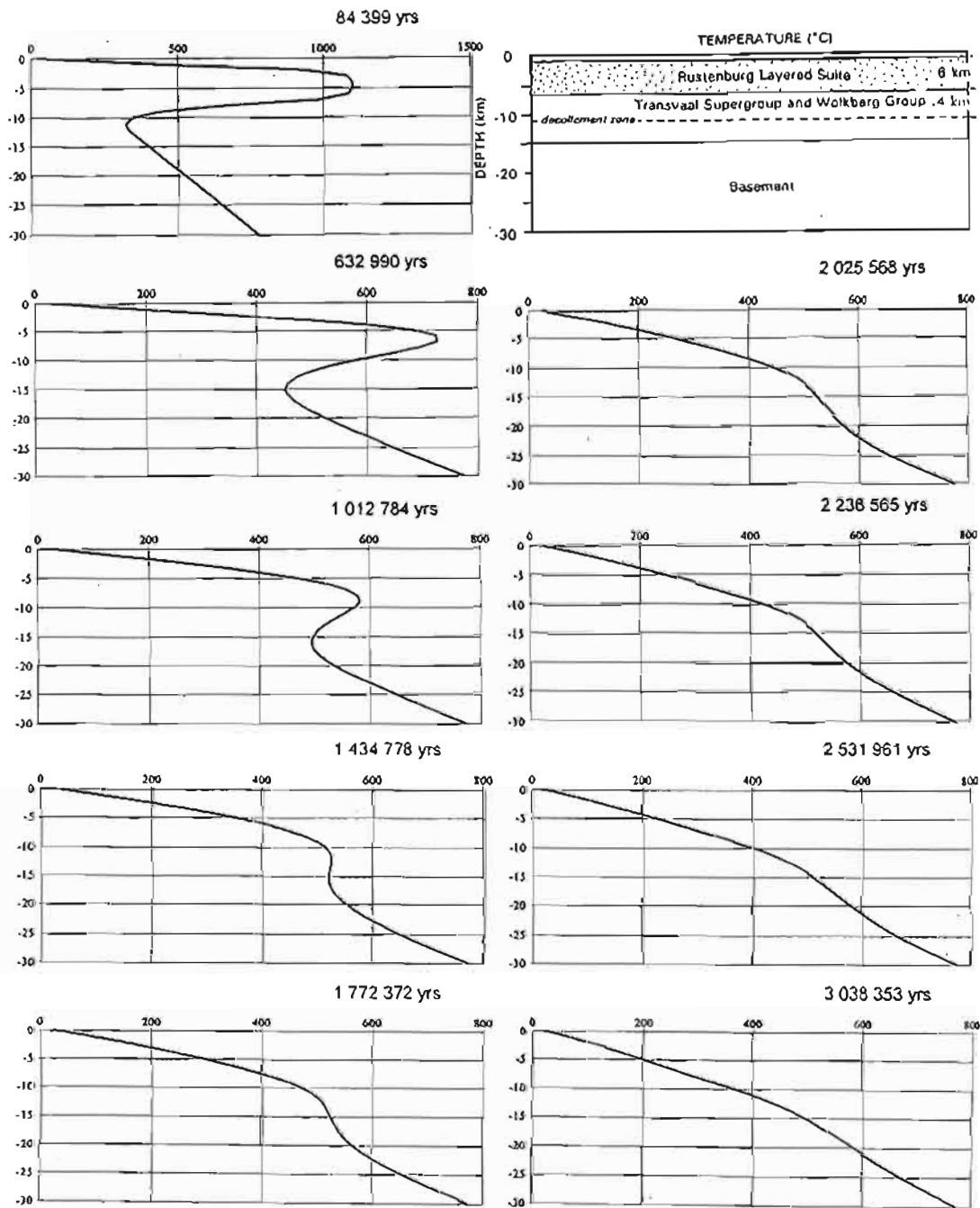
For a more regional model, the transient temperature profiles were modelled using the program “heat” of Wohletz (1995). To more accurately resemble the regional thickness of the Rustenburg Layered Suite, a 6 km thick mafic sheet was used as the intrusion with an initial intrusion temperature of 1100 °C, intruded at a depth of 1km. The base of the intrusion being at a depth of 7 km. The steady state geotherm used in the model was  $25 \text{ }^\circ\text{C.km}^{-1}$ . Thermal conductivities used were  $2.07 \text{ W.m}^{-1}.\text{k}^{-1}$  and  $2.63 \text{ W.m}^{-1}.\text{k}^{-1}$  representative of shales and gabbros respectively (Furlong *et al.*, 1991). The model indicates how peak temperatures of approximately 550 °C are attained after approximately 1 Ma after intrusion at the decollement depth of 11 km. The temperature profiles also show that thermal relaxation approaching the original geotherm is in excess of 3 Ma.

The largest of the floor domes have heights of 8 km, suggesting that they rose 8 km over a time of 1 Ma which corresponds to a minimum uplift rate of approximately  $0.8 \text{ cm.yr}^{-1}$  or  $2.5 \times 10^{-10} \text{ m.s}^{-1}$ . Maximum strains from deformed pebble conglomerates and boudinaged chistolite crystals in the interpericlinal area between the Katkloof and Schwerin Folds indicate extensions of 35% and produce strain rates in the order of  $10^{-14} \text{ s}^{-1}$ . The overall strain rate for the growth of the Phepane dome, determined from stratigraphic thickness, pericline height and geometry is estimated at  $1.9 \times 10^{-14} \text{ s}^{-1}$ , assuming a pericline height of 8 km and a width of 6 km.





7.10 Dimensionless model cooling curves for a sheet intrusion, after Jaeger (1968). Approximate “dedimensionalised” cooling times for each curve are shown for the 8 km thick Rustenburg Layered Suite having an intrusion temperature of 1100 °C. The decollement zone at 3.8 km depth indicates peak temperatures of approximately 550 °C after a time of 1 Ma.



**Figure 7.11** Model temperature profiles for the Rustenburg Layered Suite and the contact aureole using the program HEAT by Wohletz (1995).

If floor dome growth kept pace with magma addition and all the deformation occurred only within the liquidus and submagmatic stages of the Rustenburg layered Suite, between the 1300° C and 900° cooling interval, all deformation would have had to occur within the 150 000 years as predicted by Cawthorn and Walraven (1997). This produces a maximum estimate for the strain rate of deformation which is an order of magnitude higher than those predicted from the aureole cooling calculations. These give uplift rates for the domes of 5.3 cm.yr<sup>-1</sup>, and an overall strain rate for the growth of the Phepane of 1.2 x 10<sup>-13</sup> s<sup>-1</sup>.

Diapir ascent rates in the simplest form can also be calculated using Stokes law:

$$V = 2\Delta\rho gr^2 / 9\eta$$

where V is the terminal velocity, r is the sphere radius, g is the acceleration due to gravity, of magma bodies  $\Delta\rho$  is the wall rock density minus the magma density, and  $\eta$  is the country-rock viscosity.

For the Bushveld structures: r = 4 km, g = 10 ms<sup>-2</sup>,  $\Delta\rho = (-3100 \text{ kg/m}^2 - 2700 \text{ kg/m}^2 = 400 \text{ kg/m}^2)$ ,  $\eta = 10^{12} \text{ Pa s}$  which is the assumed viscosity of the Rustenburg Layered Suite in a magmatic state. This indicates an ascent velocity of 1.4 x 10<sup>-8</sup> m.s<sup>-1</sup> (~400 cm/yr). This is considerably faster than the calculated value of 2.5 x 10<sup>-10</sup> m.s<sup>-1</sup> from the geometry and heat flow calculations.

It is clear that the critical parameter for the Stokes law is the wall-rock viscosity (Rustenburg Layered Suite) parameter  $\eta$ . More realistically the Rustenburg Layered Suite did not maintain a magmatic stage throughout the evolution of the floor periclinal but entered submagmatic and semi solid state conditions during the final stages of the diapir development, slowing diapir ascent rates. Marsh (1981, 1989) showed that a 50 % crystallinity is considered the threshold between a material that is effectively solid and one that can have fluid-like behaviour. For a basic magma this corresponds to a temperature of approximately 900 °C (Figure 7.12). Numerous examples of cumulate flow type fabrics and strained cumulate crystals in the Rustenburg Layered Suite (This study, Marlow and Van der Merwe, 1977) indicate that internal deformation continued throughout the crystal mush stage and that as the diapirs were

growing, crystallisation of the Rustenburg Layered Suite was occurring, increasing the viscosity.

More realistic average viscosity values are therefore in the order  $10^{14}$  Pa s representative of the submagmatic stage for a basaltic magma (7.12) (Cruden, 1988). This slows the ascent velocity down to  $1.4 \times 10^{-10}$  m.s<sup>-1</sup> and is in the same magnitude of that calculated using the geometry and heating time of the aureole to peak metamorphic conditions.

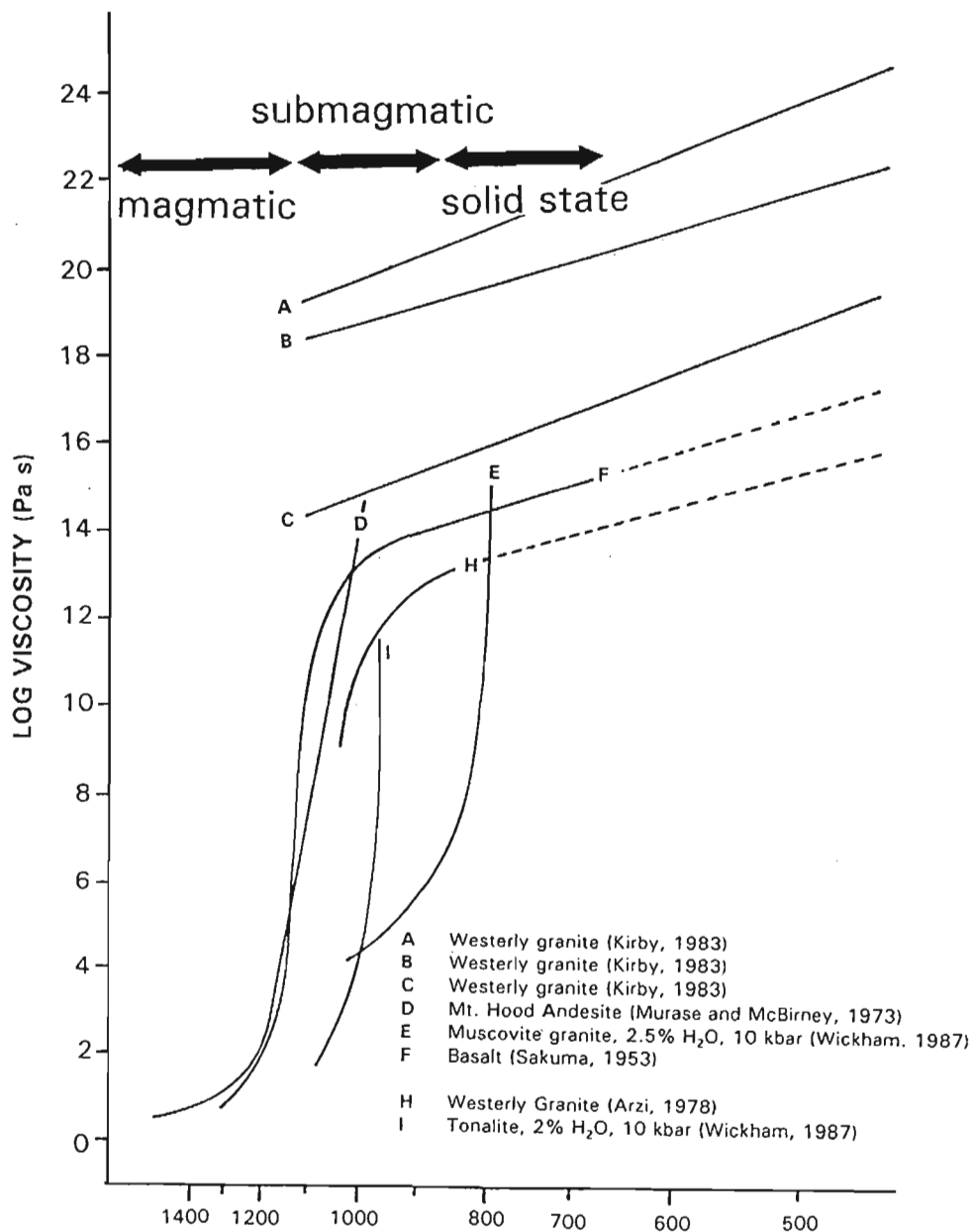


Figure 7.12 Diagram showing the generalised relationship between temperature and viscosity of a crystal-melt system (after Paterson *et al.*, 1991).

These values compare well with estimates of fold growth rates in Holocene fold belts which range between  $0.25 \text{ cm yr}^{-1}$  (Suppe, 1989) to  $1.7\text{-}3.2 \text{ cm yr}^{-1}$  (Vita-Finzi, 1979).

### 7.3.3 Rates of foliation development and porphyroblast growth

Cleavages in rocks tend to become visible in rocks only after approximately 20% shortening (Ramsay, 1967). Pfiffner and Ramsay (1982) showed that typical strain rates during cleavage formation vary between  $10^{-13}$  and  $10^{-15} \text{ s}^{-1}$  and that strain accumulation varies for pure and simple shear, with simple shear being the less efficient process. Higher strain rates ( $10^{-10}$  -  $10^{-13} \text{ s}^{-1}$ ) are associated with zones of very high strain such as mylonite zones. At an average strain rate of  $10^{-14} \text{ s}^{-1}$  visible cleavages will develop in rocks within a time of 700 000 years (Paterson and Tobisch, 1992). This is well within the 1 Ma years established for the aureole from the above cooling calculations.

Porphyroblast matrix relationships (Chapter 5) show that porphyroblastesis generally preceded fabric development - except in the earliest high strain zones - and that foliation development continued after porphyroblast growth had terminated. This suggests that porphyroblastesis was relatively rapid compared to foliation development. Porphyroblast growth rates are less well constrained than foliation formation rates and attempts to quantify porphyroblast growth rates have produced wide ranges of growth speeds.

Coetzee and Kruger (1992) used the Rb-Sr method on 4 cm diameter garnet porphyroblasts from the eastern Bushveld Complex aureole to try and estimate growth speeds and to determine the length of time for the contact metamorphic event. Their results suggested a period of growth of approximately 8 Ma. This is far longer than the cooling calculations predict and gives growth rates of  $2.5 \times 10^{-7} \text{ cm.yr}^{-1}$ . These are extremely slow growth rates well below those estimated for regional metamorphism (Ridley 1986) of about  $2 \times 10^{-5} \text{ cm.yr}^{-1}$  and  $1.3 \times 10^{-2} \text{ cm.yr}^{-1}$  in contact aureoles (Joesten and Fischer, 1988).

In the case of the Bushveld Complex contact aureole, the porphyroblast matrix relationships provide evidence that porphyroblast growth was fast. At the fast rates presented by Joesten and Fischer (1988), a 10 cm long andalusite crystal could have grown within a time of only 600 years.

## 7.4 RATE DEPENDENT EMPLACEMENT MECHANISMS

Magma emplacement will require significant wall-rock deformation to make space for the intrusion. Wall-rock deformation rates are thus a rate limiting process on the accumulation rates of magma, providing all the deformation is accommodated by a single deformation mechanism (Paterson and Tobisch, 1992). In the case of the Bushveld Complex, the present basin shape (lopolith) was produced by regional crustal subsidence suggesting that crustal subsidence was the main process involved in the accommodation of this huge volume of magma (Sharpe and Chadwick, 1982). From the above magma accumulation and wall rock deformation rates, it is possible to provide some constraints on the relative timing of metamorphism and deformation in the aureole and also to establish if the emplacement rates require unnecessary fast and unrealistic wall-rock deformation and crustal subsidence rates.

### 7.4.1 Pre-Bushveld Complex uplift

Lithospheric extension is generally considered to fall within two end-member types: passive extension in which the tensional stresses in the continental lithosphere cause thinning and passive upwelling of hot asthenosphere or active extension in which the impingement of a thermal plume on the base of the lithosphere causes convective thinning resulting in domal uplift due to isostatic adjustment from rapid thinning of the lithosphere. This is then followed by rifting as a result of the uplift (Sengor and Burke, 1978; Turcotte, 1982)

Basins formed by the latter active process, should show evidence of early uplift immediately preceding the main phase of eruption with the production of regional unconformities (Cox, 1989; White and McKenzie, 1989). The recognition of a regional unconformity at the base of the Dullstroom lavas (Cheney and Twist, 1991; Hartzer, 1995), as well as the recognition that the Dullstroom lavas represent the start of the Bushveld magmatic event (Hatton and Schweitzer, 1995; Schweitzer *et al.*, 1995) is considered good evidence for uplift immediately preceding Bushveld Complex magmatism. In the southern portion of the eastern Bushveld Complex an extensive sand sheet was present during the eruption of the Dullstroom lavas (Schweitzer and Hatton, 1997). This sheet is relatively undisturbed, but shows a north-to-south palaeocurrent direction. As Schweitzer and Hatton (1997) pointed out, this area was not subjected to extensive pre-eruption uplift, arguing against the presence of the plume head in this area.

The pre-Bushveld unconformity gradually cuts downward into the underlying Pretoria Group from the south to the north in the main Bushveld basin. A rapid truncation occurs in the Potgietersrus area, north of the Thabazimbi-Murchison Lineament where the complete Transvaal Supergroup has been removed prior to the eruption of the Rooiberg Group lavas. This differential uplift indicates that the northern part of the Kaapvaal Craton was the locus of the Pre-Bushveld uplift and that the uplift was largely controlled by pre-existing crustal lineaments, such as the Thabazimbi-Murchison Lineament. This also indicates that the plume locus was situated towards the northern part of the Kaapvaal Craton and that the Bushveld Complex mafic magmas were derived from intraplated magmas (Schweitzer and Hatton, 1997).

Experimental studies show that a plume will develop a mushroom-shaped head with a likely diameter of between 800 and 1200 km as it reaches the base of the lithosphere (Griffiths and Campbell, 1990). Further flattening, caused by interaction with the lithosphere results in a maximum diameter of 2000 km (White and McKenzie, 1989; Griffiths and Campbell, 1990). Mechanisms of crustal uplift and doming are due to the addition of igneous material to the crust and accompanying density reduction of the upper mantle source reservoir (White and McKenzie, 1989). This uplift precedes magmatism by between 10 and 20 Ma. To remove the entire Transvaal Supergroup thickness of approximately 7000 m in this time would require denudation rates of approximately  $0.35 \text{ mm. yr}^{-1}$  within the northern part of the Kaapvaal Craton.

Geochronology records a 2.0 Ga tectonothermal event within Vredefort Dome (Gibson and Stevens, 1997), the Central Zone of the Limpopo Belt as well as extending into the southern marginal zone on the Kaapvaal Craton and the northern marginal zone on the Zimbabwe Craton (Holzer *et al.*, 1995). Gibson and Stevens (1997) consider the widespread 2.0 Ga event to represent a stage of crustal intraplate magmatism by mafic magmas of Bushveld Complex age and the arrival of a mantle plume at the base of the Kaapvaal Craton.

#### **7.4.2 Bushveld Complex subsidence**

Thermal weakening of the crust, is known to greatly reduce the effective viscosity allowing gravitational collapse at much lower stress levels (Liu and Furlong, 1994). Houseman and England (1986) provided a dynamic model of lithospheric extension in which the continental

lithosphere consists of two layers, crust and mantle lithosphere, each with a density as a linear function of temperature. In this model, impingement on the base of the lithosphere by a hot plume results in an elevation of the lithosphere which produces an increment of vertical stress and a resulting horizontal strain called the stretch factor  $\beta$ .

Crustal sags, failed rifts and passive margins each result from various degrees of extension ( $\beta$ ) and thermal supply time. Due to a lack of extensional faulting, the Bushveld Complex basin has often been likened to that of a true sag basin (Sharpe and Snyman, 1980) with a stretch factor of  $\beta = 1$ . Extensional contact aureole fabrics described in this study as  $S_2$  however, indicate that higher degrees of extension were associated with basin formation than expected for a simple sag basin especially along the Thabazimbi-Murchison Lineament. Extension was largely accommodated by ductile deformation in the contact aureole producing a regional asymmetric basin geometry that approximates that of a half-graben. Fabric development thus also records the duration of the extensional episode.

Liu and Furlong (1994) showed that the lithosphere can reach its minimum strength within a few million years of mafic underplating in the lower crust. In their model, the crust intruded by a 4 km thick mafic sill at between 17 and 20 km depth, would require 1 Ma to reach the minimum strength. Strengthening of the overlying volcanic field occurs within a time of 5 Ma. Very shallow level plume emplacement (10-20 km depths) is also suggested for the Bushveld Complex (Hatton, 1995), implying rapid rates for crustal strength loss and also a short period of time to strengthen the crust. Evidence for short periods of extension, related to fast intrusion rates and shallow level plume impingement are provided by the fact that extensional fabrics in the aureole had occurred before retrograde mineral growth (Chapters 5 and 6). This according to the Jaeger (1968) cooling models limits the extension time to a maximum of approximately 1 Ma, corresponding to the time taken for the lithosphere above the Bushveld plume to reach minimum strength.

Palaeomagnetic studies indicate near horizontal layering in the Rustenburg Layered Suite before most of the subsidence occurred (Hattingh, 1986). Initial accommodation of the magma must therefore have involved a considerable amount of initial roof doming followed by floor subsidence. This would have created a large positive gravity anomaly which then returned



towards a situation of isostatic equilibrium at rates an order of magnitude slower than intrusion rates.

The sunken nature of layered mafic intrusions was investigated by Petraske *et al.* (1978) by using a simple plain-strain theory of elastic plates. They showed that an intrusion of magma along a subhorizontal discontinuity in the lithosphere will deform strata above and below. They found that the amount of downward deflection of the floor is greater the deeper the magma is emplaced. Conversely, the greatest roof deflections are associated with shallow intrusions. They also found that large underburden deflections are also associated with a relatively thin lithosphere. Country-rock response is initially elastic by almost instantaneous emplacement of magma producing both overburden and underburden deflections. With time the country rock deforms viscoelastically due to loading of the intrusion and contact metamorphism.

## **7.5 A DIAPYRIC ORIGIN FOR THE BUSHVELD COMPLEX DOMES**

A feature of the Bushveld Complex is its close association with a range of domal structures (Chapter 1). Based on the evidence from this study and more recent work on the contact aureole the origin of these structures is important in developing emplacement models for the Bushveld Complex. The domes can be classified into three distinct types based on their size, contact metamorphism, deformation and relationship to the Rustenburg Layered Suite. The three structural fold sizes were originally identified by Pretorius (1964) and used by Hunter (1975) and subsequently by Hartzler (1995) to explain the domes associated with the Bushveld Complex. They suggested that the domes resulted from the interference of NW-trending and ENE-trending fold axes of three progressively increasing wavelengths that compliment each other and assist in building antiforms and synforms. In the authors opinion these domes and basins do not conform to any regional trend but are a reflection of three important crustal components on the Kaapvaal Craton and were produced by a combination of high heat flow and gravitational instability on the Kaapvaal Craton during the Bushveld magmatothermal event.

### **7.5.1 Basement domes**

The largest domes range in width between 60 and 120 km and have an average spacing of 120 km. They are found around the margins of the Bushveld Complex and a hidden dome of this

size is considered to occupy the central Bushveld Complex as indicated by the gravity low and the absence of mafic Rustenburg Layered Suite in that area (Cousins, 1959). The size suggests that they form deep crustal flexures affecting the complete thickness of the continental crust, a thickness of approximately 35 km. Contact metamorphism does not appear to have played a part in the dome development. Examples are the Johannesburg, Gaborone and Pietersburg domes and the central dome of the Bushveld Complex. Although the Vredefort Dome is of similar size, it is considered to be of an impact origin and unrelated to the origin of the other domes (Kamo *et al.*, 1995; Reimold and Gibson, 1996). Courtnege *et al.* (1995) have shown that the Johannesburg Dome developed before the Vredefort Dome. They interpreted the Bushveld Complex-age fabrics around the northern margin of the dome as a result of gravitational loading by the Bushveld Complex which produced southward-verging bedding parallel thrusts with movement away from the Bushveld Complex.

#### **7.5.2 Transvaal Supergroup domes**

These domes are smaller than the Basement domes and visibly affect the complete thickness of the Transvaal Supergroup with only minor basement involvement in the doming. They have an average width of approximately 40 km and are characterised by intensely deformed and contact metamorphosed Transvaal Supergroup. Examples are the Dennilton-Marble Hall dome and the Crocodile River dome.

#### **7.5.3 Pretoria Group domes**

These are the smallest domes and are characterised by the diapiric structures described in this thesis. They are only found in the northeastern Bushveld Complex and range in diameter between 6-8 km with an average spacing of approximately 30 km. Only rocks of the Pretoria Group, from contact amphibolite grade upwards, are involved in the deformation.

#### **7.5.4 Diapiric origin for the domes**

The close association of the domes with the Bushveld Complex and recent fabric analysis from the contact aureole shows that the domes are an integral part of syn-Bushveld Complex tectonism. The most likely cause for the development of the large basement domes is that they are a direct response to the disturbed gravity field formed by the Rustenburg Layered Suite and the crustal isostatic response towards equilibrium. Basement doming was further aided by a

higher geothermal gradient and thermal weakening of the lithosphere by the magmatothermal event.

Porphyroblast-matrix relationships from this study, suggest that Bushveld Complex subsidence was concomitant with basement doming to the north (Pietersburg dome) resulting in the top-to-south, down-dip sense of shear in the aureole (extensional). The interpretation by Courtnege *et al.* (1995) however, shows that the Johannesburg dome, although developing during Bushveld Complex time, developed in a compressional top-to-south, up-dip sense of shear.

The larger Transvaal Supergroup domes (Dennilton-Marble Hall and Crocodile River domes) are similarly considered to have developed during Bushveld Complex emplacement. This is contrary to previous interpretations. Hartzler (1995) considered that much of the deformation in the Crocodile River fragment and the Dennilton-Marble Hall dome developed prior to the emplacement of the Bushveld Complex. The reasons given for this are that fold direction interpretations within the domes can be related to regional trends on the Kaapvaal Craton. Although pre-Bushveld deformation of the Transvaal Supergroup is present towards the western margin of the Craton in Botswana (Crockett, 1972), the Transvaal Supergroup preserved on the central Kaapvaal Craton is remarkably undeformed. Deformation of the Transvaal Supergroup immediately preceding Bushveld Complex emplacement was mainly uplift related to the arrival of the Bushveld Complex plume at the base of the crust.

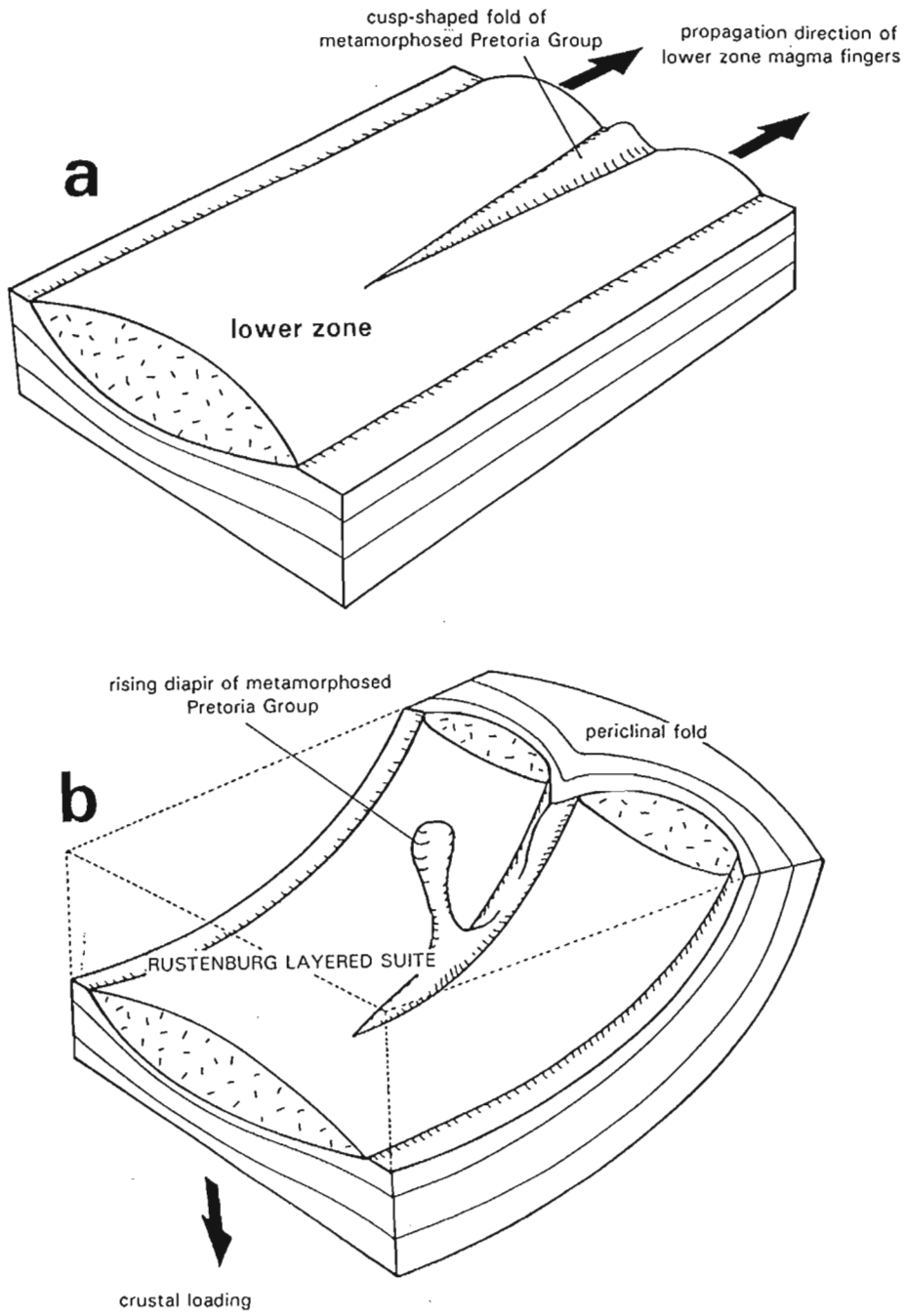
The nature of the internal deformation of these structures can be interpreted as constrictional type folding which produced interference fold structures within a single progressive syn-Bushveld Complex deformation event. The fold orientations are therefore not necessarily related to pre-existing fold orientations found outside the Bushveld Complex.

The Pretoria Group diapirs of the type described from the field area, have not been identified elsewhere in the Bushveld Complex and are considered unique to the northeastern margin of the Bushveld Complex. The truncation of lower zone magmas against the Pretoria Group diapirs suggests that floor doming was initiated in the early stages of Rustenburg Layered Suite emplacement and continued as the magma pile thickened, interacting with the highest levels of the Rustenburg Layered Suite. This mechanism of floor deformation played a major role during

the early part of Bushveld magma chamber development by isolating lower zone magmas into a number of basins, each with a unique succession of ultramafic rocks (Hatton and von Gruenewaldt, 1989). The possible reasons for the unique occurrence of the Pretoria Group diapiric structures is not certain, but it is most likely related to a combination of factors that make this part of the Bushveld Complex aureole unique such as depth of emplacement and the influence of the Thabazimbi-Murchison Lineament.

The Rustenburg Layered Suite can be interpreted as an inverted diapir, the driving force behind the generation of the periclinal structures being the subsidence of the magma chamber into a ductile contact aureole. Backstripping of the Rustenburg Layered Suite in the northeastern Bushveld Complex shows that the emplacement of lower zone magmas was initiated as a series of isolated finger-shaped intrusions separated by interfinger areas (Figure 7.13). These structures are similar to the satellite intrusions of the Rustenburg Layered Suite, the Uitkomst (Gauert *et al.*, 1995) and Uitloop (Nell, 1984) intrusions (Figure 7.15), that occur along base of the Transvaal Supergroup and are well documented from the sills associated with the Shonkin Sag Laccolith, Montana (Pollard *et al.*, 1975). Folds are developed between adjacent intrusion fingers which remain as cusp-shaped folds once the fingers have coalesced into a single sheet (Figure 7.13). During emplacement of the lower zone magmas, deformation of the interfinger zone provided suitable floor perturbations, which formed the loci to subsequent floor diapirism with further magma additions and increased floor ductility.

The structural evolution of the diapirs is shown schematically against the calculated temperature-time profile from the decollement zone near the base of the Pretoria Group (Figure 7.14a). Prograde porphyroblast growth and foliation development is complete in approximately 1 Ma, with retrograde growth occurring later. Regional subsidence is considered to have continued for much longer, controlling Waterberg Group deposition (Figure 7.14b). The evolution of the viscosity contrasts with time are also schematically presented (Figure 7.14c). The viscosity of the Rustenburg Layered Suite increases rapidly with crystallisation. The immediate contact zone (migmatite zone) becomes less viscous than the overlying mafic magmas. At approximately 0.5 Ma after emplacement, conditions at the decollement zone also become less viscous than the Rustenburg Layered Suite. Type A diapirs will tend to form early on, followed by type C diapirs in the final stages of diapiric growth.



**Figure 7.13** Diagram showing the initiation of diapirs in the interfinger areas of the lower zone intrusion. **a)** early lower zone times. **b)** post upper zone times.

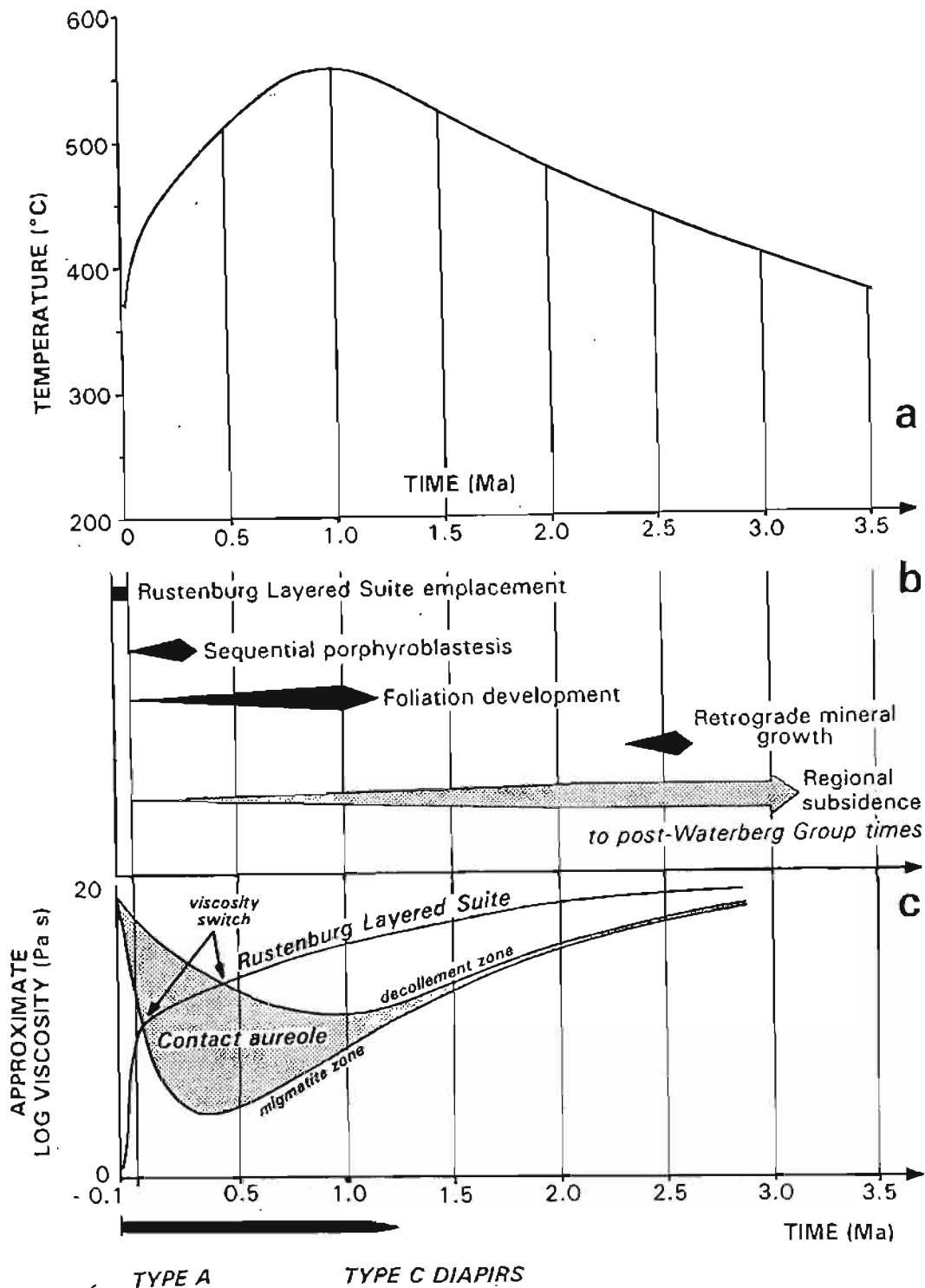


Figure 7.14 a) Temperature-time plot for the decollement zone near the base of the Pretoria Group calculated from the cooling model for the Rustenburg Layered Suite using the program HEAT (Wohletz, 1995). Note that the thermal peak is achieved at approximately 1Ma. b) Summary of process rates. The emplacement of the mafic magmas are an order of magnitude faster than the development of the contact aureole and regional thermal relaxation subsidence rates. c) Viscosity-time relationships between the contact aureole and the Rustenburg Layered Suite based on the data presented in Figure 7.12 and modelled temperature-time profiles. Note that during prograde deformation the relative viscosity contrast changes continuously with aureole diapirs evolving from Type A to Type C geometries.

As shown from kinematic indicators in Chapter 4, the Pretoria Group diapiric structures were growing under extensional conditions. Floor rocks elsewhere in the Bushveld Complex were subjected to compression during syn-Bushveld Complex times (Roering *et al.*, 1990; Courtnage *et al.*, 1995; Harley and Charlesworth, 1991, 1993, 1995). Recent analysis of the world's major basins containing salt diapirs, have shown that all these basins were subjected to extension. Non-extended basins, although having all the ingredients for salt diapirism, were found not to develop diapirs (Jackson and Vendeville, 1994). In these models however, the salt overburden is extended in a brittle manner, producing rifts that trigger the diapirs below.

Rapid subsidence of the Rustenburg Layered Suite along the Thabazimbi-Murchison Lineament possibly provided the extensional regime necessary to trigger diapirism. The diapirs are also mainly confined to the area between the Wonderkop and the Steelpoort Faults. Although no evidence was found for syn-Bushveld Complex movement on these faults, it is not impossible that the present post-Bushveld Complex displacement may have been reactivated from an older fault system. Syn-Bushveld Complex extension may have been accommodated by these structures and in the encompassing area. Maximum extension and subsidence in this area also led to the development of a greater aureole thickness with slower cooling rates than elsewhere, factors that further promoted the development of active deformation and diapirism.

## **7.6 THE BUSHVELD COMPLEX FEEDERS**

Little attention has been given to intrusion mechanisms and the nature of the Rustenburg Layered Suite feeder systems. Hunter (1975) stressed the importance of crustal flexures in locating the Bushveld intrusions, whereas Sharpe *et al.* (1981) suggested that magma chambers developed at the intersection of a Hertzian fracture system, induced by mantle diapirism, with regional lineaments. These regional lineament trends in the eastern Kaapvaal Craton are imparted by mafic dyke swarms of various ages which provide important constraints on the timing of deformation and crustal trends in relation to the eastern Bushveld Complex. Dyke swarms have proven useful in the determination of regional crustal stress patterns through time and may relate to past plate configurations. They also serve as indicators of precursor or terminal events associated with other geological phenomena and can be useful in establishing magma provenance, lithospheric thickness, erosion level and crustal warping (Halls, 1982; 1987).

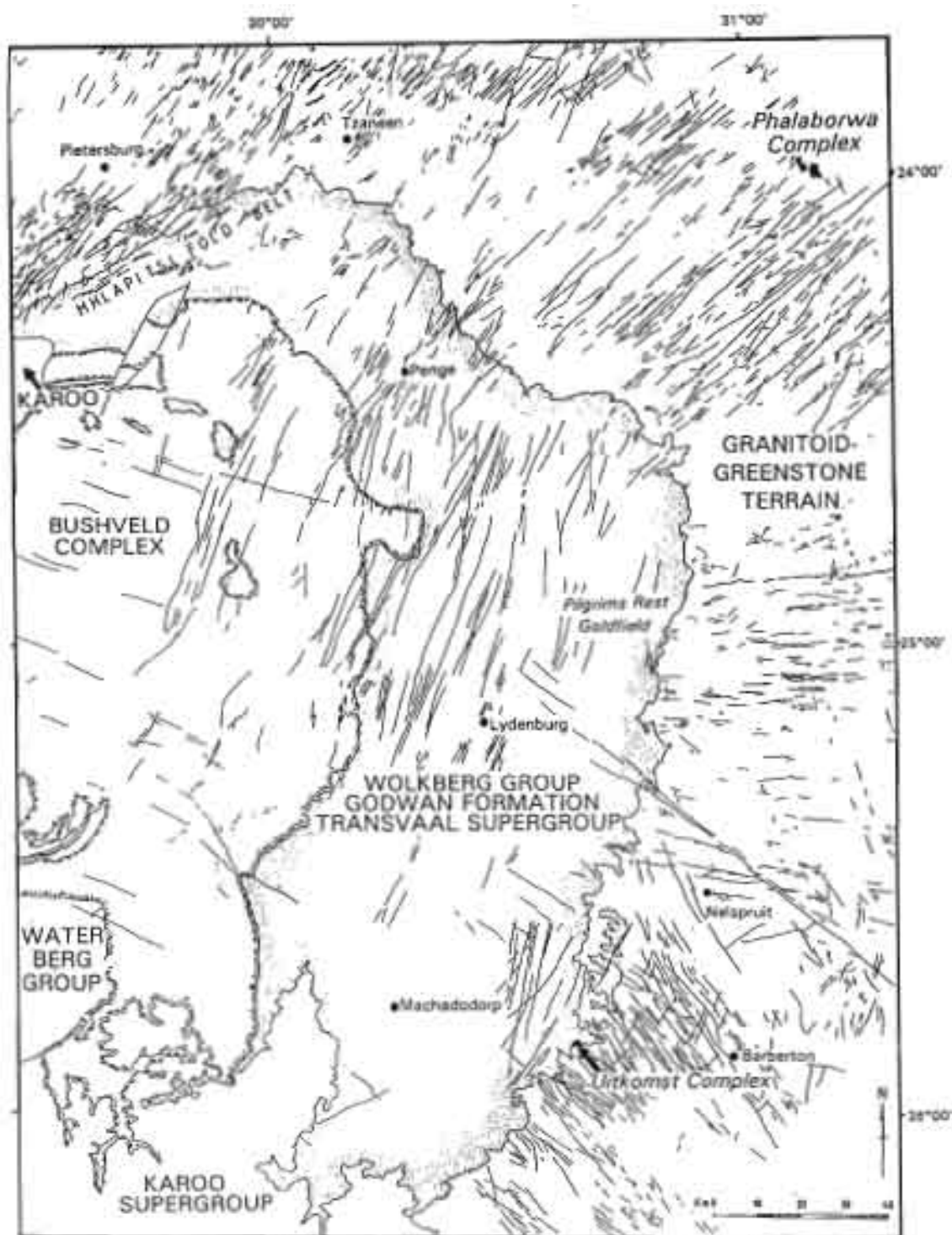
### 7.6.1 EW-trending dykes: a Rustenburg Layered Suite trend

Ernst and Buchan (1997) proposed that large layered complexes are fed by dykes or via pipes spawned from dykes. Uken and Watkeys (1997) suggested that the most likely candidate for such a feeder dyke system was the major EW-trending group of dykes that forms the axis of the Bushveld Complex (Figure 7.15 and 7.16) and extends westwards into the Molopo Farms Complex in Botswana, a layered mafic intrusion of Bushveld Complex age (Wilhelm and Von Gruenewaldt, 1990). A prominent xenolithic dyke, the Rykoppies Dyke, marks the central axis of the diabase dyke swarm (Schutte, 1982; Walraven, 1989) with an age that predates the Timbavati mafic intrusion, dated at  $1450 \pm 50$  Ma (Bristow *et al.*, 1982). The dykes do not cut the Transvaal Supergroup cover and are considered by Hunter and Reid (1987) to be of Archaean age, pre-dating the Transvaal Supergroup.

The onset of magmatic activity at the end of Transvaal Supergroup deposition was initiated by the eruption of the Dullstroom Basalt Formation and felsites of the Rooiberg Group. The maximum thickness of these volcanics is approximately 6000 metres. Associated with the volcanism are numerous diabase and minor felsic sills. In places the sills comprise up to 35 percent of the stratigraphy, a total thickness of approximately 2500 m (Sharpe, 1982). Geochronological data indicate that the Bushveld Complex igneous event began at  $2061 \pm 2$  Ma (Walraven, 1997) marked by the Dullstroom and Rooiberg volcanism (Schweitzer, 1986), and was in part synchronous with the emplacement of the Rustenburg Layered Suite at  $2061 \pm 27$  Ma (Walraven *et al.*, 1990). Although the field relations between the diabase dykes and sills are not clear, it is significant that the only sills occurring at the base of the Transvaal Supergroup are coincident with the EW-trending dyke swarm. To the north and south of the dyke swarm, diabase sills are only found higher up in the Transvaal Supergroup stratigraphy.

An interpretation of gravity data by Sharpe *et al.* (1981) suggested an elliptical distribution of conical-shaped feeder sites to the Bushveld Complex. However, the same gravity data may also be used to model the Rustenburg Layered Suite of the Bushveld Complex as a dipping sheet that becomes narrower and more steeply dipping passing into a vertical dyke at depth (Du Plessis and Kleywegt, 1987). Based on this model the most plausible orientation of Bushveld Complex feeders would be in the EW direction, implying crustal palaeostress patterns with NS extension and EW compression. The most likely source of this crustal deviatoric stress was





**Figure 7.15** Dyke swarm map of the eastern Kaapvaal Craton showing the relationship between dykes, successive supercrustal sequences and the eastern Bushveld Complex (Uken and Watkeys, 1997).

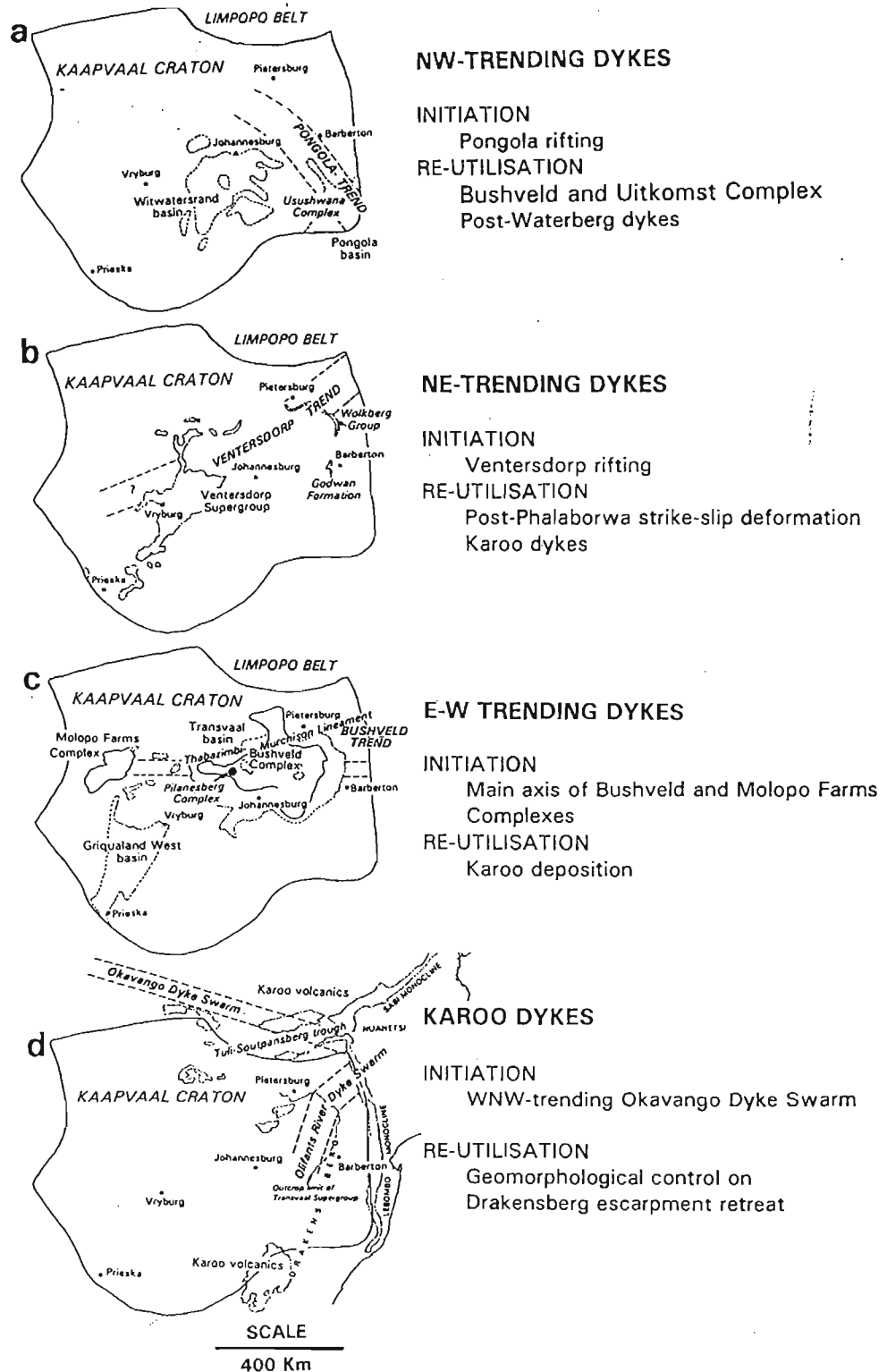


Figure 7.16 Interpretation of dyke swarm ages and trends in terms of their initiation and re-utilisation on the Kaapvaal Craton (Uken and Watkeys, 1997).

produced by the Kheis orogeny (Stowe, 1986; Beukes and Smit, 1987) on the western margin of the Kaapvaal Craton, spanning the time of Bushveld Complex emplacement, at between ~1.9 and ~2.1 Ga (Duane and Kruger, 1991).

A dyke-like Bushveld Complex feeder system that is similar to those exposed in more deeply eroded Proterozoic layered mafic complexes such as the Great Dyke of Zimbabwe (Podmore and Wilson, 1987) and the Jimberlana Complex, western Australia (Campbell *et al.*, 1970) is thus proposed. Both are associated with dyke swarms, and consist of contiguous canoe-shaped layered complexes with dyke-like feeders, within a steeply-dipping V-shaped intrusion (Campbell *et al.*, 1970; McClay and Campbell, 1976; Podmore and Wilson, 1987; Hatton, 1988).

## 7.9 CONCLUSION

The Bushveld Complex metamorphic aureole is a superb natural laboratory to study processes of metamorphism, deformation and magma emplacement. The uniqueness of the Bushveld Complex, in terms of its large size, the relatively shallow and previously undeformed and metamorphosed nature of the country rocks, make it ideal for investigating the interrelationships between emplacement processes and contact metamorphism. These provide an insight into the rates of geologic processes such as magma accumulation and crystallisation; metamorphic processes of nucleation and porphyroblast growth as well as foliation development. The aureole also forms an important time marker in unravelling regional tectonic events.

The recognition of metamorphic diapirs in the Pretoria Group floor further add to the uniqueness of the Bushveld Complex and its contact aureole. These structures have not been found associated with any other large mafic intrusions exposed on the earth's surface and thus provide an end member situation in terms of contact aureole and magma intrusion processes. The range of erosional levels through the diapirs offer a complete cross-section of both the diapir and source layer, making this an ideal area to study progressive deformation in diapiric processes.

This study has shown that the diapirs were initiated on the margins of Rustenburg Layered Suite lower zone magma intrusions, analogous to the fingered intrusions of mafic sills. Regional extension, focussed on the Thabazimbi Murchison Limeament, acted as a trigger for diapiric processes in this part of the Bushveld Complex. Viscosity relations in the contact aureole restricted the growth of diapirs to metamorphic grades above the 550 °C isotherm in the floor. Diapirs were produced by strain rates in the order of  $10^{-14} \text{ s}^{-1}$  giving diapir uplift rates of approximately  $0.6 \text{ cm.yr}^{-1}$ .

Larger Transvaal Supergroup domes and basement domes associated with the Bushveld Complex are further regarded as a product of regional crustal scale deformation. Dyke swarm orientations and lineaments suggest that emplacement of the Bushveld Complex occurred during EW craton-wide compression and NS extension.

## REFERENCES

- Andersen, T.B. (1984). Inclusion patterns in zoned garnets from Magerøy, north Norway. *Mineral. Mag.*, **48**, 21-26.
- Andreoli, M.A.G. (1988). The discovery of a hidden and strange African Orogeny: the Transvaalide Fold Belt. *Abstr., 4th Annual Conference, Tectonics Division, Geol. Soc. S. Afr.*, Silverton, Pretoria, 17.
- Armstrong, R.A., Compston, W., Retief, E.A., Williams, I.S. & Welke, H.J. (1991). Zircon ion microprobe studies bearing on the age and evolution of the Witwatersrand Triad. *Precamb. Res.*, **53**, 243-266.
- Arnold, J. & Sandiford, M. (1990). Petrogenesis of cordierite-orthoamphibole assemblages from the Springton region, South Australia. *Contrib. Mineral. Petrol.* **106**, 100-109.
- Arzi, A.A. (1978). Critical phenomena in the rheology of partially melted rocks. *Tectonophysics*, **44**, 173-184.
- Barker, A.J. (1994). Interpretation of porphyroblast inclusion trails: limitations imposed by growth kinetics and strain rates. *J. metamorphic Geol.*, **12**, 681-694.
- Barton, M.D., Staude, J.-M., Snow, E.A. & Johnson, D.D. (1991). Aureole Systematics. In: Kerrick, D.M. (Ed.), *Contact metamorphism. Reviews in Mineralogy, Min. Soc. Am.*, **26**, 723-846.
- Bastin, H.A. (1968). *Zur tectonic und Stratigraphie am nord-östlichen Bushveld-Rand*. Ph.D. thesis (unpubl.), Technische Hochschule, Aachen, 52pp.
- Batchelor, R.A. & Bowden, P. (1985). Petrogenetic interpretation of granitoid rock series using multicationic parameters. *Chem. Geol.*, **48**, 43-55.
- Bateman, R. (1984). On the role of diapirism in the segregation, ascent and final emplacement of granitoid magmas. *Tectonophysics*, **110**, 211-231.
- Bateman, R. (1985). Aureole deformation by flattening around a diapir during in situ ballooning: The Cannibal Creek granite. *Journal of Geology*, **93**, 293-310.
- Bell, T.H. (1981). Foliation development—the contribution, geometry and significance of progressive bulk inhomogeneous shortening. *Tectonophysics*, **75**, 273-296.
- Bell, T.H. (1985). Deformation partitioning and porphyroblast rotation in metamorphic rocks: a radical reinterpretation. *J. metamorphic Geol.*, **3**, 109-118.
- Bell, T.H. (1986). Foliation development and refraction in metamorphic rocks: reactivation of earlier foliations and decrenulation due to shifting patterns of deformation partitioning. *J. metamorphic Geol.*, **4**, 421-444.
- Bell, T.H., Rubenach, M. J. (1983). Sequential porphyroblast growth and crenulation cleavage during progressive deformation. *Tectonophysics*, **92**, 171-194.
- Bell, T.H. & Johnson, S.E. (1989). Porphyroblast inclusion trails: the key to orogenesis. *J. metamorphic Geol.*, **7**, 279-310.
- Bell, T.H. & Johnson, S.E. (1992). Shear sense: a new approach that resolves conflicts between criteria in metamorphic rocks. *J. metamorphic Geol.*, **10**, 99-124.
- Bell, T.H., Rubenach, M.J. & Flemming, P. D. (1986). Porphyroblast growth and dissolution in regional metamorphic rocks as a function of deformation partitioning during foliation development. *J. metamorphic Geol.*, **4**, 37-67.
- Bell, T.H., Johnson, S.E., Davis, B., Forde, A., Hayward, N., & Wilkins, C. (1992). Porphyroblast inclusion-trail orientation data: eppure non son girate. *J. metamorphic Geol.*, **10**, 295-307.
- Bell, T.H., Hickey, K.A & Wang, J. (1997). Spiral and staircase inclusion trail axes within garnet and staurolite porphyroblasts from schists of the Bolton Syncline, Connecticut: timing of porphyroblast growth and the effects of fold development. *J. metamorphic Geol.*, **15**, 467-478.
- Bence, A.E. & Albee, A.L. (1968). Empirical correction factors for the electron microanalysis of silicates and oxides. *J. Geol.*, **76**, 328-483.
- Beukes, N.J. (1986). The Transvaal Sequence in Griqualand West. In: Anhaeusser, C.R. & Maske, S. (Eds.), *Mineral Deposits of Southern Africa*, I. Geol. Soc. S. Afr., Johannesburg, 819-828.
- Beukes, N.J. & Smit, C.A. (1987). New evidence for thrust faulting in Griqualand West, South Africa: implications for stratigraphy and the age of red beds. *S. Afr. J. Geol.*, **90**, 378-394.
- Beukes, N.J., Klein, C., Kaufmann, A.J. & Hayes, J.M. (1990). Carbonate petrography, kerogene distribution, and carbon and oxygen isotope variations in Early Proterozoic transition from limestone to iron formation deposition, Transvaal Supergroup, South Africa. *Econ. Geol.*, **85**, 663-690.
- Bisschoff, A.A. (1969). *The petrology of the igneous and metamorphic rocks in the Vredefort Dome and adjoining parts of the Pochefstroom Syncline*. Ph.D. thesis (unpubl.), Univ. Pretoria, Pretoria, 230pp.
- Bisschoff, A.A. (1982). Thermal metamorphism in the Vredefort Dome. *Trans. geol. Soc. S. Afr.*, **85**, 43-57.

- Blain, M.R. (1974). The occurrence of andalusite in the lower Daspoort and Timeball Hill shales of the Pretoria Series in the western Transvaal. *Unpubl. Rep. geol. Surv. S. Afr.*, 0086.
- Blain, M.R. (1975). The occurrence of andalusite in the metamorphic aureole of the Bushveld Complex in the Eastern Transvaal. *Unpubl. Rep. geol. Surv. S. Afr.*, 0103.
- Bohlen, S.R. & Essene, G.J. (1980). *Geol. Soc. Am. Bull.*, **91**, 107-109.
- Bosazza, V.L. & Levin, J. (1939). Andalusite from the Marico District. Some experiments on its concentration and use as a refractory. *Bull. Mines. Res. Lab. S. Afr.*, **3**, 18-32.
- Bristow, J.W., Armstrong, R.W. and Allsopp, H.L. (1982). A note on the geology and geochronology of the Tshanga Gabbros. *Trans. geol. Soc. S. Afr.*, **8**, 135-139.
- Brock, B.B. (1956). Structural Mosaics and related concepts. *Trans. geol. Soc. S. Afr.*, **56**, 147-194.
- Brock, B.B. (1957). World Patterns and lineaments. *Trans. geol. Soc. S. Afr.*, **60**, 127-160.
- Brock, B.B. & Pretorius, D.A. (1964). Rand basin sedimentation and tectonics. In: Haughton, S.H. (Ed.), *The geology of some Ore Deposits in Southern Africa*, I. Geol. Soc. S. Afr., Johannesburg, 549-599.
- Bucher, K. & Frey, M. (1994). *Petrogenesis of Metamorphic Rocks*. 6th edition. Springer-Verlag. Berlin 318pp.
- Buddington, A.F. (1959). Granite emplacement with special reference to North America. *Geol. Soc. Amer. Bull.*, **70**, 671-747.
- Buick, I.S., Uken, R., Gibson, R.L. & Wallmach, T. (1998). High  $\delta^{13}\text{C}$  metacarbonates from the Transvaal Supergroup, South Africa: implications for Palaeoproterozoic carbon isotope excursions. *Geology*, **26**, 875-878.
- Burger, A.J. & Coertze, F.J. (1975). Age determinations-April 1972 to March 1974. *Ann. geol. Surv. S. Afr.*, **10**, 135-141.
- Busa, M.D. & Gray, N. H. (1992). Rotated staurolite porphyroblasts in the Littleton Schist at Bolton, Connecticut, USA. *J. metamorphic Geol.*, **10**, 627-636.
- Button, A. (1973). *A regional study of the stratigraphy and development of the Transvaal basin in the eastern and northeastern Transvaal*. Ph.D. thesis (unpubl.), Univ. Witwatersrand, Johannesburg, 352pp.
- Button, A. (1976). Stratigraphy and relations of the Bushveld floor in the eastern Transvaal. *Trans. geol. Soc. S. Afr.*, **79**, 3-12.
- Button, A. (1978). Diapiric structures in the Bushveld, north-eastern Transvaal. *Econ. Geol. Res. Unit, Univ. Witwatersrand, Inf. Circ.*, **123**, 6pp.
- Cameron, E.N. (1978). The lower zone of the eastern Bushveld Complex in the Olifants River trough. *J. Petrol.*, **19**, 437-462.
- Cameron, E.N. (1980). Evolution of the lower critical zone, central sector, eastern Bushveld Complex, and its chromite deposits. *Econ. Geol.*, **75**, 845-871.
- Cameron, E.N. (1982). The upper critical zone of the Bushveld Complex, South Africa. *Econ. Geol.*, **77**, 1307-1327.
- Campbell, I.H., McCall, G.J.H. & Tyrwhitt, D.S. (1970). The Jimberlana norite, Western Australia - a smaller analogue of the Great Dyke of Rhodesia. *Geol. Mag.*, **107**, 1-11.
- Castro, A. (1987). On granitoid emplacement and related structures. A review. *Geol. Rundschau*, **76**, 101-124.
- Cawthorn, R.G. & Biggar, G.M. (1993). Crystallisation of titaniferous chromite, magnesian ilmenite and armalcolite in tholeiitic suites in the Karoo Igneous Province. *Contrib. Mineral. Petrol.*, **114**, 221-235.
- Cawthorn, R.G. & Walraven, F. (1997). The Bushveld Complex: a time to fill and a time to cool. *Economic Geology. Res. Unit, Inf. Circ.*, **307**, Univ. Witwatersrand, Johannesburg, 11pp.
- Chandrasekhar, S. (1955). The character of the equilibrium of an incompressible heavy viscous fluid of variable density. *Proc. Camb. Philos. Soc.*, **51**, 162-178.
- Cheney, E.S. & Twist, D. (1988). The conformable emplacement of the Bushveld mafic magmas along a regional unconformity. *Ext. Abstr., Geocongress '88, 22nd Earth Science Congress*, Geol. Soc. S. Afr., Durban, 465-467.
- Cheney, E.S. & Twist, D. (1991). The conformable emplacement of the Bushveld mafic rocks along a regional unconformity in the Transvaal succession of South Africa. *Precamb. Res.*, **52**, 115-132.
- Cheney, E.S., Roering, C. & Stettler, E. (1988). Vaalbara. *Ext. Abstr., Geocongress '88, 22nd Earth Science Congress*, Geol. Soc. S. Afr., Durban, 85-88.
- Cheney, E.S., Roering, C. & Winter, H. de la R. (1990). The Archaean-Proterozoic boundary in the Kaapvaal province of Southern Africa. *Precamb. Res.*, **46**, 329-340.
- Clemens, J.P. & Mawer, C.K. (1992). Granitic magma transport by fracture propagation. *Tectonophysics*, **204**, 339-360.

- Clemens, J.P., Petford, N. & Mawer, C.K. (1997). Ascent mechanisms of granitic magmas: Causes and consequences. In: *Deformation-Enhanced Fluid Transport in the Earth's Crust and Mantle*. Holness, M.B. (Ed.). The Mineralogical Society Series, **8**, Chapman and Hall, 145-172.
- Clendenin, C.W. (1989). *Tectonic influence on the evolution of the Early Proterozoic Transvaal Sea, southern Africa*. Ph.D. thesis (unpubl.), Univ. Witwatersrand, Johannesburg, 367pp.
- Clendenin, C.W., Charlesworth, E.G. & Maske, S. (1988). An early Proterozoic three stage rift system, Kaapvaal Craton, South Africa. *Tectonophysics*, **145**, 73-86.
- Clendenin, C.W., Henry, G. & Charlesworth, E.G. (1991). Characteristics of and influences on the Black Reef depositional sequence in the eastern Transvaal. *S. Afr. J. Geol.*, **94**, 321-328.
- Clubley-Armstrong, A.R. & Sharpe, M.R. (1979). The structural evolution of the Dennilton Dome and its relationship to the intrusion of the Bushveld Complex. *Trans. geol. Soc. S. Afr.*, **82**, 23-36.
- Cobbold, P.R., Cosgrove, J.W. & Summers, J.M. (1971). The development of internal structures in deformed anisotropic rocks. *Tectonophysics*, **12**, 23-53.
- Coertze, F.J. (1974). The geology of the basic portion of the Western Bushveld Igneous Complex. *Geol. Surv. S. Afr. Mem.*, **66**, 147pp.
- Coertze, F.J., Jansen, H. & Walraven, F. (1977). The transition from the Transvaal Sequence to the Waterberg Group. *Trans. geol. Soc. S. Afr.*, **80**, 145-156.
- Coetzee, H. & Kruger, J. (1992). Monitoring the cooling of the Bushveld Complex using the Rb-Sr method on garnets from Transvaal shales. *Abstracts, 24th Congress of the Geological Society of South Africa, Bloemfontein*, 76-78.
- Cornel, D.H., Armstrong, R.A. & Walraven, F. (1998). Geochronology of the Proterozoic Hartley Basalt Formation, South Africa: Constraints on the Kheis tectogenesis and the Kaapvaal Craton's earliest Wilson Cycle. *J. Afr. Earth Sci.*, **26**, 5-27.
- Courtnage, P.M., Gibson, R.L., Charlesworth, E.G. & Andreoli, M.A.G. (1995). Post-Transvaal Deformation between the Johannesburg Dome and the Bushveld Complex. *Ext. Abstr., Centennial Geocongress*, Geol. Soc. S. Afr., Johannesburg, 287-290.
- Cousins, C.A. (1959). The structure of the mafic portion of the Bushveld Complex. *Trans. geol. Soc. S. Afr.*, **62**, 179-201.
- Coward, M.P. (1981). Diapirism and gravity tectonics: report of a Tectonic Studies Group conference held at Leeds University, 25-26 March 1980. *J. Struct. Geol.*, **3**, 89-95.
- Cox, K.G. (1989). The role of mantle plumes in the development of continental drainage patterns. *Nature*, **342**, 873-876.
- Crockett, R.N. (1971). Some aspects of post-Transvaal System tectogenesis in southeastern Botswana with particular reference to the Lobatse and Ramotswa areas. *Trans. geol. Soc. S. Afr.*, **74**, 211-235.
- Crockett, R.N. (1972). The Transvaal System in Botswana: Its geotectonic and depositional environment and special problems. *Trans. geol. Soc. S. Afr.*, **75**, 275-291.
- Cruden, A.R. (1988). Deformation around a rising diapir modeled by creeping flow past a sphere. *Tectonics*, **7**, 1091-1101.
- Cruden, A.R. (1990). Flow and fabric development during the diapiric rise of magma. *J. Geol.*, **98**, 681-698.
- Currie, K.L. (1971). The reaction  $3 \text{ cordierite} = 2 \text{ garnet} + 4 \text{ sillimanite} + 5 \text{ quartz}$  as a geological thermometer in the Opinicon Lake region, Ontario. *Contrib. Mineral. Petrol.*, **33**, 215-226.
- Dallmeyer, R.D. (1974). Metamorphic history of the northeastern Reading Prong, New York and northern New Jersey. *J. Petrol.*, **15**, 325-359.
- Daly, R.A. (1928). *Our Mobile Earth*. Charles Scribner, New York. 342p.
- De la Roche, H., Leterrier, J., Grand Claude, P. & Marchal, M. (1980). A classification of volcanic and plutonic rocks using R1 - R2 diagrams and major element analyses - its relationships with current nomenclature. *Chem. Geol.*, **34**, 183-210.
- De Waal, S.A. (1970). Interference folding of Bushveld Complex age in the Transvaal System north of Marble Hall. *Spec. Publ. geol. Soc. S. Afr.*, **1**, 283-298.
- De Wit, M.J., Jones, M.G. & Buchanan, D.L. (1992a). The geology and tectonic evolution of the Pietersburg Greenstone Belt, South Africa. *Precambrian Research*, **55**, 123-153.
- De Wit, M.J., Roering, C., Hart, R.J., Armstrong, R.A., De Ronde, C.E.J., Green, R.W.E., Tredoux, M., Peberdy, E. & Hart, R.A. (1992b). Formation of an Archaean continent. *Nature*, **357**, 553-562.
- Dietvorst, E.J.L. (1991). Instability and basin formation on the Kaapvaal Craton, southern Africa. *J. Afr. Earth Sci.*, **13**, 359-365.
- Dietz, R.S. (1961). Vredefort Ring Structure: meteorite impact scar? *J. Geol.*, **69**, 499-576.

- Dietz, R.S. (1963). Vredefort Ring-Bushveld complex impact event and lunar maria. *Spec. Pap. Geol. Soc. Am.*, **73**, 35pp.
- Dixon, J.M. & Summers, J.M. (1985). Recent developments in centrifuge modelling of tectonic processes: equipment, model construction techniques and rheology of model materials. *J. Struct. Geol.*, **7**, 83-102.
- Dreyer, C.J.B. (1982). *Amphibole asbestos in South Africa*. Ph.D. thesis (unpubl.), Rand Afrikaans University, Johannesburg, 295pp.
- Duane, M.J. & Kruger, F.J. (1991). Geochronological evidence for tectonically driven brine migration during the Early Proterozoic Kheis orogeny of Southern Africa. *Geophys. Res. Lett.*, **18**, 975-978.
- Duane, M.J., Kruger, F.J., Roberts, P.J. & Smith, C.B. (1991). Pb and Sr isotope and origin of Proterozoic base metal (fluorite) and gold deposits, Transvaal Sequence, South Africa. *Econ. Geol.*, **86**, 1491-1505.
- Duncan, A.R., Erlank, A.J. & Betton, P.J. (1984). Appendix 1. Analytical techniques and database descriptions. In: Erlank, A.J. (Ed.), *Petrogenesis of the Volcanic Rocks of the Karoo Province*. *Spec. Publ. geol. Soc. S. Afr.*, **13**, 389-395.
- Du Preez, J.W. (1944). The structural geology of the area east of Thabazimbi and the genesis of the associated iron ores. *Ann. Univ. Stellenbosch*, **43**, 263-360.
- Du Plessis, C.P. (1987). New perspectives on early Waterberg Group sedimentation from the Gatkop area, northwestern Transvaal. *S. Afr. J. Geol.*, **90**, 395-408.
- Du Plessis, C.P. & Clendenin, C.W. (1988). The Bobbejaanwater Fault System south of Thabazimbi, western Transvaal. *S. Afr. J. Geol.*, **91**, 97-105.
- Du Plessis, A. & Kleywegt, R.J. (1987). A dipping sheet model for the mafic lobes of the Bushveld Complex. *S. Afr. J. Geol.*, **90**, 1-6.
- Du Plessis, C.P. & Walraven, F. (1990). The tectonic setting of the Bushveld Complex in southern Africa, Part 1. Structural deformation and distribution. *Tectonophysics*, **179**, 305-319.
- Dymoke, P. & Sandiford, M. (1992). Phase relationships in the Buchan facies series pelitic assemblages: calculations with application to the andalusite-staurolite paragenesis in the Mount Lofty Ranges, South Australia. *Contrib. Mineral. Petrol.*, **110**, 121-132.
- Elston, W.E. (1995). Bushveld Complex and Vredefort Dome: The case for multiple-impact origin. *Ext. Abstr., Centennial Geocongress*, Geol. Soc. S. Afr., Johannesburg, **1**, 504-507.
- Engelbrecht, J.P. (1976). Metasediments of the Pretoria Group in the Enselburg area, Marico District. *Trans. geol. Soc. S. Afr.*, **79**, 61-75.
- Engelbrecht, J.P. (1988). *Die Bosveld Komplex en sy Vloergesteentes in die omgewing van Nietverdiend West-Transvaal*. Ph.D. thesis (unpubl.), Univ. of Pretoria, 327pp.
- Engelbrecht, J. P. (1990a). The Marico Hypabyssal Suite, and the marginal zone of the Bushveld Complex in the Marico District, western Transvaal, South Africa. *S. Afr. J. Geol.*, **93**, 318-328.
- Engelbrecht, J.P. (1990b). Contact metamorphic processes related to the aureole of the Bushveld Complex in the Marico District, western Transvaal, South Africa. *S. Afr. J. Geol.*, **93**, 339-349.
- England, R.W. (1990). The identification of granitic diapirs. *J. Geol. Soc. London*, **147**, 931-933.
- Eriksson, P.G. (1988). A palaeoenvironmental review of the Pretoria Group, Transvaal Sequence. *Ext. Abstr., Geocongress '88, 22nd Earth Science Congress*, Geol. Soc. S. Afr., Durban, 187-190.
- Eriksson, P.G. & Clendenin, C.W. (1990). A review of the Transvaal Sequence, South Africa. *J. Afr. Earth Sci.*, **10**, 101-116.
- Eriksson, P.G., Schreiber, U.M. & Van der Neut, M. (1991). A review of the sedimentology of the Early Proterozoic Pretoria Group, Transvaal Sequence, South Africa: implications for tectonic setting. *Precambrian sedimentary basins of Southern Africa*. Terra Nova Abstr. Suppl., **3**, 12.
- Eriksson, P.G., Schweitzer, J.K., Bosch, P.J.A., Schreiber, U.M., Van Devender, J.L. & Hatton, C.J. (1993). The Transvaal Sequence: an overview. *J. Afr. Earth Sci.*, **16**, 25-51.
- Eriksson, P.G. & Reczko, B.F.F. (1995). The sedimentary and tectonic setting of the Transvaal Supergroup floor rocks to the Bushveld Complex. *J. Afr. Earth Sci.*, **21**, 487-504.
- Ernst, R.E. & Buchan, K.L. (1997). Layered mafic intrusions: a model for their feeder systems and relationship with giant dyke swarms and mantle plume centres. *S. Afr. J. Geol.*, **100**, 319-334.
- Evans, B.W. and Guidotti, C.V. (1966). The sillimanite -potash feldspar isograd in western Maine, USA. *Contrib. Mineral. Pet.*, **12**, 25-62.
- Ferry, J.F. & Spear, F.S. (1978). Experimental calibration of the partitioning of Fe and Mg between biotite and garnet. *Contrib. Mineral. Petrol.*, **66**, 123-117.
- Fleuty, M.J. (1964). The description of folds. *Proc. Geol. Assoc.*, **75**, 461-489.



- Furlong, K.P., Hanson, R.B. & Bowers, J.R. (1991). Modeling thermal regimes. *In: Contact Metamorphism* (Ribbe, P.H. (Ed.), *Reviews in Mineralogy*, **26**, Mineralogical Society of America, 437-506.
- Fyfe, W.S. (1969). Some second thoughts on  $Al_2O_3$ - $SiO_2$ . *Chem Geology*, **2**, 67-76.
- Ganguly, J. & Kennedy, G.C. (1974). The energetics of natural garnet solid solution 1. Mixing of the aluminosilicate end-members. *Contrib. Mineral. Petrol.* **48**, 137-148.
- Gau, W.J. (1907). Geological notes on a portion of the Bushveld in the neighbourhood of the junction of the Elands and Olifants rivers. *Joh. Trans. geol. Soc. S. Afr.*, **XI**, (1906), 67-73.
- Gastil, R.G., Phillips, R.P., & Allison, E.C. (1975) Reconnaissance geology of the state of Baja, California. *Geol. Soc. Amer. Memoir*, **140**, 170pp.
- Gauert, C.D.K., De Waal, S.A. & Wallmach, T. (1995). Geology of the ultrabasic to basic Uitkomst Complex, eastern Transvaal, South Africa: an overview. *J. Afr. Earth Sci.*, **21**, 553-570.
- Ghosh, S.K., Khan, D. & Sengupta, S. (1995). Interfering folds in constrictional deformation. *J. Struct. Geol.*, **17**, 1361-1373.
- Gibson, R.L. (1992). Sequential, syndeformational porphyroblast growth during Hercynian low-pressure/high-temperature metamorphism in the Canigou massif, Pyrenees. *J. metamorphic Geol.*, **10**, 637-650.
- Gibson, R.L. (1993). When is a hornfels a hornfels? Metapelitic rocks from the lower Witwatersrand Supergroup, Vredefort Dome, South Africa. *S. Afr. J. Geol.*, **96**, 42-48.
- Gibson, R.L. & Stevens, G. (1997). Regional metamorphism due to anorogenic intracratonic magmatism. *Econ. Geol. Res. Unit Inf. Circ. No. 311*, University of the Witwatersrand, Johannesburg.
- Gibson, R.L. & Stevens, G. (1998). Regional metamorphism due to anorogenic intracratonic magmatism. *In: Treloar, P.J. & O'Brien, P.J. (Eds.) What Drives Metamorphism and Metamorphic Reactions?* *Geol. Soc. London Spec. Publ.*, **138**, 121-135.
- Gibson, R.L. & Wallmach, T. (1995). Low pressure-high temperature metamorphism in the Vredefort Dome, South Africa: anticlockwise pressure-temperature path followed by rapid decompression. *Geological Journal*, **30**, 319-331.
- Good, N. & De Wit, M.J. (1997). The Thabazimbi-Murchison Lineament of the Kaapvaal Craton, South Africa: 2700 Ma of episodic deformation. *J. Geol. Soc. London*, **154**, 93-97.
- Gough, D.I. & Van Niekerk, C.B. (1959). A study of Palaeomagnetism of the Bushveld gabbro. *Philos. Mag.*, **4**, 126-136.
- Griffiths, R.W. & Campbell, I.H. (1990). Stirring and structure in mantle starting plumes. *Earth and Planetary Science Letters*, **99**, 66-78.
- Hälbich, I.W., Lamprecht, D.F., Altermann, W. & Horstmann, U.E. (1992). A carbonate-banded iron formation in the early Proterozoikum of South Africa. *J. Afr. Earth Sci.*, **15**, 217-236.
- Hälbich, I.W., Scheepers, R.S., Lamprecht, D., Van Deventer, J.N. & de Kock, N.J. (1993). The Transvaal-Griqualand West banded iron formation: geology, genesis, iron exploitation. *J. Afr. Earth Sci.*, **16**, 63-120.
- Hall, A.L. (1907). The Geology of the Central Portion of the Lydenburg District between Lydenburg and Belvedere. *Pret. Ann. Rep. geol. Surv. Transvaal*, (1906), 75-100.
- Hall, A.L. (1932). The Bushveld Igneous Complex of the Central Transvaal. *Mem. geol. Surv. S. Afr.*, **28**, 386-420.
- Halls, H.C. (1982). The importance and potential of mafic dyke swarms in studies of geodynamic processes. *Geosci. Can.*, **9**, 145-154.
- Halls, H.C. (1987). Dykes swarms and continental rifting: Some concluding remarks. Halls H.C. and W.F. Fahrig (Eds.), *Mafic Dyke Swarms Volume*. *Geol. Assoc. Can. Spec. Pap.*, **34**, 483-491.
- Hamilton, W. (1970). Bushveld Complex - product of impacts? *Spec. Publ. geol. Soc. S. Afr.*, **1**, 367-379.
- Hamilton, P.J. (1977). Sr-isotope and trace element studies of the Great Dyke and Bushveld mafic phase and their relation to early Proterozoic magmatic genesis in Southern Africa. *J. Petrol.*, **18**, 24-52.
- Hammerbeck, E.C.I. (1986). Andalusite in the metamorphic aureole of the Bushveld Complex. *In: Anhaeusser, C.R. & Maske, S. (Eds.), Mineral Deposits of Southern Africa*, **1**. *Geol. Soc. S. Afr.*, Johannesburg, 993-1004.
- Harker, A. (1950). *Metamorphism: A study of the Transformation of Rock-Masses*. Methuen and Co. Ltd., London 362pp.
- Harley, M. & Charlesworth, E.G. (1991). Compressive deformation in a pre-Bushveld sill, Sudwala, eastern Transvaal. *S. Afr. J. Geol.*, **94**, 348-354.
- Harley, M. & Charlesworth, E.G. (1993). Formation of bedding-parallel, thrust-hosted gold deposits, Sabie-Pilgrims Rest goldfield, eastern Transvaal: The role of fluid pressure. *Inform. Circ. Econ. Geol. Res. Unit, Univ. Witwatersrand, Johannesburg*, **262**, 19pp.

- Harley, M. & Charlesworth, E.G. (1995). Structural development and controls to epigenetic mesothermal gold mineralization in the Sabie-Pilgrims Rest goldfield, eastern Transvaal, South Africa. *Ext. Abstr., Centennial Geocongress*, Geol. Soc. S. Afr., Johannesburg, **I**, 73-76.
- Harmer, R.E. & Von Gruenewaldt, G. (1991). A review of magmatism associated with the Transvaal Basin - implications for its tectonic setting. *S. Afr. J. Geol.*, **94**, 104-122.
- Harte, B. & Hudson, N.F.C. (1979). Pelite facies series and the temperatures and pressures of Dalradian metamorphism in E Scotland. In: The Caledonides of the British Isles. In: Harris, A.L., Holland, C.H. & Leake, B.E. (Eds.), *Geol. Soc. London Spec. Publ.*, **8**, 323-336.
- Hartzer, F.J. (1988). Die Geologie van die Krokodilrivierfragment, Transvaal. *Bull. geol. Surv.*, **92**, 93pp.
- Hartzer, F.J. (1989). Stratigraphy, structure and tectonic evolution of the Crocodile River Fragment. *S. Afr. J. Geol.*, **92**, 110-124.
- Hartzer, F.J. (1995). Transvaal Supergroup inliers: geology, tectonic development and relationship with the Bushveld Complex, South Africa. *J. Afr. Earth Sci.*, **21**, 521-547.
- Hatch, F.H. (1905). The Geology of the Marico District. *Trans. geol. Soc. S. Afr.*, **VII**, (1904) 1-6.
- Hattingh, P.J. (1980). The structure of the Bushveld Complex in the Groblersdal-Lydenberg-Belfast area of the eastern Transvaal. *Trans. geol. Soc. S. Afr.*, **83**, 125-133.
- Hattingh, P. J. (1986). The palaeomagnetism of the main zone of the Bushveld Complex. *Tectonophysics*, **124**, 271-295.
- Hatton, C.J. (1988). Formation of the Bushveld Complex at a plate margin. *Ext. Abstr., Geocongress '88, 22nd Earth Science Congress*, Geol. Soc. S. Afr., Durban, 251-254.
- Hatton, C.J. (1989). Continental configuration during the formation of the Bushveld Complex. *Abstr., 28th International Geol. Congr.*, Washington, **2**, 40.
- Hatton, C.J. (1995). Primary magmas in the Ventersdorp and Bushveld Igneous Provinces: Magma Extraction from a Lower Mantle Plume. *Centennial Geocongress. Extended Abstracts*. Geol. Soc. S. Afr. Rand Afrikaans University, **1**, 520-521.
- Hatton, C.J. & Schweitzer, J.K. (1995). Evidence for synchronous extrusive and intrusive Bushveld magmatism. *J. Afr. Earth Sci.*, **21**, 579-594.
- Hatton, C.J. & Von Gruenewaldt, G. (1987). The geological setting and petrogenesis of the Bushveld chromitite layers. In: Stowe, C.W., (Ed.), *Guidelines to the Evolution of Chromite Ore Fields*. Hutchinson and Ross, Stroudsburg, 109-143.
- Hatton, C.J. & Von Gruenewaldt, G. (1989). Early Precambrian layered intrusions. In: Hall, R.P. & Hughes, D.J. (Eds.), *Early Precambrian Basic Magmatism*. Blackie and Son, New York, 56-82.
- Hensen, B.J. & Green, D.H. (1971). Experimental study of the stability of cordierite and garnet in pelitic compositions at high pressures and temperatures. I. Compositions with excess aluminosilicate. *Contrib. Mineral. Petrol.*, **33**, 309-330.
- Hensen, B.J. & Green, D.H. (1973). Experimental study of the stability of cordierite and garnet in pelitic compositions at high pressures and temperatures. III. Synthesis of experimental data and geological applications. *Contrib. Mineral. Petrol.*, **38**, 151-166.
- Hensen, B.J. (1977). Cordierite-garnet bearing assemblages as geothermometers and barometers in granulite facies terranes. *Tectonophysics*, **43**, 73-88.
- Hilliard, P. (1994). *The structural evolution of the Johannesburg Dome, Kaapvaal Craton, South Africa*. M.Sc thesis (unpubl.), Univ. Pretoria, Pretoria, 99pp.
- Hilliard, P. (1997). *Structural evolution and tectonostratigraphy of the Kheis Orogen and its relationship to the southwestern margin of the Kaapvaal Craton*. PhD thesis (unpubl.), Univ. Durban-Westville, Durban, 229pp.
- Hodges, K.V. & Spear, F.S. (1982). Geothermometry, geobarometry and the Al<sub>2</sub>SiO<sub>5</sub> triple point at Mt. Moosilauke, New Hampshire. *Amer. Mineral.*, **67**, 1118-1134.
- Holdaway, M.J. (1976). Mutual compatibility relations of the Fe<sup>+2</sup>-Mg-Al silicates at 800°C and 3kb. *Am. J.Sci.*, **276**, 285-308.
- Holdaway, M.J. & Lee, S.M. (1977). Fe-Mg cordierite stability in high-grade pelitic rocks based on experimental, theoretical and natural observations. *Contrib. Mineral. Petrol.* **63**, 175-198.
- Holland, T.J.B. & Powel, R. (1990). An enlarged and updated internally consistent thermodynamic dataset with uncertainties and corrections: the system K<sub>2</sub>O-Na<sub>2</sub>O-CaO-MgO-MnO-FeO-Al<sub>2</sub>O<sub>3</sub>-TiO<sub>2</sub>-SiO<sub>2</sub>-C-H<sub>2</sub>-O<sub>2</sub>. *J. metamorphic Geol.*, **8**, 89-124.
- Hollister, L.S. (1966). Garnet zoning - an interpretation based on the Rayleigh fractionation model. *Science* **154**, 1647-1651.

- Hollister, L.S. & Crawford, M.L. (1986). Melt-enhanced deformation: a major tectonic process. *Geology*, **14**, 558-561.
- Holmes, G.G. (1906). The Geology of part of the Rustenburg District. *Joh. Trans. geol. Soc. S. Afr.*, **VIII**, (1905) 167-174.
- Holzer, L., Kamber, B.S., Kramers, J.D. & Frei, R. (1995). The tectono-metamorphic event at 2 Ga in the Limpopo Belt and the resetting behaviour of chronometers at high temperature. *Communs geol. Surv. Namibia*, **10**, 129-140.
- Houseman, G. & England, P.C. (1986). A dynamical model of lithosphere extension and sedimentary basin formation. *J. Geophys. Res.*, **91**, 719-729.
- Hulbert, L.J. & Sharpe, M.R. (1981). Metamorphics Project. *Inst. Geol. Res. Bushveld Complex, Univ. Pretoria, Ann. Rep.*, **980**, 30-32.
- Human, D.R. (1975). The geology and metamorphic petrology of part of the basal argillaceous zone, Daspoort Stage, Pretoria Series on the Farm Havercroft, North Eastern Transvaal. *Petros*, **6**, 25-43.
- Human, D.R. & Collins, L.A. (1986). The Havercroft-Streatham Andalusite Deposit, Eastern Transvaal. In: Anhaeusser, C.R. & Maske, S., (Eds.), *Mineral Deposits of Southern Africa*. I. Geol. Soc. S. Afr., Johannesburg, 1005-1008.
- Hunter, D.R. (1974). Crustal development of the Kaapvaal Craton. Part II: The Proterozoic. *Precamb. Res.*, **1**, 295-326.
- Hunter, D.R. (1975). *The regional geological setting of the Bushveld Complex. (An adjunct to the provisional Tectonic map of the Bushveld Complex)*. Wainwright, E.H. (Ed.), Econ. Geol. Res. Unit. Univ. Witwatersrand. 18pp.
- Hunter, D.R. (1976). Some enigmas of the Bushveld Complex. *Econ. Geol.*, **71**, 229-248.
- Hunter, D.R. & Hamilton, P.J. (1975). The Bushveld Complex. In: Tarling, D.H. (Ed.), *Evolution of the Earth's Crust*. Academic Press, London, 107-103.
- Hunter, D.R. & Reid, D.L. (1987). Mafic dyke swarms in southern Africa. Hall, H.C. and Fahrig, W. F. (Eds.), *Mafic Dyke Swarms Volume*. Geol. Assoc. Can. Spec. Pap., **34**, 445-456.
- Irvine, T.N. (1970). Heat transfer during solidification of layered intrusions. I. Sheets and sills. *Can. J. Earth Sci.*, **7**, 1031-1061.
- Jackson, M.P.A. & Talbot, C.J. (1986). External shapes, strain rates, and dynamics of salt structures. *Geol. Soc. Am. Bull.*, **97**, 305-323.
- Jackson, M.P.A. & Talbot, C.J. (1989). Anatomy of mushroom-shaped diapirs. *J. Struct. Geol.*, **11**, 211-230.
- Jackson, M.P.A. & Vendeville, B.C. (1994). Regional extension as a geologic trigger for diapirism. *Geol. Soc. Amer. Bull.*, **106**, 57-73.
- Jaeger, J.C. (1957). The temperature in the neighborhood of a cooling intrusive sheet. *Amer. J. Sci.*, **255**, 306-318.
- Jaeger, J.C. (1959). Temperatures outside a cooling intrusive sheet. *Amer. J. Sci.*, **257**, 44-54.
- Jaeger, J.C. (1961). The cooling of irregularly shaped igneous bodies. *Amer. J. Sci.*, **259**, 721-734.
- Jaeger, J.C. (1964). Thermal effects of intrusions. *Rev. Geophysics*, **2**, 443-466.
- Jaeger, J.C. (1968). Cooling and solidification of igneous rocks. In: H.H. Hess and Plodervaart, A. (Eds.), *Basalts*, Interscience, Wiley, New York, **2**, 503-536.
- Jansen, H. (1970). Volcanic rocks and associated sediments in the southern portion of the Waterberg basin. *Ann. geol. Surv. S. Afr.*, **78**, 25-33.
- Jansen, H. (1975). Precambrian basins on the Transvaal Craton and their sedimentological and structural features. *Trans. geol. Soc. S. Afr.*, **78**, 25-33.
- Joesten, R. & Fisher, G. (1988). Kinetics of diffusion-controlled mineral growth in the Christmas Mountains (Texas) contact aureole. *Bull. Geol. Soc. Am.*, **100**, 714-732.
- Johnson, S.E. (1990). Lack of porphyroblast rotation in the Otago schists, New Zealand: implications for crenulation development, folding and deformation partitioning. *J. metamorphic Geol.*, **8**, 13-30.
- Johnson, S.E. (1992). Sequential porphyroblast growth during progressive deformation and low-P high-T (LPHT) metamorphism, Cooma Complex, Australia: the use of microstructural analysis in better understanding deformation and metamorphic histories. *Tectonophysics*, **214**, 311-339.
- Johnson, S.E. (1993a). Unravelling the spirals: a serial thin-section study and three dimensional computer-aided reconstruction of spiral-shaped inclusion trails in garnet porphyroblasts. *J. metamorphic Geol.*, **11**, 621-634.
- Johnson, S.E. (1993b). Testing models for the development of spiral-shaped inclusion trails in garnet porphyroblasts: to rotate or not to rotate, that is the question. *J. metamorphic Geol.*, **11**, 635-659.

- Kamo, S.L., Reimold, W.U., Krogh, T.E. & Colliston, W.P. (1995). Shocked zircons in Vredefort pseudotachylite and the U-Pb zircon age of the Vredefort impact event. *Ext. Abstr., Centennial Geocongress*, Geol. Soc. S. Afr., Johannesburg, 1, 566-569.
- Kaneko, Y. & Miyano, T. (1990). Contact metamorphism by the Bushveld Complex in the northeastern Transvaal, South Africa. *J. Min. Pet. and Economic Geol.* **85**, 66-81.
- Kerrick, D.M. (1987). Fibrolite in contact aureoles of Donegal, Ireland. *Amer. Mineral.*, **72**, 240-254.
- Kerrick, D.M. (1990). The  $Al_2SiO_5$  polymorphs: *Mineral. Soc. Am. Rev. Mineral.*, **72**, 406pp.
- Kerrick, D.M. & Speer, J.A. (1988). The role of minor element solid solution on the andalusite-sillimanite equilibrium in metapelites and peraluminous granitoids. *Amer. J. Sci.*, **288**, 152-192.
- Kerrick, D.M. & Woodsworth, G.J. (1989). Aluminum silicates in the Mount Raleigh pendant, British Columbia. *J. metamorphic Geol.*, **7**, 547-563.
- Kirby, S.H. (1983). Rheology of the lithosphere. *Rev. Geophys. Space Phys.*, **21**, 1458-1487.
- Klein, C. & Beukes, N.J. (1989). Geochemistry and sedimentology of facies transition from limestone to Iron-Formation deposition in the Early Proterozoic Transvaal Supergroup, South Africa. *Econ. Geol.*, **84**, 1733-1774.
- Klemm, D.D. (1991). The Formation of highly concentrated iron ore bodies within the BIF. The Sishen case. In: Pagel, M. & Leory, J.L. (Eds.), *Source, transport and deposition of metals*. Balkema, Rotterdam. 63-64.
- Kouchi, A., Sugawara, Y., Kashima, K. & Sunagawa, I. (1983). Laboratory growth of sector-zoned clinopyroxenes in the system  $CaMgSi_2O_6$ - $CaTiAl_2O_6$ . *Contrib. Mineral. Petrol.*, **83**, 177-184.
- Kretz, R. (1983). Symbols for rock-forming minerals. *Amer. Mineral.* **68**, 277-279.
- Kruger, F.J. & Marsh, J.S. (1982). Significance of  $^{87}Sr/^{86}Sr$  ratios in the Merensky cyclic unit of the Bushveld Complex. *Nature*, **298**, 53-55.
- Kruger, F.J., Cawthorn, R.G., Meyer, P.S. & Walsh, K.C. (1986). Sr-isotopic, chemical and mineralogical variations across the pyroxenite marker and in the Upper Zone of the Bushveld Complex. *Ext. Abstr., Geocongress '86*, Geol. Soc. S. Afr., Johannesburg, 609-612.
- Lang, H. M. & Dunn, G.R. (1990). Sequential porphyroblast growth during deformation in a low-pressure metamorphic terrain, Orrs Island-Harpswell Neck, Maine. *J. metamorphic Geol.*, **8**, 199-216.
- Lapinsky, L. (1981). *An electron microprobe investigation of some rocks from the Bushveld Complex contact aureole*. M.Sc. thesis (unpubl.), Univ. Natal, Durban, 222pp.
- Leube, A. (1960). Structural control in the Rooiberg tinfields (South Africa). *Trans. geol. Soc. S. Afr.*, **63**, 265-282.
- Lister, G.S. & Snoke, A.W. (1984). S-C Mylonite. *J. Struct. Geol.* **6**, 617-638.
- Liu, M. & Furlong, K.P. (1994). Intrusion and underplating of mafic magmas: thermal-rheological effects and implications for Tertiary tectonism in the North American Cordillera. *Tectonophysics*, **237**, 175-187.
- Mahar, E.M., Baker, J.M., Powel, R., Holland, T.J.B. & Howell, N. (1997). The effect of Mn on mineral stability in metapelites. *J. metamorphic Geol.*, **15**, 223-238.
- Marsh, B.D. (1981). On the crystallinity, probability of occurrence, and rheology of lava and magma. *Contrib. Mineral. Petrol.*, **78**, 85-98.
- Marsh, B.D. (1989). Magma Chambers. *Ann. Rev. Earth Planet Sciences*, 439-474.
- Matthews, P.E. (1988). Breccia sheets and dykes: evidence of hydraulic fracturing in Palaeozoic Natal Group sandstones near Durban, Natal. *Ext. Abstr., Geocongress '88, 22nd Earth Science Congress*, Geol. Soc. S. Afr., Durban, 387-389.
- Marlow, A. G. & Van der Merwe, M. J. (1977). The geology and the potential economic significance of the Malope area, north-eastern Bushveld Complex. *Trans. geol. Soc. S. Afr.*, **80**, 117-123.
- Martin, D.McB., Charlesworth, E.G., Clendenin, C.W., Maske, S. & De Gasparis, A.A. (1988). The nature and influences of the Thabazimbi-Murchison Line, west of Thabazimbi, on a number of Early Proterozoic basins. *Ext. Abstr., Geocongress '88, 22nd Earth Science Congress*, Geol. Soc. S. Afr., Durban, 383-386.
- Martini, J.E.J. (1992). The metamorphic history of the Vredefort dome at approximately 2 Ga as revealed by coesite-stishovite-bearing pseudotachylites. *J. metamorphic Geol.*, **10**, 517-527.
- Master, S. (1990). Bolide Impact, Subduction and the Bushveld Complex: An Hypothesis. *Ext. Abstr., Annual Conference*, Tectonics Division Geol. Soc. S. Afr., Pretoria, 1-2.
- Master, S. (1991). *The origin and controls on the distribution of copper and precious metal mineralization at the Mangula and Norah Mines, Mhangura, Zimbabwe*. PhD thesis (unpubl.), Univ. Witwatersrand, Johannesburg, 385pp.
- McCarthy, T.S., Charlesworth, E.G. & Stanistreet, I.G. (1986). Post-Transvaal structural features of the northern portion of the Witwatersrand Basin. *Trans. geol. Soc. S. Afr.*, **89**, 311-324.

- McClay, K.R. & Campbell, I.H. (1976). The structure and shape of the Jimberlana intrusion, Western Australia, as indicated by an investigation of the Bronzite Complex. *Geol. Mag.*, **113**, 129-139.
- McCourt, S. & Vearncombe, J.R. (1987). Shear zones bounding the central zone of the Limpopo Mobile Belt, Southern Africa. *J. Struct. Geol.*, **9**, 127-138.
- McCourt, S. & Vearncombe, J.R. (1992). Shear zones of the Limpopo Belt and adjacent granitoid-greenstone terranes: implications for late Archaean collision tectonics in southern Africa. *Precambrian Res.*, **55**, 553-570.
- McLellan, E.L. (1982). Problems of structural analysis in migmatitic terranes. In: Atherton, M.P. & Gribble, C.D. (Eds.), *Migmatites, Melting and Metamorphism*. Shiva, Cheshire, 299-302.
- Meinster, B. (1974). Thrusting and block-faulting around Gatkop east of Thabazimbi, Transvaal. *Ann. geol. Surv. S. Afr.*, **10**, 57-72.
- Mellor, E.T. (1908). The geology of the Hoekbergen in the Waterberg District, including Gatkop. *Ann. Rep. geol. Surv., Transvaal*.
- Misch, P. (1971). Porphyroblasts and 'crystallisation force': some textural criteria. *Geol. Soc. Am. Bull.*, **88**, 245-251.
- Miyano, T., Beukes, N.J. & Van Reenen, D.D. (1987). Metamorphic evidence for early post-Bushveld sills in the Penge Iron Formation, Transvaal Sequence, eastern Transvaal. *S. Afr. J. Geol.*, **90**, 37-43.
- Molengraaff (1894) in Hall, A.L. (1932). The Bushveld Igneous Complex of the Central Transvaal. *Mem. geol. Surv. S. Afr.*, **28**, 386-420.
- Molengraaff (1906) in Hall, A.L. (1932). The Bushveld Igneous Complex of the Central Transvaal. *Mem. geol. Surv. S. Afr.*, **28**, 386-42
- Molyneux, T.G. & Klinkert, P.S. (1978). A structural interpretation of part of the eastern mafic lobe of the Bushveld Complex and its surrounds. *Trans. geol. Soc. S. Afr.*, **81**, 359-368.
- Müller, R.F. (1972). Stability of biotite: a discussion. *Amer. Mineral.*, **57**, 300-316.
- Murase, T. & McBirney, A.R. (1973). Properties of some common igneous rocks and their melts at high temperature. *Geol. Soc. Am. Bull.*, **84**, 3563-3592.
- Myers, R.E. (1990). *The Geology of the Godwan Basin, Eastern Transvaal*. Ph.D. thesis (unpubl.), Univ. Witwatersrand, Johannesburg, 320pp.
- Nell, J. (1984). *Geochemical and Thermodynamic Controls in the formation of mineral assemblages from the metamorphic Aureole of the Bushveld Complex in the Potgietersrus area*. M.Sc. thesis (unpubl.), Univ. Pretoria, Pretoria, 332pp.
- Nell, J. (1985). The Bushveld metamorphic aureole in the Potgietersrus area: Evidence for a two-stage metamorphic event. *Econ. Geol.*, **80**, 1129-1152.
- Nicolaysen, L.O. & Ferguson, J. (1990). Cryptoexplosion structures, shock deformation and siderophile concentration related to explosive venting of fluids associated with alkaline ultramafic magmas. *Tectonophysics*, **191**, 303-335.
- Norrish, K. & Hutton, J.J. (1969). An accurate X-ray spectrographic method for analysis of a wide range of geological samples. *Geochim. Cosmochim. Acta*, **33**, 431-453.
- Partridge, F.C. (1934). The andalusite sands of the western Transvaal. *Bull. geol. Surv. S. Afr.*, **2**, 16pp.
- Parrisch, D.K., Krivz, A.L. & Cater, N.L. (1976). Finite element folds of similar geometry. *Tectonophysics*, **32**, 183-207.
- Passchier, C.W., Trouw, R.A.J., Zwart, H.J. & Vissers, R.L.M. (1992). Porphyroblast rotation: eppur si muove? *J. Metamorphic Geol.*, **10**, 283-294.
- Passchier, C.W. & Trouw, R.A.J. (1996). *Microtectonics*. Springer-Verlag, Berlin Heidelberg, 289pp.
- Paterson, S.R. (1988). Cannibal Creek Granite: post-tectonic 'ballooning' pluton or pre-tectonic piercement diapir? *J. Geol.*, **96**, 730-736.
- Paterson, S.R. & Fowler, T.K.J. (1993). Re-examining pluton emplacement processes. *J. Struct. Geol.*, **15**, 191-206.
- Paterson, S.R. & Tobisch, O.T. (1992). Rates of processes in magmatic arcs: implications for the timing and nature of pluton emplacement and wall rock deformation. *J. Struct. Geol.*, **14**, 291-300.
- Paterson, S.R., Tobisch, O. T. & Vernon, R.H. (1991). Emplacement and deformation of granitoids during volcanic arc construction in the Foothills terrane, central Sierra Nevada, California. *Tectonophysics*, **191**, 89-110.
- Paterson, S.R., Vernon, R.H., Fowler, Jr., T.K. (1991). Aureole Tectonics. In: Contact Metamorphism. Kerrick, D.M. (Ed.), *Reviews in Mineralogy*, Min. Soc. Am., **26**, 672-722.
- Pattison, D.R.M. & Harte, B. (1985). A petrogenetic grid for pelites in the Ballachulish and other Scottish thermal aureoles. *J. Geol. Soc London*, **142**, 7-28.

- Pattison, D.R.M. & Harte, B. (1991). Petrography and mineral chemistry of pelites. In: Voll, G., Topel, J., Pattison, D.R.M. & Seifert, F. (Eds.), *Equilibrium and kinetics in contact metamorphism: The Ballachulish Igneous Complex and its aureole*. Springer Verlag, Heidelberg.
- Pattison, D.R.M. & Tracy, R.J. (1991). Phase equilibria and thermobarometry of metapelites. In: Contact Metamorphism. Kerrick, D.M. (Ed.), *Reviews in Mineralogy*, Min. Soc. Am., **26**, 105-182.
- Pearce, J.A., Harris, N.W. & Tindle, A.G. (1984). Trace element discrimination diagrams for the tectonic interpretation of granitic rocks. *J. Petrol.*, **25**, 956-983.
- Petford, N. (1996). Dikes or diapirs. *Trans. Royal Soc. Edinburgh: Earth Sciences*, **87**, 105-114.
- Petrasko, A.K., Hodge, D. & Shaw, R. (1978). Mechanics of emplacement of basic intrusions. *Tectonophysics*, **46**, 41-63.
- Perchuk, L.L. (1977). Thermodynamic control of metamorphic processes. In: Saxena, S.K. & Bhattacharji, S. (Eds.), *Energetics of Geological Processes*. Springer Verlag, New York, 285-352.
- Pfiffner, O.A. & Ramsay, J.G. (1982). Constraints on geologic strain rates: arguments from finite strain states of naturally deformed rocks. *J. Geophys. Res.*, **87**, 311-321.
- Pitcher, P.S. & Berger, A.R. (1972). *The geology of Donegal: a study of granite emplacement and unroofing*. Wiley, New York, 435pp.
- Platt, J.P. & Vissers, R.L.M. (1980). Extensional structures in anisotropic rocks. *J. Struct. Geol.* **2**, 397-410.
- Podmore, F. & Wilson, A.H. (1987). A reappraisal of the structure, geology and emplacement of the Great Dyke, Zimbabwe. In: Hall, H.C. & Fahrig, W.F. (Eds.), *Mafic Dyke Swarms Volume*. Spec. Pap. Geol. Assoc. Can., **34**, 317-330.
- Pollard, D.D., Muller, O.H. & Dockstader, D.R. (1975). The form and growth of fingered sheet intrusions. *Geol. Soc. Am. Bull.*, **86**, 351-363.
- Potgieter, G.J. (1988). The Structural Evolution of the Transvaal rocks of the area between Potgietersrus and the Murchison Range. *Ext. Abstr., Geocongress '88*. Geol. Soc. S. Afr., Durban, 465-467.
- Potgieter, G. (1991). Inversion tectonics along the northeastern boundary of the Transvaal basin. *Precambrian sedimentary basins of Southern Africa*. Terra Nova Abstr. Suppl., **3**, 32.
- Powell, R. & Holland, T. (1990). Calculated mineral equilibria in the pelitic system KFMASH (K<sub>2</sub>O-FeO-MgO-Al<sub>2</sub>O<sub>3</sub>-SiO<sub>2</sub>-H<sub>2</sub>O). *Amer. Mineral.*, **75**, 367-380.
- Pretorius, D.A. (1964). The geology of the Central Rand Goldfield. In: Haughton, S.H. (Ed.), *The Geology of some Ore deposits in Southern Africa*. Geol. Soc. S. Afr., Johannesburg, 62-108.
- Price, N.J. & Cosgrove, J.W. (1990). *Analysis of geological structures*. Cambridge University Press, Cambridge. 502pp.
- Quandling, K. & Cawthorn, R.G. (1994). The layered gabbro-norite sequence, Main Zone, eastern Bushveld Complex. *S. Afr. J. Geol.*, **97**, 442-454.
- Ramberg, H. (1963). Experimental study of gravity tectonics by means of centrifuged models. *Bull. Geol. Inst. Univ. Uppsala*, **42**, 1-97.
- Ramberg, H. (1970). Model studies in relation to intrusion of plutonic bodies. *Geol. J. Spec. Issue*, **2**, 261-286.
- Ramberg, H. (1981). Gravity, Deformation and the Earth's Crust. Academic Press, London, 452pp.
- Ramsay, J.G. (1967). *Folding and fracturing of rocks*. McGraw-Hill, New York, 568pp.
- Ramsay, J.G. (1980). Shear zone geometry: a review. *J. Struct. Geol.* **2**, 83-99.
- Ramsay, J.G. & Huber, M.I. (1983). *The techniques of modern structural geology. Volume 1: Strain Analysis*. Academic Press, London, 307pp.
- Reimold, W.U. (1993). A review of the geology of and deformation related to the Vredefort structure, South Africa. *J. geol. Edu.*, **41**, 106-117.
- Reimold, W.U. & Gibson, R.L. (1996). Geology and evolution of the Vredefort Impact Structure, South Africa. *J. Afr. E. Sci.*, **23**, 125-162.
- Reinhardt, J. & Rubenach, M.J. (1989). Temperature-time relationships across metamorphic zones: evidence from porphyroblast-matrix relationships in progressively deformed metapelites. *Tectonophysics*, **158**, 141-161.
- Reischmann, T. (1995). Precise U/Pb age determination with baddeleyite (ZrO<sub>2</sub>), a case study from the Phalaborwa Igneous Complex, South Africa. *S. Afr. J. Geol.*, **98**, 1-4.
- Rhodes, R.C. (1975). New evidence for impact origin of the Bushveld Complex. *Geology*, **3**, 549-554.
- Rhodes, R.C. & Du Plessis, M.D. (1976). Notes on some stratigraphic relations in the Rooiberg Felsite. *Trans. geol. Soc. S. Afr.*, **79**, 183-185.
- Rice, A. H. N. & Mitchell, J. I. (1991). Porphyroblast textural sector-zoning and matrix displacement. *Mineral. Mag.*, **55**, 379-396.

- Ridley, J. (1986). Modeling of the relations between reaction enthalpy and the buffering of reaction progress in metamorphism. *Mineralog. Mag.*, **50**, 375-384.
- Roering, C., Barton, J.M. & Winter, H. de la R. (1990). The Vredefort structure: A perspective with regard to new tectonic data from adjoining terranes. *Tectonophysics*, **171**, 7-22.
- Saggerson, E.P. (1974). Porphyroblastesis and displacement: some new textural criteria from pelitic hornfels. *Mineral. Mag.*, **39**, 793-797.
- Saggerson, E.P. & Turner, L.M. (1992). Metamorphic Map of the Republics of South Africa, Transkei, Bophuthatswana, Venda and Ciskei and the Kingdoms of Lesotho and Swaziland. *Dept. of Mineral and Energy Affairs, Geol. Surv. S. Afr.*
- Saggerson, E.P. & Turner, L.M. (1995). A Review of metamorphism in the Republic of South Africa and the kingdoms of Lesotho and Swaziland. Expl: 1:1 000 000 scale Metamorphic Map, *Geol. Sur. S. Afr.*, 285pp.
- Saxena, S.K. (1969). Silicate solid solutions and geothermometry. 3. Distribution of Fe and Mg between coexisting garnet and biotite. *Contrib. Mineral. Petrol.*, **22**, 259-267.
- Schoneveld, C. (1977). A study of typical inclusion patterns in strongly paracrystalline rotated garnets. *Tectonophysics*, **39**, 453-460.
- Schreyer, W. (1983). Metamorphism and fluid inclusions in the basement of the Vredefort Dome, South Africa: guidelines to the origin of the structure. *J. Petrology*, **24**, 26-47.
- Schutte, I.C. (1982). Eerste verslag oor die geologie van die suid-sentrale gedeelte, Nasionale Krugerwildtuin. *S. Afr. Geol. Surv. Rep.* (unpubl.), 25pp.
- Schweitzer, J. (1986). The geochemical transition from the Dullstroom Basalt Formation to the Rooiberg Felsite Group. *Inst. Geol. Res. Bushveld Complex, University of Pretoria, Annu. Rep.*, 1985, 72-81.
- Schweitzer, J.K. & Hatton, C.J. (1997). Sedimentary rocks at the base of the Ventersdorp and Bushveld plume events. *Abstracts, Precambrian sedimentation systems, 23 October 1997, Sedimentology Division of the Geological Society of South Africa.*
- Schweitzer, J.K., Hatton, C.J. & De Waal, S.A. (1995). Regional lithological stratigraphy of the Rooiberg Group, upper Transvaal Supergroup: A proposed new subdivision. *S. Afr. J. Geol.*, **98**, 245-255.
- Schwellnus, J.S.I. (1956). *The basal portion of the Bushveld Igneous Complex and the adjoining metamorphosed sediments in the northeastern Transvaal.* D.Sc. dissertation (unpubl.), Univ. Pretoria, Pretoria, 207pp.
- Schwellnus, J.S.I., Engelbrecht, L.N.J., Coertze, F.J., Russel, H.D., Malherbe, S.J., Van Rooyen, D.P. & Cooke, R. (1962). The geology of the Olifants River area, Transvaal. Expl: 1:250 000 scale Sheet 2429B Chuniespoort and 2430A Wolkberg. *Geol. Surv. S. Afr.*, 87pp.
- Schwerdtner, W.M. (1990). Structural tests of diapir hypothesis in Archean crust of Ontario. *Canadian. J. Earth Sci.*, **27**, 387-402.
- Selig, F. (1965). A theoretical prediction of salt dome patterns. *Geophysics*, **30**, 633-643.
- Sengor, A.M.C. & Burke, K. (1978). Relative timing of rifting and volcanism on earth and its tectonic implications. *Geophys. Res. Lett.*, **5**, 419-421.
- Sharpe, M. R. (1982). Petrography and Chronology of intrusion of Mafic Sills beneath the eastern Bushveld Complex. *Inst. Geol. Res. Bushveld Complex, Res. Rept.*, **37**, 51 pp.
- Sharpe, M.R. (1984). Petrography, classification and chronology of mafic sill intrusions beneath the eastern Bushveld Complex. *Bull. geol. Surv. S. Afr.*, **77**, 40pp.
- Sharpe, M.R. (1985). Strontium isotope evidence for preserved density stratification in the main zone of the Bushveld Complex, South Africa. *Nature*, **316**, 119-126.
- Sharpe, M.R. (1986). Eastern Bushveld Complex Excursion Guidebook. *Ext. Abstr., Geocongress '86*, Geol. Soc. S. Afr., Johannesburg, 135pp.
- Sharpe, M.R., Bahat, D. & Von Gruenewaldt, G. (1981). The concentric elliptical structure of feeder sites to the Bushveld Complex and possible economic implications. *Trans. geol. Soc. S. Afr.*, **84**, 239-244.
- Sharpe, M.R., Brits, R.J.N. & Engelbrecht, J.P. (1983). Rare earth and trace element evidence pertaining to the petrogenesis of 2.3 Ga old continental andesites and other volcanic rocks from the Transvaal Sequence, South Africa. *Inst. Geol. Res. Bushveld Complex, Univ. Pretoria, Res. Rep.*, **40**, 63pp.
- Sharpe, M.R. & Chadwick, B. (1981). The geometry and origin of structures in certain Transvaal Sequence rocks within and adjacent to the eastern compartment of the Bushveld Complex. *Inst. Geol. Res. Bushveld Complex, Res. Rep.*, **27**, 19pp.
- Sharpe, M.R. & Chadwick, B. (1982). Structures in Transvaal Sequence rocks within and adjacent to the eastern Bushveld Complex. *Trans. Geol. Soc. S. Afr.*, **86**, 29-41.

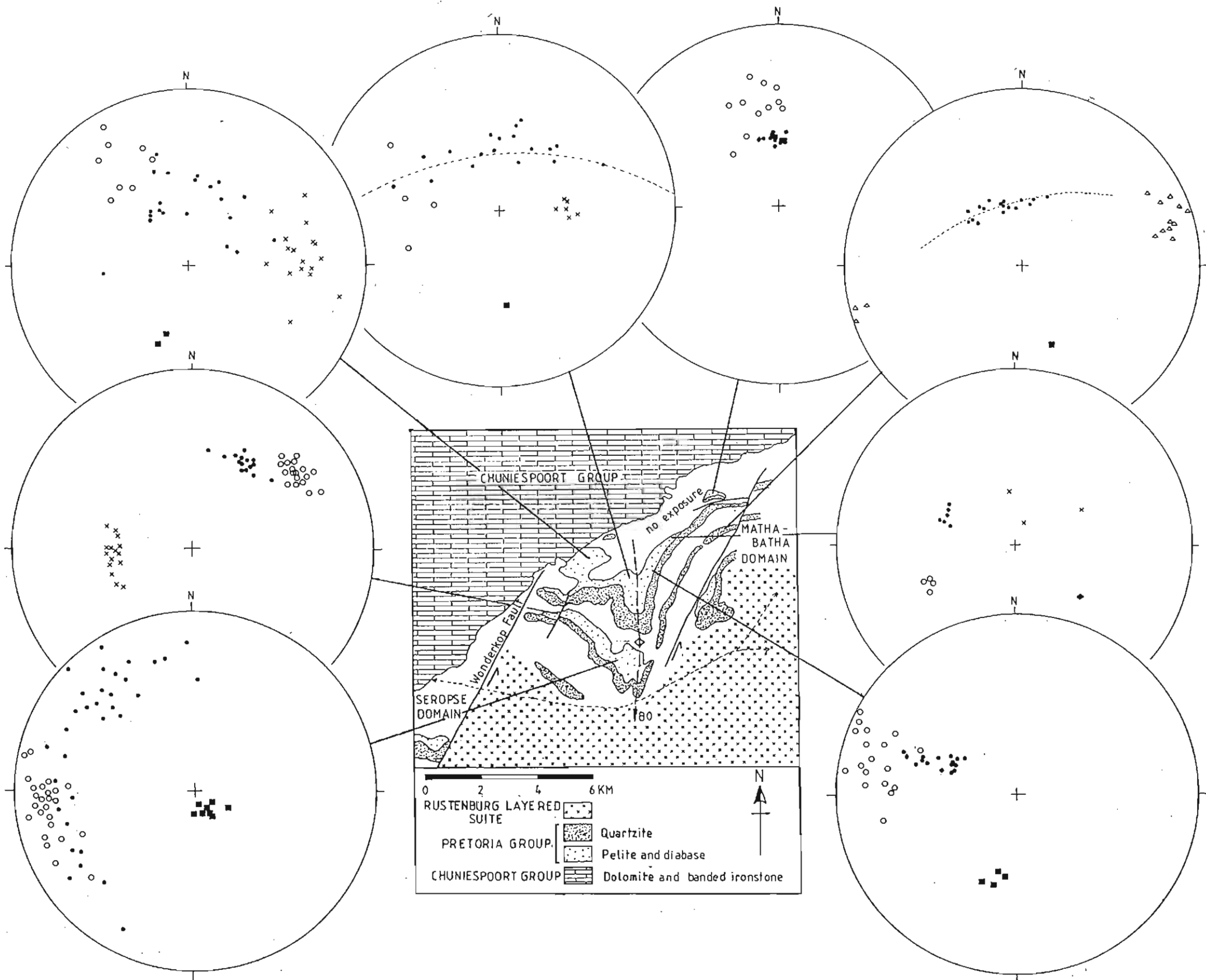
- Sharpe, M.R., Everson, N.M. & Naldrett, A.J. (1986). Sm/Nd and Rb/Sr isotopic evidence for liquid mixing, magma generation and contamination in the eastern Bushveld Complex. *Ext. Abstr., Geocongress '86*, Geol. Soc. S. Afr., Johannesburg, 621-624.
- Sharpe, M.R. & Snyman, J.A. (1980). A model for the emplacement of the eastern compartment of the Bushveld Complex. *Tectonophysics*, **65**, 85-110.
- Shaw, D.M. (1956). Geochemistry of pelitic rocks. Part III: Minor elements and general geochemistry. *Geol. Soc. America Bull.*, **67**, 919-935.
- Smit, C.A., Roering, C. & Van Reenen, D.D. (1992). The structural framework of the southern margin of the Limpopo Belt, South Africa. *Precambrian Res.*, **55**, 51-67.
- Smith, D.B. (1996). Deformation in the late Permian Boulby Halite (EZ3Na) in Teeside, NE England. In: Alsop, G.I., Blundell, D.J. & Davidson, I. (Eds.), *Salt Tectonics*, Geological Society Special Publication No. **100**, 77-87.
- Snyman, C.P. (1958). 'n Gneis, 'n Koepelstruuktur en die metamorphose van die Sisteem Transvaal suid van Marble Hall, Transvaal. *Trans. geol. Soc. S. Afr.*, **61**, 225-262.
- South African Committee for Stratigraphy (SACS), (1980). Stratigraphy of South Africa. Part 1 (Comp. L.E.Kent). *Lithostratigraphy of the Republic of South Africa, South West Africa/Namibia, and the Republics of Bophuthatswana, Transkei and Venda*: Handb. Geol. Surv. S. Afr., **8**.
- South African Geological Survey & Department of Mines. (1978). 1:250 000 scale geological series. 2428 Nylstroom.
- South African Geological Survey & Department of Mineral and Energy Affairs. (1986). 1:250 000 scale geological series. 2430 Pilgrims Rest.
- Spear, F.S. & Cheney, J.T. (1989). A petrogenetic grid for pelitic schists in the system  $\text{SiO}_2\text{-Al}_2\text{O}_3\text{-FeO-MgO-K}_2\text{O-H}_2\text{O}$ . *Contrib. Mineral. Petrol.*, **101**, 149-164.
- Spencer, R.M. (1986). A model for the tectonic evolution of the South Rand Basin. *Ext. Abstr., Geocongress '86*, Geol. Soc. S. Afr., Johannesburg, 63-66.
- Spry, A. (1969). *Metamorphic Textures*. Pergamon Press, New York, 352pp.
- Spry, A. (1972). Porphyroblasts and 'crystallisation force': some new textural criteria: discussion. *Geol. Soc. Am. Bull.*, **88**, 1201-1202.
- Spry, A. (1974). Spherically arranged inclusions in post-tectonic garnet porphyroblasts: a comment. *Mineral. Mag.*, **39**, 723-724.
- Stanistreet, I.G., McCarthy, T.S., Charlesworth, E.G., Meyers, R.G. & Armstrong, R.A. (1986). Pre-Transvaal wrench tectonics along the northern margin of the Witwatersrand Basin, South Africa. *Tectonophysics*, **131**, 53-74.
- Stear, W.M. (1976). *The geology and ore controls of the Northern Rooiberg Tin-field, Transvaal*. M.Sc. thesis (unpubl.), Stellenbosch University, Stellenbosch, South Africa, 89pp.
- Stepo, D. (1990). The geology and gravity field in the central core of the Vredefort structure. *Tectonophysics*, **171**, 75-103.
- Stevens, G., Gibson, R.L. & Droop, G.T.R. (1996). Polyphase granulite metamorphism in the Vredefort Dome: A window into the deep Kaapvaal Craton at 2.06 Ga. *Inform. Circ. Econ. Geol. Res. Unit, Univ. Witwatersrand, Johannesburg*, **297**, 27pp.
- Stowe, C.W. (1986). Synthesis and interpretation of structures along the north-eastern boundary of the Namaqua tectonic province, South Africa. *Trans. geol. Soc. S. Afr.*, **89**, 185-189.
- Stowe, C.W. (1993). Compositions and tectonic settings of chromite deposits through time. *Inf. Circ. Precambrian Res. Unit, Univ. of Cape Town*, **10**, 25pp.
- Stowe, C.W. (1994). Compositions and tectonic setting of chromite deposits through time. *Econ. Geol.*, **89**, 528-546.
- Strutt, J.W., Lord, Rayleigh (1900). *Investigation of the Character of the Equilibrium of an Incompressible Heavy Fluid of Variable Density*. Cambridge University Press, **2**, Cambridge, Scientific Papers, **2**, 200-207.
- Suppe, J. (1989). Rates of fault slip and fault growth. *Geol. Soc. Am. Abs. W. Prog.*, **21**, A28.
- Talbot, C.J. (1992). Centrifuged models of Gulf of Mexico profiles. *Marine and Petroleum Geology*, **9**, 412-432.
- Talbot, C.J. & Jackson, M.P.A. (1987). Internal Kinematics of Salt Diapirs. *Bull. Am. Assoc. Pet. Geol.*, **71**, 1068-1093.
- Talbot, C.J. & Sokoutis, D. (1992). The importance of incompetence. *Geology*, **20**, 951-953.
- Tankard, A.J., Jackson, M.P.A., Eriksson, K.A., Hobday, D.K., Hunter, D.R. & Minter, W.E.L. (1982). *Crustal Evolution of Southern Africa*. Springer-Verlag, New York, U.S.A., 523pp.



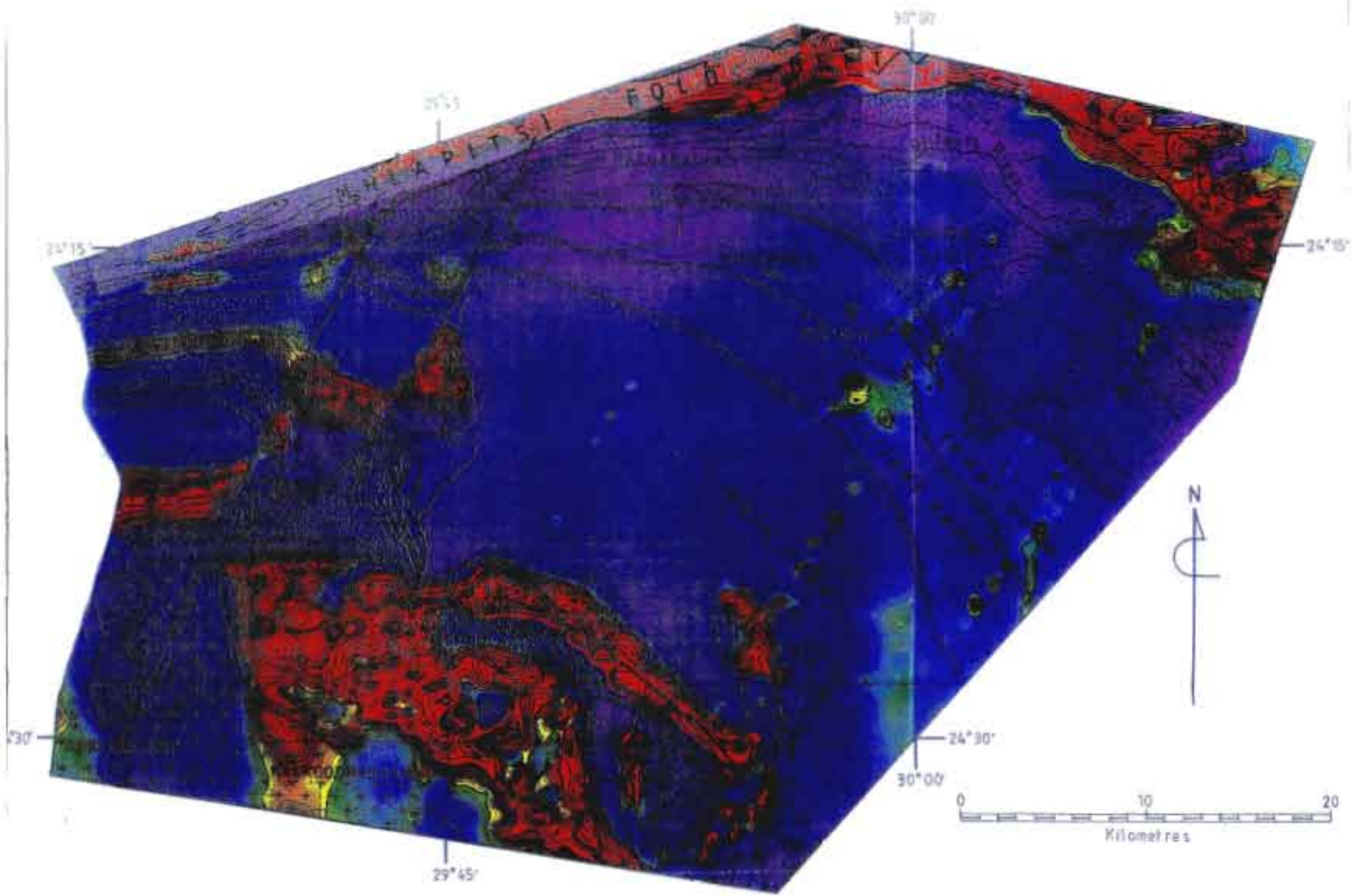
- Taylor, G.I. (1950). The instability of liquid surfaces when accelerated in a direction perpendicular to their planes. I. *Proc. R. Soc. London, Ser. A*, **201**, 192-196.
- Thompson, J.B.Jr. (1957). The graphical analysis of mineral assemblages in pelitic schists *Amer. Mineral.* **42**, 842-858.
- Thompson, A.B. (1976). Mineral reactions in pelitic rocks: I. Prediction of P-T-X (Fe-Mg) phase relations, II. Calculation of some P-T-X (Fe-Mg) phase relations. *Amer. J. Sci.* **276**, 401-454.
- Tozer, E.T. & Thorsteinsson, R. (1964). Western Queen Elizabeth Islands, Arctic Archipelago. *Mem. Geol. Surv. Canada*, **332**.
- Trusheim, F. (1960). Mechanism of salt migration in N. Germany. *Am. Assoc. Petrol. Geol. Bull.*, **44**, 1519-1540.
- Turcotte, D.L. (1982). Magma migration, *Ann. Rev. Earth Planet Sci.*, **10**, 397-408.
- Turcotte, D.L. & Schubert, G. (1982). *Geodynamics: Applications of Continuum Physics to Geological Problems*. Wiley, New York, 450pp.
- Tuttle, O.F. & Bowen, N.L. (1958). Origin of granite in the light of experimental studies in the system  $\text{NaAlSi}_3\text{O}_8$ - $\text{KAlSi}_3\text{O}_8$ - $\text{SiO}_2$ - $\text{H}_2\text{O}$ . *Geol. Soc. Am. Mem.*, **74**, 1-153.
- Twist, D. (1985). Geochemical evolution of the Rooiberg silicic lavas in the Loskop Dam area, southeastern Bushveld. *Econ. Geol.*, **80**, 1153-1165.
- Twist, D. & Harmer, R.E.J. (1987). Geochemistry of contrasting siliceous magmatic suites in the Bushveld Complex: genetic aspects and implications for tectonic discrimination diagrams. *J. Volcanol. Geothermal Res.*, **32**, 83-98.
- Uken, R. & Watkeys, M.K. (1990). Structures in the northern margin of the Bushveld Complex. *Tectonics Division of the Geological Society of South Africa, Annual Conference Abstracts*, University of Pretoria.
- Uken, R. & Watkeys, M.K. (1994). Deformation, timing and emplacement mechanisms for the eastern Bushveld Complex. *Tectonics Division of the Geological Society of South Africa, 10th Anniversary Conference Abstracts*, University of Pretoria, Pretoria, 4.
- Uken, R. & Watkeys, M.K. (1995). The Bushveld Complex aureole: Structural processes in a low pressure, high temperature contact metamorphic terrane. *Ext. Abstr., Centennial Geocongress*, Geol. Soc. S. Afr., Johannesburg, 688-690.
- Uken, R. & Watkeys, M.K. (1997). An interpretation of mafic dyke swarms and their relationship with major mafic magmatic events on the Kaapvaal Craton and Limpopo Belt. *S. Afr. J. Geol.*, **100**, 341-348.
- Vail, J.R. (1977). Further data on the alignment of basic igneous intrusive complexes in southern and eastern Africa. *Trans. geol. Soc. S. Afr.*, **80**, 87-92.
- Van Biljon, S. (1949). The transformation of the upper part of the Pretoria Series in the Bushveld Igneous Complex. *Trans. geol. Soc. S. Afr.*, **52**, 1-198.
- Van Biljon, W.J. (1976). Goud is nie waar dit gevind word nie! *Trans. geol. Soc. S. Afr.*, **79**, 155-167.
- Van Rooyen, D.P. (1951). Fluvial andalusite deposits in the Marico District. *Bull. geol. Surv. S. Afr.*, **19**, 16pp.
- Van der Molen, I. & Paterson, M.S. (1979). Experimental deformation of partially melted granite. *Contrib. Mineral. Petrol.*, **70**, 299-318.
- Vermaak, C.F. (1970). The geology of the lower portion of the Bushveld Complex and its relationship to the floor rocks in the area west of Pilansberg, western Transvaal. *Spec. Publ. geol. Soc. S. Afr.*, **1**, 242-262.
- Vernon, R.H. (1979). Formation of late sillimanite by hydrogen metasomatism (base-leaching) in some high-grade gneisses. *Lithos*, **12**, 143-152.
- Vernon, R.H. (1987). Growth and concentration of fibrous sillimanite related to heterogeneous deformation in K-feldspar-sillimanite metapelites. *J. metamorphic Geol.*, **5**, 51-68.
- Vernon, R.H. (1988). Microstructural evidence of rotation and non-rotation of mica porphyroblasts. *J. Metamorphic Geol.*, **6**, 595-601.
- Vernon, R.H. & Powell, C.McA. (1976). Porphyroblastesis and displacement: some new textural criteria from pelitic hornfels-a comment. *Mineral. mag.*, **40**, 787-788.
- Vernon, R.H., Collins, W.J. & Paterson, S.R. (1993a). Pre-foliation metamorphism in low-pressure/high-temperature terrains. *Tectonophysics*, **219**, 241-256.
- Vernon, R.H., Paterson, S.R. & Foster, D. (1993b). Growth and deformation of porphyroblasts in the Foothills terrane, central Sierra Nevada, California: negotiating a microstructural minefield. *J. Metamorphic Geol.*, **11**, 203-222.
- Verwoerd, W.J. (1963). Die geologiese struktuur van die Krokodilrivierfragment. *Trans. geol. Soc. S. Afr.*, **66**, 49-74.
- Visser, J.N.J. (1971). The deposition of the Griquatown Glacial Member in the Transvaal Supergroup. *Trans. geol. Soc. S. Afr.*, **71**, 187-199.

- Vita-Finzi, C. (1979). Rates of Holocene folding in the coastal Zagros near Bandar Abbas, Iran. *Nature, Lond.*, **278**, 632-633.
- Von Gruenewaldt, G. (1973). The main and upper zones of the Bushveld Complex in the Roossenekal area, Eastern Transvaal. *Trans. geol. Soc. S. Afr.*, **76**, 53-61.
- Von Gruenewaldt, G., Sharpe, M.R. & Hatton, C.J. (1985). The Bushveld Complex: introduction and review. *Econ. Geol.*, **80**, 803-812.
- Wallmach, T. (1986). Calc-silicate xenoliths in the eastern Bushveld Complex. *Inst. Geol. Res. Bushveld Complex, Annual Report*, 81-92.
- Wallmach, T., Hatton, C.J. & Droop, G.T.R. (1989). Extreme facies of contact metamorphism developed in calc-silicate xenoliths in the eastern Bushveld Complex. *Can. Mineral.*, **27**, 509-523.
- Walraven, F. (1985). Genetic aspects of the granophyric rocks of the Bushveld Complex. *Econ. Geol.*, **80**, 1166-1180.
- Walraven, F. (1989). The Geology of the Pilgrims Rest Area. Explanation to Sheet 2430 (Pilgrims Rest). *S. Afr. Geol. Surv. Map Scale 1:250 000*, 24pp.
- Walraven, F. (1997). Geochronology of the Rooiberg Group, Transvaal Supergroup, South Africa. *Econ. Geol. Res. Unit, Univ. Witwatersrand, Inf. Circ.*, **316**, 21pp.
- Walraven, F., Armstrong, R.A. & Kruger, F.J. (1990). A chronostratigraphic framework for the north-central Kaapvaal Craton, Bushveld Complex and the Vredefort structure. *Tectonophysics*, **171**, 23-48.
- Walraven, F., Frick, C. & Lubabla, R.T. (1992). Pb-isotope geochronology of the Schiel Complex, Northern Transvaal, South Africa. *J. Afr. Earth Sci.*, **15**, 103-110.
- Walraven, F. & Hattingh, E. (1993). Geochronology of the Nebo Granite, Bushveld Complex. *S. Afr. J. Geol.*, **96**, 31-42.
- Walraven, F. & Martini, J. (1995). Zircon Pb-evaporation age determinations of the Oak Tree Formation, Chuniespoort Group, Transvaal Sequence: implications for Transvaal-Griqualand West basin correlations. *S. Afr. J. Geol.*, **98**, 58-67.
- Walraven, F. & Coertze, F.J. (1988). Acid rocks within the Rustenburg Layered Suite in eastern Transvaal and their significance for emplacement models of basic Bushveld magmas. *Ext. Abstr., Geocongress '88, 22nd Earth Science Congress*, Geol. Soc. S. Afr., Durban, 705-708.
- Wang, P. & Spear, F.S. (1991). A field and theoretical analysis of garnet + chlorite + chloritoid + biotite assemblages from the tri-state (MA, CT, NY) area, USA. *Contrib. Mineral. Petrol.*, **106**, 217-235.
- Watkeys, M.K. (1984). *The Precambrian geology of the Limpopo Belt north and west of Messina*. Ph.D. thesis (unpubl.), Univ. Witwatersrand, Johannesburg, 349pp.
- Watkeys, M.K. (1996). The Klondike steep structure, Okiep Copper District, South Africa. *S. Afr. J. Geol.*, **99**, 169-183.
- Watkeys, M.K. & Sweeney, R.J. (1988). Tuli-Lebombo volcanism and Gondwana Rifting. *Ext. Abstr., Geocongress '88, 22nd Earth Science Congress*, Geol. Soc. S. Afr., Durban, 725-728.
- Wells, P.R.A. (1976). Late Archaean metamorphism in the Buksefjorden region, southwest Greenland. *Contrib. Mineral. Petrol.*, **56**, 229-242.
- Wells, P.R.A. (1979). Chemical and thermal evolution of Archaean silicic crust, southern west Greenland. *J. Petrol.*, **20**, 187-226.
- White, S.H., Burrows, S.E., Carreras, J., Shaw, N.D. & Humphyreys, F.J. (1980). On mylonites in ductile shear zones. *J. Struct. Geol.*, **2**, 175-187.
- White, R.S. & McKenzie, D. (1989). Magmatism at rift zones: The generation of volcanic continental margins and flood basalts. *J. Geophys. Res.*, **94**, 7685-7729.
- Whitehead, J.A. (1988). Fluid models of geological hotspots. *Ann. Rev. Fluid Mech.*, **20**, 61-87.
- Whitehead, J.A. & Helfrich, K.R. (1990). Magma waves and diapiric dynamics. In: *Magma Transport and Storage*, Ryan, M.P. (Ed.), John Wiley & Sons, Ltd., 53-76.
- Whitehead, J.A. & Luther, D.S. (1975). Dynamics of laboratory diapir and plume models. *J. Geophys. Res.*, **80**, 705-717.
- Wickham, S.M. (1987). The segregation and emplacement of granitic magmas. *J. Geol. Soc. Lond.*, **144**, 281-297.
- Wilhelm, H.J., Von Gruenewaldt, G. and Behr, S.H. (1990). Investigations on the MolopoFarms Complex, Botswana: Stratigraphy and petrology. *Geocongress '88, 22nd Earth Science Congress, Extended Abstracts*. Geol. Soc. S. Afr. Univ. of Natal, Durban. 733-736.
- Willemse, J. (1959). The floor of the Bushveld Igneous Complex and its relationships with special reference to the eastern Transvaal. *Trans. geol. Soc. S. Afr.*, **62**, 21-83.

- Willemse, J. (1964). A brief outline of the geology of the Bushveld Igneous Complex. *In: Haughton, S.H. (Ed.), The geology of some ore deposits in southern Africa*. Geol. Soc. S. Afr., **2**, 91-128.
- Willemse, J. (1969). The geology of the Bushveld Igneous Complex, the largest repository of magmatic ore deposits in the world. *Econ. Geol. Monogr.*, **4**, 1-22.
- Willemse, J. & Bensch, J.J. (1964). Inclusions of original carbonate rocks in gabbro and norite of the eastern part of the Bushveld Complex. *Trans. geol. Soc. S. Afr.*, **67**, 1-87.
- Willemse, J. & Viljoen, E.A. (1970). The fate of argillaceous material in the gabbroic magma of the Bushveld Complex. *Spec. Publ. geol. Soc. S. Afr.*, **1**, 336-366.
- Wilson, R.W. (1971). On syntectonic porphyroblast growth. *Tectonophysics*, **11**, 239-260.
- Winkler, H.G.F. (1979). *Petrogenesis of Metamorphic Rocks*. Springer Verlag, New York, 348pp.
- Wintsch, R.P. & Andrews, M.S. (1988). Deformation induced growth of sillimanite: "stress" minerals revisited. *J. Geol.*, **96**, 143-161.
- Wohletz, K.H. (1995). HEAT, Version 3, A 2-D Heterogeneous Heat Flow Code. 16-Bit Version 16.37. [Http://geont1.lanl.gov/wohletz/heat.htm](http://geont1.lanl.gov/wohletz/heat.htm)
- Wones, D.R. & Eugester, H.P. (1965). Stability of biotite; experiment, theory, and application. *Am. Mineralogist*, **50**, 1228-1272.
- Xu, G., Will, T. & Powell, R. (1994). A calculated petrogenetic grid for the system  $K_2O$ - $FeO$ - $MgO$ - $Al_2O_3$ - $SiO_2$ - $H_2O$ . *Journal of Metamorphic Geology*, **12**, 99-119.
- Yardley, B.W.D., Barber, J.P. & Gray, J.R. (1987). The metamorphism of the Dalradian rocks of western Ireland and its relation to tectonic setting. *Phil. Trans. R. Soc. Lond.*, **A321**, 243-268.
- Zaleski, S. & Julien, P. (1992). Numerical simulation of Rayleigh-Taylor instability for single and multiple salt diapirs. *Tectonophysics*, **206**, 55-69.
- Zwart, H.J. (1962). On the deformation of ploymetamorphic mineral associations, and its application to the Bosost area (Central Pyrenees). *Geologische Rundschau*. **52**, 38-65.



**Appendix 1G** Aeromagnetic map of the study area with an overlay of the main geological units.  
Map supplied by Geodass for the Nylstroom 2428 and Pilgrims Rest 2430 1 :250000 scale sheets.



GEOLOGICAL LEGEND

-  Pretoria Group
-  Chuniespoort Group

-  Lebowa Granite Suite
-  Rustenburg Layered Suite

# APPENDIX 2

# MINERAL ASSEMBLAGES

## APPENDIX 2A

### Andalusite zone pelitic mineral assemblages

X - Prograde phase, R - Retrograde phase. Mineral abbreviations from Kretz (1983).

Samples with mineral chemical data are shaded, ■ Whole rock analysis

Sample	Locality	And	Bt	St	Grt	Crd	Oam	Cld	Pl	Chl	Mus	Ser	Qtz	Accessory
■ C7	Hoogenoeg	X	X	X					R	R	X	X	X	Tur, Zrn, Ilm
C4a	Hoogenoeg	X	X	X					R	R	X	X	X	Tur, Zrn, Ilm
■ C4	Hoogenoeg	X	X	X					R	R	X	X	X	Tur, Zrn, Ilm
HOEG STZ2	Hoogenoeg	X	X	X	X			R	X	R	X	X	X	Zrn, Ilm
H7	Hoogenoeg	X	X		X	X			X				X	Zrn, Ilm
HAPL	Hoogenoeg		X	X					X	R	X	X	X	Tur, Ilm, Zrn
HOEG ST.2.1	Hoogenoeg	X	X	X					X	R	X	X	X	Ilm, Tur, Zrn
■ AG/X	Hoogenoeg		X	X	X						X		X	Ilm, Tur, Zrn
OB3a	Hoogenoeg	X	X	X	X				X		R		X	Ilm
H4	Hoogenoeg	X	X	X	X			R	X	R	R	X	X	Ilm, Zrn
HOEG OB653a	Hoogenoeg		X							R	X	X	X	Zrn, Tur, Ilm
■ HWU	Hoogenoeg	X	X	X	X	X	X		X	R	R		X	Ilm, Zrn, Tur
72S36	Hoogenoeg	X	X	X					X	R	R	X	X	Zrn., Tur, Ilm
Cop 110 62:	Copper	X	X	X	X				X	R	R	X	X	Zrn, Ilm Tur
Cop2	Copper	X	X	X	X				X	R	R	X	X	Zrn, Tur, Ilm
COP11440	Copper	X	X	X	X				X		R		X	Tur, Zrn, Ilm
COP4B	Copper	X	X			X			X	R	R	X	X	Tur, Zrn, Ilm
UP/TH	Copper		X	X	X		X		X	R			X	Zrn
GTS/HFS	Copper	X	X	X	X	X			X				X	Ilm
OB3b	Hoogenoeg	X	X		X				X	R			X	Ilm, Zrn
■ OB5	Hoogenoeg	X	X	X	X				X		X		X	Ilm, Tur, Zrn

Sample	Locality	And	Bt	St	Grt	Crd	Qam	Cld	Pl	Chl	Mus	Ser	Otz	Accessory
■ B/1	Hoogenoeg	X	X	X		X			X	R			X	Tur, Zrn, Ilm
H10	Hoogenoeg		X	X	X								X	Tur, Ilm, Zrn
5A	Hoogenoeg		X	X	X					R			X	Ilm, Zrn, Tur
OB5	Hoogenoeg	X	X	X	X				X		R		X	Tur, Zrn, Ilm
■ X/A	Hoogenoeg	X	X	X					X	R	R	X	X	Ilm
C2	Hoogenoeg		X	X								X	X	Ilm, Zrn
H4A	Hoogenoeg		X		X				X	X			X	Ilm, Zrn
CB2	Hoogenoeg	X	X	X	X						R		X	Tur, Ilm, Zrn
H10A	Hoogenoeg		X		X				X			X	X	Zrn, Ilm
B9	Hoogenoeg				X				X	X			X	Ilm
H5	Hoogenoeg	X	X	X					X	R	R	R	X	Tur, Ilm,
H15	Hoogenoeg		X		X					X			X	Ilm
HA7	Hoogenoeg	X	X	X	X					R	R		X	Ilm, Zrn, Tur
HA7a	Hoogenoeg		X	X					X	R			X	Ilm, Zrn
■ 16/7	Tuinplaats	X	X		X	X				R	R		X	Ilm
K8	Tuinplaats	X	X								R	X	X	Ilm
■ 16/8	Tuinplaats	X	X								R	X	X	Ilm
W.KOP6	Wondakop	X	X	X	X						R	X	X	Ilm, Zrn
T16/4	Tuinplaats		X	X	X				X	R	R		X	Ilm, Zrn
16/7A	Tuinplaats		X		X	X				R			X	Ilm,
CB042	Copper	X	X	X	X				X		R	X	X	Ilm, Zrn
ODH 80.5	Copper	X	X	X						R	R	X	X	Ilm, Zrn
UIT.LHB	Uitkyk	X	X	X	X				X		R	X	X	Ilm, Zrn, Tur
UT2.5	Hoogenoeg	X	X	X	X				X		R	X	X	Ilm, Zrn, Tur
X KOP1	Copper	X	X	X	X				X	R	R		X	Ilm, Zrn, Tur
COP2	Copper		X	X	X				X	R		R	X	Ilm, Zrn
COP 106/3B	Copper	X	X	X	X				X	R	R		X	Ilm, Zrn, Tur



Sample	Locality	And	Bt	St	Grt	Crđ	Oam	Clđ	Pl	Chl	Mus	Ser	Qtz	Accessory
H6	Hoogenoeg	X	X	X	X				X		R		X	Ilm, Zrn
V08	Voorspoed	X	X	X	X				X		R		X	Ilm
X11	Hoogenoeg	X	X	X						R	R	R	X	Ilm
O/B4	Tuinplaats		X		X				X	X,R			X	Ilm
16/17-042552	Toornkop		X		X	X			X	R	R		X	Ilm, Zrn
16/18	Toornkop	X	X	X	X	X	X		X	R			X	Zrn, Ilm, Tur
O/B4	Hoogenoeg		X		X				X	X,R			X	Ilm
RU99	Hoogenoeg	X	X	X	X				X		R		X	Ilm, Zrn, Tur
H.NOEGB/D	Hoogenoeg	X	X	X	X				X		R		X	Ilm, Zrn
HOEGM.A.H	Hoogenoeg	X	X	X	X				X	R	R		X	Ilm, Zrn
O/B3b	Hoogenoeg	X	X		X				X				X	Ilm, Tur
MH (A)	Uitkyk	X	X	X	X				X		R		X	Ilm, Tur
LHA	Uitkyk	X	X	X	X				X		R	X	X	Ilm, Tur, Zrn
■ H3	Hoogenoeg	X	X	X					X		R	X	X	Ilm, Zrn, Tur
H9	Hoogenoeg	X	X	X	X	X	X		X	R			X	Ilm, Zrn
UITMAH	Uitkyk	X	X	X	X				X	R			X	Ilm, Tur, Zrn
M4	Hoogenoeg		X	X	X				X	R			X	Ilm, Zrn
M2	Hoogenoeg		X	X					X	R		X	X	Ilm, Zrn
HAB	Hoogenoeg	X	X	X					X		R		X	Ilm, Zrn
■ B7	Hoogenoeg	X	X	X				R	X	R	R	X	X	Ilm, Tur, Zrn
B2	Hoogenoeg		X	X					X		R	X	X	Ilm, Zrn
SC	Hoogenoeg		X	X					X	R	R	X	X	Ilm, Tur, Zrn
■ M/1	Hoogenoeg		X	X	X				X	R	R		X	Ilm, Zrn
12Aa	Hoogenoeg		X	X	X				X	R	R		X	Zrn
14A	Hoogenoeg	X	X	X					X		R	X	X	Zrn, Tur, Ilm
C3a	Hoogenoeg		X	X					X		R	X	X	Tur, Zrn, Ilm

Sample	Locality	And	Bt	St	Grt	Crd	Oam	Cld	Pl	Chl	Mus	Ser	Qtz	Accessory
COP4	Copper	X	X			X			X	R	R	X	X	Ilm, Zrn, Tur
THF1.B	Hoogenoeg	X	X	X		X				R	R	X	X	Zrn, Ilm, Tur
THF1.B	Hoogenoeg	X	X	X		X					R	X	X	Zrn, Ilm, Tur
THF/10	Hoogenoeg	X	X	X	X				X	R	R	X	X	Ilm, Zrn
CONZ	Hoogenoeg				X				X	X			X	Ilm, Tur

## APPENDIX 2B

## Fibrolite zone pelitic mineral assemblages

X - Prograde phase, R - Retrograde phase. Mineral abbreviations from Kretz (1983).

Samples with mineral chemical data are shaded, ■ Whole rock analysis

Sample	Locality	And	Fib	Bt	Grt	Crd	Kfs	Pl	St	Chl	Mus	Ser	Qtz	Accessory
■ 27/8	Koedoeskop	X	X	X			X	X			R		X	Tur, Zrn, Ilm
■ 27/10	Koedoeskop	X	X	X		X		X			X		X	Tur, Zrn, Ilm
RU/2	Fonteinplaats	X	X	X				X			R		X	Tur, Zrn, Ilm
17/13	Tigerpoort	X	X	X		X					X		X	Ap, Zrn
■ 19/12	Katkloof			X	X	X		X		Il	R		X	Zrn, Ilm
JOB14	Jobskop	X	X	X			X	X			R		X	Zrn, Tur
DP2	De Paarl	X	X	X		X	X	X		R	R		X	Zrn, Ilm
DP1	DePaarl	X	X	X				X		R	X		X	Zrn, Ap
M.LELE	Mphatlale	X	X	X			X	X		R	X		X	Zrn, Ilm
MAL6852	Mphatlale	X		X				X			R	X	X	Zrn, Ilm
MAL-A06652	Mphatlale	X	X	X	X		X	X		R	R		X	Zrn, Ilm
KOED161-10	Koedoeskop			X				X			R		X	Tur, Zrn
ROO3A	Roodekrans	X	X	X		X	X	X		R	R		X	Tur, Zrn, Ilm
ROO3B	Roodekrans	X	X	X		X	X	X		R	R		X	Tur, Zrn, Ilm
WIS 1	Wismar, Ledingwe	X	X	X		X	X	X		R	R		X	Tur, Zrn, Ilm
WIS2	Wismar, Ledingwe	X	X	X		X	X	X		R	R		X	Tur, Zrn, Ilm
UD3	Wismar, Lidingwa990	X	X	X		X	X	X		R	R		X	Zrn, Tur, Ilm

## APPENDIX 2C

### Migmatite zone pelitic mineral assemblages

X - Prograde phase, R - Retrograde phase. Mineral abbreviations from Kretz (1983).

*Samples with mineral chemical data are shaded, ■ Whole rock analysis*

Sample	Locality	And	Crn	Sil	Fib	Bt	Hcy	Mt	Grt	Crd	Opx	Kfs	Pl	Chl	Mus	Qtz	Accessory
■ 26/3	Koedooskop					X				X		X			X	X	Zrn
26/3a	Koedooskop					X						X	X			X	Zrn
■ 27/3	Koedooskop					X				X		X	X			X	Tur, Zrn
27/6	Koedooskop					X						X	X		X	X	Ilm, Zrn
■ 3/4	Groenfontein					X						X	X			X	Tur, Zrn
29/6	Koedooskop					X						X	X			X	Zrn, Tur, Ilm
■ 26/9A	Koedooskop					X						X	X			X	Zrn, Tur, Ilm
JOB5A	Jobskop	X		X		X						X	X				Zrn
JOB5B	Jobskop	X		X		X						X	X				Zrn
Par220	Phepane W- limb					X				X		X	X	R		X	Zrn, Tur
060SE52	Phepane W-limb					X						X	X	R	R		Zrn, Tur
PAR2	Phepane Core					X				X				R	R	X	Zrn
PAR3	Phepane Core	X				X	X			X		X	X				Zrn
PAR6	Phepane core	X				X	X			X		X	X	R	R		Zrn, Tur
PAR1072	Phepane core East limb	X				X	X			X		X	X	R	R	X	Zrn
PAR1108	Phepane NE limb					X						X	X		R	X	Zrn, Ilm
PAR1108a	Phepane NE limb					X						X	X				Ilm, Zrn
PAR4C	Phepane core	X				X	X			X		X	X	R	R	X	Ilm, Zrn
CORPAR A	Phepane core W limb	X				X	X			X		X	X	R	R		Zrn, Tur
CORPAR B	Phepane core W limb	X				X	X			X		X	X	R	R		Zrn, Tur
PAR5C	Phepane core	X				X	X			X		X	X	R	R		Ilm, Zrn
PAR1123	Phepane NE-limb		X	X		X				X		X	X	R			Zrn
PAR1128 (HILL 11382)	Phepane	X	X	X		X				X		X	X	R			Zrn

Sample	Locality	And	Crn	Sil	Fib	Bt	Hcy	Mt	Grt	Crd	Opx	Kfs	Pl	Chl	Mus	Qtz	Accessory
PAR 1-95	Phepane core					X						X	X		R	X	Zrn
PAR2C	Phepane core	X				X	X			X		X	X	R	R	X	Zrn, Tur
PAR5C	Phepane core	X				X	X			X		X	X	R	R	X	Zrn, Tur
PRAM1	Pramkoppies	X			X	X				X		X	X	R	R	X	Zrn
924A	Pramkoppies Hill 924					X			X	X		X	X	R		X	Zrn, Ilm
924B	Pramkoppies	X				X	X		X	X		X	X	R	R	X	Zrn, Tur
KOAM.MKW	Pramkoppies	X				X	X		X	X		X	X	R	R	X	Zrn, Tur
MASET3	Pramkoppies 1184.8				X			X		X	X	X	X	R	R		Zrn
MASET2	Pramkoppies 1184.8							X		X	X	X	X	R	R		Zrn
MOS C	Pramkoppies				X			X		X	X	X	X	R	R		Zrn
PRAM1B	Pramkoppies	X		X		X				X		X	X	R	R	X	Zrn, Tur
MOSS840A	Pramkoppies					X		X		X	X	X	X	R	R		Zrn, Tur
LEK1	Lekurung Pramkoppies	X			X	X	X			X		X	X	R	R	X	Tur, Zrn, Ap
LEK2	Lekurung Pramkoppies					X				X		X	X			X	Tur, Zrn
LEK3	Lekurung Pramkoppies	X				X	X			X		X	X	R	R	X	Tur, Zrn
LEK5	Lekurung Pramkoppies	X				X	X			X		X	X	R	R	X	Tur, Zrn
MA1	Pramkoppies					X				X		X	X			X	IZrn
GROP1	Grootkop					X				X		X	X		R	X	Zrn, Tur
Z2	Zaalkloof					X						X	X			X	Tur, Zrn
MABELA	Mphatlele					X			X	X			X			X	Tur, Zrn
MALEL A	Mpatlele					X			X	X			X			X	Tur, Zrn
MALEL F	Mphatlele					X			X	X			X			X	Tur, Zrn
LES 992A	Mphatlele					X						X	X			X	Zrn
PHOS1023A	Zaalkloof	X			X	X				X		X	X	R	R	X	Tur, Zrn

Sample	Locality	And	Crn	Sil	Fib	Bt	Hcy	Mt	Grt	Crd	Opx	Kfs	Pl	Chl	Mus	Qtz	Accessory
PHOS1023B	Zaalkloof					X	X			X		X	X	R	R	X	Tur, Zrn
PHOS1023C	Zaalkloof	X				X	X		X	X		X	X	R	R		Zrn, Ilm
PHOS1023B1	Zaalkloof Phosiri	X				X	X			X		X	X	R	R	X	Tur, Zrn
PHOS1023H	Zaalkloof					X				X		X	X		R	X	Tur, Zrn
P107B	Zaalkloof, Phosiri	X				X	X			X		X	X	R	R	X	Tur, Zrn
P1078A	Zaalkloof, Phosiri	X		X	X	X				X		X	X	R	R	X	Tur, Zrn
PHOS1078E	Zaalkloof	X			X	X				X		X	X	R	R	X	Zrn, Tur
POS4	Zaalkloof	X		X		X				X		X	X	R	R	X	Zrn, Tur
KRG	Tigerpoort Katkloof fold			X	X	X		X		X	X	X	X	R	R		Zrn
HAAI-1	Haakdoorn-draai					X		X		X	X	X	X	R			Zrn
HAAI-3	Haakdoorn-draai					X		X		X	X	X	X				Zrn

# APPENDIX 3

# GEOCHEMISTRY

## APPENDIX 3A

## Analytical methods and operating conditions for XRF analysis

A problem with pelitic rock analysis is that the samples are usually banded on a millimetre to centimetre-scale and chemical differences are likely to exist between individual layers. To avoid risk of contamination from layers of differing chemistry, 5 kilogram samples were selected that had few and thicker bands. A rock splitter was used to remove adjacent layers that visibly had a differing mineralogical composition, as well as surface weathering effects. A steel faced Watson jaw crusher reduced the sample to 10 mm sized chips. These were further reduced to -300 mesh powder using a Siebtechnik agate swing-mill. Fusion disks were prepared according to the method of Norrish and Hutton (1969) by the Geochemistry department of the Geological Survey in Pretoria. Analyses were done using a Phillips 1400 X-ray spectrometer. Wet chemical techniques were used to determine the FeO concentration. Infra-red detection of SO<sub>2</sub> and CO<sub>2</sub> gases were determined using a Leco CS244 carbon and sulphur determinator. Infra-red detection of H<sub>2</sub>O<sup>-</sup> and H<sub>2</sub>O<sup>+</sup> were done with a Leco RMC100 rapid moisture analyser, where H<sub>2</sub>O<sup>-</sup> was determined at approximately 120 °C and H<sub>2</sub>O<sup>+</sup> at between 750 and 1200 °C.

## APPENDIX 3B

## Whole rock major element chemistry

SAMPLE NO UND NO	X/A UND951	19/12 UND952	26/3 UND954	16/7 UND955	16/8 UND957	27/8 UND958	C4 UND959	27/3 UND960	AQ/X UND961	27/10 UND962	OB5 UND963	26/9A UND964	3/4 UND966	H3 UND967	HWU UND968	M/1 UND969	C7 UND970	B7 UND971	B/1 UND972
SiO <sub>2</sub>	57.67	60.47	76.95	53.01	54.19	59.50	54.01	60.02	57.07	61.94	56.04	70.85	60.45	57.70	57.87	65.21	66.38	56.04	56.30
TiO <sub>2</sub>	0.99	0.63	0.38	1.35	0.88	0.71	0.66	0.78	0.59	0.90	1.03	0.48	0.71	0.71	1.30	0.62	0.83	0.96	1.22
Al <sub>2</sub> O <sub>3</sub>	27.57	19.70	11.99	23.39	28.61	20.30	22.52	19.93	15.62	18.43	22.16	14.42	20.35	26.28	22.80	14.61	17.85	28.05	23.07
FeO	3.97	8.14	2.88	12.25	7.41	6.83	9.06	7.80	18.84	7.72	13.12	3.36	7.69	8.95	9.89	12.64	3.20	8.74	10.57
MnO	0.08	0.07	0.04	0.22	0.12	0.09	0.06	0.11	0.07	0.07	0.07	0.10	0.14	0.11	0.11	0.12	0.06	0.05	0.12
MgO	0.49	2.77	0.60	3.57	2.23	2.82	1.61	3.17	1.90	3.17	2.72	2.34	3.31	1.62	3.54	2.07	0.01	1.36	3.75
CaO	0.12	0.55	0.37	1.53	0.01	0.01	0.01	0.44	0.01	0.43	0.03	1.03	1.00	0.01	0.61	0.53	0.01	0.01	0.18
Na <sub>2</sub> O	0.77	2.81	2.49	1.87	0.60	0.25	0.28	1.01	0.09	1.13	0.25	2.19	1.01	0.79	2.12	0.75	0.30	1.07	1.26
K <sub>2</sub> O	5.84	2.06	2.52	0.64	3.78	4.49	4.75	4.74	3.68	3.89	3.21	3.41	5.02	3.02	1.73	3.22	4.52	3.42	2.62
P <sub>2</sub> O <sub>5</sub>	0.34	0.10	0.10	0.20	0.17	0.08	0.12	0.22	0.13	0.07	0.10	0.16	0.16	0.09	0.08	0.15	0.09	0.30	0.09
CR <sub>2</sub> O <sub>3</sub>	0.18	0.31	0.15	0.23	0.20	0.22	0.14	0.22	0.13	0.20	0.27	0.15	0.29	0.16	0.23	0.22	0.25	0.26	0.20
H <sub>2</sub> O <sup>+</sup>	1.55	2.15	0.61	1.15	0.74	0.96	2.30	1.10	0.75	1.11	1.00	0.30	0.61	0.54	0.93	0.81	1.69	0.64	1.15
H <sub>2</sub> O <sup>-</sup>	0.16	0.13	0.01	0.13	0.01	0.11	0.20	0.39	0.05	0.05	0.17	0.01	0.06	0.02	0.05	0.02	0.07	0.01	0.17
CO <sub>2</sub>	0.14	0.04	0.15	0.52	2.07	3.77	3.05	0.10	0.04	0.18	0.89	0.08	0.29	0.12	0.17	0.11	7.36	0.12	0.10
S	0.00	0.00	0.06	0.00	0.01	0.02	0.00	0.00	0.00	0.00	0.00	0.00	0.00	0.01	0.01	0.01	0.02	0.00	0.00
TOTAL	99.87	99.92	99.30	100.06	101.01	100.14	98.75	100.01	98.96	99.30	101.07	98.88	101.09	100.11	101.43	101.08	102.62	101.01	100.80
A	0.56	0.41	0.40	0.45	0.50	0.25	0.30	0.19	0.10	0.23	0.32	0.24	0.17	0.50	0.43	0.15	0.41	0.52	0.37
F	0.82	0.62	0.73	0.66	0.65	0.58	0.76	0.58	0.85	0.58	0.73	0.45	0.57	0.76	0.61	0.77	1.0	0.78	0.61
Mn	0.02	0.01	0.01	0.01	0.01	0.01	0.00	0.01	0.00	0.01	0.00	0.01	0.01	0.01	0.01	0.01	0.02	0.00	0.01

$$A = (Al_2O_3) - 3(K_2O) / (Al_2O_3) - 3(K_2O) + (MgO) + (FeO); F = (FeO) / (FeO) - (MgO); Mn = (MnO) / (MnO) + (FeO) + (MgO)$$

## **APPENDIX 3C Analytical methods used in microprobe analysis**

Samples were selected for mineral chemical analysis for geothermometry and geobarometry. Carbon-coated polished thin sections were analysed for major elements using the wave-length dispersive automated Cameca Camebax electron probe analyser at the Department of Geochemistry, University of Cape Town. Instrumental conditions were: a normal acceleration voltage of 15 kV, a specimen current which varied between 0.50 and 0.10 microamps; an integrating time of 10 seconds and an electron beam diameter of 1-2 microns. Anhydrous multi-element silicates and oxides were used as standards. Data correction for atomic number, fluorescence and absorption were made using the methods of Bence and Albee (1968)



# APPENDIX 3D

# Mineral analysis used for geothermometry and geobarometry

## Garnet

	OB5		OB5s		AQ/X		16/7c		16/7b		19/12		M/1		HWU		HWUc		HWUs	
	CORE	RIM	CORE	RIM	CORE	RIM	CORE	RIM	CORE	RIM	CORE	RIM	CORE	RIM	CORE	RIM	CORE	RIM	CORE	RIM
SiO <sub>2</sub>	36.26	36.41	36.26	37.19	36.27	36.02	36.76	36.44	36.18	37.03	36.98	37.37	37.39	34.96	36.16	36.63	36.67	36.30	36.16	36.30
TiO <sub>2</sub>	0.21	0.04	0.21		0.13	0.05	0.08				0.08		0.25			0.06				
Al <sub>2</sub> O <sub>3</sub>	21.30	21.30	21.30	21.88	21.04	20.99	21.30	21.98	21.57	21.60	21.29	21.19	21.56	21.48	21.19	21.29	21.10	20.96	21.19	20.96
Cr <sub>2</sub> O <sub>3</sub>					0.05						0.08				0.07				0.07	
FeO	36.55	38.64	36.55	38.57	38.04	40.39	38.03	38.14	36.64	37.36	35.19	36.01	31.31	39.92	36.67	37.74	37.07	37.85	36.67	37.85
MnO	2.25	0.70	2.25	0.37	0.92	0.19	2.07	1.89	2.84	2.05	2.83	0.83	3.99	0.70	2.37	2.01	2.15	2.06	2.37	2.06
MgO	1.57	1.88	1.57	2.00	0.93	0.97	1.41	2.29	2.21	2.32	2.52	3.05	2.05	1.66	2.39	2.37	2.43	2.30	2.39	2.30
CaO	1.97	2.07	1.97	1.81	2.90	1.67	1.48	0.96	1.28	1.07	1.30	1.90	4.78	1.51	1.06	0.81	1.00	0.77	1.06	0.77
TOTAL	100.11	101.04	100.11	101.82	100.28	100.28	101.13	101.70	100.72	101.43	100.27	100.35	101.33	100.23	99.91	100.85	100.48	100.24	99.91	100.24

ATOMIC PROPORTIONS BASED ON 12 OXYGEN ATOMS

Si	2.951	2.942	2.951	2.963	2.959	2.952	2.969	2.920	2.928	2.963	2.983	2.995	2.970	2.873	2.946	2.957	2.967	2.956	2.946	2.956
Ti	0.013	0.003	0.013		0.008	0.003	0.005				0.005		0.015			0.003				
Al	2.043	2.029	2.043	2.055	2.023	2.027	2.028	2.076	2.057	2.036	2.024	2.001	2.019	2.080	2.035	2.026	2.012	2.012	2.035	2.012
Cr					0.003						0.005	0.002			0.005				0.005	
Fe	2.408	2.611	2.408	2.57	2.596	2.769	2.569	2.556	2.480	2.500	2.374	2.413	2.000	2.744	2.499	2.548	2.508	2.578	2.499	2.578
Mn	0.155	0.048	0.155	0.025	0.063	0.013	0.142	0.128	0.195	0.139	0.193	0.056	0.268	0.049	0.163	0.137	0.148	0.142	0.163	0.142
Mg	0.191	0.227	0.191	0.237	0.113	0.119	0.170	0.274	0.267	0.277	0.303	0.364	0.243	0.203	0.291	0.285	0.293	0.279	0.291	0.279
Ca	0.172	0.179	0.172	0.154	0.254	0.146	0.128	0.083	0.111	0.092	0.113	0.163	0.407	0.133	0.092	0.070	0.087	0.067	0.092	0.067
SUM	8.013	8.039	8.013	8.004	8.019	8.029	8.011	8.037	8.038	8.007	8.000	7.994	8.002	8.082	8.031	8.023	8.018	8.034	8.031	8.034

\* all iron reported as FeO

## Biotite

	OB5	AQ/X	M/1	HWU	16/7b
SiO <sub>2</sub>	36.31	34.42	34.66	35.79	35.50
TiO <sub>2</sub>	1.63	1.77	1.80	1.44	1.57
Al <sub>2</sub> O <sub>3</sub>	21.11	21.19	20.49	21.12	21.52
FeO	22.72	27.46	23.77	22.11	21.60
MnO	0.02	nd	nd	0.09	nd
MgO	6.65	4.33	7.16	8.57	7.66
CaO	0.01	nd	nd	0.04	nd
Na <sub>2</sub> O	0.35	0.29	0.29	0.30	0.28
K <sub>2</sub> O	7.29	8.76	8.06	8.09	8.50
TOTAL	96.09	98.22	96.23	97.55	96.63

ATOMIC PROPORTIONS BASED ON 22 OXYGEN ATOMS

Si	5.456	5.249	5.287	5.323	5.326
Ti	0.184	0.203	0.206	0.161	0.178
Al	3.740	3.807	3.683	3.702	3.805
Fe	2.855	3.502	3.032	2.750	2.711
Mn	0.002	nd	nd	0.011	nd
Mg	1.488	0.985	1.628	1.899	1.714
Ca	0.018	nd	nd	0.007	nd
Na	0.101	0.084	0.085	0.087	0.082
K	1.396	1.703	1.567	1.535	1.628
SUM	15.240	15.533	15.488	15.475	15.444

nd=not detected; \* all iron reported as FeO

## Staurolite

	AQ/X	HWUs	OB5s	M/1
SiO <sub>2</sub>	27.63	28.02	27.35	26.26
TiO <sub>2</sub>	0.17	0.25	0.42	0.40
Al <sub>2</sub> O <sub>3</sub>	52.77	53.13	52.57	54.62
FeO	15.85	14.25	14.53	15.51
MnO	nd	0.13	0.01	nd
MgO	0.83	1.63	1.31	0.92
CaO	nd	nd	nd	nd
ZnO	0.39	0.28	0.17	0.19
K <sub>2</sub> O	nd	nd	nd	0.02
TOTAL	97.64	97.69	96.38	97.90

ATOMIC PROPORTIONS BASED ON 23 OXYGENS

Si	3.884	3.906	3.871	3.678
Ti	0.018	0.026	0.045	0.042
Al	8.740	8.728	8.769	9.016
Fe	1.862	1.660	1.720	1.817
Mn	nd	0.015	0.001	nd
Mg	0.174	0.338	0.275	0.192
Ca	nd	nd	nd	nd
Zn	0.041	0.028	0.018	0.020
K	nd	nd	0.003	nd
SUM	14.719	14.701	14.702	14.765

nd=not detected; \* all iron reported as FeO

## Cordierite

	16/7c	19/12	HWUc
SiO <sub>2</sub>	47.75	48.60	48.32
TiO <sub>2</sub>	nd	nd	nd
Al <sub>2</sub> O <sub>3</sub>	32.68	32.26	32.53
Cr <sub>2</sub> O <sub>3</sub>	nd	nd	nd
FeO	10.25	7.80	9.68
MnO	0.08	nd	0.13
MgO	7.04	8.20	7.13
CaO	nd	nd	nd
Na <sub>2</sub> O	0.42	0.46	0.26
K <sub>2</sub> O	nd	nd	nd
TOTAL	98.22	97.32	98.05

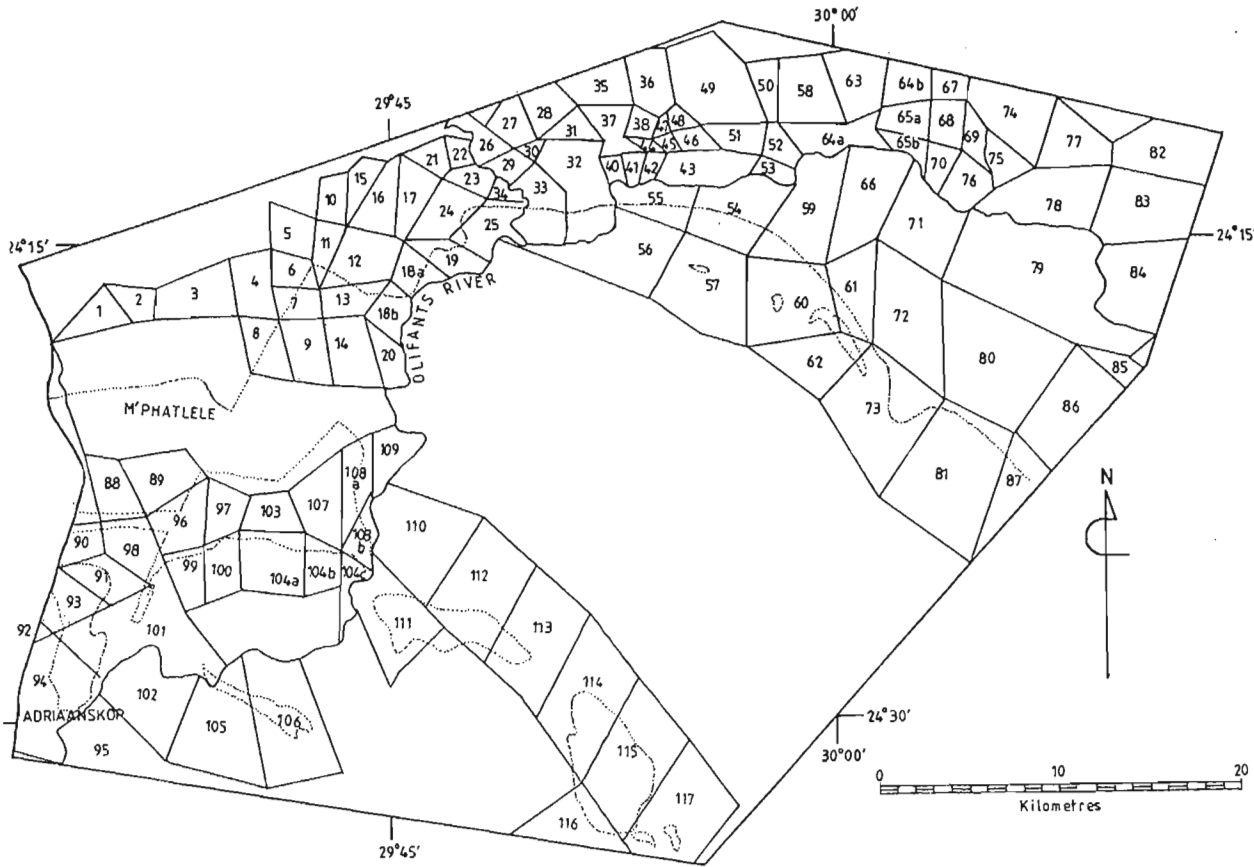
ATOMIC PROPORTIONS BASED ON 6 OXYGEN ATOMS

Si	1.658	1.681	1.673
Ti	nd	nd	nd
Al	1.337	1.315	1.328
Cr	nd	nd	nd
Fe	0.298	0.226	0.280
Mn	0.002	nd	0.004
Mg	0.364	0.423	0.368
Ca	nd	nd	nd
Na	0.028	0.031	0.017
K	nd	nd	nd
SUM	3.687	3.676	3.670

nd=not detected; \* all iron reported as FeO

# APPENDIX 1F

# KEY TO FARM NAMES




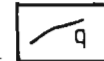



1	Middelkop	42	Success	81	Mecklenburg
2	Schipadnek	43	Groenfontein	82	Dalton
3	Naauwpoort	44	Ongegund	83	Dublin
4	Groothoek	45	Uitrecht	84	Geneva
5	Muiskraal	46	Lot 275	85	Tivoli
6	Witgat	47	Weltevreden	86	Putney
7	Kaffernek	48	Uitkyk	87	Croydon
8	Molagat	49	Hoogenoeg	88	Doorloop
9	Zondernaam	50	Lot 280	89	Vleiplaats
10	Honingkop	51	Lot 28	90	Spitskop
11	Bakenkop	52	Copper	91	Grootkop
12	Katkloof	53	Begroting	92	Vlaklaagte
13	Diepsloot	54	Rostok	93	Boschplaats
14	Tabakplaas	55	Haakdoornhoek	94	Badfontein
15	Benauwdheid	56	Jachtlust	95	Veeplaats
16	Wonderkop	57	Winterveld	96	Pramkoppies
17	Toornkop	58	Tubex	97	Koppiesdam
18a	Tigerpoort	59	Jobs Kop	98	Kameelbult
18b	Fonteinplaats	60	Moeijelijk	99	Platdoorns
19	Leeukop	61	Schwerin	100	Davidspoort
20	Grootdraai	62	Zwartkoppies	101	Taaiboschspruit
21	Beesthoek	63	Lot 297	102	Wonderboom
22	Tuinplaats	64a	Rooipoort	103	Stofpoort
23	Goedhoek	64b	Lot 296	104a	Dwarsrand
24	Grootplaats	65a	Lot 287	104b	Zwarthoek
25	Scheiding	65b	Lot 288	104c	Fortdraai
26	Lagerdraai	66	Roodekrans	105	Vlakplaats
27	Lot 251	67	Ska	106	Haakdoorndraai
28	Lot 262	68	Lot 294	107	Zaakloof
29	Lot 253	69	Lot 293	108a	Spelonk
30	Lot 252	70	Lot 290	108b	Olifantspoort
31	Lot 261	71	Stavenhagen	109	Koppieskraal
32	Matabatas	72	Wismar	110	Eersterecht
33	Koedooskop	73	Waterkop	111	Mooiplaats
34	Inkomst	74	Horn Gate	112	Hoeraroep
35	Lot 263	75	Lot 292	113	Goedverwacht
36	Parker's Pass	76	Lot 290	114	Driekop
37	Voorspoed	77	Elton	115	Paradys
38	Klein Geluk	78	Nice	116	Zoetvelden
40	Plaats	79	Stellenbosch	117	Geeneinde
41	Ebenhaezer	80	De Paarl		

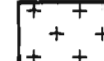


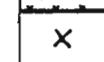
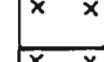


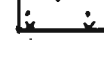
**GEOLOGICAL LEGEND**

**GEOLOGICAL SYMBOLS**

**INTRUSIVE ROCKS**

-  Dolerite
-  Diabase
-  Quartz-feldspar porphyry
-  Quartz vein
-  Pegmatite

**Roodekrans Complex**




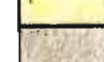


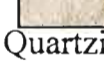

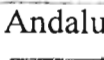
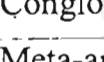
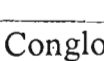
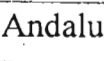
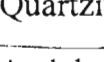
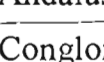

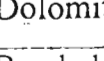
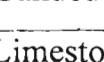




-  Coarse-grained pink granite
-  Ferrogabbro, with minor troctolite and anorthosite (magnetite layer )
-  Gabbro, norite, anorthosite
-  Pyroxenite, norite, anorthosite (chromite layer  chr) (Merensky Reef  MR)
-  Melanorite, pyroxenite and harzburgite

- Nebo Granite
- Upper zone
- Main zone
- Critical zone
- Lower zone

**LEBOWA GRANITE SUITE**

**RUSTENBURG LAYERED SUITE**

**CONTACT METAMORPHOSED VOLCANOSEDIMENTARY SUCCESSION**

-  Alluvium
-  Quartzite
-  Quartzite, semi-pelite, pelite and calc-silicate
-  Quartzite with subordinate semipelite
-  Migmatitic fibrolite-andalusite-cordierite-biotite schist
-  Meta-mafic lavas, pyroclastics and breccias
-  Calc-silicate (graphitic shale )
-  Andalusite-fibrolite-biotite schist
-  Quartzite
-  Andalusite-fibrolite-biotite schist
-  Conglomerate, quartzite and intercalated muscovite schist
-  Meta-amygdaloidal mafic lavas
-  Conglomerate
-  Andalusite-staurolite-garnet-biotite fels
-  Quartzite
-  Andalusite-staurolite-garnet-biotite fels
-  Conglomerate and chert breccia
-  Dolomite, chert, limestone, chert breccia with interbedded shale, sandstone and quartzite
-  Banded ironstone, shale and subordinate carbonate and breccia
-  Limestone, dolomite, chert, shale, quartzite, diamictite, hornfels and conglomerate

- Lakenvalei Quartzite Formation
- Vermont Hornfels Formation
- Magaliesberg Quartzite Formation
- Lydenburg Shale Member
- Machadodorp Member
- Boven Shale Member
- Daspoort Quartzite Formation
- Strubenkop Shale Formation
- Dwaalheuwel Quartzite Formation
- Hekpoort Andesite Formation
- Boshoek Formation
- Upper pelitic unit
- Klapperkop Quartzite Member
- Lower pelitic unit
- Bevets Conglomerate Member
- Duitschland Formation
- Penge Formation
- Ma
- Malmani Subgroup


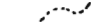












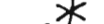








**Silverton Shale Formation**

**PRETORIA GROUP**






**Timeball Hill Formation**

**Rooihogte Formation**

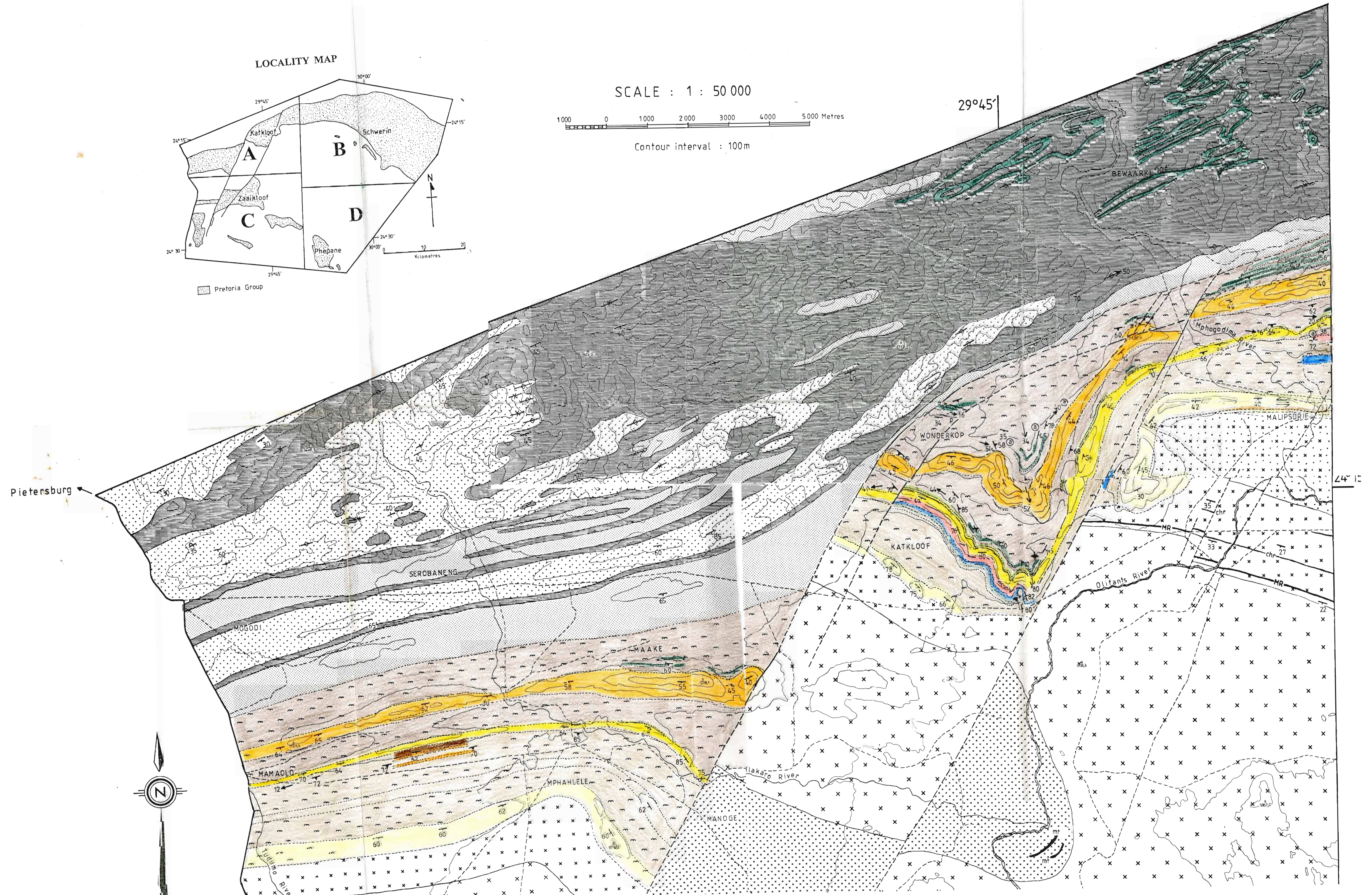
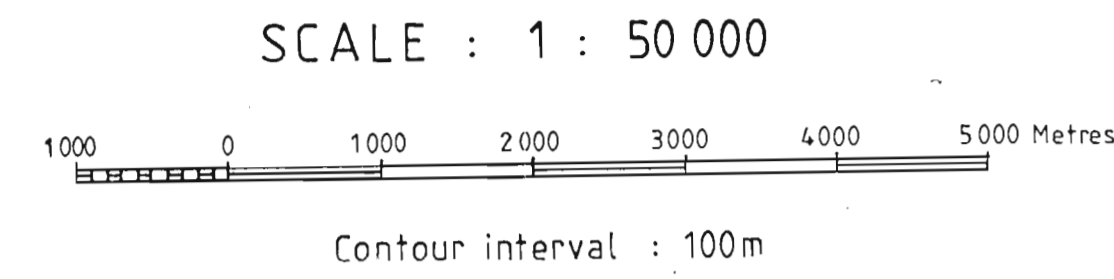
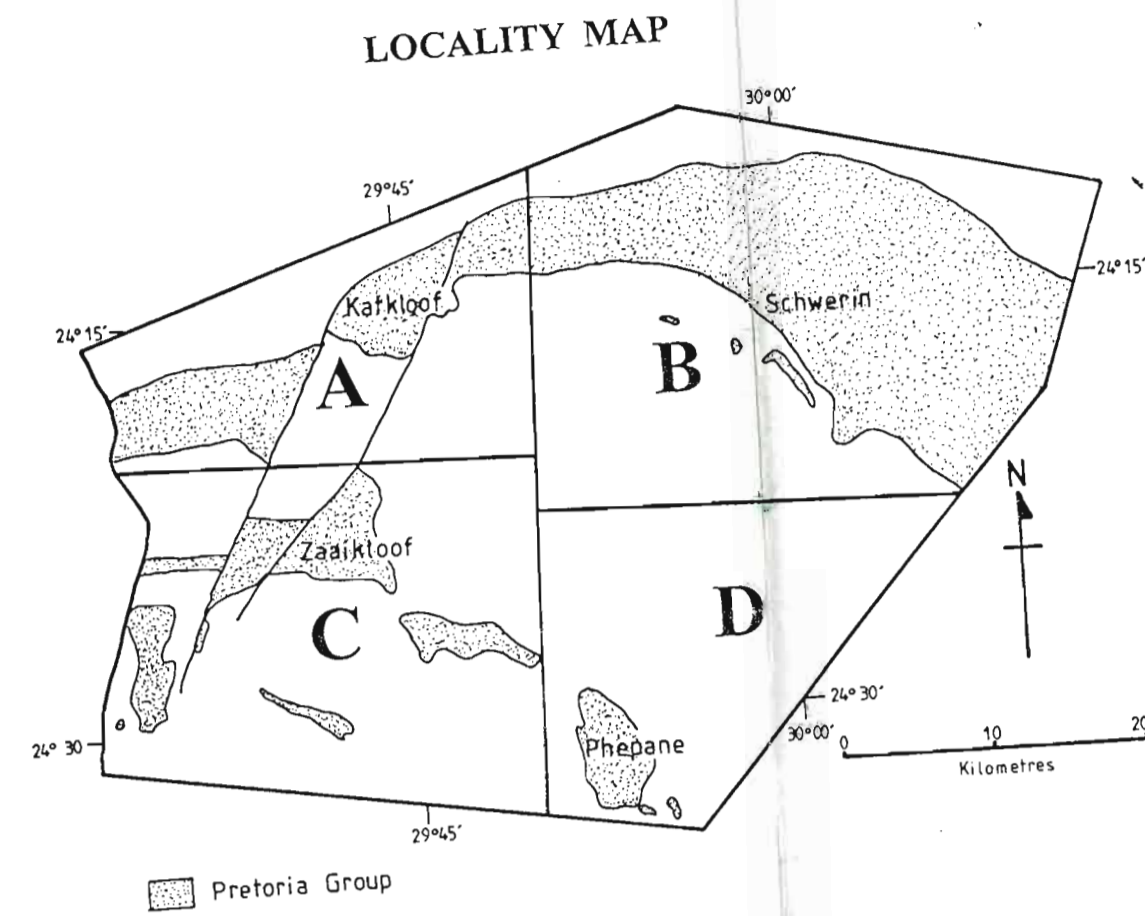
**CHUNIESPOORT GROUP**

-  Observed lithological boundary
-  Inferred lithological boundary
-  Dip and strike of sedimentary and igneous stratification
-  Dip and strike of overturned bedding
-  Vertical bedding
-  Younging direction
-  Form lines
-  Dip and strike of foliation
-  Vertical foliation
-  Plunge and azimuth of mineral stretching lineation
-  Plunge and azimuth of minor fold axis
-  Plunge and azimuth of anticlinal fold axis
-  Plunge and azimuth of synclinal fold axis
-  Axial trace of major anticlinal fold structure
-  Axial trace of major synclinal fold structure
-  Magma flow direction indicator
-  Ductile shear sense indicator
-  Observed fault
-  Inferred fault
-  Extensional fault with downthrown side indicated
-  Contractional fault with teeth on hangingwall
-  Operating mines
-  Old andalusite workings and trenches

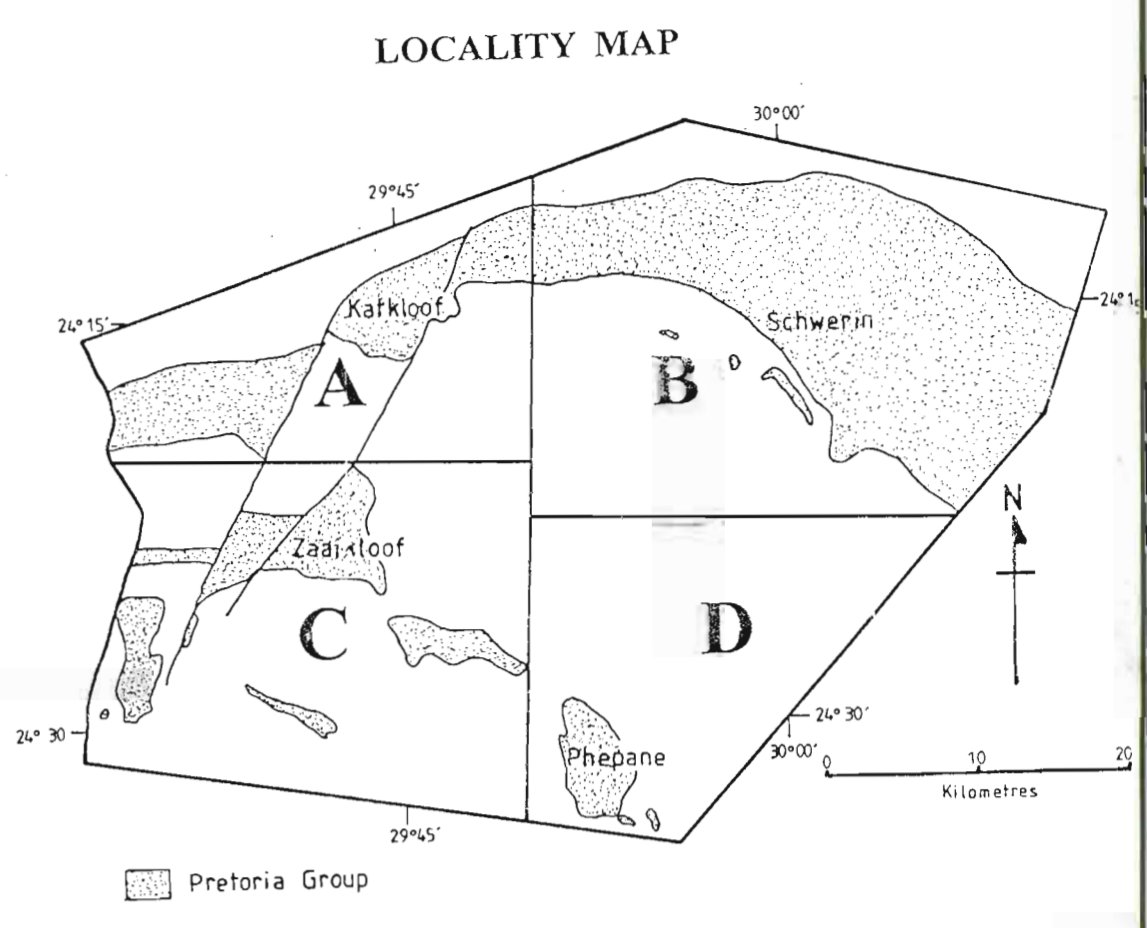
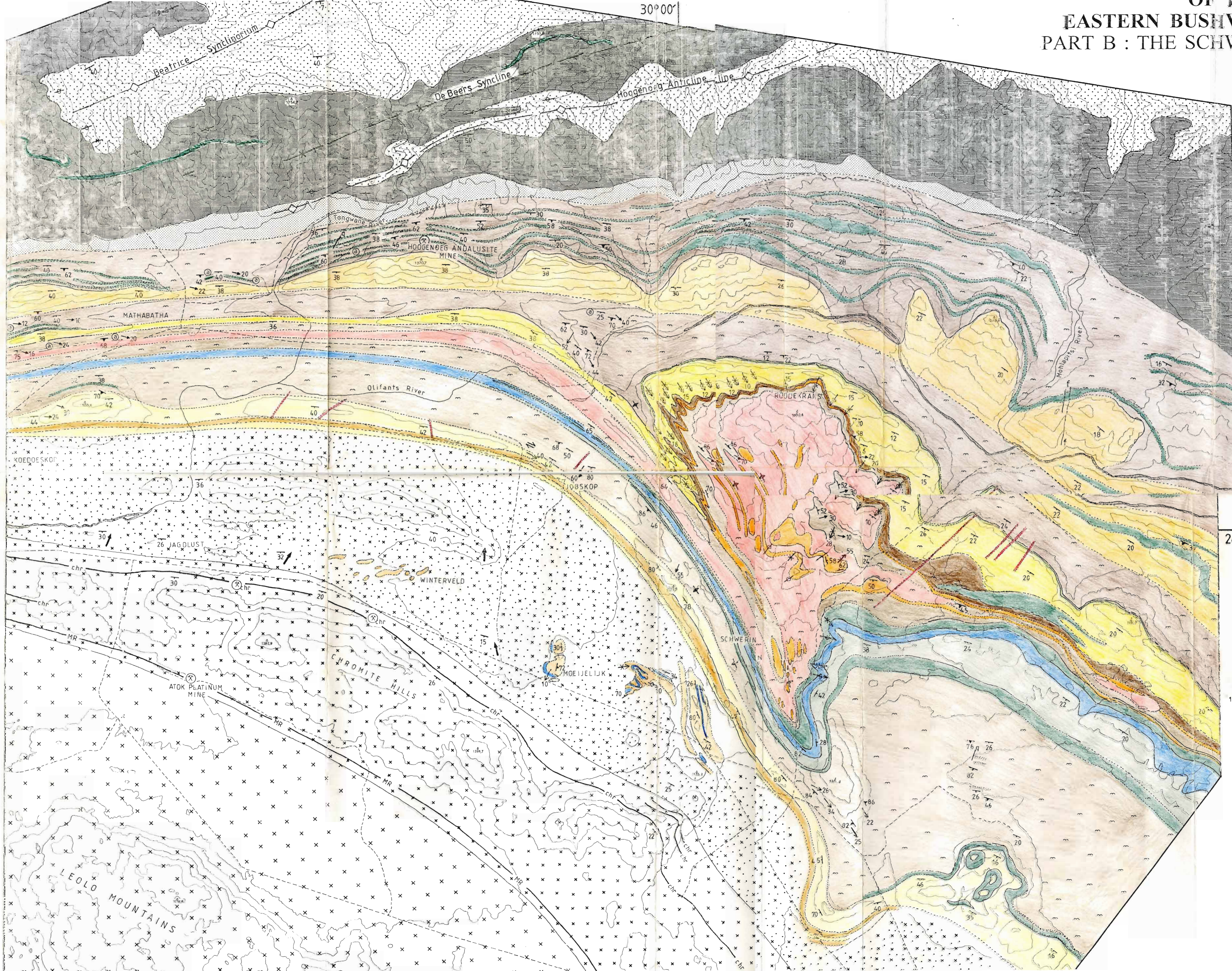
**TOPOGRAPHICAL SYMBOLS**

-  Contours at 100m intervals
-  Trigonometric beacons with ground heights
-  Roads and tracks
-  Minor perennial rivers
-  Major perennial rivers

NORTHERN MARGIN  
OF THE  
EASTERN BUSHVELD COMPLEX  
PART A : THE KATKLOOF FOLD AREA

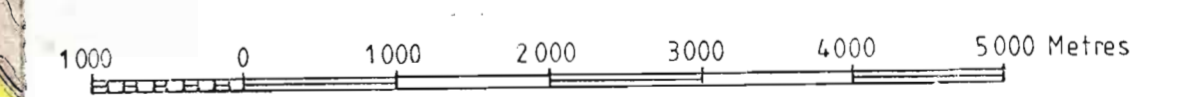


**EASTERN BUSHVELD COMPLEX**  
**PART B : THE SCHWERIN FOLD AREA**



24°15'

SCALE : 1 : 50 000

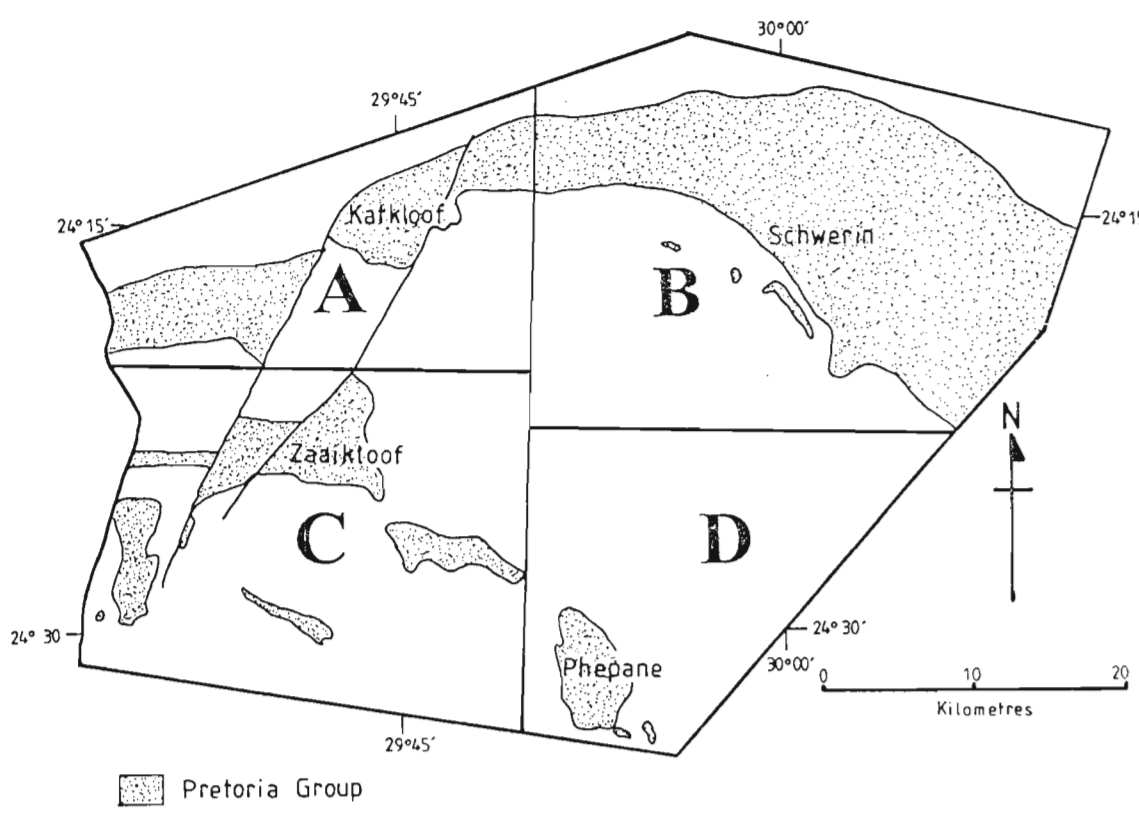


Contour interval : 100m

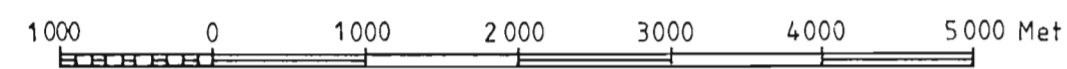


# PART C : THE ZAAIKLOOF FOLD AREA

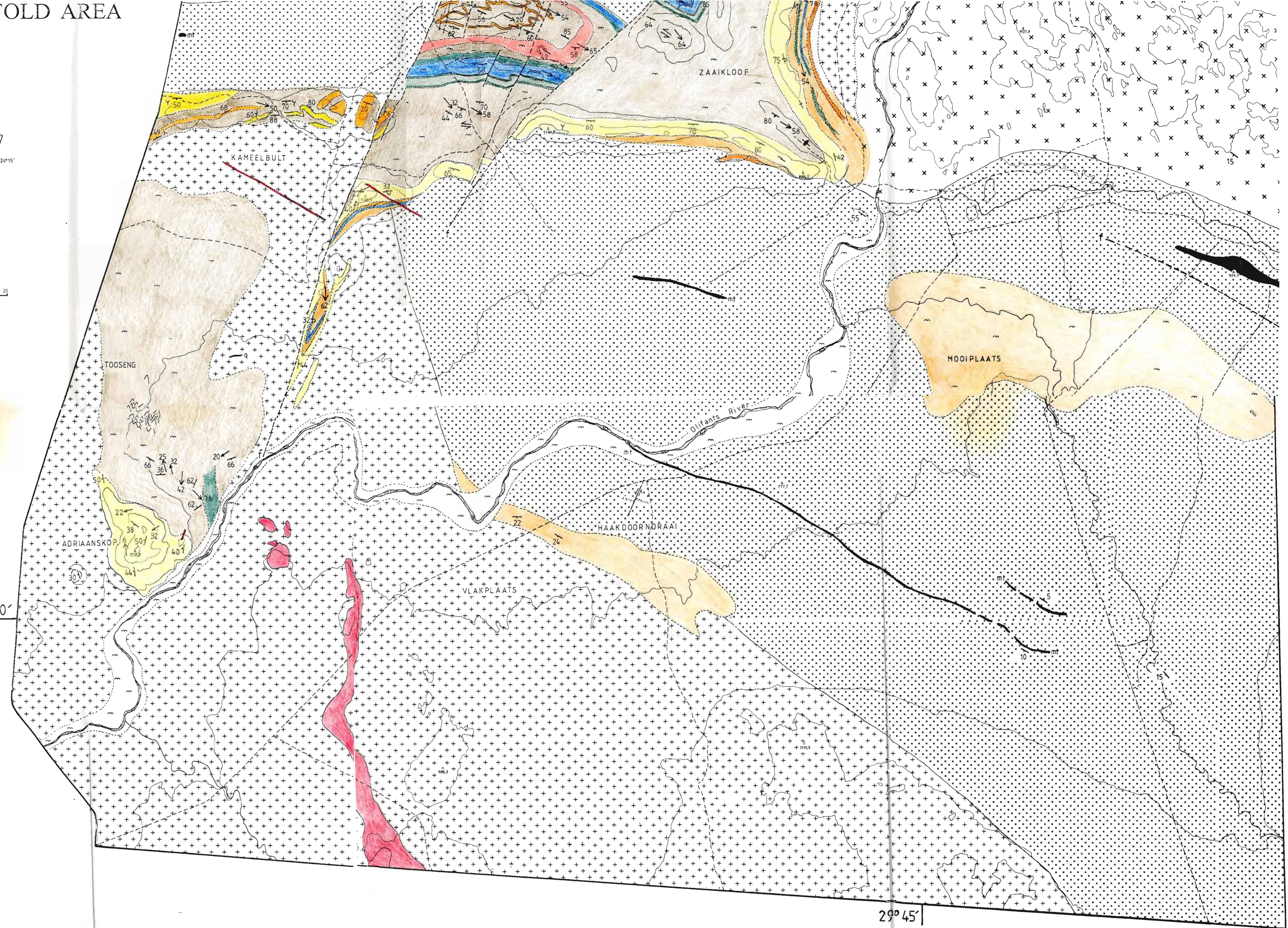
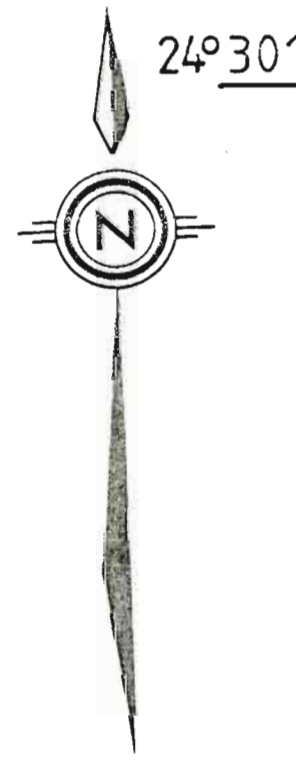
LOCALITY MAP



SCALE : 1 : 50 000



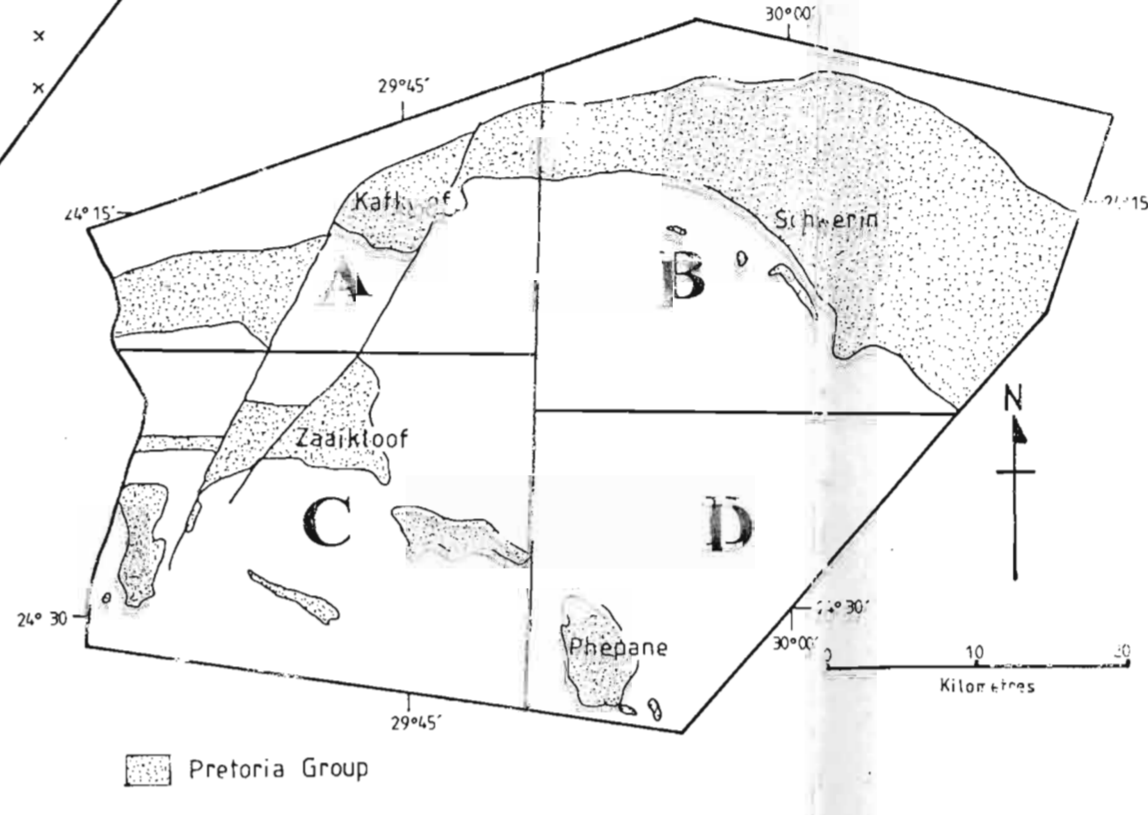
Contour interval : 100m



# GEOLOGICAL MAP OF THE NORTHERN MARGIN OF THE EASTERN BUSHVELD COMPLEX PART D : THE PHEPANE FOLD AREA



LOCALITY MAP



SCALE : 1 : 50 000

1000 0 1000 2000 3000 4000 5000 Metres

Contour interval : 100m

24° 30'